12-1-2016

Characterizing Crystal Populations for the Petrogenesis of the Post-Collapse Rhyolites in The Long Valley Caldera, California

William Joseph
University of Nevada, Las Vegas

CHARACTERIZING CRYSTAL POPULATIONS FOR THE PETROGENESIS OF THE POST-COLLAPSE RHYOLITES IN THE LONG VALLEY CALDERA, CALIFORNIA

By

William T. Joseph

Bachelor of Arts – Geology
DePauw University
2014

A thesis submitted in partial fulfillment of the requirement for the

Master of Science – Geoscience

Department of Geoscience
College of Sciences
The Graduate College

University of Nevada, Las Vegas
December 2016

UNLV | GRADUATE COLLEGE

Thesis Approval

The Graduate College
The University of Nevada, Las Vegas

November 18, 2016

This thesis prepared by

William T. Joseph

entitled

Characterizing Crystal Assemblages for the Petrogenesis of Post-Collapse Rhyolites in the Long Valley Caldera, California

is approved in partial fulfillment of the requirements for the degree of

Master of Science – Geoscience
Department of Geoscience

Terry Spell, Ph.D.
Examination Committee Chair

Kathryn Hausbeck Korgan, Ph.D.
Graduate College Interim Dean

Rodney V. Metcalf, Ph.D.
Examination Committee Member

Minghua Ren, Ph.D.
Examination Committee Member

George Rhee, Ph.D.
Graduate College Faculty Representative

ABSTRACT

Post-collapse rhyolites of the Long Valley in eastern California are the product of remelting of crystal mush bodies via mafic rejuvenation following the eruption of the Bishop Tuff. This is supported by mineral textures and major element geochemistry from the Resurgent Dome rhyolite, the Moat rhyolite, the Hot Creek Flow, and the Deer Mountain rhyolite. New $^{40}Ar/^{39}Ar$ eruptive ages are reported for the Moat rhyolites (525 ka, 333 ka, 118 – 94 ka), Hot Creek Flow (312 – 295 ka), and the Deer Mountain rhyolite (65 ka). The initial post-collapse eruptions, resulting in the Resurgent Dome rhyolite, appear to be derived from the residual Bishop Tuff magma chamber and are characterized by euhedral, juvenile plagioclase and orthopyroxene phenocrysts in crystal poor rhyolites.

At 525 ka, Moat rhyolites mark a major increase in mafic rejuvenation inducing rhyolitic magma production. Reverse zonation (An_{18} – An_{39}) present in plagioclase populations indicates mafic magma injecting into the crystal mush zone. Similarly, anti-rapakivi textures and plagioclase cores with labradorite compositions (An_{56}) found within 333 ka Moat rhyolites indicate mixing between mafic and rhyolitic melts. Spatially and temporally related Hot Creek Flow rhyolites appear to be the results of crystal poor rhyolitic melt extracted from the same magma body. A decrease in mafic inputs is exhibited the youngest Moat rhyolite where andesine core and oligoclase rim overgrowths are separated by dissolution surfaces in plagioclase populations. This relationship is displayed again in the culminating Deer Mountain eruption, but decrease in mafic input indicates a waning of the Long Valley magmatic system.

ACKNOWLEDGMENTS

I would like to thank all those that have helped me during my time at UNLV. First, I would like to thank my advisor Dr. Terry Spell for his help as a trusty field assistant, his thoughtful critiques, and most of all his dry wit. I would also like to thank my committee members Dr. Minghua Ren, Dr. Rod Metcalf and Dr. George Rhee. I would especially like to thank Dr. Minghua Ren for his help assisting with the electron microprobe, Kathy Zanetti for her help at the Nevada Isotope and Geochronology Lab, and Dr. Ayra Udry for use of her petrographic microscope. Lastly I would like to thank Dr. Steven Singletary and Syed Gilani at the Southeastern North Carolina Regional Microanalytical and Imaging Consortium for assistance with EPMA analysis, as well as their generous hospitality while in Fayetteville.

This thesis is dedicated to all of my friends and family that have nurtured my interested in Geology from an early age to my time here at UNLV. While I had my fair share of setbacks completing this research, the encouragement and love I received from my family and friends kept me on track. I would especially like to thank my friends Billy Fischer, Billy Pilesky, Chad Crotty, and Steve Dobbs who have supported me since my arrival at UNLV. I am forever grateful to them and all those I met along this journey.

This thesis was funded by the Geological Society of America and the Bernada E. French and Edwards and Olswang scholarships. I am grateful for the financial support these institutions provided in completing my research. Data collected at the facility at FSU was funded by the U.S. Department of Defense grant W911NF-09-1-0011.

TABLE OF CONTENTS

LIST OF TABLES

LIST OF FIGURES

CHAPTER 1

INTRODUCTION

The evolution of high volume, silicic volcanic systems remains a highly debated topic. Whereas extensive studies of voluminous (100-1000 km^3) caldera forming eruptions have been conducted in areas such as the Jemez Volcanic Field in New Mexico (Smith and Bailey, 1966; Wolf and Ramos, 2003; Rowe et al., 2007), the Yellowstone caldera in Wyoming (Smith and Braile, 1994; Perkins and Nash, 2002), the San Juan Volcanic Field in Colorado (Bachman and Bergantz, 2003), and the Long Valley caldera in California (Bailey et al., 1976; Hildreth, 2004; Gualda and Ghiorso, 2013; Simon et al., 2014), there has been less emphasis on post-collapse volcanism within these systems. A reassessment continental volcanic systems, like that of the Long Valley, with an emphasis on post-collapse rhyolites may place further constraints the long-term evolution of the magmatic plumbing systems that produce large caldera forming eruptions. Thus, further understanding of the magma chamber dynamics beneath the Long Valley caldera during the late Pleistocene can provide insights to the development of supervolcanoes.

Following the voluminous (600 km^3) (Bailey et al., 1976) Bishop Tuff eruption at approximately 780 ka (Bailey et al., 1976), post-collapse volcanism produced the Resurgent Dome rhyolite (700 ka) (Simon et al, 2014), the Moat rhyolites (576 ka) (Simon et al, 2014), the Hot Creek Flow (335 ka) (Simon et al., 2014)), and the Deer Mountain rhyolites (101 ka) (Heumann et al., 2002) Traditional models for the production of large volumes of rhyolite in caldera systems (like Long Valley) were first formalized by Smith (1979) and later by Hildreth (1981). These models suggest that a single, long lived magma chamber can produce the entire volume of material involved in pre-caldera, caldera forming and post-caldera eruptive events. Additionally, temperature and compositional gradients recorded in eruptive units reflect the

simple evolution of basaltic to silicic magmatism within the chamber. However, more recent models (Hupert and Sparks, 1988; Bachman and Bergantz, 2004) argue that melt segregation and independent magma batches can be generated on short (10^2 to 10^3 years) timescales and are responsible for individual eruptive events. Compositional variations exhibited in the resulting eruptive units are the product of subsequent melts rejuvenating and recycling previous material in the shallow crust (Bachman and Bergantz, 2004).

An initial model for the magmatic plumbing system of Long Valley was proposed by Bailey et al. (1976). This model fits with the models of Smith (1979) and Hildreth (1981) as it was hypothesized that a voluminous, long-lived magma chamber was responsible for eruptions prior to caldera formation, during the eruption of the Bishop Tuff, and for subsequent post-caldera eruptions.

While the model proposed by Bailey et al. (1976) can resolve some simple geochemical trends observed throughout eruptive stratigraphy, it does not address the nuances throughout the evolution of Long Valley and most certainly cannot account for geochemical trends within the post-collapse units. More recent work for the Long Valley caldera (Simon et al., 2014) combines high precision age data with Hf-Nd isotopic compositions of zircon populations for pre-eruptive conditions of post-collapse rhyolites. Zircon populations from two periods of post-collapse volcanism (700 ka – 400 ka and 400 ka – 100 ka) suggest a system whereby mafic magmas recharged and mixed with previous crustal melts and assimilated crystallized Pleistocene age granitic intrusions. This represents an extreme contrast from the initial model proposed by Bailey et al. (1976) in that eruptions and melt production are not driven by the entirety of the magmatic system but are subject to distinct evolutionary paths localized to different areas of the caldera. However, the timing and interaction of magma mixing and assimilation for the production of the

post-collapse rhyolites is not well understood. Thus, the goal of this study is to examine the crystal assemblages of the post-collapse rhyolites to further constrain magma system dynamics beneath the post-collapse Long Valley caldera towards the end of the Pleistocene.

1.1 Previous Work

Multiple models have been proposed regarding the magmatic plumbing system that produced the Long Valley rhyolites and their respective mineral assemblages. Descriptions of crystal assemblages for post-collapse rhyolites are not well documented and are generally described by Bailey et al. (1976) as well as by Hildreth (2004). Mineral assemblages of the Resurgent Dome rhyolites are comprised of less than 3% phenocrysts of quartz, plagioclase, biotite and hypersthene (Bailey et al., 1976). This coincides with Hildreth (2004) who reports similar sparse phenocrysts (0-3%) with additional euhedral, unresorbed orthopyroxene, Fe-Ti oxides, apatite, zircon, and pyrrhotite.

Moat rhyolites contain 20% phenocrysts of hornblende, biotite, quartz, sanidine, and plagioclase (Bailey et al., 1976). Hildreth (2004) also observed similar phenocryst populations in these NW-trending rhyolites. The Hot Creek Flow is not well documented by Bailey et al. (1976), but Hildreth (2004) describes this southeastern rhyolite as phenocryst poor with no quartz but sparse crystals of feldspar, biotite, clinopyroxene, and Fe-Ti oxides. The Deer Mountain rhyolite dome is phenocryst rich (20 – 30%) and contains quartz, sanidine, plagioclase, biotite, hornblende, and Fe-Ti oxides (Hildreth, 2004).

Bailey et al. (1976) was the first to attempt to reconcile initial descriptions of mineral textures within the framework of magma evolution. As previously mentioned his model inferred a voluminous, long-lived (>1 Ma) magma chamber that was thermally and compositionally

zoned and produced a succession of less-evolved rhyolites with decreasing SiO_2 content. Therefore, subsequent eruptions reflect the progressive withdrawal of deeper magmas with time culminating with mafic volcanism. These less-evolved mantle derived magmas provided a thermal input for the production of a large volume of silicic magma. The mafic inputs also sustained and drove volcanism for the lifetime of the system.

Work offered by Heumann and Davies (1997) suggest a modified version of the model presented by Bailey et al. (1976). Their interpretation supports Bailey et al. (1976) claim that the Bishop Tuff magma chamber remained active following the 780 ka eruption. Early and late post-caldera rhyolites were the result of gradual differentiation of the residual Bishop Tuff melt with and addition of mafic material near the base of the chamber. However, a second rhyolitic melt mixing with residual melt accounts for major oxide (high and low SiO_2) and trace element distinctions between early ($\geq$ 400 ka) and late ($\leq$ 400 ka) post-collapse rhyolites. Moreover, instances of trace element variability in some post-collapse units (i.e. the Mammoth Knolls Dome) infer isolated magma chambers separated from the main body (Huemann and Davies, 1997). Thus, it is implied that early post-collapse rhyolites reflect the bulk composition of the Long Valley magma chamber and later erupted post-collapse rhyolites represent smaller, chemically evolved magma bodies (Heumann and Davies, 1997)

Hildreth (2004) also offered an alternative mechanism to his initial model (Hildreth, 1981) and the model proposed by Bailey et al. (1976) for compositional gradients observed in Long Valley rhyolites. Hildreth (2004) argueed that post-collapse eruptive units in the Long Valley reflect silicic melt segregation from a larger crystal mush body. Mafic magmas and dikes that penetrated the upper crust periodically rejuvenated the crystal mush and drove melt

segregation. However, the thermal influence of mafic intrusions are increasingly less involved after 650 ka (Hildreth, 2004).

More recently, Gualda and Ghiorso (2013) argue that the reconstruction of magmatic plumbing systems based solely on the inversion of eruptive stratigraphy is speculative at best. Furthermore, initial models cannot account for compositional variations and eruptive frequency demonstrated by the Long Valley volcanic stratigraphy. Based on new geobarometric data, a single voluminous magma chamber is not viable for the production of even single eruptions such as the Bishop Tuff (Gualda and Ghiorso, 2013). For Example, zircon emplacement temperatures and pressures (~740-750°C and ~175-200 MPa) are quite similar between early and latest erupted members of the Bishop Tuff (Gualda and Ghiorso, 2013). A bimodal distribution between phenocryst and glass compositions with respect to Both Bishop Tuff members suggests compositional distinction (Gualda and Ghiorso, 2013). Thus, similar crystallization conditions and distinct compositional differences with phenocryst and glass populations from each member suggest a coeval eruption from "laterally juxtaposed" magma chambers (Gualda and Ghiorso, 2013).

These data from Gualda and Ghiorso (2013), coupled with refined $^{40}Ar/^{39}Ar$ dates and zircon U-Pb ages from post-collapse rhyolites (Simon et al., 2014), suggest a system of short-lived independent magma chambers, as melt bodies are inferred to have short pre-eruptive residence times on the order of 10 – 100 ka (Simon et al., 2014). Additionally, an increase in Nd (-2.5 to -1.0) and Hf (1.0 to 2.5) isotopic compositions from zircon populations and pumice clasts suggest an increase in mafic magma input following the eruption of the Bishop Tuff, facilitating remelting and eruptive events (Simon et al., 2014). These inputs decrease with time until the culminating eruption of the Deer Mountain rhyolite (Simon et al., 2014).

CHAPTER 2

GEOLOGIC SETTING

2.1 The Long Valley Caldera and Volcanic Field

The Long Valley caldera is a 450 km^2 elliptical depression on the eastern escarpment of the Sierra Nevada, California, USA (Fig. 2.01) (Bailey et al., 1976; Bailey, 1989). The caldera resides in the Long Valley-Mono Craters volcanic field within the larger (approximately 4000 km^2) Owens Valley Graben (Bailey, 2004; Hill, 2006). Volcanism occurring in the Long Valley region is associated with transtensional deformation on the margin of the Eastern California Shear Zone (ECSZ) and western border of the Basin and Range Province (Bailey, 2004; Hill, 2006). Magmatism occured as response to transform movement in the ECSZ and extension in the Walker Lane (WL) area (Hill, 2006). Upwelling magma reached the surface due to crustal thinning in response to dextral slip along the ECSZ-WL region (Hill, 2004). Basaltic, dacitic, and rhyolitic lavas erupted to the surface reside upon Mesozoic Sierra Nevadan basement rocks composed of granite to granodiorite (Bailey, 2004).

Volcanism occurring in the Long Valley area commenced around 4 Ma (Bailey, 2004). The volcanic interval prior to caldera formation (2.5 Ma – 800 ka) resulted in the eruption of the high-silica Glass Mountain rhyolites (Metz and Mahood, 1985). At approximately 780 ka, eruption of the Bishop Tuff produced 600 km^3 of welded ignimbrite deposits (Bailey et al., 1976). Following this, roof collapse occurred along ring fracture faults on the boundary of the caldera after partial evacuation of the magma chamber. Two main periods of intracaldera volcanism occurred following collapse producing the early phase Resurgent Dome rhyolite (700 ka) and Moat rhyolites (576 ka) (Simon et al., 2014). Hot Creek Flow (335 ka; Simon et al.,

2014), and the Deer Mountain rhyolite (101 ka; Heumann et al., 2002) compromise the bulk of eruptions occurring during the late phase post-caldera sequence.

2.2 The Resurgent Dome Rhyolite

After the formation of the Long Valley caldera, initial post-collapse eruptions resulted in the formation of the low silica (74-75%) Resurgent Dome rhyolite (Bailey et al., 1976; Hueman and Davies, 1997; Hildreth, 2004). This unit is by far the most voluminous of all post-collapse rhyolites (~100 km^3) and is composed of 14 obsidian and rhyolite flows and domes located in the west central area of the caldera (Bailey, 1989; Hildreth, 2004) (Fig. 2.01). These domes and flows were erupted subaqueously within the paleo- Lake Long Valley (Bailey, 1989). Faulting associated with dome resurgence caused the formation of a northwest trending medial graben towards the center of the caldera (Bailey, 1989). Both of these factors contribute heavily to alteration observed in the groundmass of this unit.

Recent $^{40}Ar/^{39}Ar$ dating of the Resurgent Dome plagioclase indicate an eruptive age of approximately 700 ka (Simon et al., 2014). This largely aphyric unit contains approximately 0-3% phenocrysts with a quartz-free mineral assemblage consisting of plagioclase, orthopyroxene, biotite, Fe-Ti oxides, (Bailey et al., 1976, 1989; Hildreth, 2004; Huemann and Davies, 1997) and in rare instances amphibole. The chemically associated Bishop Tuff contains this same mineral assemblages as well as the presence of quartz and sanidine (Hildreth, 2004).

2.3 The Moat Rhyolites

Following formation of the Resurgent Dome three porphyritic Moat rhyolites erupted in clockwise fashion within the caldera approximately every 200 ka (Huemann and Davies, 1997) (Fig. 2.01). The first moat eruption (≤1 km^3; Hildreth, 2004), occurring North of the Resurgent Dome, was at approximately 576 ka (Simon et al., 2014). Emplacement of a smaller flow

occurred in the southeast moat at approximately 362 – 333 ka (Simon et al., 2014). The most voluminous (~4 km^3; Hildreth, 2004) and culminating moat eruption (sometimes referred to as the western coulee) occurred around 151 – 147 ka (Huemann, 2002).

These crystal rich units (20 – 30 % phenocrysts; Hildreth 2004) are petrographically similar and contain plagioclase, sanidine, quartz, biotite, amphibole, and Fe-Ti oxides. Chemically, each Moat rhyolite unit show variability in silica content with the western most unit showing the least evolved compositions (72 – 73% SiO_2) while the Northern and Southeast Moat units contain 74 – 75% SiO_2 and 76% SiO_2 respectively (Hildreth, 2004).

2.4 The Hot Creek Flow Rhyolite

The Hot Creek Flow rhyolite erupted in a close temporal (336 ka; Simon et al., 2014) and spatial (≤ 1km) relationship with the intermediate Moat rhyolite eruption. Moreover, the Hot Creek Flow is located in the southeastern geomorphic intracaldera moat (Fig. 2.01). However, the Hot Creek Flow is petrographically distinct from the Moat rhyolites. The Hot Creek Flow contains a sparse assemblage of phenocrysts (0 – 3%) which lack quartz but contain plagioclase, sanidine, biotite, and Fe-Ti oxides (Hildreth, 2004). While the Hot Creek Flow shares chemical similarities with the intermediate Moat rhyolite (76% SiO_2; Hildreth, 2004), the Hot Creek Flow is more voluminous, with eruptive material occupying approximately 10 km^2 north of its central vent (Fig. 2.01).

2.5 The Deer Mountain Rhyolite

The Deer Mountain rhyolite is the youngest eruptive unit examined in this study. Recent $^{40}Ar/^{39}Ar$ dates obtained from step heating of sanidine, indicate dome emplacement occurred at approximately 101 ka (Huemann et al, 2002). This dome is petrographically similar to the hornblende-biotite bearing rhyolite of the latest erupted Moat unit. However, the Deer Mountain

rhyolite was emplaced approximately 2.5 km to the west of the geomorphic moat (Hildreth, 2004) (Fig. 2.01). This unit is one of a cluster of four western domes that total approximately 1 km^3. The Deer Mountain rhyolite is crystal rich like that of the youngest Moat unit and contains upwards of 20% phenocrysts consisting of sanidine, plagioclase, quartz, biotite, amphibole, and Fe-Ti oxides (Hildreth, 2004). Additionally, the Deer Mountain rhyolite and southwestern Moat rhyolite are less evolved with 72 – 73% SiO_2 and 110 – 200 ppm Ba (Hildreth, 2004).

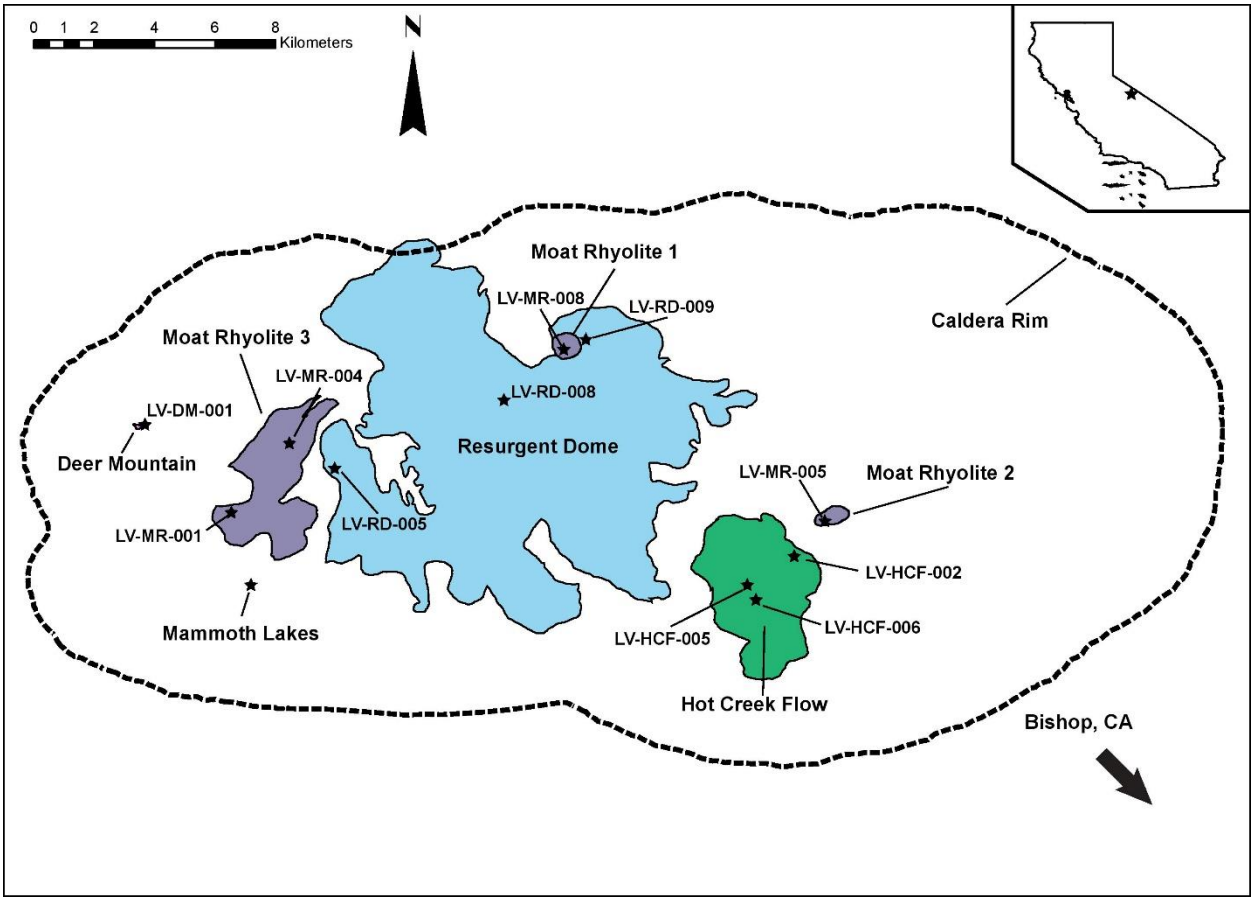

Figure 2.01. Location of eruptive units within the Long Valley caldera adapted from Bailey (1989). Stars represent sampling sites, while the dashed line represents the caldera rim. Inset displays the location of Long Valley within the state of California.

CHAPTER 3

METHODS AND ANALYTICAL TECHNIQUES

3.1 Sampling Techniques

Twenty-two samples were collected from the Resurgent Dome rhyolite, Moat rhyolites, Hot Creek Flow, and Deer Mountain rhyolite outcrops within the Long Valley caldera. Field work and sample collection occurred in July and September of 2015. Sample collection was based on the geologic mapping of Bailey (1989). After returning to UNLV eleven samples (Fig. 2.01) were selected for thin section preparation, petrographic analysis, and EPMA work based on lack of alteration and representative crystal assemblages.

3.2 Sample Preparation

Samples were cut to standard billet size for thin and probe section preparation. Forty billets were sent to Quality Thin Section in Tucson, AZ for completion. One additional billet was sent to Wagner Petrographic as sample LV-MR-008 was damaged during sample preparation.

Hand samples were then crushed and sieved for the recovery of sanidine phenocrysts for $^{40}Ar/^{39}Ar$ geochronology. Samples were crushed using the Bico chipmunk crusher and Bico disk mill to obtain material suitable for sieving. Crushed material was sieved through 1700 µm to 250 µm sieve size fractions to obtain minerals for hand picking under a binocular microscope. Sanidine crystals were picked from sieved size fractions based on blocky crystalline habit, vitreous luster, and translucent diaphaneity.

Fourteen thin sections were selected for polishing for use on the JEOL JXA-8900 probe at the University of Nevada, Las Vegas and the JEOL JXA-8530F probe at Fayetteville State University in Fayetteville, North Carolina. Samples were polished by hand using a series of 9, 6, 3, 1, 0.5, and 0.25 µm silicon diamond solutions and a 1 µm alumina solution placed on an 8”

Buehler Texmet polishing cloth covered glass plates. Samples were then cleaned with water and isopropanol and placed in a desiccation vacuum desiccator to remove remaining moisture. Following desiccation, samples were carbon coated for EPMA work. This was achieved by placing samples in a DV-502 A carbon evaporator and a Denton Vacuum BTT-IV Evaporator. In both methods the chamber was evacuated to approximately 10^{-5} millitorr. Once the correct vacuum was achieved, electric current passed through the ultra-pure carbon rod to make deposition of approximately 20 µm of carbon coating on the surface of the thin section.

3.3 $^{40}Ar/^{39}Ar$ Geochronology

Eleven samples were chosen for $^{40}Ar/^{39}Ar$ Geochronology based on lack of alteration and the presence of sanidine and plagioclase. These samples are: LV-RD-005, LV-RD-008, LV-RD-009, LV-MR-001, LV-MR-004, LV-MR-005, LV-MR-008, LV-HCF-002, LV-HCF-005, LV-HCF-006, and LV-DM-001. Crushed samples were sieved using a series of 1700 µm, 800 µm, 700 µm, 600 µm, 500 µm, 425 µm, 420µm, and 250 µm sieves. 1700 µm sieves were used to remove coarse rock chips while smaller sieve sizes obtain finer crystal populations. LV-RD-005 plagioclase crystals were picked from 600 - 425 µm. LV-RD-008 plagioclase crystals were picked from 425 - 250 µm. LV-RD-009 plagioclase crystals were picked from 700 - 600 µm. LV-MR-001, LV-MR-004, and LV-MR-005 sanidine crystals were picked from 800 - 500 µm. LV-MR-008 sanidine crystals were picked from 800 - 420 µm. LV-HCF-002 sanidine crystals were picked from 600 - 425 µm. LV-HCF-005 and LV-HCF-006 sanidine crystals were picked from 800 - 420 µm. LV-DM-001 sanidine crystals were picked from 1700 - 800 µm. Thirty feldspar crystals were picked from each sample. The crystals were then placed in 10 ml of 4% hydrofluoric acid solution for two minutes, rinsed with 30 ml of acetone, and finally put into an ultrasonic bath for the removal of remaining groundmass.

Samples were sent to the U.S. Geological Survey TRIGA reactor in Denver, CO for irradiation. Samples were wrapped in foil and placed inside a fused silica tube measuring 6 mm in diameter. Fluence monitors were placed together with samples every 5 to 10 mm along the tube. The fluence monitor used was Fish Canyon Tuff FC-2 sanidine, with an age of 28.02 ± 0.16 Ma (Spell and McDougall, 2003). K-glass and optical grade CaF were also included within the silica tubes to monitor argon interference from K and Ca. Loaded silica tubes were then packed inside an Al container and placed inside a Cd Lined In-Core Irradiation Tube (CLICIT) and then irradiated for one hour inside the 1 MW TRIGA reactor.

The irradiated samples were analyzed in the Nevada Isotope Geochronology laboratory using the laser fusion method. Each sample were placed in Cu sample tray by placing a single crystal in each well. In some instances, crystals were too small or discovered to be plagioclase which greatly reduced the yield of ^{40}Ar. Thus, when necessary, multiple crystals were placed in single wells to obtain a higher yield of sample gas (LV-RD-008, LV-RD-009, LV-HCF-006, and LV-MR-004 samples utilized multiple crystal fusions). Crystals were fused for one minute using a 20 W CO_2 laser to approximately 1600°C. Gasses were removed by three GP-50 SAES getters and then transferred to a MAP 251-50 mass spectrometer. Relative volumes of the laser section of the extraction line and mass spectrometer allow for approximately 80% of the gas to be analyzed when using laser fusion. Peak intensities were measured using a Balzers electron multiplier over seven cycles. Linear regression of the seven measurements cycles were used to calculate initial peak intensities for ^{36}Ar, ^{37}Ar, ^{38}Ar, ^{39}Ar, and ^{40}Ar.

Mass spectrometer discrimination was obtained by analyzing atmospheric argon and blanks. A discrimination correction for measured sample isotope ratios was applied after measuring atmospheric $^{40}Ar/^{36}Ar$ ratios. For samples LV-MR-001, LV-MR-005, and LV-HCF-

006 the following discrimination correction was applied (all 1-sigma uncertainties): = 1.0669 ± 0.27%. For samples LV-HCF-002, LV-HCF-005, LV-RD-005, and LV-RD-009 the following discrimination correction was applied 1.0737 ± 0.10. For samples LV-HCF-005, LV-MR-004, LV-MR-008, and LV-RD-008 the following discrimination correction was applied: 1.0835 ± 0.30. Blanks were measured approximately every hour and average as follows: ^{40}Ar = 2.414 mv, ^{39}Ar = 0.080 mv, ^{38}Ar = 0.030 mv, ^{37}Ar = 0.026 mv, ^{36}Ar = 0.016 mv.

Operation of the CO_2 laser, sample stage, and mass spectrometer, as well as data reduction and age calculations, were done using LabSPEC software. Isochron regression and weighted mean plots were done using Isoplot software. Reliable ages were determined for each sample by calculating a mean age and standard deviation for each data set. Mean ages for each data set were further refined by removing anomalous analyses (≥2-sigma uncertainty). Anomalous analysis were caused by fusion of small crystals and plagioclase, greatly reducing the yield of ^{40}Ar.

After removing 2-sigma outliers, a weighted mean and isochron age was calculated for each data set. Weighted mean and isochron ages were evaluated for each refined data set using the mean square of weighted deviates (MSWD). MSWD analysis evaluates the statistical goodness of fit for a data set. If a weighted mean or isochron does not meet MSWD criteria (Wendt and Carl, 1991) for a specific number of data points, then it is not statistically valid. For both the weighted mean and isochron, data points were plotted with MSWD residuals and replotted with outliers removed to satisfy MSWD criteria. However, a weighted mean calculated from laser fusion analyses is referred to as an apparent age as they assume atmospheric initial argon ($^{40}Ar/^{36}Ar$ = 295.5). If actual initial argon $^{40}Ar/^{36}Ar$ exceeds the atmospheric value this will cause ages to be overestimated. Thus, isochron ages are considered more desirable. In

addition to MSWD criteria an isochron is considered statistically valid when the minimum number of points that define a best fit line is 4. A good isochron age is not only defined by these parameters but also by the degree to which the data set is dispersed along the calculated line. When data is spread along this line it better constrains atmospheric and radiogenic intercepts and thus reduces uncertainties (McDougall and Harrison, 1999). All $^{40}Ar/^{39}Ar$ ages are quoted at 1 sigma analytical uncertainty.

3.4 Petrography

Each eruptive unit was examined in hand sample and thin section for petrographic descriptions. Examination of hand samples produced initial observations of crystal assemblages and relative abundances of minerals. Thin section analysis allowed for the identification of major and accessory mineral phases as well as crystal textures. Point counts provided further determination of abundances by distinguishing proportions of crystals and groundmass and the modal abundances of each mineral phase. Exactly 600 points were counted on each thin section.

3.5 EPMA

Thin sections selected for EPMA analysis were chosen based on the presence of representative crystal assemblages, textures, and lack of alteration. Samples were prepared as previously described by polishing and coating with carbon for use on the JEOL JXA-8900 probe at the UNLV Electron Microanalysis and Imaging Laboratory (EMIL) and the JEOL JXA-8530F probe at the Southeastern North Carolina Regional Microanalytical and Imaging Consortium (SENCR-MIC) at Fayetteville State University in Fayetteville, North Carolina. The probe was utilized to collect major element data in targeted crystals by obtaining point analyses along transects and individual spots in plagioclase, sanidine, biotite, hornblende and pyroxene.

Prior to probe analysis, photomicrographs were produced to image and locate targeted crystals on each thin section. Once carbon coated, thin sections were placed in the probe and electron dispersive spectroscopy (EDS) was performed on targeted crystals not thoroughly identified under the petrographic microscope. Following EDS, back scatter electron (BSE) images were produced for each target to analyze textural and chemical changes in each crystal. BSE images are produced by bombarding a target area by scanning a focused electron beam, which rebound scattered electrons off the surface of the sample. The rebounded electrons are recorded by the detectors as a digital signal. The number of electrons reaching the detector is proportional to the mean atomic number of the targeted crystal or sample. Thus, brighter samples correlate with a higher atomic number. With this information, rim to rim and rim to core transects were plotted to decipher relationships between textural and chemical variations in targeted crystals. Once BSE images and transects were set mineral standards were analyzed to ensure the probe was properly calibrated to prevent poor data collection for each element and desirable oxide totals were achieved. Standards used at EMIL were as follows: SM-Anorthoclase, SM-Ilmenite, SM-Cr-Augite, SM-Olivine, Olivine-SM-fa, SM-Microcline, SM-Plagioclase, MAC-fluorite, AP-ilmenite, AP-scapolite, SM-Chromite, and AP-apatite. Standards used at SENCR-MIC were from Astimex block MINM53 and are as follows: 41 – Orthoclase, 2 – Almandine Garnet, 40 – Rutile, 23 – Fluorite, 1 – Albite, 4 – Apatite, 6 – Benitoite, 10 – Bustamite, 45 – Tugtapite, 34 – Olivine, 17 – Chromium Oxide, and 12 – Diposide. Once these steps were completed, individual analysis was performed on points within targeted crystals.

CHAPTER 4

RESULTS

4.1 $^{40}Ar/^{39}Ar$ Geochronology Results

4.1.1 LV-RD-005 Plagioclase

This sample produced 14 single crystal analyses. Ages range from 1.68 Ma to 0.05 Ma with a mean age of 840 ± 53 ka (n=14). MSWD criteria omit 11 of these analyses for a weighted mean age of 411 ± 15 ka (MSWD = 0.067, n = 3). No reliable isochron was defined by these data. Ca/K ratios are consistently high (~9.40) indicating a homogenous plagioclase feldspar population. No reliable age was produced for this sample (Fig. 4.01).

4.1.2 LV-RD-008 Plagioclase

This sample produced 4 multiple crystal analyses. Ages range from 2.05 Ma to 0.78 Ma with a mean age of 1.38 ± 0.56 Ma (n=4). No reliable isochron or weighted mean was produced for this data. Ca/K ratios are consistently high (~7.71) indicating a homogenous plagioclase feldspar population. No reliable age was produced for this sample (Fig. 4.01).

4.1.3 LV-RD-009 Plagioclase

This sample produced 8 multiple crystals analyses. Ages range from 2.63 Ma to 0.12 Ma with a mean age of 1.31 ± 0.79 Ma (n=8). MSWD criteria omit 2 of these analyses for a weighted mean age of 1.09 ± 0.20 Ma (MSWD = 2.2, n = 6). No reliable isochron was produced for this data. Ca/K ratios are consistently high (~5.37) indicating a homogenous plagioclase feldspar population. No reliable age was produced for this sample (Fig. 4.01).

4.1.4 LV-RD-005, LV-RD-008, LV-RD-009 Combined Plagioclase

When all 14 single crystal analyses and 12 multiple crystal analyses from the 3 samples are combined, Resurgent Dome samples produced an age range from 2.63 Ma to 0.05 Ma with a

mean age of 1.07 ± 0.65 Ma (n=26). MSWD criteria omit 23 analyses and yield a weighted mean age of 411 ± 15 ka. (MSWD = 0.067, n = 3). Combined Resurgent Dome plagioclase analyses did not produce a reliable isochron. Ca/K ratios are consistently high indicating a homogenous plagioclase feldspar population. No reliable age was produced for these combined analyses, thus no reliable age was obtained for the Resurgent Dome rhyolite (Fig. 4.01).

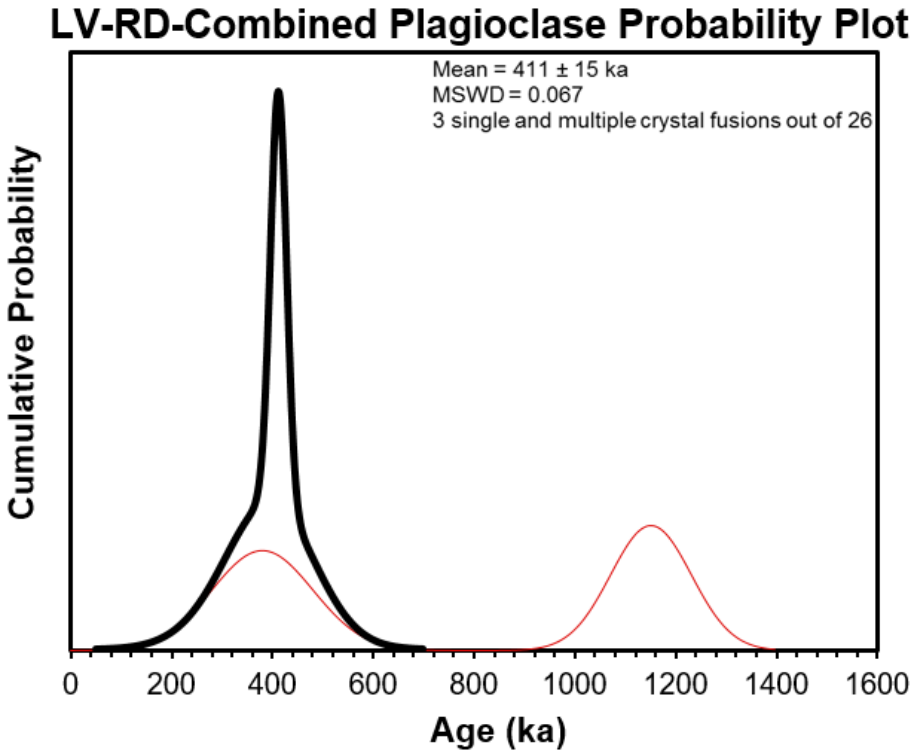

Figure 4.01. Cumulative Probability plot of combined Resurgent Dome plagioclase age data. Red line indicates relative probability of ages before MSWD analysis. Black line indicates cumulative probability of ages deemed acceptable after MSWD analysis.

4.1.5 LV-MR-008 Sanidine

This sample produced 30 single crystal analyses. Ages range from 573 ka to 499 ka with a mean age of 536 ± 19 ka (n=30). MSWD criteria omit 7 of these analyses for a weighted mean age of 534 ± 2 ka (MSWD = 1.5, n = 23). A statistically valid isochron is defined by 17 points for an age of 525 ± 2 ka (MSWD = 0.71) (Fig. 4.02). The initial $^{40}Ar/^{36}Ar$ ratio is 302 ± 1, indicating a small amount of excess argon is present in analyzed crystals. Ca/K ratios are

consistently low (~ 0.030) and coincide with a homogenous alkali feldspar population. The isochron age should be considered most reliable for this sample.

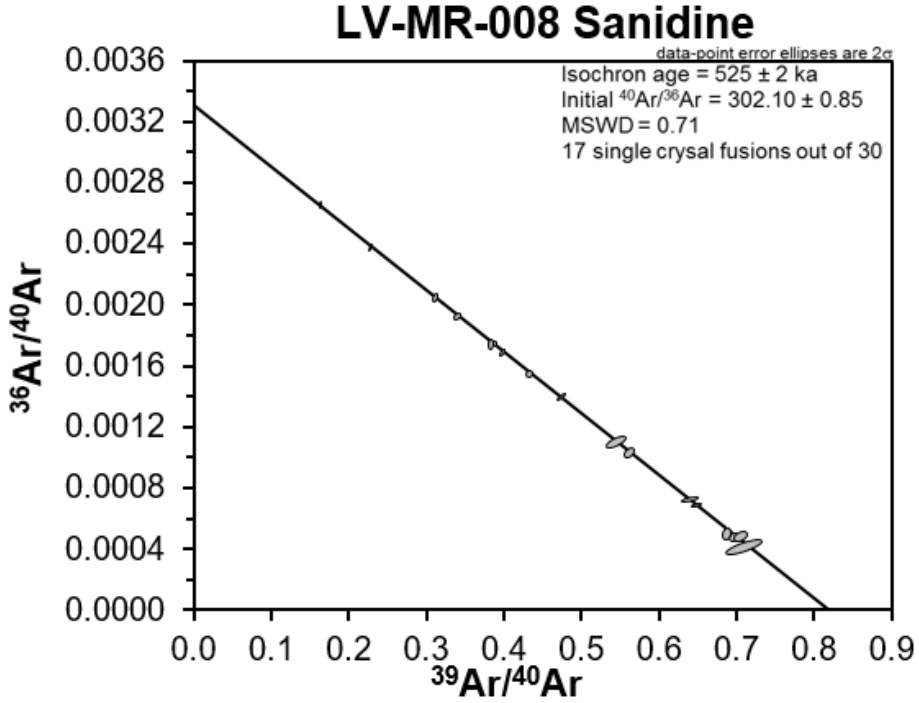

Figure 4.02. Isochron plot for LV-MR-008 Sanidine.

4.1.6 LV-MR-005 Sanidine

This sample produced 20 single crystal analyses. Ages range from 374 ka to 326 ka with a mean age of 348 ± 15 ka (n=18). MSWD criteria omit 5 of these analyses for a weighted mean age of 343 ± 3 ka (MSWD = 1.6, n = 15). A statistically valid isochron is defined by 8 points for an isochron age of 333 ± 4 ka (MSWD = 2.1) (Fig. 4.03). The initial $^{40}Ar/^{36}Ar$ ratio of 310 ± 13 does not indicate the presence of excess argon but suggests inherited non-atmospheric initial argon when considering high uncertainty. Ca/K ratios are consistently low (~ 0.13) and coincide

with a homogenous alkali feldspar population. The isochron age should be considered most reliable for this sample due to the presence of excess argon.

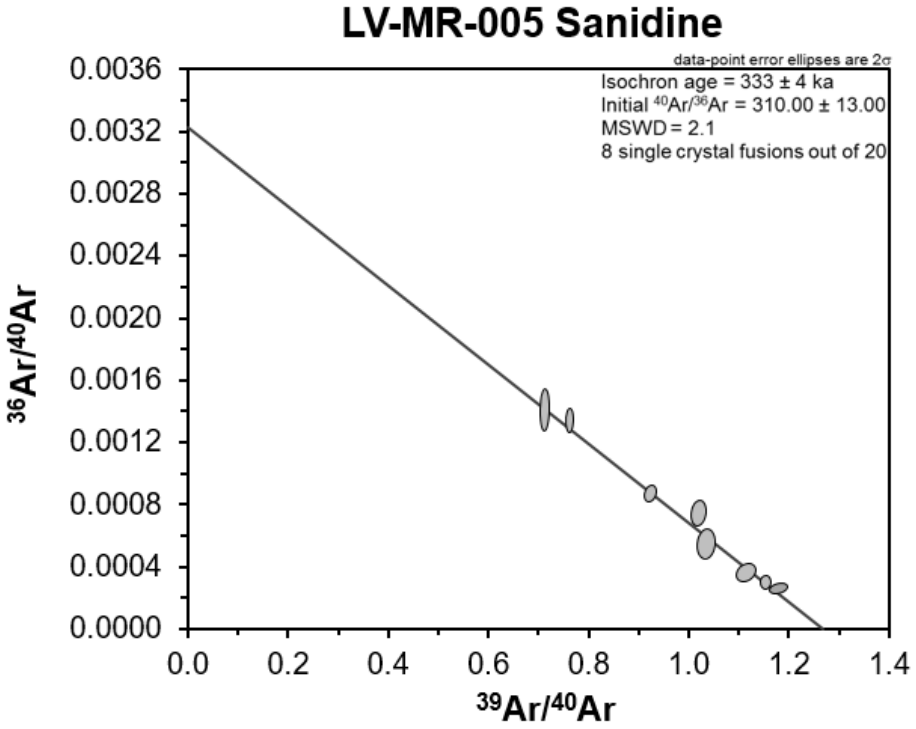

Figure 4.03. Isochron plot for LV-MR-005 Sanidine.

4.1.7 LV-HCF-002 Sanidine

This sample produced 17 single crystal analyses. Ages range from 389 ka to 243 ka with a mean age of 320 ± 39 ka (n=17). MSWD criteria omit 1 analysis for a weighted mean age of 320 ± 7 ka (MSWD = 1.7, n = 16). A statistically valid isochron is defined by 9 points for an isochron age of 312 ± 7 ka (MSWD = 1.7) (Fig. 4.04). The initial $^{40}Ar/^{36}Ar$ ratio of 299 ± 4 indicates that no excess argon is present. Ca/K ratios are consistently low (~0.10) and coincide with a homogenous alkali feldspar population. When considering uncertainty, mean, weighted

mean, and isochron ages are indistinguishable, however the isochron should be considered the most reliable.

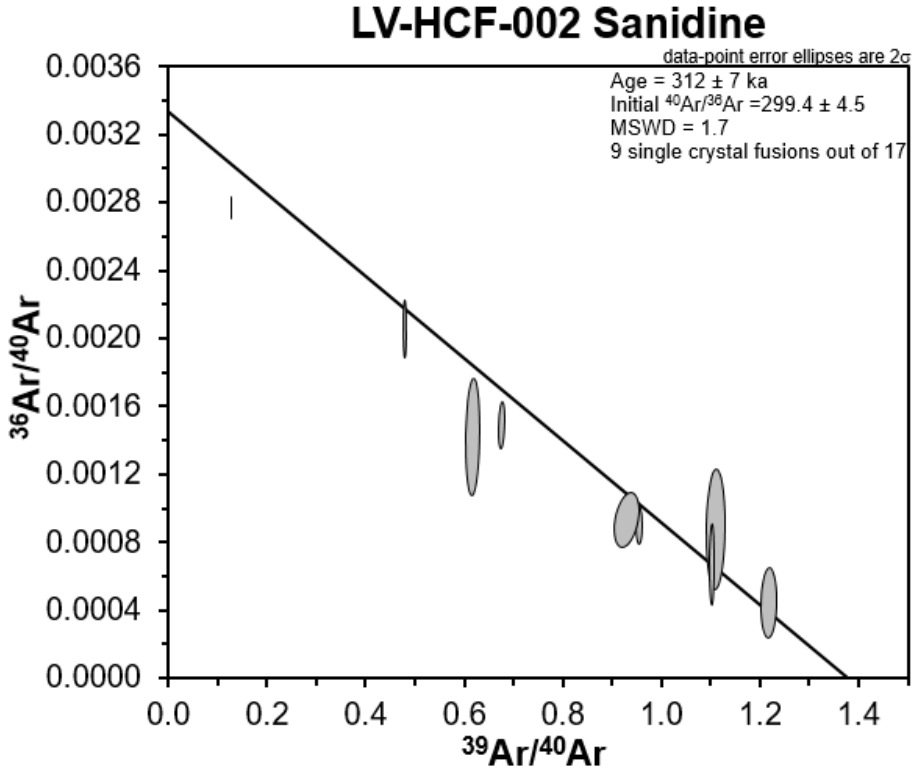

Figure 4.04. Isochron plot for LV-HCF-002 Sanidine.

4.1.8 LV-HCF-005 Sanidine

This sample produced 24 single crystal analyses. Ages range from 599 ka to 185 ka with a mean age of 377 ± 121 ka (n=24) (Fig 4.05). MSWD criteria omit 14 of these analyses for a weighted mean age of 297 ± 7 ka (MSWD = 2, n = 10). A statistically valid isochron is defined by 5 points for an isochron age of 331 ± 6 ka (MSWD = 2.1). The initial $^{40}Ar/^{36}Ar$ ratio of 291 ± 2 indicating loss of argon. Ca/K ratios are consistently low (~0.31) which coincide with a homogenous alkali feldspar population. The weighted mean age should be considered the most reliable for this sample due to high uncertainty of the isochron.

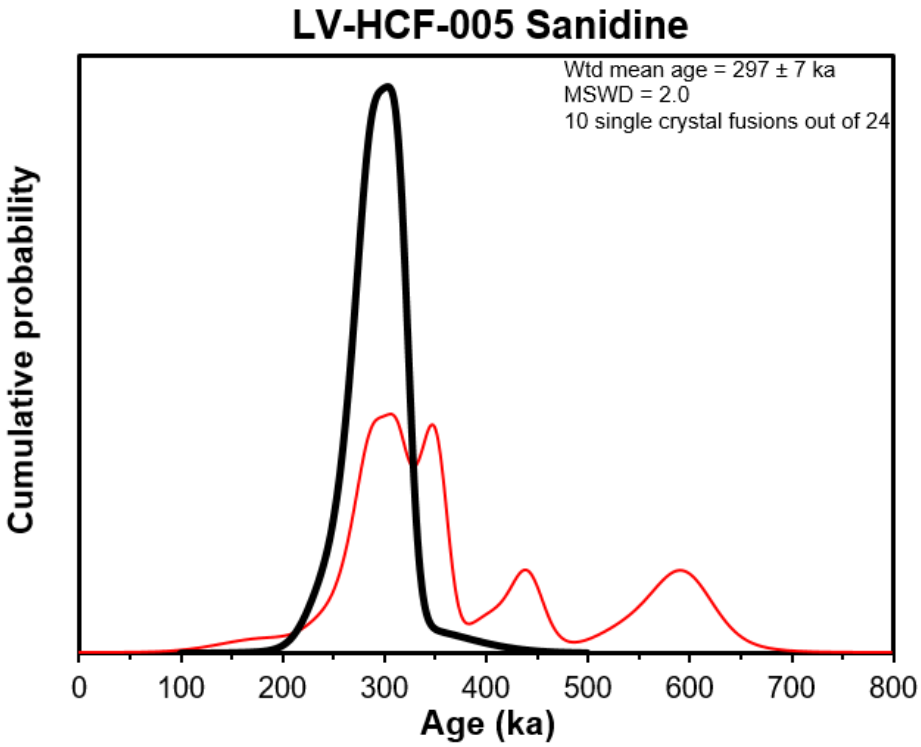

Figure 4.05. Cumulative probability plot for LV-HCF-005 Sanidine. Red line indicates relative probability of ages before MSWD analysis. Black line indicates cumulative probability of ages deemed acceptable after MSWD analysis.

4.1.9 LV-HCF-006 Sanidine

This sampled produced 20 multiple crystal analyses. Ages range from 456 ka to 284 ka with a mean age of 342 ± 57 ka (n=20). MSWD criteria omit 6 of these analyses for a weighted mean age of 305 ± 4 ka (MSWD = 1.2, n = 14). A statistically valid isochron is defined by 14 points for an isochron age of 295 ± 3 ka (MSWD = 1.8) (Fig. 4.06). The initial $^{40}Ar/^{36}Ar$ ratio of 299 ± 1 indicates a small amount of excess argon present in the crystals analyzed. Ca/K ratios are consistently low (~0.30) indicating a population of homogenous alkali feldspars. The isochron age should be considered the most reliable for this sample due to the presence of excess argon.

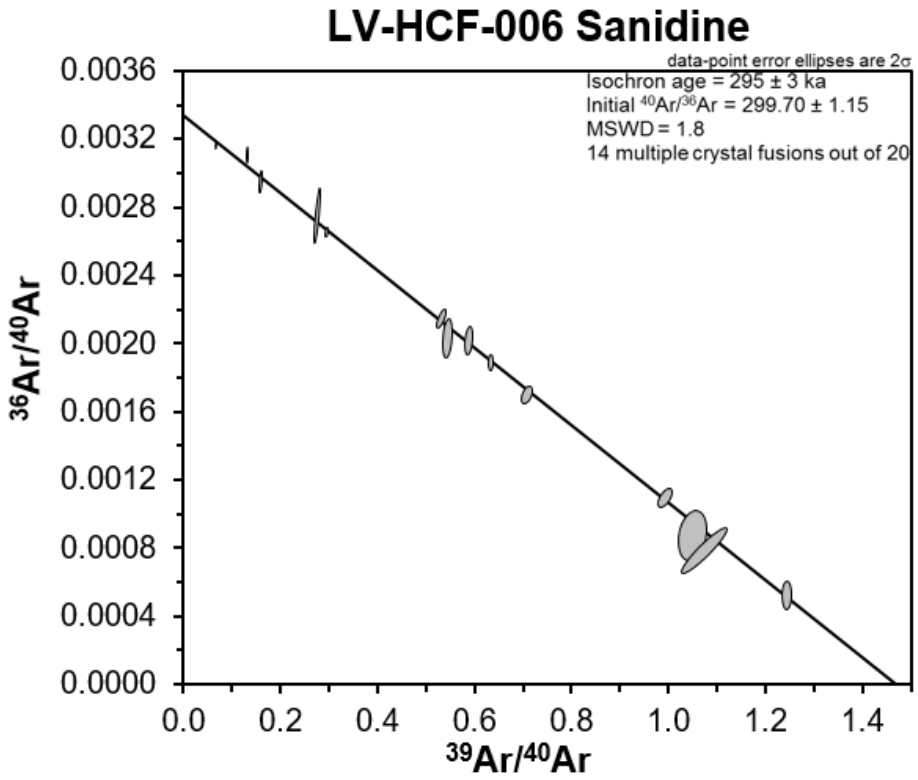

Figure 4.06. Isochron plot for LV-HCF-006 Sanidine.

4.1.10 LV-MR-004 Sanidine

This sample produced 28 single and multiple crystal analyses. Ages range from 144 ka to 98 ka with a mean age of 124 ± 12 ka (n=27). MSWD criteria omit 2 of these analyses for a weighted mean age of 124 ± 2 ka (MSWD = 1.3, n = 26). A statistically valid isochron is defined by 16 points for an isochron age of 118 ± 1 ka (MSWD = 1.6) (Fig. 4.07). The initial $^{40}Ar/^{36}Ar$ ratio of 310 ± 2 indicates the presence of excess argon in the crystals analyzed. Ca/K ratios are

consistently low (~0.035) indicating a population of homogenous alkali feldspars. The isochron age should be considered most reliable for this sample due to the presence of excess argon.

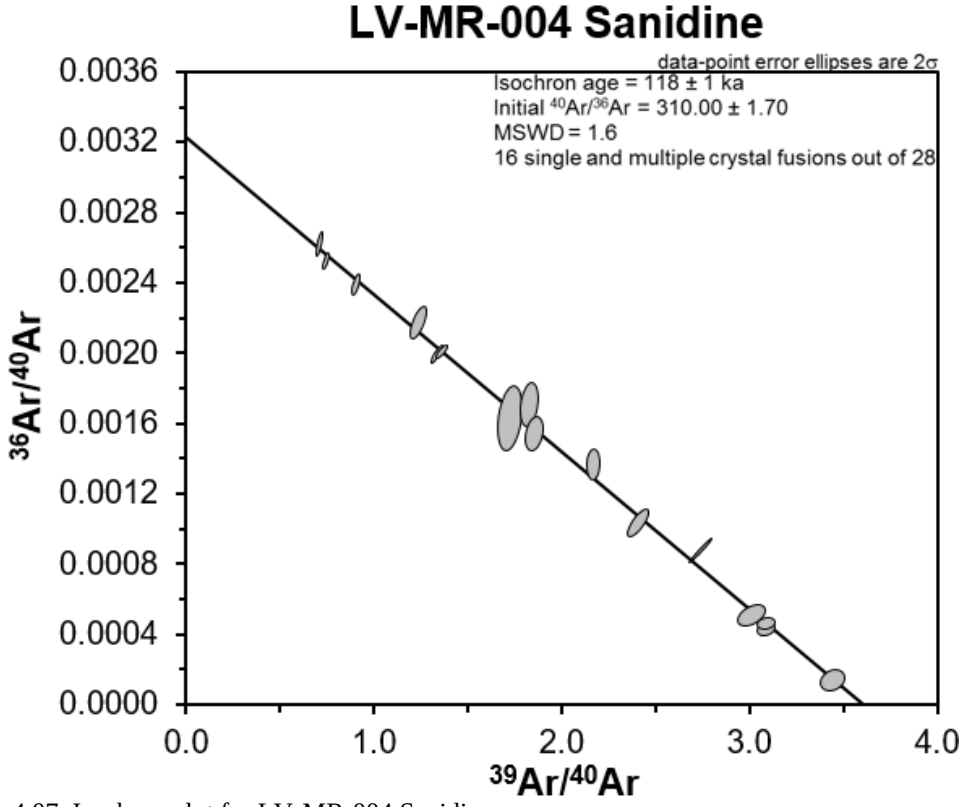

Figure 4.07. Isochron plot for LV-MR-004 Sanidine.

4.1.12 LV-MR-001 Sanidine

This sample produced 11 single crystal analyses. Ages range from 117 ka to 99 ka with a mean age of 109 ± 6 ka (n=11). MSWD criteria retained all 11 analyses for an indistinguishable weighted mean age of 109 ± 3 ka (MSWD = 0.45, n = 11). A statistically valid isochron is defined by 7 points for an isochron age of 94 ± 2 ka (MSWD = 1.8) (Fig. 4.08). The initial $^{40}Ar/^{36}Ar$ ratio of 301 ± 2 indicates the presence of small amount of excess argon in the crystals analyzed. Ca/K ratios are consistently low (~0.040) indicating a population of homogenous alkali feldspars. The isochron age should be considered most reliable for this sample due to the presence of excess argon.

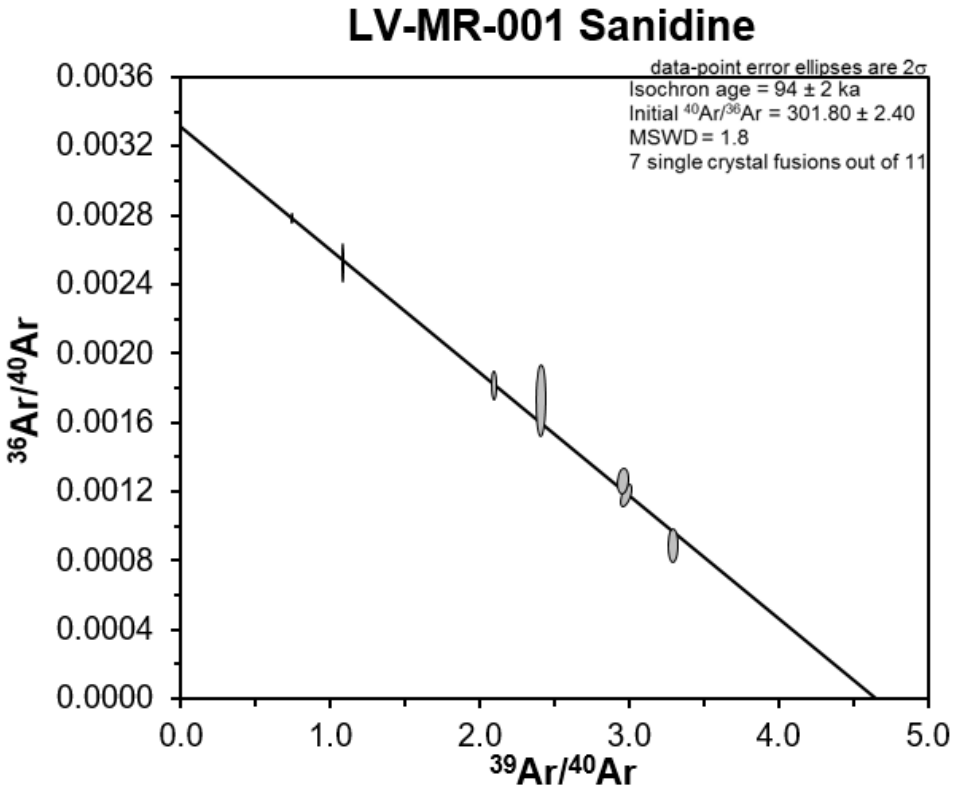

Figure 4.08. Isochron plot for LV-MR-001 Sanidine.

4.1.13 LV-DM-001 Sanidine

This sample produced 28 single crystal analyses. Ages range from 82 ka to 48 ka with a mean age of 67 ± 8 ka (n=26). MSWD criteria omit 2 of these analyses for a weighted mean age of 67 ± 2 ka (MSWD = 1.10, n = 26). A statistically valid isochron is defined by 10 points for an isochron age of 65 ka ± 1 ka (MSWD = 2.0) (Fig. 4.09). The initial $^{40}Ar/^{36}Ar$ ratio of 300 ± 1 indicates the presence of a small amount of excess argon in the samples analyzed. Ca/K ratios are consistently low (~0.030) indicating a population of homogenous alkali feldspars. The isochron age should be considered the most reliable for this sample due to the presence of excess argon.

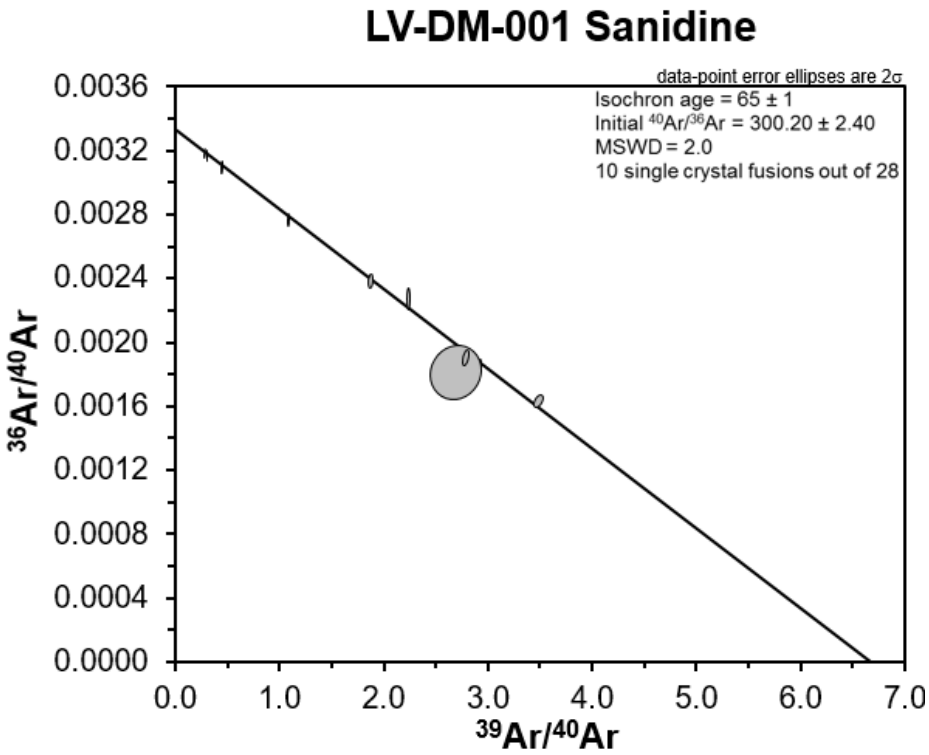

Figure 4.09. Isochron plot for LV-DM-001 Sanidine.

4.2 Petrography Results

4.2.1 Petrography of the Resurgent Dome Rhyolite

Resurgent Dome samples (LV-RD-008 and LV-RD-009) are sparsely porphyritic (2% crystals; Table 4.01) with crystals set in a vitrophyric groundmass. Primary minerals include (in order of decreasing abundance) plagioclase, orthopyroxene, biotite and hornblende with accessory oxides, apatite, and zircon.

Plagioclase within the Resurgent Dome samples ranges in size from approximately 1.98 to 0.24 mm and are euhedral to subhedral. Polysynthetic albite and carlsbad twins are common in plagioclase crystals as is the presence of concentric, oscillatory zonation and inclusions of oxides, apatite, and zircon. Orthopyroxene crystals are predominately glomeroporphyritic clusters (Fig. 4.10) in association with plagioclase crystals. Orthopyroxenes are commonly euhedral to subhedral and range in length from 1.08 to 0.24 mm.

Biotite and amphibole crystals are sparse in the Resurgent Dome. Moreover, hornblende was only observed in LV-RD-009-1A. Biotite crystals are euhedral and range from approximately 1.74 to 0.33 mm. Amphibole is considerably larger (1.92 mm) and euhedral. Both phases contain inclusions of oxides.

4.2.2 Petrography of the Moat Rhyolite

The Moat rhyolites are subdivided into three units (Qmr_1, Qmr_2, and Qmr_3) based on the map of Bailey (1989). All Moat rhyolites are porphyritic (12-23% crystals; Table 4.01) with a pumiceous groundmass. Mineral assemblages common to all Moat rhyolite units are sanidine, plagioclase, biotite, quartz, and amphibole with accessory oxides and apatite. In each unit sanidine and plagioclase are dominant mineral phases (Table. 4.01).

LV-MR-008 (Qmr_1)

LV-MR-008 (as well as LV-MR-005) is the most sparsely porphyritic Moat rhyolite unit with only 12% crystals (Table 4.01). Plagioclase crystals range from approximately 4.14 to 0.24 mm and display a wide array of textures. Plagioclase crystals are euhedral to subhedral with inclusions of oxides, biotite, zircon, and apatite. Concentric zoning and carlsbad, polysynthetic albite, and pericline twinning are common to most plagioclase populations. In one LV-MR-008 plagioclase crystal, inclusions coincide with zoning and distinct core and rim overgrowths (Fig. 4.10). Plagioclase form as individual phenocrysts but in some instances form as glomerocrysts or as inclusions in resorbed sanidines. Dissolution features are common in plagioclase populations and are often present as sieved or resorbed cores with clear rim overgrowths. In one instance a twinned plagioclase containing inclusions of euhedral biotite and plagioclase displays a sieved core with a distinct rim overgrowth.

Sanidine crystals are in similar size (5.64 to 0.42 mm) and morphology (euhedral to subhedral) to plagioclase crystals. Crystals contain inclusions of biotite, zircon, oxides, and less commonly plagioclase. Sanidine phenocrysts are present as aggregates but more often appear as individual crystals. Dissolution features are less common in sanidine crystals, however slightly embayed margins are observed in subhedral sanidines.

Biotite crystals are smaller (1.74 to 0.12 mm) and are euhedral to slightly subhedral. While biotite form as individual phenocrysts they are often found as inclusions in plagioclase and sanidine; biotite is sometimes intergrown between fractures within plagioclase. In some cases, biotite crystals contain oxides as inclusions. Quartz crystals have a similar size range (1.02 to 0.36 mm) and are subhedral to anhedral in shape. Hornblende, which are approximately 1.02 to 0.18 mm in length and is present as euhedral to subhedral crystals. Simple twins and oxide inclusions are sometimes observed in hornblende phenocrysts.

LV-MR-005 (Qmr_2)

LV-MR-005 is also sparsely porphyritic with only 12% crystals (Table 4.01). Plagioclase and sanidine are dominant phases within this unit and are similar in size and morphology; plagioclase crystals range from 3.24 to 0.21 mm and sanidine crystals range from 3.18 to 0.33 mm. Plagioclase crystals are euhedral to subhedral and contain carlsbad, polysynthetic albite, and pericline twinning. Concentric zoning is typical in most plagioclase crystals as is the presence of biotite, oxide, and apatite inclusions. One LV-MR-005 plagioclase crystal contains a strongly zoned core, middle growth band, and distinct rim overgrowth coinciding with a dissolution surfaces (Fig. 4.10). Other common dissolution features occur in the form of slightly resorbed margins. Sanidine crystals are euhedral to subhedral with inclusions of biotite and

oxides and occasional carlsbad twinning. While resorption features are uncommon in sanidine populations, rare instances of rim embayment are observed in subhedral sanidine crystals.

Biotite crystals are smaller (1.92 to 0.18 mm) and range in shape from euhedral to slightly subhedral and contain inclusions of oxides. They are generally present as individual crystals and are also commonly found as inclusions in plagioclase, sanidine, and quartz and rarely occur as aggregates in association with other biotite. Associated quartz crystals are subhedral to anhedral (1.11 to 0.33 mm) with strong resorption and embayment of rims.

Hornblende is the least abundant phase within LV-MR-005. These crystals range from 1.98 to 0.25 mm, are euhedral to subhedral, and contain oxide inclusions. Euhedral hornblende form as individual phenocrysts but sometimes form as crystal aggregates with other subhedral amphibole.

LV-MR-004 and LV-MR-001(Qmr_3)

LV-MR-004 and LV-MR-001 contain the highest abundance of crystals (23% and 18% respectively; Table 4.01) of all Moat rhyolite units. Sanidine crystals are the dominant phase within this unit (Table 4.01) and are euhedral to slightly anhedral with inclusions of oxides, biotite, apatite, and less often plagioclase. In some instances biotite has grown along fractures in sanidines. Crystal sizes range in length from approximately 4.44 to 0.18 mm. Crystals commonly form individually but some sanidine are present as glomerocrysts with plagioclase and biotite. Moderate to intense rim resorption is observed in subhedral to anhedral crystals, while euhedral crystals do not show any indication of dissolution. Additionally, subhedral crystals sometimes show instances of weak concentric zoning and carlsbad twinning which are absent in euhedral populations.

The morphology of plagioclase phenocrysts (5.82 to 0.25 mm) in this unit range from euhedral to slightly anhedral. These crystals commonly contain inclusions of biotite, oxides, and zircon and display carlsbad and polysynthetic-albite twinning. Plagioclase is present as individual crystals but also as glomerocrysts with sanidine, biotite, and other plagioclase crystals. Plagioclase are present less commonly as inclusions in sanidine. Concentric (sometimes oscillatory) zoning is common in plagioclase crystals. This is observed in a slightly anhedral plagioclase intergrown between sanidine crystals (Fig. 4.10). Plagioclase populations usually contain rim dissolution and intense embayment but also display overgrowths. In one instance, a coarse subhedral LV-MR-001 plagioclase crystal (Fig. 4.10) contains a distinct cellular rim overgrowth. Another example of disequilibrium is displayed in an LV-MR-004 plagioclase (Fig. 4.11) where pervasive resorption has dissolved from rim to core. These characteristics are common in both euhedral and anhedral crystals.

Smaller biotite crystals (3.78 to 0.11 mm; most crystals do not exceed 1 mm) within this unit are euhedral to subhedral and form as individual phenocrysts but are often contained as inclusions in sanidine, plagioclase, quartz. In some instances, euhedral biotite has interstitially grown between plagioclase crystals and glomerocrysts with plagioclase and sanidine. Biotite contain inclusions of oxides. Quartz crystals range in size similar to biotite crystals (2.16 to 0.18 mm) but are often subhedral to anhedral. Quartz crystals sometimes contain oxides and apatite. Heavy resorption and embayment is also observed in quartz populations. Hornblende crystals are smaller than all other crystals (1.00 to 0.66 mm) and are euhedral, show simple twins, and often contain oxide inclusions.

4.2.3 Petrography of the Hot Creek Flow Rhyolite

Hot Creek Flow samples (LV-HCF-002, LV-HCF-005, and LV-HCF-006) are sparsely porphyritic (3-8% crystals; Table 4.01) with a pumiceous groundmass. LV-HCF-002 groundmass has undergone intense silicic alteration. Primary minerals include sanidine, plagioclase, and biotite; accessory minerals include oxides, apatite and zircon.

Sanidine is the dominant feldspar phase within the Hot Creek Flow (Table 4.01). Crystals range in size from 2.28 to 1.05 mm and are commonly euhedral to subhedral, contain inclusions of oxides, and often display simple twins. Plagioclase crystals can be divided into two populations ranging from 4.02 to 0.46 mm. The larger population (towards the larger end of the size range) found in LV-HCF-002-2, are subhedral, display simple twins, and contain sieved or resorbed cores with rim overgrowths as well as oxide and biotite inclusions (Fig. 4.11). Cores often contain concentric zonation that terminates at dissolution surfaces coinciding with rim overgrowths.

Smaller plagioclase crystals are euhedral to subhedral, slightly embayed, and sometimes form as glomeroporphyritic aggregates (observed in LV-HCF-005-1, LV-HCF-005-2, LV-HCF-006-1) with biotite crystals. Subhedral crystals are found in glomerocrysts. Carlsbad and polysynthetic albite twinning are common to this assemblage along with the occurrence of minor pericline twinning. Concentric zonation is strongly visible within this population as is the presence of oxides contained within crystals.

Biotite crystals appear similar in morphology to plagioclase compositions. Subhedral, slightly resorbed crystals are found in glomeroporphyritic clusters while more euhedral crystals have formed individually. Additionally, biotite crystals commonly contain oxide inclusions. One

lamellar LV-HCF-006-1 biotite measures 2.12 mm in length but most crystals are fine grained and average approximately 1 mm.

4.2.4 Petrography of the Deer Mountain Rhyolite

The Deer Mountain rhyolite (LV-DM-001-1) is porphyritic (22% crystals; Table 4.01) with a pumiceous groundmass. Primary minerals include sanidine, plagioclase, and biotite; accessory minerals include hornblende with minor oxides, apatite, and zircon.

Sanidine is the dominant mineral phase within the Deer Mountain rhyolite (Table 4.01). These crystals have a large variation in size ranging from 5.04 to 0.33 mm. The range of morphologies is quite variable, with euhedral to anhedral crystals. Subhedral and anhedral crystals are commonly poikilitic with inclusions of euhedral plagioclase, biotite, oxides, and apatite. Resorption is observed in anhedral sanidine phenocrysts, while subhedral crystals less commonly contain dissolution textures. All varieties of sanidine contain instances of concentric zoning, subtle rim overgrowths, and carlsbad twinning.

Plagioclase crystals of the Deer Mountain are euhedral to subhedral, ranging in length from 3.93 to 0.33 mm, and display similar morphology and size to sanidine populations. Euhedral plagioclase crystals do form as individual crystals, but are more commonly found as inclusions within coarse sanidine. Plagioclase crystal aggregates, associated with sanidine and biotite, are also present (Fig. 4.11). Subhedral plagioclase tends towards the larger end of the size range and contain inclusions of oxides, biotite, and apatite. Carlsbad and polysynthetic albite twinning is observable in both euhedral and subhedral plagioclase crystals; pericline twinning is present within one euhedral crystal. Dissolution features are present in plagioclase phenocrysts and can be observed in one LV-DM-001-1 crystal (Fig. 4.11) with pervasive rim dissolution.

Biotite is a less abundant primary mineral phase within the Deer Mountain. These crystals range in length from 4.23 – 0.24 mm; abundant crystals are less than 2.4 mm and few crystals exceed the upper echelon of this size range. Larger, euhedral biotite crystals contain many inclusions and display ≤ 1 mm rims (Fig. 4.11) visible in cross polarized light. Smaller biotite crystals (≤ 2.44 mm) are euhedral to subhedral (sometimes interstitial) but also contain oxide inclusions. Smaller biotite are commonly present as inclusions within plagioclase and sanidine populations; inclusions occur less commonly within glomerocrysts.

Like biotite, hornblende crystals have a variable size range (1.82 mm to 0.18 mm) but do not commonly exceed 0.94 mm in length. Hornblende crystals are euhedral to subhedral and can display simple twins. They are often found as subhedral inclusions in sanidine or as euhedral clusters with biotite.

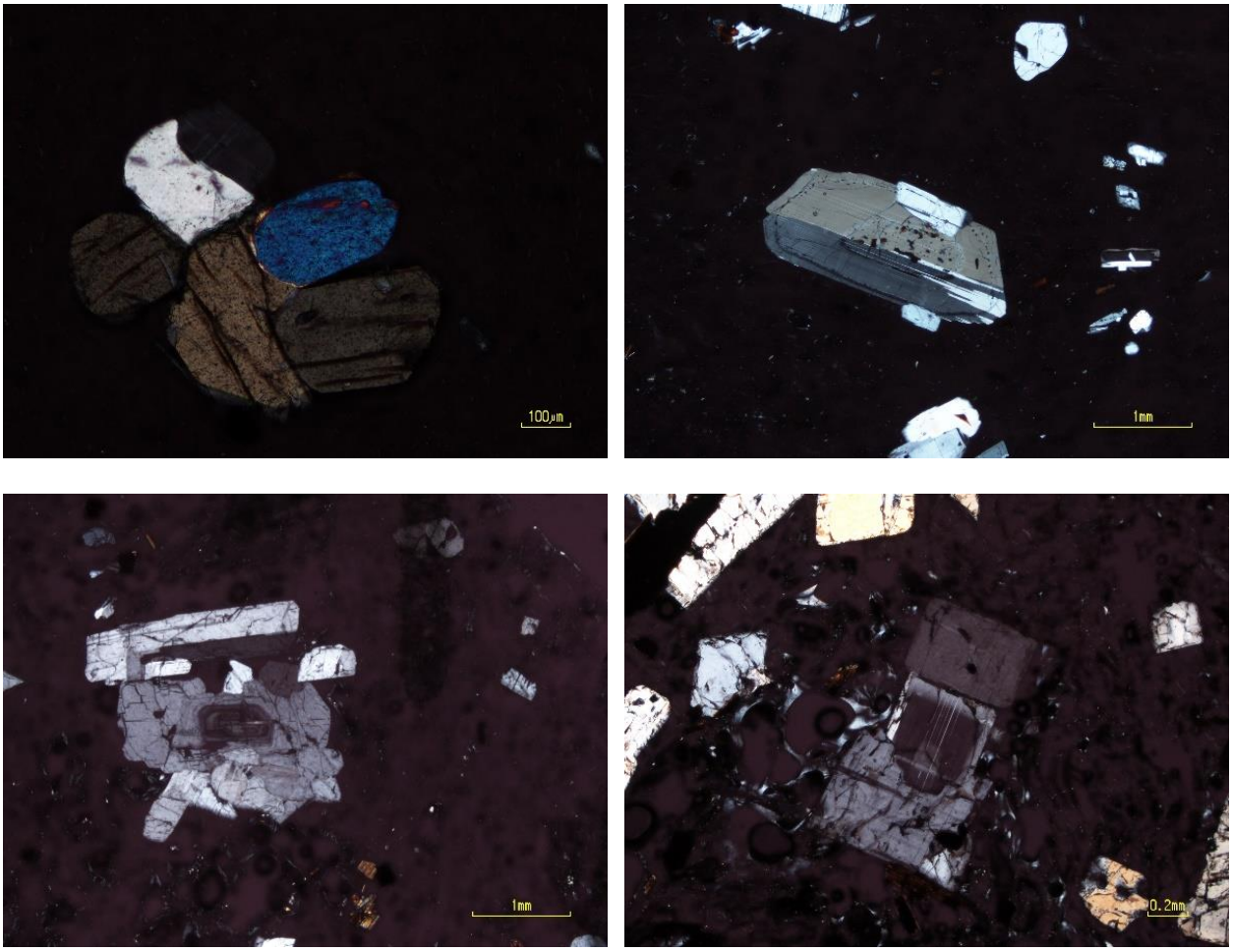

Figure 4.10. Clockwise from Top left. LV-RD-008-2 orthopyroxene and plagioclase glomerocryst in cross polarized light. Top Right – LV-MR-008-1 plagioclase phenocryst with core, rim and growth band separated by inclusions. Bottom right – LV-MR-004-1 oscillatory zoned plagioclase intergrown between subhedral plagioclase and sanidine. LV-MR-005-1 anti-rapakvi plagioclase with strongly zoned core and sanidine rim overgrowth. All photomicrographs were imaged under cross polarized light.

Table 4.01. Modal abundances of crystals and ground mass from post-collapse rhyolites based on point count results.

Sample Name:	LV-RD -008-1	LV-RD -008-2	LV-RD -009-1	LV-RD -009-2	LV-MR -008-1	LV-MR -005-1	LV-HCF -002-1	LV-HCF -005-1	LV-HCF -005-2	LV-HCF -006-1	LV-HCF -006-2	LV-MR -004-1	LV-MR -001-1	LV-DM -001-1
Plagioclase	12	11	10	12	40	28	8	3	2	5	3	33	35	20
Sanidine	0	0	0	0	32	29	12	4	3	7	5	77	52	96
Orthopyroxene	1	0	1	0	0	0	0	0	0	0	0	0	0	0
Amphibole	0	0	0	0	3	4	0	2	0	0	0	1	2	3
Biotite	0	0	0	0	6	8	2	1	1	1	1	14	11	13
Quartz	0	0	0	0	5	5	0	0	0	0	0	9	4	0
Oxides	0	0	0	0	1	0	0	0	0	0	0	4	1	1
Vesicles	0	0	2	3	7	17	46	17	17	10	0	26	32	20
Groundmass	587	589	587	585	506	509	532	575	577	577	591	436	463	447
Total	600	600	600	600	600	600	600	600	600	600	600	600	600	600
Modal Abundance of Crystals														
Plagioclase	92	100	91	100	46	38	36	30	33	38	33	24	33	15
Sanidine	0	0	0	0	37	39	55	40	50	54	56	56	50	72
Orthopyroxene	8	0	9	0	0	0	0	0	0	0	0	0	0	0
Amphibole	0	0	0	0	3	5	0	20	0	0	0	1	2	2
Biotite	0	0	0	0	7	11	9	10	17	8	11	10	10	10
Quartz	0	0	0	0	6	7	0	0	0	0	0	7	4	0
Oxides	0	0	0	0	1	0	0	0	0	0	0	3	1	1
Modal Abundance of Groundmass														
Vesicles	0	0	0	1	1	3	8	3	3	2	0	6	6	4
Groundmass	100	100	100	99	99	97	92	97	97	98	100	94	94	96
Percent Crystals	2	2	2	2	12	12	4	1	1	4	2	23	18	22
Percent Groundmass	98	98	98	98	88	88	96	99	99	96	98	77	82	78

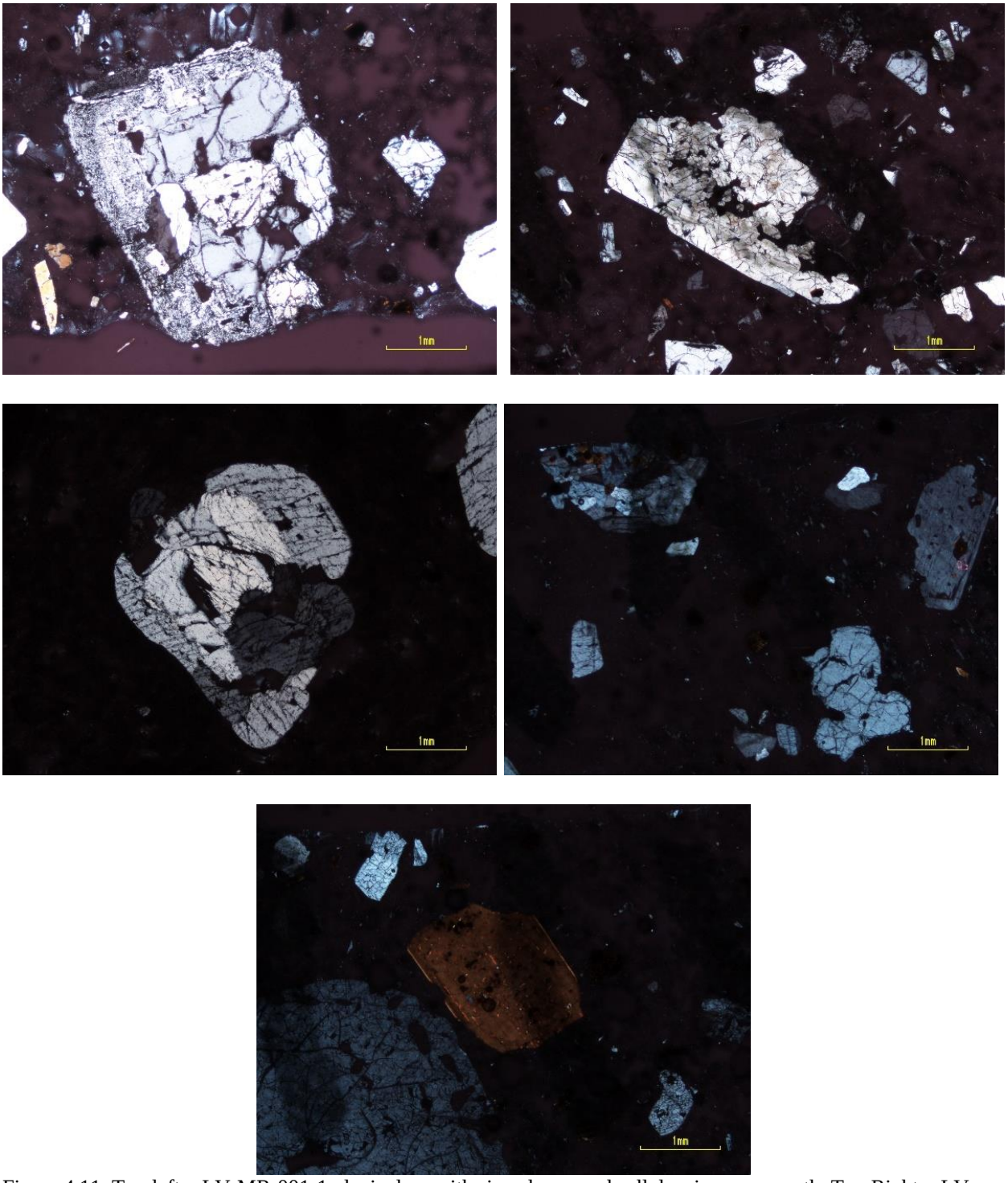

Figure 4.11. Top left – LV-MR-001-1 plagioclase with sieved core and cellular rim overgrowth. Top Right – LV-MR-004-1 plagioclase with pervasive rim dissolution. Middle right - LV-DM-001-1 glomerocryst (upper left) containing sanidine, plagioclase and biotite; LV-DM-01-1 plagioclase (upper right) with embayed rims. Middle left – LV-HCF-002-2 anti-rapakivi plagioclase with sieved core and sanidine rim overgrowth. Bottom – LV-DM-001-1 biotite with oxide inclusions and slight rim overgrowths. All photomicrographs are were imaged under cross-polarized light.

4.3 Electron Probe Micro-Analysis Results

Feldspar phenocrysts were analyzed in samples LV-RD-008, LV-RD-009, LV-MR-001, LV-MR-004, LV-MR-005, LV-MR-008, LV-HCF-002, LV-HCF-005, LV-HCF-006, and LV-DM-001. Crystals with obvious dissolution textures were targeted as well as well-formed euhedral phenocrysts. When feasible, rim to rim transects were performed.

Biotite phenocryst were analyzed in samples LV-RD-008, LV-RD-009, LV-MR-001, LV-MR-004, LV-MR-005, LV-MR-008, LV-HCF-002, LV-HCF-005, LV-HCF-006, and LV-DM-001. Biotite crystals were usually small and mostly suitable for spot analysis rather than transects, but a euhedral biotite was analyzed in LV-DM-001-1. Hornblende phenocrysts were analyzed in samples LV-RD-009, LV-MR-001, LV-MR-004, LV-MR-005, LV-MR-008, and LV-DM-001. Like biotite, hornblende crystals were usually small and point analyses were performed as well as transects. The total weight percent for biotite and hornblende phenocrysts were affected by the presence of volatiles (H_2O). Additionally, LV-MR-001, LV-MR-004, LV-MR-005, LV-MR-008, and LV-DM-001 biotite and amphibole were not analyzed for TiO_2, which affected total weight percent and did not allow for structural recalculation.

Pyroxene phenocrysts were analyzed in samples LV-RD-008 and LV-RD-009. Crystals were often euhedral and rim to rim transects were performed on phenocrysts when possible. Fe-Ti oxides were analyzed in samples LV-RD-008, LV-RD-009, LV-MR-001, LV-MR-004, LV-MR-005, LV-MR-008, LV-HCF-002, LV-HCF-005, LV-HCF-006, and LV-DM-001-1.

4.3.1 EPMA of the Resurgent Dome Rhyolite

Feldspar

Resurgent Dome feldspar populations are composed of large (1.98 to 0.24mm), euhedral plagioclase crystals, which display concentric and often oscillatory zonation in thin section. No

sanidine were present in Resurgent Dome rhyolites. Large plagioclase crystals were preferentially targeted for analysis.

For samples LV-RD-008-1, LV-RD-008-2, LV-RD-009-1, and LV-RD-009-2 normal zonation (An-rich core with An-poor rim) was found in all plagioclase transects (Fig. 4.12). However, most core and rim compositions of plagioclase are almost indistinguishable. Core compositions generally plot within the andesine field ($An_{50} - An_{30}$), whereas rim compositions tend towards andesine-oligoclase compositional boundary (An_{30}) (Fig. 4.13). In rare instances, core compositions are considerably more calcium rich than rim compositions. For example, RD-009-1A4 plagioclase core compositions plot as high as An_{53}, but average approximately An_{34} (Fig. 4.14). Similarly, RD-008-2A2 plagioclase core compositions are as high as An_{60} and average approximately An_{42} (Fig. 4.13).

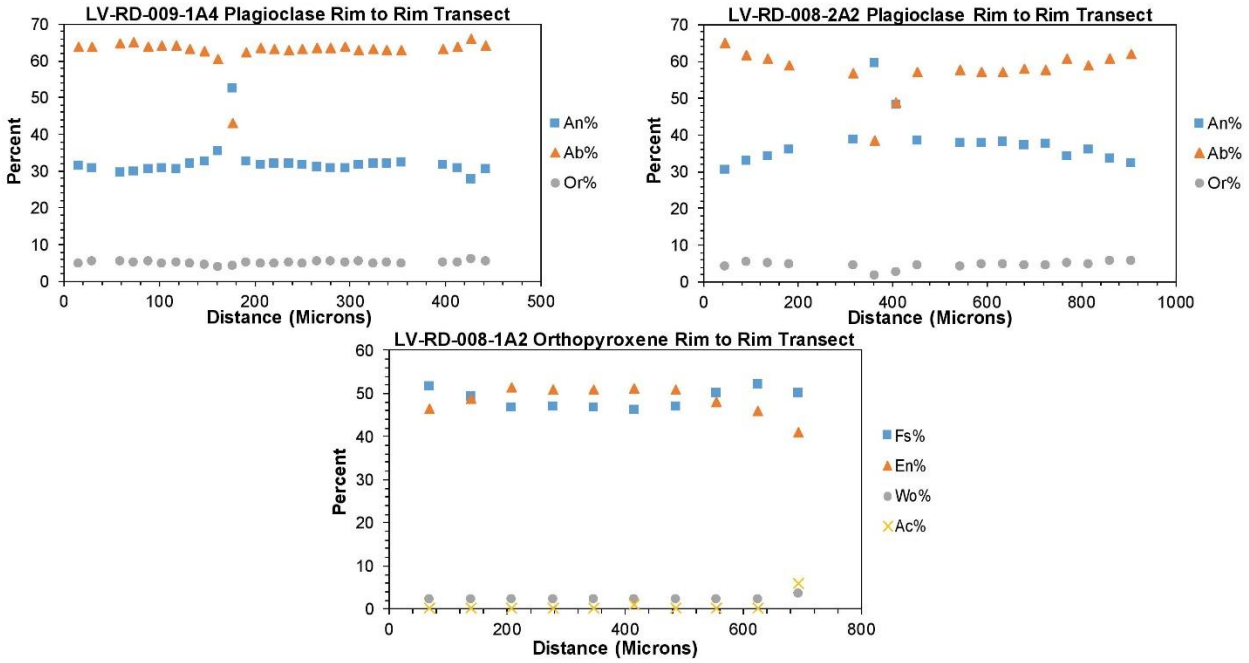

Figure 4.12. EPMA transects of 700 ka Resurgent Dome plagioclase and orthopyroxene.

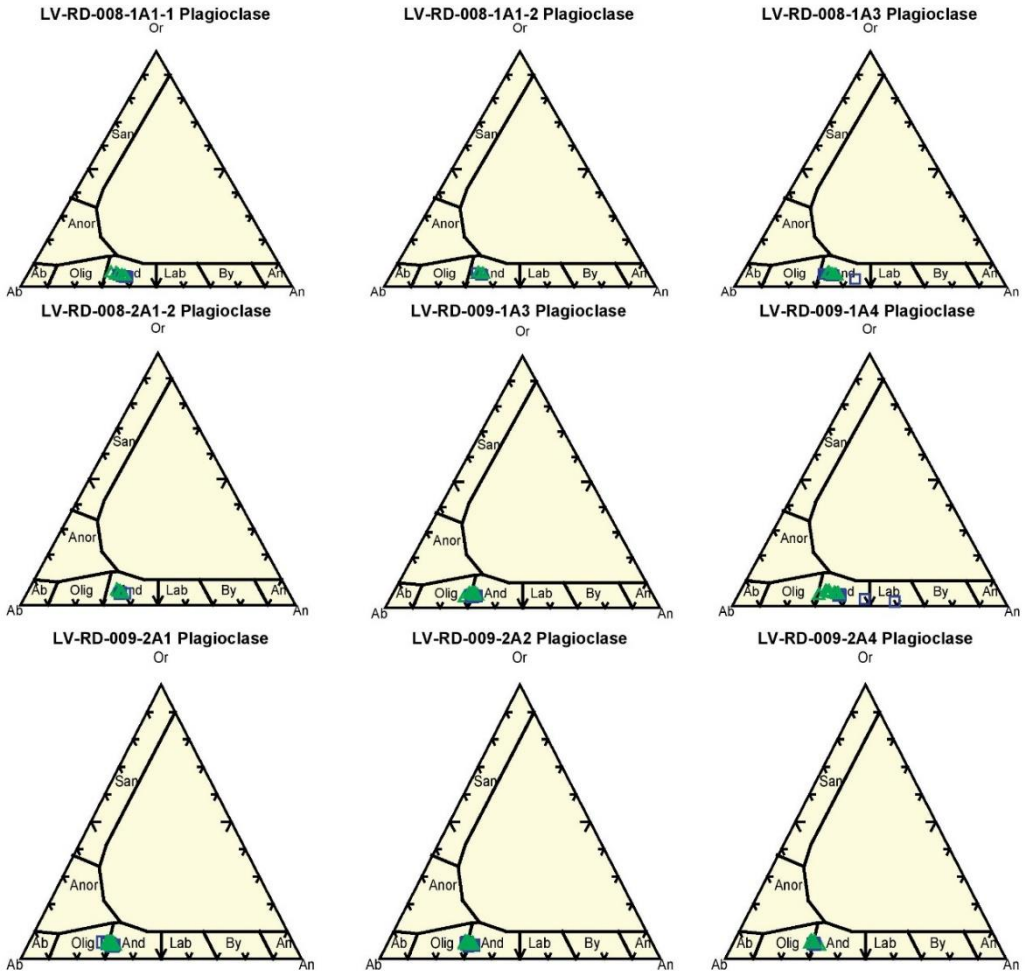

Figure 4.13. Ternary plots of Resurgent Dome plagioclase. Blue squares represent core compositions. Green Triangles represent rim compositions.

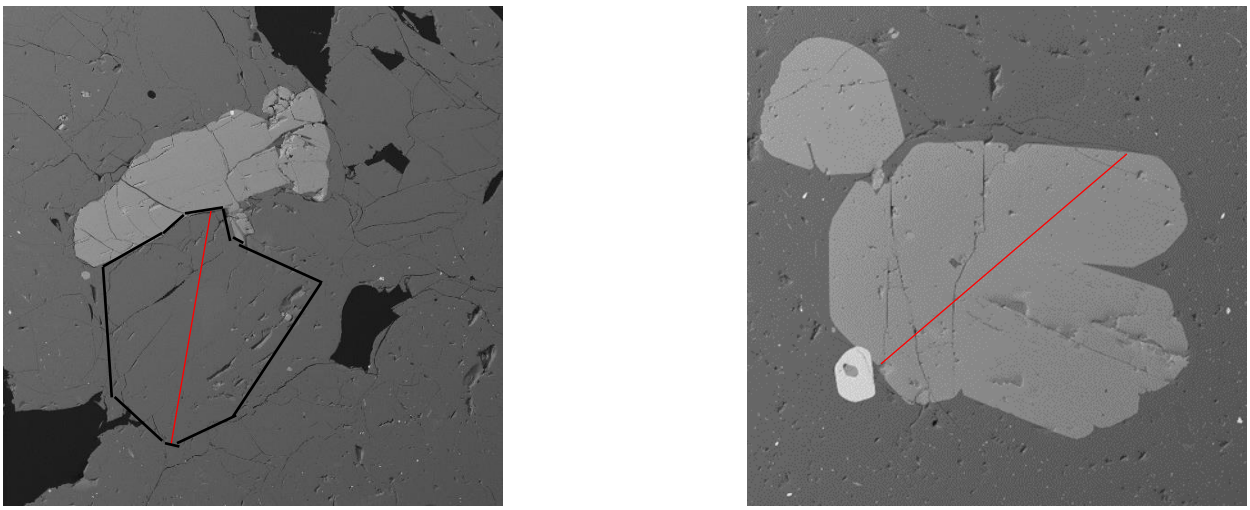

Fig. 4.14. Back scatter electron (BSE) image of LV-RD-009-1A4 plagioclase (left) and LV-RD-008-2A1-1 orthopyroxene. Rim to rim transect highlighted by red lines. Plagioclase outlined by black lines.

Pyroxene

Pyroxene phenocrysts within the Resurgent Dome are sparse however, small, euhedral crystals yielded some analyses. Rim to rim transects (Fig. 4.12) were performed on pyroxene phenocrysts, although small crystals inhibited favorable data collection. Like Resurgent Dome plagioclase, pyroxene crystals display weak normal zonation. Unlike plagioclase, zonation was only detected by variations in FeO, MgO, and CaO and not by petrographic methods. Pyroxene phenocrysts generally plot with subequal ferrosillite and enstatite compositions (Fs_{51}, Wo_2). However, rims are more Fe-rich when compared to Mg-rich cores (Fig. 4.13).

4.3.2 EPMA of the Moat Rhyolites

QMR_1

Feldspar

The 525 ka Moat rhyolite unit contains feldspar populations consisting of both plagioclase and sanidine. As discussed in the Petrography chapter, plagioclase phenocrysts are the dominant phase and display euhedral to subhedral morphologies but also exhibit concentric zoning, rim overgrowths, and are resorbed when observed in thin section. Sanidine populations display similar euhedral to subhedral morphologies and show instances of disequilibrium textures such as embayed rims. Rim to rim and core to rim transects were performed on larger plagioclase and sanidine crystals to detect compositional variations coinciding with mineral textures. However, some intensely resorbed textures inhibited favorable data collection.

Examples of both normal and reverse zonation are present in plagioclase populations. One large, euhedral plagioclase, LV-MR-008-1-1, displays two growth bands separated by dissolutions surfaces. At each dissolution surface An content decreases (~An_{23}, ~An_{20}, ~An_{19} from core to rim respectively) (Figs. 4.16 and 4.17). However, at each dissolution surface a

distinct increase in An (An_{22} - An_{26} and An_{17} - An_{21}) occurs before a gradual decrease in An content towards the rim (Figs 4.16 and 4.17). This increase in An content also occurs in a LV-MR-008-1-10 plagioclase (Fig. 4.18), where core compositions consistently plot as oligoclase (~An_{19}) with andesine rims (~An_{38}) (Fig. 4.17).

Sanidine phenocrysts display instances of visible concentric zonation in thin section, however, this is not reflected in the major (CaO, NaO, and K_2O) element compositions. For example, a large euhedral sanidine, LV-MR-008-1-2, displays consistent potassium content of approximately Or_{64} through the entire rim to rim transect (Fig. 4.17).

Biotite

Core to rim transects were performed on biotite phenocrysts although most biotite were too small in size (≥0.25 mm) or mineral surfaces were unfavorable to data collection. The only biotite phenocryst analyzed within LV-MR-008 providing reliable data displays weak reverse zonation. This crystal displays a slight decrease in FeO (~21% - 19%) composition and increase in MgO (~9% - 10%) from core to rim (Fig. 4.17).

QMR_2

Feldspar

Feldspar populations from the 333 ka Moat rhyolite unit are predominantly plagioclase with subordinate sanidine. Both phases contain large, euhedral phenocrysts with instances of concentric zonation observable in thin section. Additionally, sanidine and plagioclase phenocrysts display instances of dissolution in the form of resorbed, irregular margins. Rim overgrowths are also apparent in plagioclase populations. Rim to rim and core to rim transects were performed on both feldspar populations. However, some intensely resorbed textures inhibited data collection.

Plagioclase phenocrysts display normal zonation but in some instances are lacking any chemical variation (Figs. 4.19 and 4.20). For example, LV-MR-005-1-5 plagioclase contains core compositions as high as An_{23} and rim compositions from An_{19-18} but one LV-MR-005-1-2 plagioclase contains nearly indistinguishable core and rim compositions of An_{20} and An_{20-19} respectively (Fig. 4.20). Sanidine phenocrysts similarly lack chemical variations with approximately Or_{67} through the entire rim to rim transect. Conversely, one LV-MR-005-1-3 (Fig. 4.21) plagioclase phenocryst displays normal zoning with a distinct core and rim compositional gap occurring at a dissolution surface. Plagioclase core compositions transition from labradorite to andesine (An_{56} - $An_{42)}$ over approximately 300 µm, followed by a sharp decreases from andesine to oligoclase compositions (An_{31} - $An_{15)}$ through the next 300 µm (Figs. 4.19 and 4.20). Subsequent rim compositions plot as sanidine (~Or_{67}) indicating anti-rapakivi texture (Figs. 4.19 and 4.20).

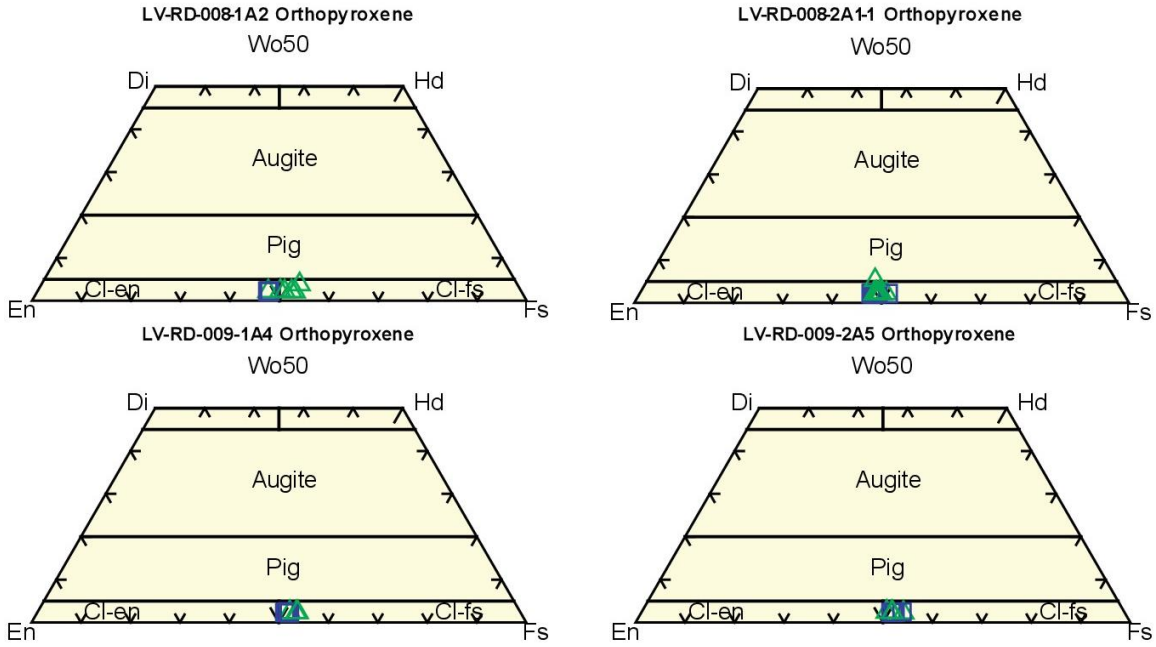

Figure 4.15. Ternary plots of Resurgent Dome orthopyroxene. Blue squares represent core compositions. Green Triangles represent rim compositions.

Amphibole

Amphibole are the least abundant mineral phase within QMR_2 and are smaller in size than feldspar populations. These phenocrysts are euhedral to subhedral. Additionally, BSE images obtained with the electron microprobe revealed core-rim zonation features not observable with petrographic microscope techniques.

All amphibole phenocrysts display the same core-rim normal zonation. Core compositions are variable but generally have MgO compositions of ~14-13% and FeO compositions of ~11-13% (Fig. 4.17). In LV-MR-005-1-1, LV-MR-005-1-1-2, and LV-MR-005-1-2-2 FeO content steadily increases to rim compositions of ~17% while MgO decreases to ~11% (Fig. 4.19).

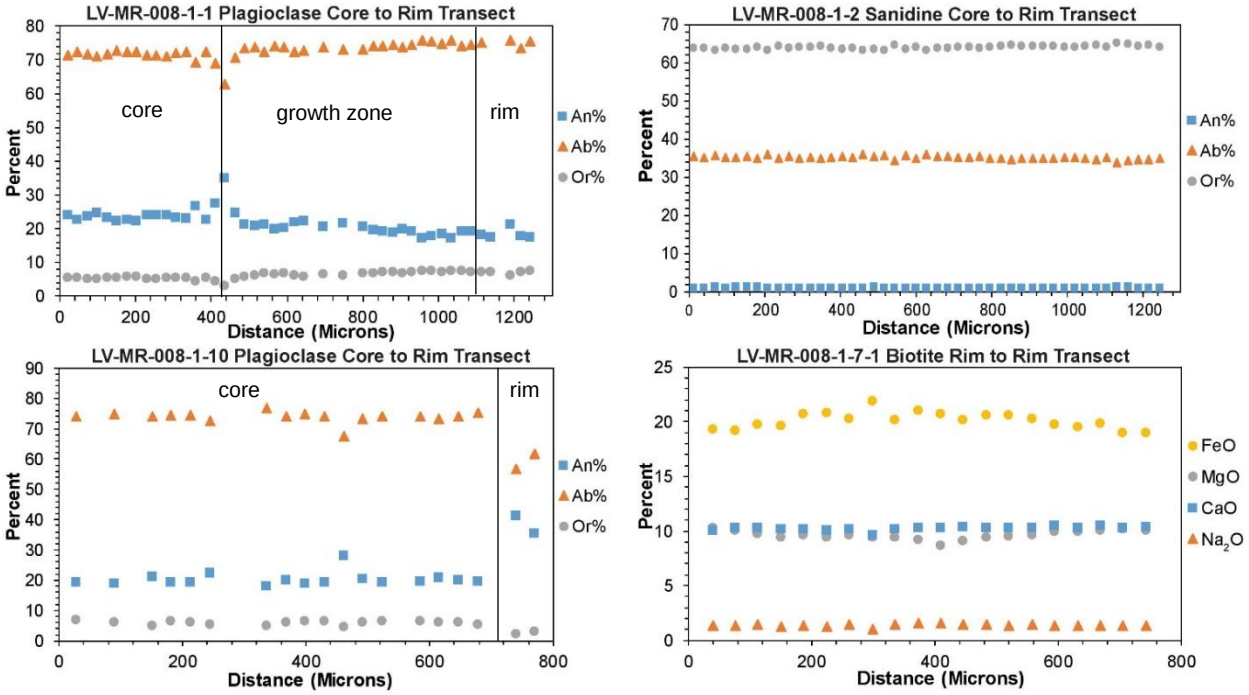

Figure 4.16. EPMA transects of 525 ka Moat rhyolite plagioclase, sanidine, and biotite.

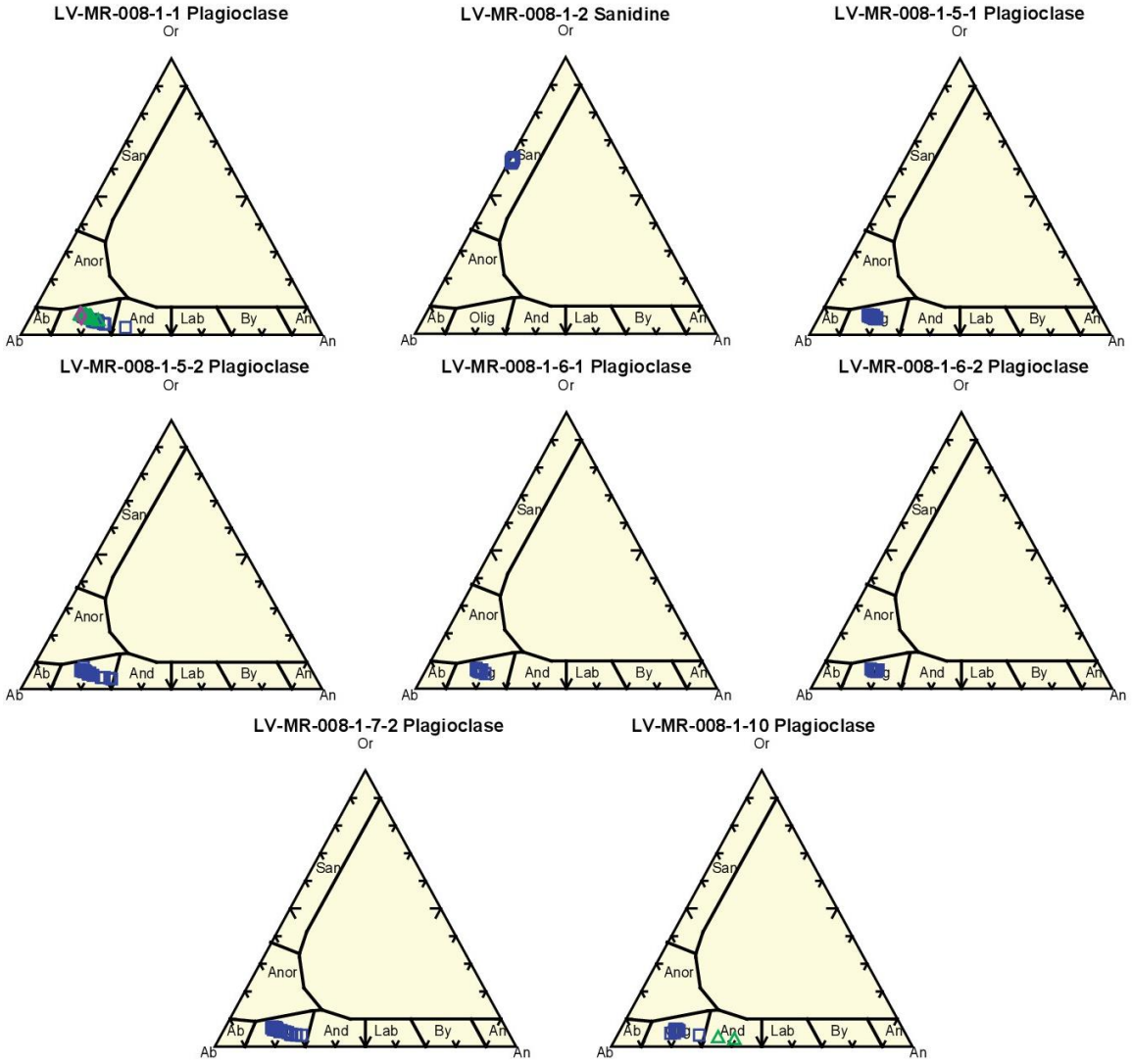

Figure 4.17. Ternary plots of 525 ka Moat rhyolite plagioclase and sanidine. Blue squares represent core compositions. Green Triangles represent rim compositions. Purple diamonds within LV-MR-008-1 represent secondary rim overgrowth.

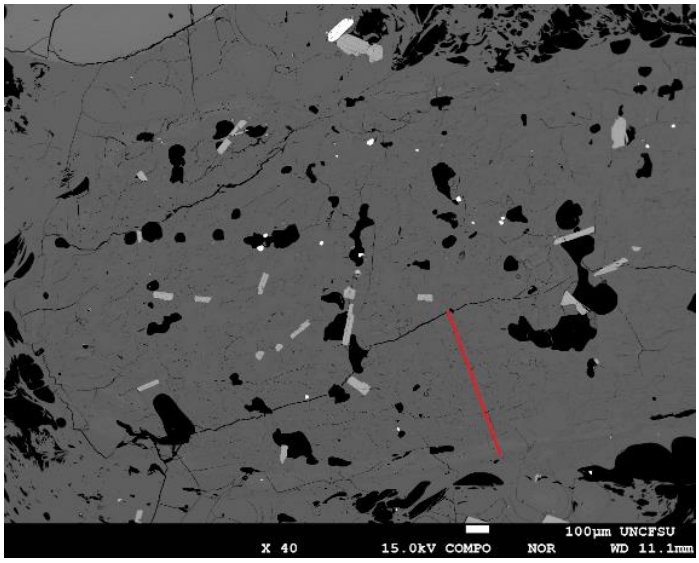

Figure. 4.18. BSE image of LV-MR-008-1-10 plagioclase. Core to rim transect highlighted by red line.

QMR_3

Feldspar populations from the 118-94 ka Moat rhyolite are predominantly sanidine phenocrysts with euhedral to anhedral morphologies. Subhedral sanidine phenocrysts display instances of concentric zoning in thin section but this phenomenon is more commonly observed in plagioclase populations regardless of disequilibrium features or morphology. Rim to rim and core to rim transects were performed on all populations but some intensely resorbed textures inhibited favorable data collection from both plagioclase and sanidine phenocrysts.

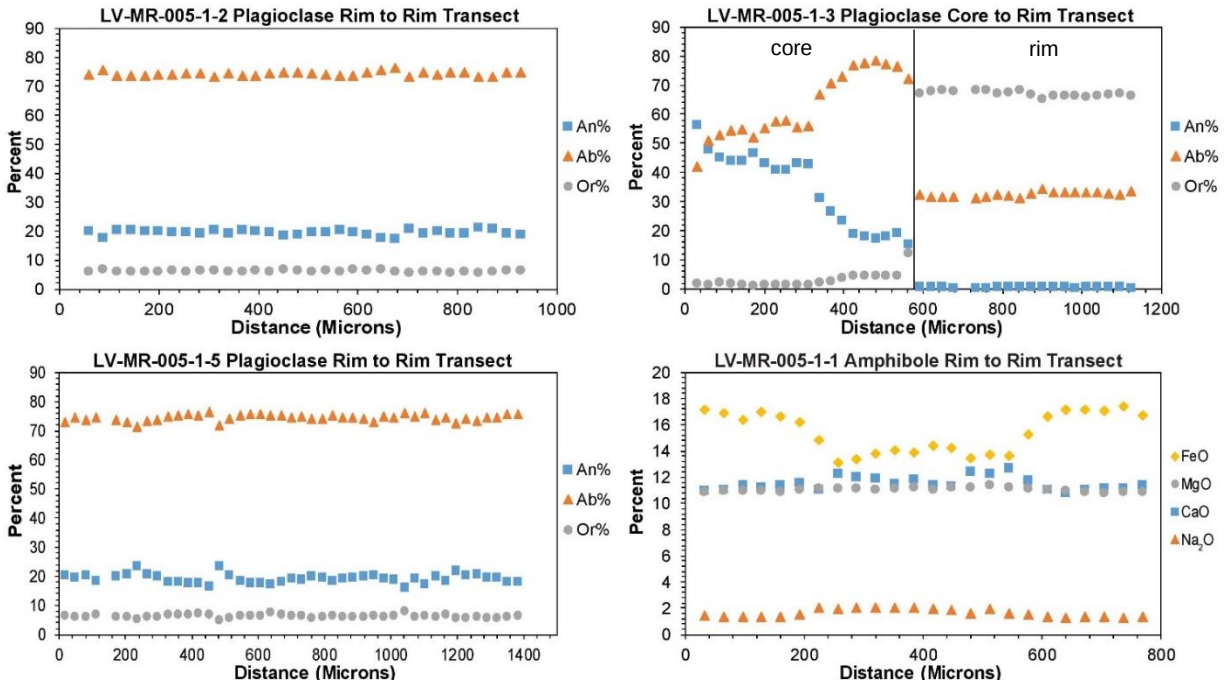

Figure 4.19. EPMA transects of 333 ka Moat rhyolite plagioclase and amphibole.

Sanidine phenocrysts lack distinct zonation patterns and commonly exhibit indistinguishable core and rim compositions. For example, a LV-MR-004-1-3 sanidine displays core and rim compositions of Or_{64}. LV-MR-004-1-1-2 sanidine exhibits similar core and rim compositions (~Or_{65} and ~Or_{65}) although one rim analysis exhibits a distinct increase in Ab content (Ab_{34} to Ab_{44} towards the rim) (Figs. 4.22 and 4.23).

Plagioclase phenocrysts display gradual and oscillatory normal zonation patterns. One LV-MR-004-1-7 plagioclase displays this type of zonation relationship as core compositions plot near the oligoclase-andesine compositional boundary (~An_{29}) while rim compositions plot in the oligoclase field (~An_{19}) (Figs. 4.22 and 4.23). Conversely LV-MR-004-1-4 (Fig. 4.24) plagioclase displays a more distinct core to rim relationship. Core compositions plot as andesine (~An_{42} - ~An_{37}) with oligoclase rims (An_{29} - An_{16}) (Figs. 4.19 and 4.20). In one instance, LV-MR-004-1-6 plagioclase intergrown with sanidine displays distinct compositional changes occurring over shorter distances. More calcic cores (~An_{33}) gradually decreases towards the rims

until a sharp decrease coincides with more sodic compositions (~An_{18}). After crossing the phenocryst boundary between plagioclase and sanidine compositions plot as sanidine (~Or_{63}) (Figs. 4.22 and 4.23).

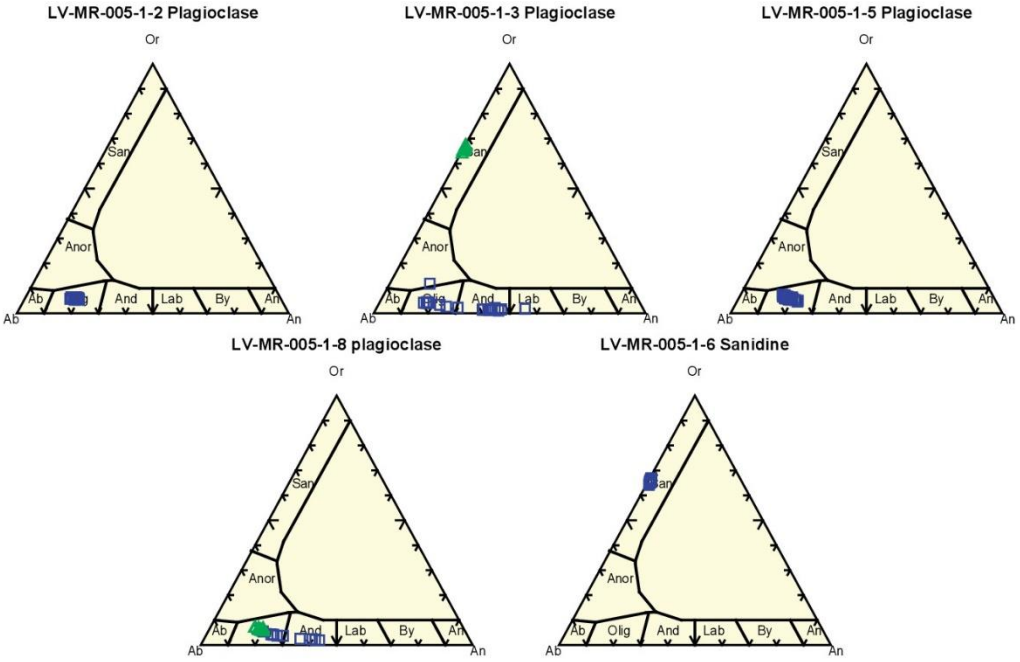

Figure 4.20. Ternary plots of 333 ka Moat rhyolite plagioclase and sanidine. Blue squares represent core compositions. Green Triangles represent rim compositions.

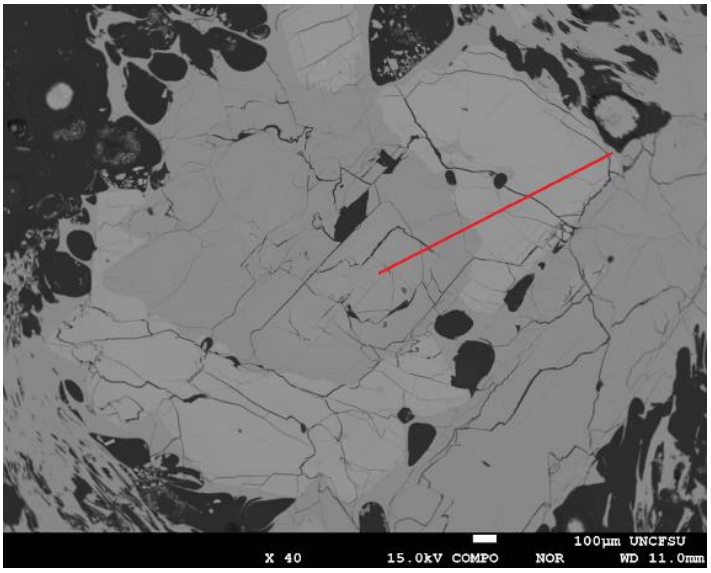

Figure. 4.21. BSE image of LV-MR-005-1-3 plagioclase. Core to rim transect highlighted by red line.

Amphibole

Like QMR_2, amphibole phenocrysts are small (< 1 mm) and euhedral. Additionally, these crystals do not display optic zonation in photomicrograph images but when images were obtained with BSE techniques, a normal core-rim compositional relationship is apparent. LV-MR-001-1-11 amphibole exhibit with a decrease in MgO content from ~10-8% and an increase in FeO content from 17-22% at the core–rim boundary (Fig. 4.23). A LV-MR-004-1-9 amphibole exhibits a similar relationship with and approximate 16-22% increase in FeO from core to rim while MgO decreases from ~10-8% (Fig. 4.23).

4.3.3 EPMA of the Hot Creek Flow Rhyolite

Feldspar

Hot Creek Flow feldspar populations consist of both sanidine and plagioclase. Sanidine is the most abundant phase and generally euhedral. Plagioclase crystals are divided into two populations based on size and textures. Larger plagioclase crystals are subhedral and display rim overgrowths while smaller plagioclase crystals are generally euhedral and lack distinct disequilibrium textures. However, concentric zoning visible in thin section is common to plagioclase populations and rim to rim transects were performed on these crystals to elucidate chemical variations.

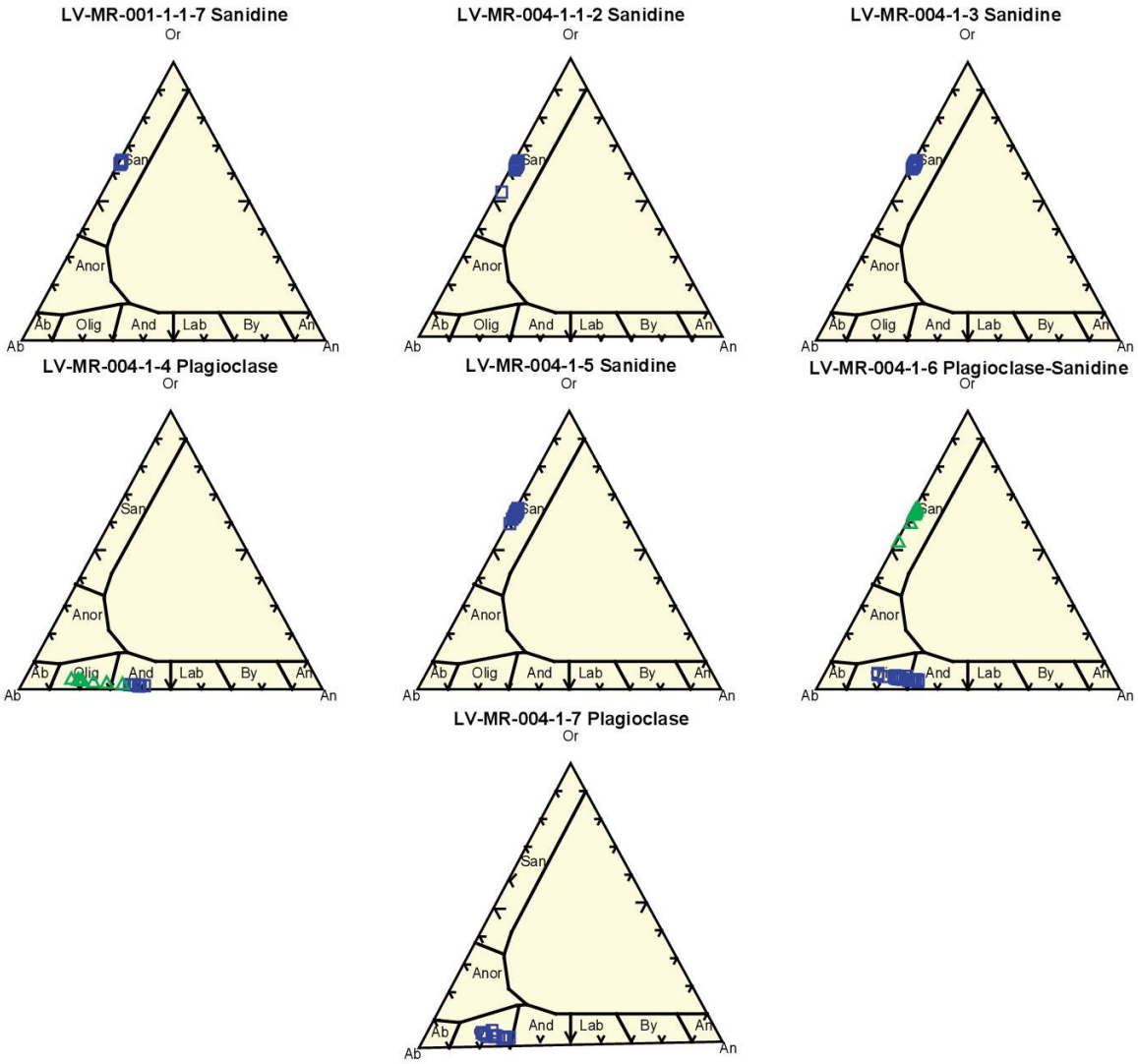

Figure 4.22. Ternary plots of 118-94 ka Moat rhyolite plagioclase and sanidine. Blue squares represent core compositions. Green Triangles represent rim compositions.

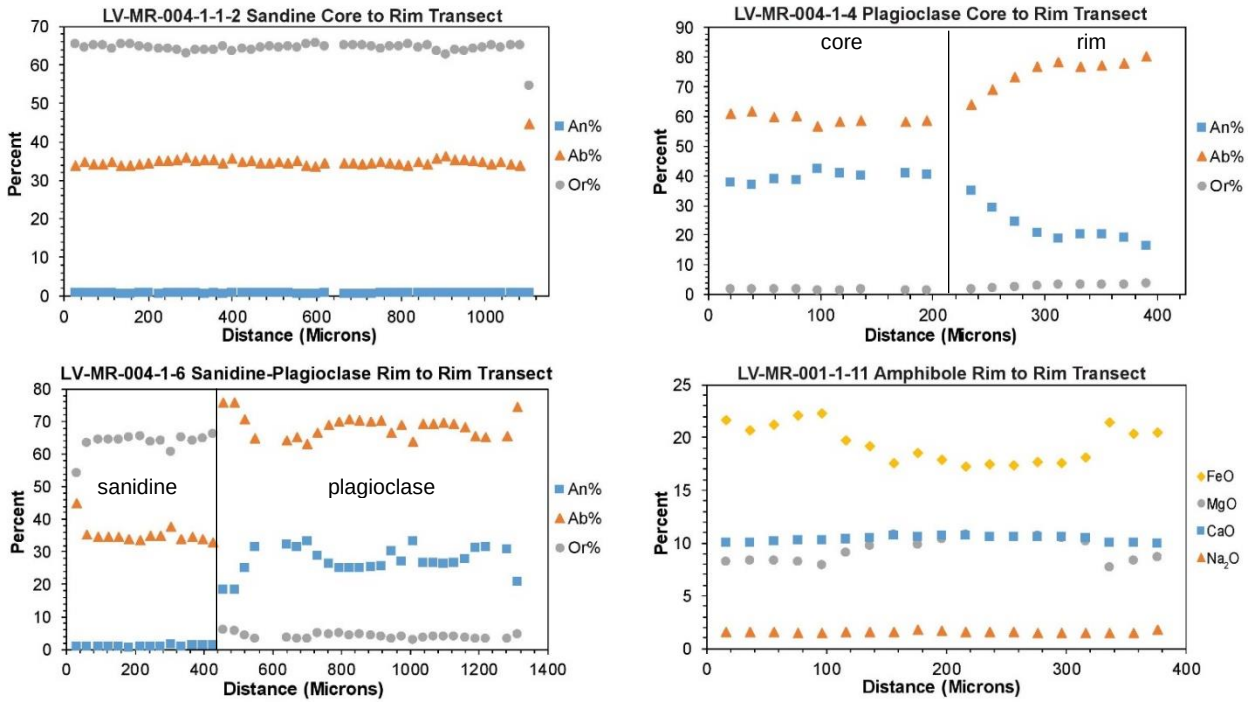

Figure 4.23. EPMA transects of 118-94 ka Moat rhyolite plagioclase, sanidine, and amphibole.

Normal, oscillatory zonation is the only type of zonation present in plagioclase populations, but larger phenocrysts are anti-rapakivi feldspars. These large plagioclase phenocrysts contain oligoclase cores (~An_{24}) and sanidine rims (~Or_{61}) (Figs. 4.25 and 4.26) as observed in LV-HCF-002-1-1 (Fig. 4.27). Small plagioclase crystals display normal, oscillatory zonation and plot within the oligoclase field. A HCF-005-1A3-1 plagioclase has moderate normal zoning from An_{27} core to An_{22} rims (Figs. 4.25 and 4.26). Conversely, sanidine lack zonation and compositional changes as core and rim values are often indistinguishable (Figs. 4.25 and 4.26). For example, a HCF-005-1A1-2 sanidine phenocryst has the same core and rim values of Or_{62} (Figs. 4.25 and 4.26).

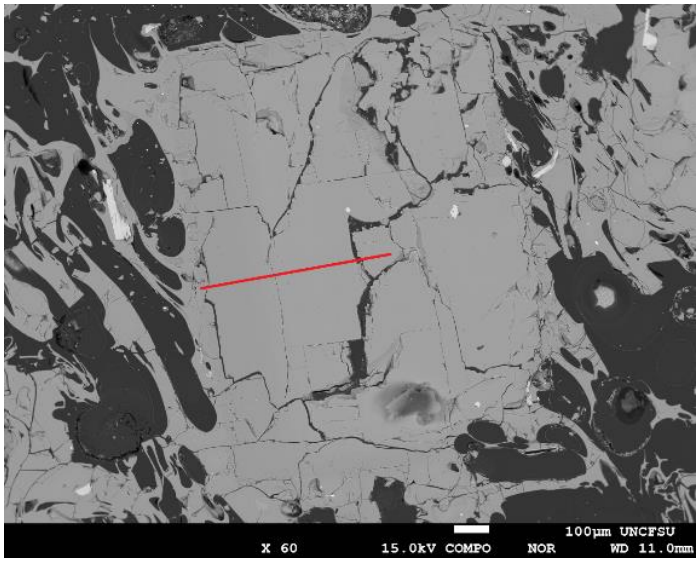

Fig. 4.24. BSE image of LV-MR-004-1-4 plagioclase. Core to rim transect highlighted by red line.

4.3.4 EPMA of the Deer Mountain rhyolite

Feldspar

Deer Mountain feldspar phenocryst populations are predominantly sanidine and plagioclase. Sanidine phenocryst morphologies range from euhedral to anhedral with resorption features more apparent in anhedral crystals. This contrasts with plagioclase phenocrysts which are largely euhedral and lack optically visible zonation features. Rim to rim and core to rim transects were performed on all populations, although some textures were not conducive to favorable data collection.

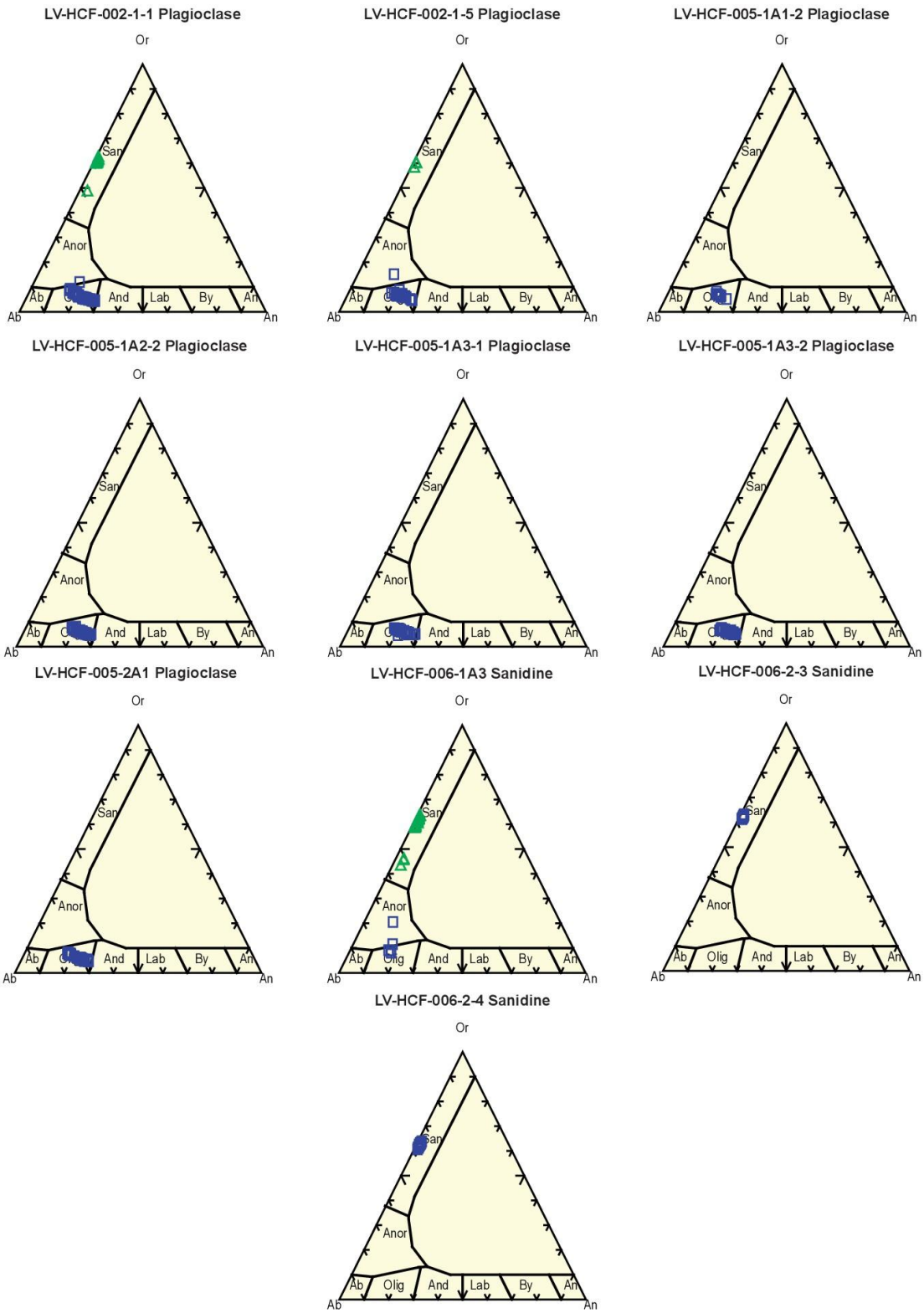

Figure 4.25. Ternary plots of Hot Creek Flow plagioclase and sanidine. Blue squares represent core compositions. Green Triangles represent rim compositions.

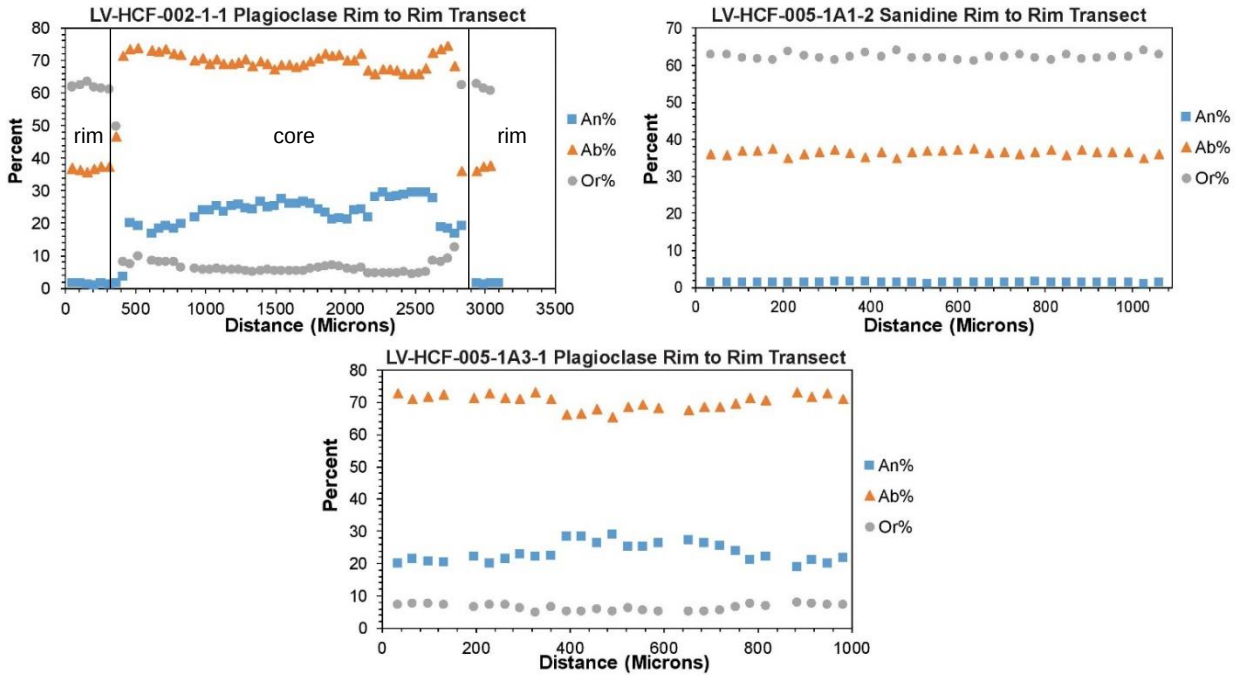

Figure 4.26. EPMA transects of 312-295 ka Hot Creek Flow plagioclase and sanidine.

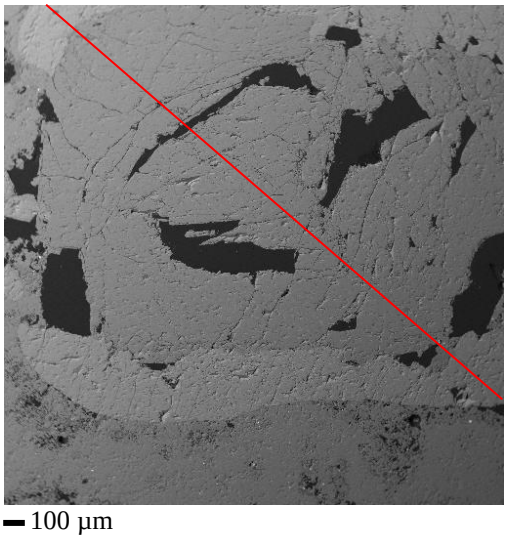

Figure. 4.27. BSE image of LV-HCF-002-1-1 plagioclase. Rim to rim transect highlighted by red line.

Sanidine phenocrysts lack major zonation features but faint normal zonation is apparent in thin section. A LV-DM-001-1-3 sanidine crystal displays this relationship as potassium compositions average ~Or_{64} throughout the entire rim to rim transect (Fig. 4.28) Additionally, more extreme rim compositions indicate a subtle overgrowth illustrated by elevated sodium values (core= ~Ab_{32}, rim= ~Ab_{48}) (Figs 4.28 and 4.29).

Plagioclase phenocrysts display instances of oscillatory, normal zonation. This is more pronounced in some phenocrysts than others. A LV-DM-001-1-7 (Fig. 4.30) plagioclase displays an initial decrease in calcium content as core compositions decrease gradually from An_{49} to An_{31} (Fig. 4.28). Compositions then sharply drop from An_{31} to An_{16} over the next 58 µm (Fig. 4.28). Compositions vary but average approximately An_{17} for the duration of the transect to the rim (Fig 4.28). Other plagioclase crystals do not display distinct growth bands and show nearly indistinguishable rim and core compositions. For example, rim and core compositions in a LV-DM-001-1-2 plagioclase range from ~An_{20-19} to An_{19} respectively (Fig. 4.28).

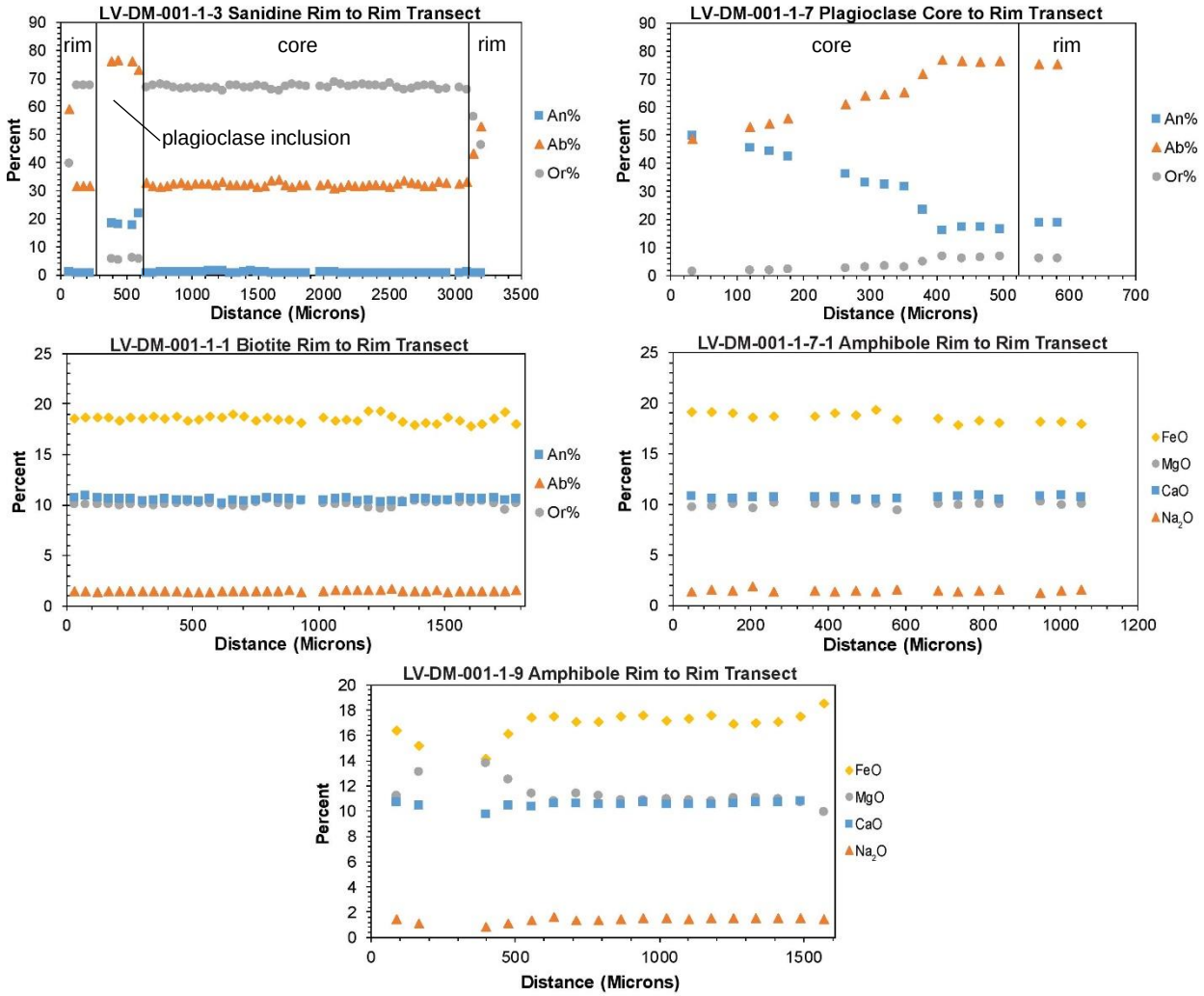

Figure 4.28. EPMA transects of Deer Mountain plagioclase, sanidine, biotite, and amphibole.

Amphibole and Biotite

Large, euhedral biotite phenocrysts and small euhedral amphibole phenocrysts are present in the Deer Mountain rhyolite. Biotite phenocrysts are considerably larger than feldspars in some cases but most crystals are smaller. Amphibole phenocrysts are considerably smaller than biotite crystals, and sometimes occur in glomerocrysts with biotite. Rim to rim transects were performed across all phenocrysts.

Biotite phenocrysts do not show significant distinctions in major element compositions, however one small phenocryst displays slight normal zonation. Core and rim compositions in a LV-DM-001-1-8 biotite exhibit an FeO increase from ~16-19% whereas MgO decreases from ~10-9% (Fig 4.28). Large, euhedral biotite phenocrysts display almost indistinguishable core (16-18% FeO; 9-11% MgO) and rim (18% Feo; 10-11% MgO) compositions (Fig 4.28).

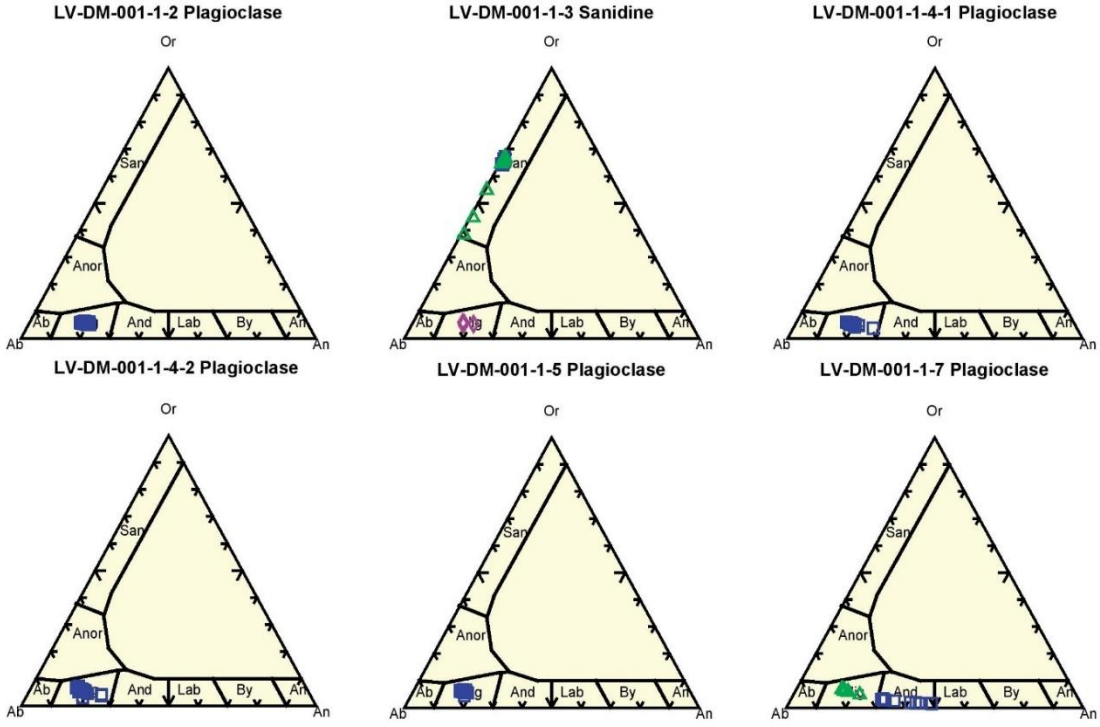

Figure 4.29. Ternary plots of Deer Mountain plagioclase and sanidine. Blue squares represent core compositions. Green Triangles represent rim compositions. Purple diamonds within LV-DM-001-1-3 represent plagioclase inclusion.

Like biotite phenocrysts, amphibole transects do not generally display distinct core to rim compositional variations. However, in one instance a LV-DM-001-1-9 amphibole appears to show oscillatory, normal zonation as compositions range from 14-19% FeO and 14-10% MgO towards the rims (Fig. 4.23). Another LV-DM-001-1-7-1 amphibole displays indistinguishable core (19% FeO; 10% MgO) and rim (19% FeO, 10 % MgO) compositions (Fig 4.23).

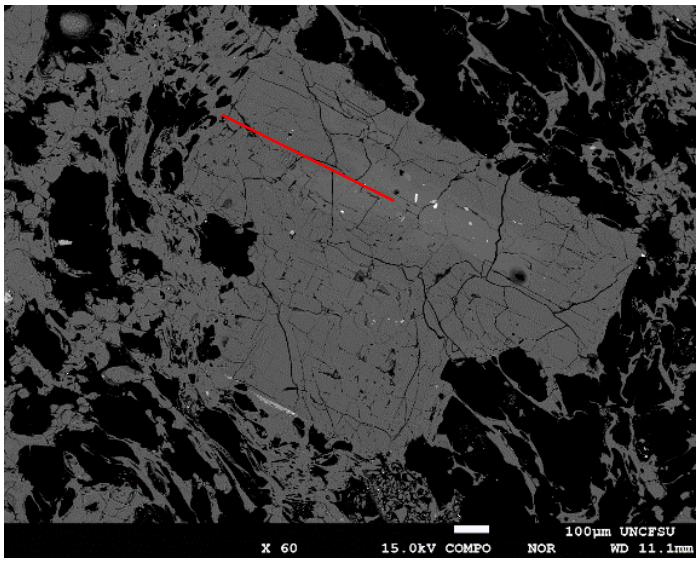

Figure. 4.30. BSE image of LV-DM-001-1-7 plagioclase. Core to rim transect highlighted by red line.

CHAPTER 5

DISCUSSION

5.1 Interpretations of $^{40}Ar/^{39}Ar$ Geochronology

New $^{40}Ar/^{39}Ar$ ages have been reported for all but one (Resurgent Dome rhyolite) of the post-collapse rhyolites examined in this study to evaluate the temporal evolution of post-collapse magmatism following eruption of the Bishop Tuff. Previously determined $^{40}Ar/^{39}Ar$ ages from Simon et al. (2014) infer that Resurgent Dome volcanism occurred at approximately 700 ka. Laser heating of plagioclase separates returned ages (all are at one sigma uncertainty) of 696 ± 40 ka and 705 ± 25 ka (Simon et al., 2014). These dates are the most recent and reliable and will be referenced throughout this study.

Ages obtained in this study from the initial Moat rhyolite eruption of 525 ± 2 ka is significantly younger than ages reported by Simon et al. (2014) at 576 ± 9 ka. However, ages obtained in this study are indistinguishable from a K/Ar date reported by Mankinen et al. (1986) of 523 ± 11 ka. Intermediate age Moat rhyolites reported in this study yielded an age of 333 ± 4 ka, similar to K/Ar ages reported by Bailey et al. (1976) of 349 ± 5 ka and Mankinen et al. (1986) at 362 ± 8 ka. Temporally related Hot Creek Flow sanidine separates from three samples yielded ages of 312 ± 7 ka, 297 ± 7 ka, and 295 ± 3 ka, which overlap with 329 ± 23 ka and 288 ± 31 ka K/Ar ages reported by Mankinen et al. (1986). However, uncertainty associated with K/Ar ages reported by Mankinen et al. (1986) is high and overlaps with slightly older ages reported by Simon et al. (2014) of 336 ± 2 ka. The youngest Moat rhyolite unit yielded ages of 118 ± 1 ka and 94 ± 2 ka, from samples LV-MR-004 and LV-MR-001 respectively. This difference in ages may be reflected in the fact that this unit is the result of a composite flow

created by multiple eruptions. (Fig. 2.01). Laser fusion and step heating analysis by Huemann et al. (2002) yielded ages (151 ± 4 ka and 147 ± 4 ka) that are older than obtained in this study.

The $^{40}Ar/^{39}Ar$ age obtained for the Deer Mountain rhyolite in this study of 65 ± 1 ka is significantly younger than plateau ages reported by Huemann et al. (2002) of 101 ± 8 ka and K/Ar ages from Mankinen et al. (1986) of 115 ± 3 ka. However, such discrepancies might be a result of a composite dome eruption.

5.2 Interpretations of Petrography

The physical characteristics of crystal populations of each eruptive unit provide evidence for different pre-eruptive evolutionary paths with respect to Resurgent Dome, Moat rhyolite, Hot Creek Flow, and Deer Mountain rhyolites. Based on distinct textures (or lack of thereof) general constraints can be placed on the evolution of the early and late post-collapse magma plumbing system. Crystals from the Resurgent Dome rhyolite contain equilibrium textures that suggest equilibrium crystallization of juvenile plagioclase and orthopyroxene phenocrysts from a rhyolitic melt. However, following 525 ka, Moat rhyolite, Hot Creek Flow, and Deer Mountain crystal populations indicate variable crystallization histories inferred by rim overgrowths, sieve textures, and dissolution features. Moreover, phenocryst assemblages can be further distinguished upon modal abundances (Table 4.01) of crystals contained within in each eruptive unit.

These observations are consistent with equilibrium crystallization of Resurgent Dome rhyolite from a rhyolitic melt derived from the residual Bishop Tuff magma chamber. Mostly euhedral populations of plagioclase, orthopyroxene, amphibole, and biotite indicate no mixing of mafic magma within the Resurgent Dome chamber. Additionally, glomerocrysts of plagioclase and orthopyroxene further suggest equilibrium crystallization facilitated by simple fractionation.

However, a plagioclase with a core composition of An_{60} indicates that some interaction with more mafic magmas did occur, which may have provided a mechanism to keep the residual Bishop Tuff magma chamber liquid for approximately 80 ka. Resurgent Dome phenocryst assemblages are similar to those of the latest erupted Bishop Tuff member (Hildreth, 2004). However, phases such as sanidine and quartz are conspicuously absent from the Resurgent Dome and the relative abundance of crystals displays a significant drop from 15 – 25 % in the Bishop Tuff to 2% in the Resurgent Dome (Table 4.01) (Hildreth, 2004).

Approximately 200 ka after the eruption of the Resurgent Dome rhyolite, the 525 ka Moat rhyolite phenocryst assemblages display distinct textural differences. There is a significant increase in the relative abundance of phenocrysts from 2% to 12% (Table 4.01). In addition to the difference in phenocryst abundances rim overgrowths on dissolution surfaces within plagioclase populations as well as sieve textures are common, and may indicate disequilibrium during crystallization caused by magma mixing. A similar phenomenon is observed within Hot Creek Flow plagioclase populations, as larger phenocrysts found in LV-HCF-002-1 contain distinct rim overgrowths on dissolution surfaces. This suggests magma mixing with a hotter mafic melt, causing dissolution followed by recrystallization. Magma mixing events also appear to have occurred in a close temporal (333 ka Moat rhyolite and 312-295 ka Hot Creek Flow) and spatial (Fig. 2.01) relationship within the intermediate Moat rhyolite magma chamber. However, mineral abundances within the Hot Creek Flow (1 – 4%) are much lower than that of the 333 ka Moat rhyolite (12%) (Table 4.01). Plagioclase populations of both units contain concentric zonation and dissolution surfaces marking the beginning of rim overgrowths. These distinct core-rim textural relationships suggest that not all phenocryst populations are truly juvenile in nature and may represent instances of xenocryst recycling. This observation suggests that although

mineral abundances of the 333 ka Moat rhyolite and the Hot Creek Flow are vastly different, when considering the close temporal and spatial relationship of these two eruptive units, as well similar plagioclase textures, extraction from the same source magma is possible.

The 118-94 ka Moat rhyolite unit as well as the Deer Mountain rhyolite display textures that may record magma mixing events as preserved in plagioclase and sanidine populations. This is exemplified by a large Moat rhyolite plagioclase crystal with a resorbed core and a cellular rim overgrowth. A similar occurrence is illustrated in Deer Mountain rhyolite feldspar populations, where a euhedral plagioclase phenocryst displays a distinct resorbed core and rim overgrowth.

The above examples of disequilibrium caused by, e.g., magma mixing and instances of xenocryst recycling are viable interpretations for later (<525 ka) erupted post-collapse units. Smaller, generally euhedral biotite, amphibole, plagioclase and sanidine crystals appear to record equilibrium crystallization after mixing events.

5.3 Interpretation of Crystal Geochemistry

While crystal textures may provide physical evidence for disequilibrium such as magma mixing events, corresponding major and minor element geochemistry can further constrain such events. Furthermore, the assumption that disequilibrium textures are direct evidence for magma mixing events may be tenuous. Disequilibrium textures within phenocrysts are the product of not only melt compositional change but also other processes such as changes in pressure, temperature, and volatile content. Based on prior studies, dissolution surfaces that coincide with major changes in composition (i.e. plagioclase An content) are most likely caused by magma mixing. For example Perguni et al (2004), Ginibre et al (2004), and Shcherbakov et al (2011) argue that large scale (≥10% An) compositional changes in feldspar phenocrysts are associated with magma recharge events. Smaller oscillatory zoning is inferred to be a function of

convection and diffusion synonymous with fractional crystallization and crystal settling (Loomis, 1982; L'Heuruex and Fowler, 1994). Large increases in An content (reverse zoning) are thus interpreted as interaction with less evolved, hotter, more mafic melts. In some instances, large compositional increase correlate with crystal recycling introducing xenocrysts (crystals foreign to a magma system) (Jerram and Martin, 2008). The opposite is true for normal zonation which indicates fractional crystallization recorded in a decrease in An content towards the crystal rim. Crystal recycling may occur in association with small compositional changes introducing antecrysts (reincorporation of chemically similar crystals) (Jerram and Martin, 2008). However, in some instances (such as anti-rapakivi texture) plagioclase phenocrysts mantled by sanidine overgrowths suggest high temperature conditions causing resorption followed by recrystallization initiated by mafic rejuvenation (Hibbard, 1981; Aslan, 2005).

Based on these observations euhedral plagioclase and subhedral orthopyroxene phenocrysts from the Resurgent Dome appear to represent equilibrium crystallization of residual melt (possibly that of the Bishop Tuff magma chamber). Normal zonation patterns (Andesine cores to oligoclase rims) observed in plagioclase phenocrysts, and ferrosillite compositions of orthopyroxene phenocrysts indicate equilibrium crystallization from a rhyolitic melt. While this does not provide a direct correlation between the Resurgent Dome and the Bishop Tuff, it does provide evidence for crystallization from melt with a similar composition with minimal interaction with less evolved melts. Studies completed by Hildreth (2004) document similar major element compositions between the latest erupted Bishop Tuff member and the Resurgent Dome (Fig. 5.01). Differences in mineral assemblages between these two units might have been caused by the disruptive Bishop Tuff eruption leading to reorganization of the magma chamber causing resorption of sanidine phenocrysts (Hildreth, 2004).

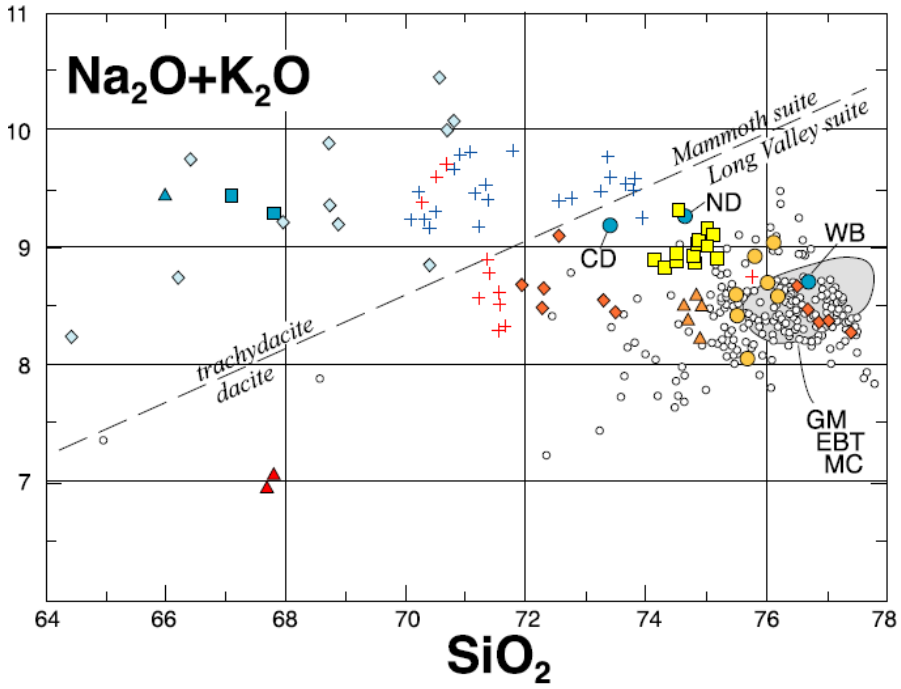

Figure 5.01. Total alkalis versus Silica plot from Hildreth (2004). White circles represent late Bishop Tuff. Yellow squares represent Resurgent Dome rhyolite. Red triangles represent a northeastern Rhyodacite Dome. Orange triangles represent initial Moat rhyolite. Orange Circles represent intermediate age Moat rhyolite and Hot Creek Flow. Orange diamonds represent youngest Moat rhyolite. Red crosses represent crystal poor Inyo Domes. Blue crosses represent crystal rich Inyo Domes. Blue circles represent all other Inyo Domes. Blue diamonds represent Mammoth mountain domes. Blue squares represent Crystal Poor Dacites. Blue triangles represent northwestern Wall Dacites. CD = tiny Cratered Dome; ND = North Deadman Dome; WB = Wilson Butte; GM = Glass Mountain; EBT = Early Bishop Tuff; MC = Mono Craters.

Early Moat rhyolites (525 ka) display major element variations within plagioclase rims that are evidence for mafic rejuvenation. This is recorded in reverse zoning of a plagioclase phenocryst with a resorbed, sieved core and rim overgrowth where An values increase from An_{19} to An_{38}. This is also consistent with biotite, where MgO content increases towards rims while FeO decreases. This may be interpreted as recording a recharge event associated with an intrusion of a more mafic magma. Smaller plagioclase and sanidine populations that lack dissolution features tend to follow normal zonation patterns consistent with equilibrium crystallization from a rhyolitic melt following recharge. This recharge event may also be recorded by εNd values of -1.95 to -1.54 (Simon et al., 2014). This contrasts with more crustal Resurgent Dome εNd values of -2.13 to -2.01. This is interpreted here as mafic recharge

inducing melting after a relatively quiescent 200 ka period following Resurgent Dome eruptions. The presence of more mafic magma may also correspond with a decrease in whole rock silica content of early Moat rhyolites to 73.4% (Heumann and Davies, 1997).

Further evidence for interaction with mafic magmas is displayed in the 333 ka Moat rhyolites by the presence of xenocrystic plagioclase cores. A plagioclase with a Ca-rich core composition of An_{56} was most likely derived from a mafic magma rather than the rhyolite it is erupted with. Moreover, this phenocryst displays anti-rapakivi texture possibly caused by less-evolved material (associated with core compositions) inducing melting. Furthermore, εNd of -1.45 to -1.29 indicates increasing mafic input (Simon et al., 2014). Lack of resorption features in other plagioclase, sanidine, and amphibole phenocrysts likely reflect crystallization of rhyolitic melt associated with anti-rapakivi sanidine overgrowths on plagioclase.

Similar crystal relationships are found in the 312 – 295 ka Hot Creek Flow where sparse phenocryst assemblages contain coarse, subhedral plagioclase crystals with sanidine overgrowths. Epsilon Nd values of -1.07 (Simon et al., 2014) are the most mantle-like of all post-caldera rhyolites, although whole rock SiO_2 content increases to 77.2% (Heumann and Davies, 1997). This could be explained by remelting of previous silicic intrusions or mush bodies by interaction with mafic melt components. However, the Hot Creek Flow may also represent stratified highly evolved melt at the top of a larger magma body.

This contrasts with the appropriately termed low-silica Moat (71.9%) rhyolite named by Heumann and Davies (1997). Epsilon Nd values begin to return to more crustal values of -1.29 to -1.44 (Heumann and Davies, 1997). These youngest (118 – 94 ka) Moat rhyolites display textures that indicate mixing of intermediate and rhyolitic melts as recorded in a plagioclase with core compositions of An_{42} and rim compositions of An_{16}. Once again, smaller euhedral feldspars

and amphiboles may record crystallization of a homogenous rhyolitic magma after mixing occurred. For example, a small (~700 μm), euhedral sanidine records consistent Or_{35} content from rim to rim and a small (~ 700 μm), euhedral amphibole has observable core compositions of approximately 11% MgO and rim compistions of 8% MgO.

Deer Mountain rhyolite εNd values (-1.76) indicate a continued waning of mafic rejuvenation either due to location within the caldera or a simple reduction in mantle-derived magmas interacting at crustal depths (Huemann and Davies, 1997). Deer Mountain rhyolites also have low whole rock SiO_2 concentrations of 71.9%. However, there is still evidence that rejuvenation is involved, as a plagioclase with a resorbed core displays andesine (An_{50}) compositions with a distinct oligoclase (An_{16}) euhedral rim overgrowth. This is evidence for intermediate magma transferring xenocrysts into a rhyolitic melt where after they continue to crystallize. Amphibole and biotite phenocrysts again appear to record the crystallization history of equilibrated rhyolitic melt compositions. This is displayed in smaller, euhedral amphibole and biotite crystals which both record consistent MgO content of 10% and 11% from rim to rim respectively.

5.4 A Petrologic Model for the Post-Collapse Magma Plumbing System

The observations outlined above suggest mafic magma rejuvenation is common based on antirapakivi textures, instances of reverse zoning, and high An plagioclase cores observed in feldspars from late erupted (≤525 ka) post-collapse rhyolites. Moreover, εNd values (Simon et al. 2014) provide supporting evidence for an increase in more mantle like components from 525 ka to 295 ka. However, the structure of the magma plumbing system beneath the Long Valley caldera remains uncertain despite recent studies. The most viable arguments for the plumbing system are alternatives to the long-lived magma chamber model (Bailey et al., 1976; Hildreth,

1981) which argue for a more a complex evolution than simple chemical stratification related to fractional crystallization. Studies by Heumann and Davies (1997), Heumann et al. (2002), Hildreth (2004), and Simon et al., (2014) suggest either: (1) isolation, storage and evolution of the upper portion of the residual Bishop Tuff magma chamber producing chemically distinct early (≥ 400 ka) and late (≤ 400 ka) rhyolites (Heumann and Davies, 1997; Heumann et al., 2002) or (2) generation of separate magma batches due to an increase in rejuvenation of crystal mush bodies by more primitive melts until approximately 400 ka. Following 400 ka less rejuvenation reduced assimilation and melting of mush bodies (Hildreth, 2004: Simon et al., 2014). The model proposed in this study incorporates concepts from arguments proposed by Heumann and Davies (1997), Heumann et al. (2002), Hildreth (2004), and Simon et al., (2014). However, new geochemical and textural data from crystal populations suggest different temporal distinctions between late and early erupted post-collapse rhyolites than previously reported.

While the geochemical (and more specifically isotopic) distinctions described previously seem to indicate independent magma batches for the production of each eruptive unit it appears that all post-collapse rhyolites may be related to a cogenetic source beginning with the Resurgent Dome rhyolite and culminating with the much younger Inyo Domes. For example, Heumann and Davies (1997) suggest that the entire post-collapse rhyolite sequence is related based on a linear Pb-Sr trend between the Resurgent Dome and the Inyo Domes (Fig. 5.02).

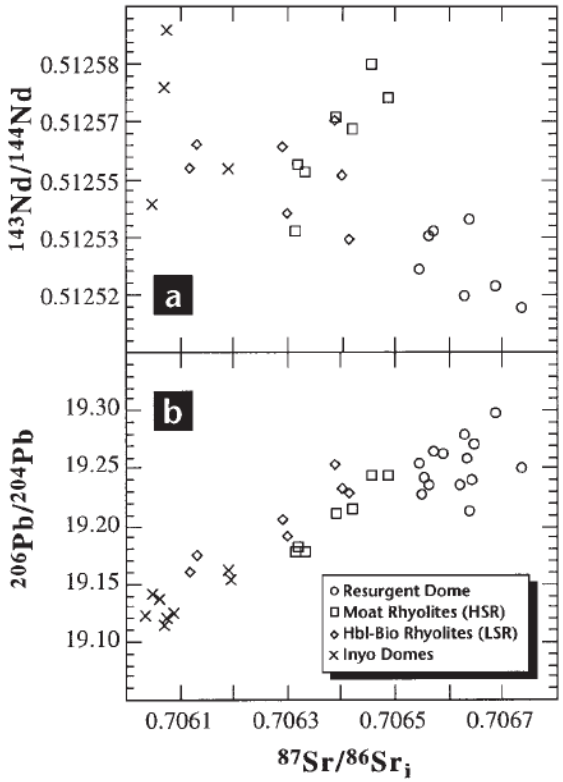

Figure 5.02. Initial $^{87}Sr/^{86}Sr$ versus $^{143}Nd/^{144}Nd$ and $^{206}Pb/^{204}Pb$ for the post-collapse rhyolites suite from Heumann and Davies (1997). HSR (High Silica Rhyolite) and LSR (Low Silica Rhyolite) refer to Moat rhyolite subtypes.

This may indicate that all melt production is the result of segregation from a larger bulk reservoir, but here this is interpreted as evidence for multiple silicic intrusions or mush bodies residing within in close proximity at variable levels in the crust (Fig. 5.03). Furthermore, Pb-Sr isotopes presented by Heumann and Davies (1997) support the notion that there is a decrease in crustal derived melt components and an increase in primitive mantle-derived sources with time. This is not to say that basaltic magmatism increased, but rather, rhyolitic mush bodies or granitic intrusions might have been preferentially remelted by interacting with hotter mafic material (Fig. 5.03). Mush bodies may have formed as a result of remelting of granitic intrusions (Huppert and Sparks, 1988) or segregation from the residual Bishop Tuff reservoir (Heumann and Davies, 1997). However, no mafic magmas ascended to the surface for 500 ka after caldera collapse (Hildreth, 2004), which suggest that the locus of activity for basaltic melts most likely interacted

beneath a barrier of silicic intrusions or mush bodies. Lastly, large (>10 km) distances and time (~91 ka) intervals between eruptions suggest that the post-collapse units formed independently and are largely unrelated. This is supported by time intervals between crystallization and eruption of post-collapse rhyolites on the order of 10's -100's ka, which may be controlled by variable mafic input (Simone et al., 2014).

These observations suggest a model for the creation of the Resurgent Dome rhyolite. After the eruption of the Bishop Tuff minimal re-melting of the residual magma chamber leads to the eruption of a crystal poor rhyolite. This might lead to the absence of mineral phases such as sanidine and quartz that are found in the latest erupted member of the Bishop Tuff. However, formation of unzoned, euhedral plagioclase and orthopyroxene from reorganization and convection of the magma chamber after the eruption of the Bishop Tuff are the pre-dominant forces. This is consistent with equilibrium, fractional crystallization and crystal settling from a relatively undisturbed melt body. Moreover, it has been suggested that crystal-poor rhyolites can be extracted from voluminous mush bodies similar to the source that supplied the voluminous Bishop Tuff eruption (Bachman and Bergantz, 2004).

This is in contrast to what occurs following 525 ka. Whereas the first Moat rhyolite might be interpreted as an eruption of crystal-rich material from a stratified magma chamber based on a decrease in whole rock SiO_2 this does not resolve the observation that εNd values are increasingly elevated and there are instances of reverse zonation within plagioclase feldspars. This suggests that a more mafic magma induced melting of a crystal rich silicic mush and ultimately led to eruption.

The close temporal (~20 ka between eruptions) and spatial (~1 km between outcrops) relationship between the 333 ka Moat rhyolite and Hot Creek Flow may be explained by both

magma models (Heumann and Davies, 1997 and Heumann et al., 2002; Hildreth, 2004 and Simon et al., 2014) in that it appears they represent subsequent eruptions from a rejuvenated mush body. Evidence for magma mixing is apparent in plagioclase feldspar populations due to xenocryst and antecryst recycling mechanisms indicated by anti-rapakvi texture and high An plagioclase cores. Epsilon Nd values also indicate interaction with more primitive magma, however the Hot Creek Flow is more highly evolved than the intermediate age Moat rhyolite flow in terms of SiO_2 content. Additionally, Hot Creek Flow plagioclase phenocrysts indicate that magma mixing occurred between two rhyolitic melts based on An content. Thus, it is possible that the Hot Creek Flow and the 333ka Moat rhyolite may represent the stratified portions of a re-melted mush body that extracted high-silica crystal poor rhyolites and low-silica crystal rich rhyolites based on a close proximity and temporal relationship.

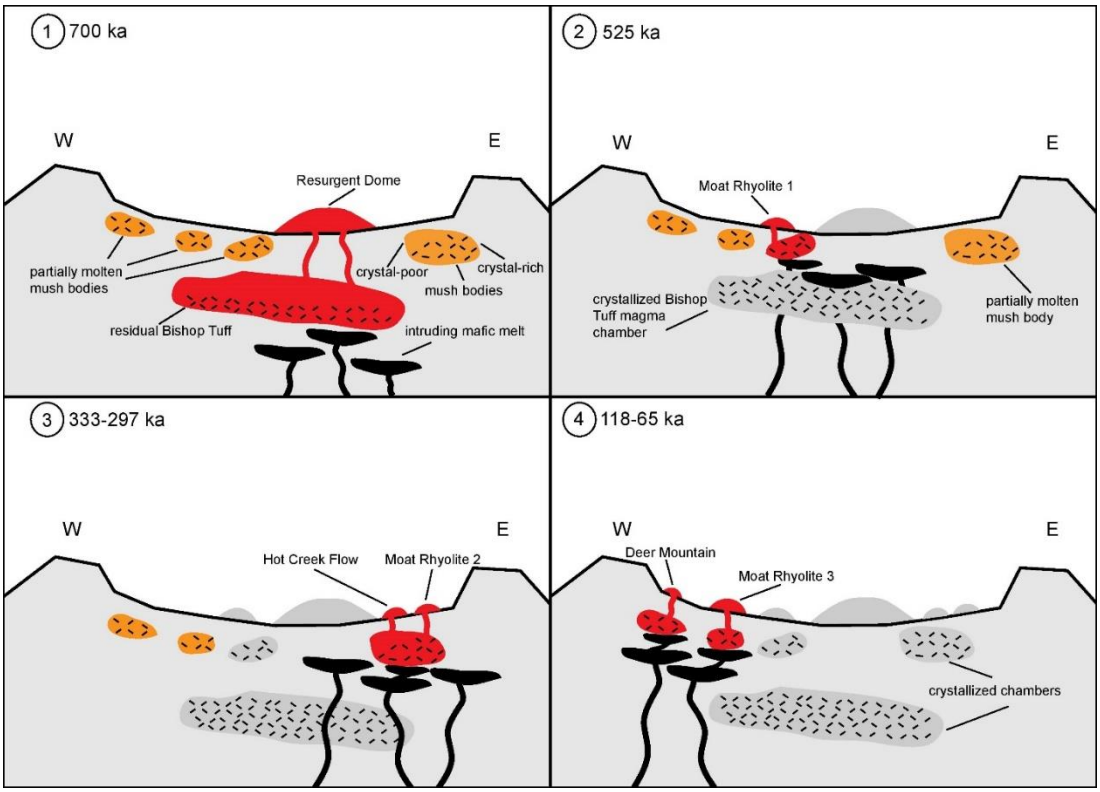

Figure 5.03. Melting model for the production of the post-collapse rhyolites (not to scale). Colors correspond to thermal state of melt; red represents molten melt bodies, orange represents partially molten mush bodies, and gray represents crystallized chambers.1. Minimal mafic melt interaction causes the 700 ka Resurgent Dome eruption. 2. North of the Resurgent Dome increased mafic melt interaction remelts a mush body prompting eruption of the 525

ka Moat rhyolites. 3. South of the Resurgent Dome mafic melt interaction prompts eruption of stratified mush body erupting the 333 ka crystal-rich Moat rhyolite and the 312-295 ka crystal poor Hot Creek Flow. 4. The last mafic rejuvenation pulse remelts crystal mush bodies and prompts the eruption of the 118-94 ka Moat rhyolite and the 65 ka Deer Mountain rhyolite. Mush bodies may cool and crystallize to form intrusions due to large time intervals between eruptions especially if at shallow crustal depths.

Following the eruption of this southeastern rhyolite cluster, magmatic conditions are better explained by the re-melting model (Hildreth, 2004; Simon et al., 2014). The youngest Moat rhyolite exhibits increasingly crustal εNd values most likely due to a reduction in mafic inputs. However, based on feldspar textures and distinct core-rim compositions interaction between rhyolitic melts occurred. This same process occurred to produce the Deer Mountain rhyolite although interactions between ascending basalt and rhyolitic mush bodies inducing melting is greatly reduced based on the most crustal εNd values and less distinct feldspar core-rim compositions.

CHAPTER 6

CONCLUSIONS

The magma plumbing system under the Long Valley caldera provides insights into the evolution of a supervolcano and the formation of large volumes of rhyolitic melt. The geochemical variations and textures of mineral assemblages coupled with temporal and spatial considerations of the Long Valley post-collapse rhyolites indicate a possible melt production model that can be applied to other caldera systems. Previously published Pb-Sr isotope data (Heumann and Davies, 1997) suggest that post-collapse units may be cogenetic in origin. However, more mafic melts are involved in the generation of rhyolitic magma as eruptive units become younger in age (Hildreth, 2004; Simon et al., 2004). Based on the data collected in this study, following caldera collapse, magma mixing fueled by a periodic increase in basaltic mantle derived melts rejuvenated silicic intrusions or crystal mush bodies within the upper crust. Following 525 ka reverse zonation and dissolution textures indicate the first major instance of mafic input. At approximately 333 ka to 295 ka anti-rapakivi textures and xenocryst recycling indicate the greatest mafic melt involvement. The culminating 118 ka – 94 ka Moat rhyolite and Deer Mountain eruption at 67 ka suggest a decrease in mafic rejuvenation as core to rim compositional changes are less distinct, although dissolution textures remain. This is in contrast the relatively quiescent equilibrium crystallization conditions within the Resurgent Dome producing phenocryst poor rhyolites with juvenile, euhedral, mineral assemblages.

APPENDIX A. EPMA ANALYSES OF FELDSPAR. ERRONEOUS DATA HAVE BEEN REMOVED.

LV-RD-008-1A1-1 Plagioclase Rim to Rim

Distance (μm)	Na_2O	TiO_2	CaO	MgO	SiO_2	FeO	K_2O	Al_2O_3	F	MnO	Cl	Cr_2O_3	P_2O_5	Total
48	3.32	0.07	2.36	1.07	70.48	3.82	4.65	12.89	0.00	0.25	0.03	0.00	0.00	98.93
192	7.02	0.05	6.08	0.00	60.06	0.20	0.96	24.38	0.03	0.05	0.00	0.01	0.00	98.84
239	6.69	0.02	6.35	0.01	59.75	0.22	0.91	24.94	0.10	0.00	0.01	0.00	0.00	98.96
287	7.01	0.03	6.64	0.02	59.57	0.19	0.82	24.84	0.00	0.01	0.02	0.01	0.02	99.18
335	6.77	0.01	6.70	0.00	59.41	0.21	0.86	24.89	0.21	0.00	0.00	0.00	0.01	98.98
383	6.52	0.00	7.32	0.00	59.17	0.22	0.75	25.58	0.06	0.00	0.00	0.01	0.00	99.62
431	6.76	0.02	7.43	0.02	58.92	0.20	0.72	25.68	0.00	0.00	0.01	0.02	0.02	99.79
479	6.41	0.02	7.43	0.01	58.91	0.21	0.71	25.70	0.10	0.00	0.00	0.00	0.00	99.46
527	6.76	0.00	7.09	0.01	58.84	0.20	0.76	25.53	0.19	0.00	0.00	0.00	0.03	99.33
574	6.51	0.05	7.10	0.01	59.04	0.21	0.79	25.44	0.00	0.02	0.01	0.00	0.00	99.19
622	6.51	0.00	7.21	0.00	58.94	0.19	0.72	25.45	0.02	0.03	0.00	0.03	0.00	99.08
670	6.68	0.04	7.02	0.01	59.04	0.24	0.78	25.49	0.00	0.01	0.01	0.01	0.03	99.35
718	6.73	0.01	6.60	0.01	60.14	0.22	0.82	25.03	0.00	0.00	0.00	0.01	0.00	99.57

LV-RD-008-1A1-2 Plagioclase Rim to Rim

Distance (μm)	Na_2O	TiO_2	CaO	MgO	SiO_2	FeO	K_2O	Al_2O_3	F	MnO	Cl	Cr_2O_3	P_2O_5	Total
63	6.94	0.00	6.34	0.00	60.50	0.24	0.87	24.87	0.00	0.02	0.01	0.00	0.00	99.79
95	6.65	0.02	6.73	0.01	59.88	0.19	0.84	25.34	0.00	0.00	0.00	0.01	0.00	99.66
126	6.77	0.03	6.71	0.00	59.76	0.21	0.84	25.03	0.00	0.00	0.00	0.01	0.00	99.36
158	6.70	0.00	6.58	0.00	59.85	0.24	0.83	25.00	0.06	0.00	0.01	0.00	0.03	99.26
189	6.73	0.03	6.03	0.01	60.53	0.20	0.95	24.73	0.02	0.00	0.01	0.01	0.01	99.24
221	6.73	0.00	6.50	0.00	60.12	0.24	0.85	24.82	0.00	0.01	0.00	0.00	0.00	99.28
284	6.74	0.02	6.70	0.01	59.69	0.20	0.85	25.31	0.00	0.00	0.00	0.00	0.00	99.52
315	6.63	0.03	6.12	0.03	60.33	0.20	0.92	24.69	0.00	0.00	0.01	0.00	0.01	98.94

LV-RD-008-1A3 Plagioclase Rim to Rim

Distance (μm)	Na_2O	TiO_2	CaO	MgO	SiO_2	FeO	K_2O	Al_2O_3	F	MnO	Cl	Cr_2O_3	P_2O_5	Total
69	6.88	0.02	6.64	0.00	60.01	0.26	0.84	24.83	0.00	0.04	0.02	0.02	0.02	99.56
104	6.55	0.00	6.81	0.01	59.47	0.18	0.77	25.16	0.16	0.00	0.01	0.00	0.01	99.07
139	6.62	0.07	6.91	0.01	59.75	0.20	0.76	25.11	0.05	0.00	0.01	0.00	0.04	99.50
174	6.57	0.03	7.00	0.00	59.36	0.23	0.75	25.17	0.13	0.00	0.00	0.04	0.00	99.21
208	6.85	0.00	6.40	0.01	60.08	0.15	0.84	24.79	0.00	0.00	0.02	0.00	0.04	99.18
243	6.82	0.01	6.38	0.00	59.74	0.15	0.86	24.88	0.00	0.00	0.02	0.00	0.00	98.85
278	6.64	0.00	6.45	0.01	59.81	0.16	0.80	24.79	0.00	0.02	0.01	0.00	0.00	98.68
312	6.79	0.03	6.42	0.01	60.26	0.21	0.85	24.64	0.05	0.00	0.00	0.00	0.00	99.24
382	5.88	0.01	8.43	0.00	57.08	0.19	0.54	26.93	0.06	0.00	0.01	0.04	0.01	99.15
416	6.62	0.03	6.70	0.00	59.72	0.21	0.79	25.20	0.00	0.02	0.00	0.00	0.00	99.29
451	7.04	0.00	5.93	0.01	60.43	0.18	0.91	24.63	0.03	0.01	0.02	0.02	0.00	99.20
486	6.78	0.00	6.17	0.00	60.94	0.21	0.91	24.57	0.00	0.02	0.02	0.00	0.03	99.11
521	6.85	0.01	6.04	0.00	60.36	0.23	0.89	24.36	0.00	0.00	0.02	0.00	0.00	98.76
555	6.67	0.00	6.61	0.00	59.53	0.19	0.80	25.07	0.00	0.00	0.01	0.01	0.02	98.91
590	6.57	0.00	6.77	0.02	59.62	0.21	0.78	25.02	0.02	0.03	0.04	0.02	0.04	99.12
625	6.80	0.02	6.29	0.00	59.91	0.21	0.94	24.57	24.57	0.10	0.03	0.00	0.06	98.79
659	6.84	0.00	6.21	0.00	60.27	0.21	0.92	24.55	0.00	0.03	0.01	0.00	0.00	99.05

LV-RD-008-2A1-2 Plagioclase Rim to Rim

Distance (μm)	Na_2O	TiO_2	CaO	MgO	SiO_2	FeO	K_2O	Al_2O_3	F	MnO	Cl	Cr_2O_3	P_2O_5	Total
27	6.62	0.02	6.22	0.03	60.37	0.22	0.91	24.72	0.00	0.00	0.00	0.00	0.00	99.11
54	6.82	0.01	6.57	0.00	60.01	0.23	0.85	25.12	0.00	0.00	0.00	0.02	0.00	99.64
108	6.61	0.04	6.73	0.00	59.27	0.24	0.83	24.96	0.00	0.02	0.00	0.00	0.00	98.70
135	6.83	0.01	6.89	0.01	59.89	0.21	0.76	25.27	0.00	0.02	0.01	0.00	0.01	99.90
162	6.44	0.02	7.01	0.01	59.17	0.23	0.75	25.11	0.00	0.01	0.00	0.01	0.02	98.77
189	7.12	0.01	7.06	0.01	59.95	0.22	0.76	25.14	0.00	0.00	0.01	0.03	0.01	100.31
216	6.96	0.05	6.90	0.00	59.77	0.33	0.85	25.00	0.05	0.02	0.00	0.00	0.00	99.91
243	6.83	0.04	7.07	0.00	59.68	0.29	0.76	25.36	0.19	0.02	0.00	0.00	0.00	100.15
270	6.81	0.01	6.81	0.02	59.83	0.34	0.82	25.13	0.00	0.01	0.00	0.00	0.00	99.78

LV-RD-008-2A2 Plagioclase Rim to Rim

Distance (μm)	Na_2O	TiO_2	CaO	MgO	SiO_2	FeO	K_2O	Al_2O_3	F	MnO	Cl	Cr_2O_3	P_2O_5	Total
45	7.25	0.01	5.81	0.03	61.29	0.20	0.68	24.28	0.05	0.00	0.00	0.00	0.00	99.57
91	6.88	0.01	6.27	0.02	60.40	0.20	0.89	24.70	0.06	0.03	0.00	0.00	0.05	99.49
136	6.91	0.05	6.59	0.02	59.65	0.25	0.82	24.88	0.03	0.00	0.00	0.03	0.03	99.25
181	6.74	0.00	7.02	0.01	59.32	0.20	0.80	25.31	0.00	0.00	0.03	0.02	0.01	99.45
317	6.35	0.02	7.36	0.03	59.17	0.23	0.72	25.52	0.03	0.01	0.00	0.00	0.00	99.42
362	4.40	0.01	11.59	0.00	53.56	0.22	0.30	29.68	0.00	0.01	0.00	0.00	0.02	99.77
408	5.65	0.04	9.48	0.01	56.24	0.19	0.47	27.72	0.00	0.00	0.01	0.00	0.02	99.82
453	6.40	0.01	7.36	0.02	59.06	0.21	0.71	25.72	0.00	0.00	0.01	0.00	0.05	99.54
544	6.60	0.00	7.37	0.03	59.19	0.23	0.69	25.85	0.00	0.00	0.01	0.00	0.00	99.95
589	6.33	0.00	7.17	0.01	58.87	0.24	0.76	25.51	0.03	0.01	0.00	0.00	0.02	98.95
634	6.31	0.04	7.18	0.03	59.27	0.24	0.77	25.64	0.00	0.00	0.00	0.00	0.01	99.47
680	6.63	0.02	7.24	0.01	59.13	0.19	0.76	25.67	0.00	0.00	0.00	0.03	0.03	99.72
725	6.37	0.02	7.08	0.00	58.31	0.27	0.74	25.70	0.02	0.00	0.01	0.00	0.03	98.54
770	6.85	0.01	6.57	0.01	60.25	0.26	0.83	25.04	0.00	0.01	0.00	0.00	0.00	99.82
815	6.58	0.01	6.85	0.00	59.86	0.20	0.79	25.15	0.19	0.00	0.00	0.00	0.03	99.58
861	6.70	0.00	6.35	0.02	60.03	0.20	0.90	24.78	0.00	0.00	0.00	0.00	0.02	99.00
906	6.86	0.00	6.14	0.00	60.65	0.21	0.90	24.77	0.00	0.00	0.00	0.02	0.01	99.56

LV-RD-009-1A3 Plagioclase Rim to Rim

Distance (μm)	Na_2O	TiO_2	CaO	MgO	SiO_2	FeO	K_2O	Al_2O_3	F	MnO	Cl	Cr_2O_3	P_2O_5	Total
74	7.23	0.00	5.97	0.02	60.93	0.21	0.85	24.59	0.00	0.01	0.00	0.01	0.00	99.82
111	7.34	0.03	5.84	0.00	60.87	0.21	0.93	24.35	0.00	0.00	0.00	0.00	0.00	99.57
148	7.52	0.02	5.96	0.00	60.19	0.20	0.87	24.52	0.00	0.00	0.00	0.02	0.00	99.30
222	7.48	0.00	5.99	0.00	60.95	0.21	0.88	24.55	0.00	0.01	0.00	0.01	0.00	100.08
296	7.49	0.03	6.33	0.01	60.21	0.23	0.80	24.72	0.00	0.01	0.00	0.00	0.00	99.83
370	7.01	0.01	6.17	0.02	60.56	0.22	0.79	24.47	0.02	0.02	0.00	0.00	0.00	99.27
407	7.26	0.02	5.74	0.01	60.92	0.23	0.89	24.40	0.18	0.01	0.00	0.00	0.00	99.57
481	7.59	0.04	5.92	0.02	60.35	0.23	0.85	24.22	0.06	0.00	0.01	0.00	0.01	99.29
519	7.66	0.01	6.32	0.01	60.56	0.23	0.76	24.95	0.08	0.00	0.00	0.02	0.00	100.56
556	7.30	0.04	6.40	0.03	60.41	0.22	0.79	25.02	0.02	0.00	0.01	0.00	0.00	100.23
630	7.90	0.00	6.18	0.00	60.55	0.22	0.79	25.74	0.00	0.00	0.01	0.01	0.00	101.39
667	7.35	0.01	6.22	0.02	61.11	0.21	0.85	24.56	0.05	0.00	0.00	0.03	0.00	100.39
704	7.12	0.00	6.25	0.02	60.43	0.21	0.79	24.75	0.00	0.00	0.00	0.00	0.00	99.57
778	7.33	0.01	5.95	0.02	60.65	0.22	0.85	24.47	0.00	0.00	0.00	0.01	0.00	99.50
815	6.92	0.04	5.65	0.02	60.24	0.76	0.84	24.13	0.08	0.00	0.00	0.00	0.00	98.64
852	7.13	0.00	6.02	0.00	60.80	0.20	0.90	24.55	0.08	0.00	0.00	0.01	0.00	99.65
889	7.35	0.01	6.22	0.03	60.04	0.17	0.80	24.69	0.00	0.00	0.00	0.00	0.00	99.32
926	7.11	0.05	5.93	0.00	60.91	0.16	0.87	24.47	0.05	0.00	0.01	0.01	0.00	99.53
963	7.25	0.00	5.81	0.00	60.91	0.21	0.91	24.30	0.05	0.03	0.01	0.00	0.00	99.45
1037	7.53	0.00	5.71	0.01	60.21	0.21	0.92	24.38	0.00	0.00	0.00	0.00	0.01	98.97

LV-RD-009-1A4 Plagioclase Rim to Rim

Distance (μm)	Na_2O	TiO_2	CaO	MgO	SiO_2	FeO	K_2O	Al_2O_3	F	MnO	Cl	Cr_2O_3	P_2O_5	Total
15	7.33	0.01	6.14	0.00	60.36	0.42	0.79	24.61	0.13	0.00	0.00	0.01	0.00	99.74
30	7.34	0.00	6.06	0.00	60.68	0.36	0.90	24.57	0.03	0.00	0.01	0.00	0.00	99.92
59	7.46	0.01	5.81	0.00	61.91	0.25	0.91	24.89	0.00	0.01	0.01	0.00	0.00	101.26
74	7.36	0.02	5.78	0.01	61.46	0.58	0.85	24.66	0.00	0.00	0.00	0.00	0.00	100.71
88	7.06	0.00	5.77	0.02	59.97	0.34	0.85	24.31	0.14	0.00	0.01	0.00	0.00	98.39
103	7.23	0.00	5.93	0.00	60.88	0.24	0.80	24.52	0.00	0.00	0.01	0.02	0.00	99.62
118	7.42	0.01	6.04	0.01	61.00	0.21	0.86	24.58	0.26	0.01	0.00	0.00	0.00	100.29
133	7.23	0.01	6.29	0.03	60.50	0.21	0.78	24.45	0.00	0.00	0.01	0.00	0.00	99.50
147	7.19	0.05	6.40	0.01	60.09	0.21	0.76	24.86	0.00	0.02	0.00	0.00	0.00	99.58
162	7.03	0.00	7.00	0.00	59.36	0.25	0.68	25.52	0.13	0.00	0.00	0.00	0.00	99.93
177	6.26	0.02	13.02	0.01	51.61	0.26	0.88	21.03	0.60	0.00	0.06	0.01	6.39	99.90
192	7.05	0.00	6.26	0.00	60.75	0.23	0.82	24.59	0.00	0.00	0.01	0.00	0.00	99.70
206	7.25	0.00	6.17	0.02	60.89	0.19	0.78	24.57	0.00	0.01	0.01	0.01	0.00	99.89
221	7.23	0.02	6.24	0.02	59.89	0.17	0.81	24.77	0.00	0.01	0.00	0.00	0.01	99.18
236	7.13	0.02	6.15	0.02	60.94	0.24	0.82	24.68	0.03	0.01	0.00	0.00	0.00	100.03
251	7.10	0.01	6.09	0.00	60.77	0.22	0.80	24.34	0.08	0.02	0.00	0.02	0.00	99.42
265	7.08	0.00	5.92	0.00	60.45	0.19	0.87	24.48	0.14	0.00	0.00	0.00	0.00	99.07
280	7.11	0.00	5.87	0.00	60.52	0.24	0.90	24.38	0.06	0.00	0.00	0.00	0.00	99.07
295	7.36	0.00	6.07	0.02	60.81	0.24	0.85	24.61	0.18	0.01	0.00	0.00	0.02	100.07
309	7.03	0.04	6.03	0.02	60.53	0.39	0.87	24.55	0.00	0.00	0.00	0.00	0.00	99.46
324	7.32	0.02	6.32	0.00	60.15	0.23	0.79	24.53	0.00	0.00	0.00	0.01	0.00	99.38
339	7.16	0.02	6.21	0.01	60.88	0.18	0.84	24.70	0.00	0.00	0.00	0.01	0.00	100.01
354	7.20	0.00	6.31	0.00	60.37	0.19	0.82	24.62	0.02	0.01	0.00	0.00	0.00	99.51
398	7.16	0.01	6.15	0.02	59.46	0.20	0.81	24.88	0.00	0.00	0.00	0.00	0.00	98.68
413	7.19	0.00	5.93	0.00	59.89	0.20	0.84	24.49	0.00	0.00	0.00	0.01	0.00	98.55
427	7.43	0.00	5.34	0.00	61.71	0.20	0.99	23.92	0.03	0.00	0.00	0.00	0.00	99.62
442	7.32	0.00	5.94	0.01	60.99	0.21	0.88	24.49	0.03	0.00	0.01	0.02	0.00	99.88

LV-RD-009-2A1 Plagioclase Rim to Rim

Distance (μm)	Na_2O	TiO_2	CaO	MgO	SiO_2	FeO	K_2O	Al_2O_3	F	MnO	Cl	Cr_2O_3	P_2O_5	Total
59	7.33	0.02	6.17	0.00	60.01	0.21	0.81	24.52	0.00	0.00	0.00	0.00	0.00	99.08
79	7.18	0.01	6.14	0.00	60.65	0.20	0.86	24.56	0.00	0.00	0.00	0.00	0.00	99.59
98	7.23	0.03	6.01	0.01	60.69	0.20	0.83	24.65	0.02	0.00	0.00	0.00	0.00	99.67
118	7.04	0.01	5.93	0.00	60.37	0.21	0.82	24.43	0.03	0.00	0.01	0.00	0.01	98.86
137	7.34	0.05	6.07	0.00	59.79	0.21	0.82	24.32	0.06	0.00	0.00	0.00	0.00	98.64
157	7.49	0.00	5.90	0.00	60.52	0.21	0.92	24.17	0.10	0.00	0.01	0.00	0.00	99.28
196	7.40	0.03	5.91	0.01	60.21	0.21	0.87	24.51	0.14	0.01	0.00	0.00	0.00	99.24
216	7.09	0.04	6.28	0.00	60.25	0.24	0.78	24.71	0.24	0.00	0.01	0.00	0.00	99.53
236	7.31	0.00	6.05	0.00	60.76	0.18	0.89	24.34	0.11	0.01	0.00	0.01	0.00	99.62
255	7.15	0.02	5.99	0.01	60.85	0.18	0.86	24.47	0.00	0.01	0.01	0.00	0.00	99.55
314	7.24	0.01	6.21	0.01	60.19	0.25	0.81	24.83	0.19	0.01	0.00	0.03	0.00	99.67
334	7.53	0.05	5.19	0.02	61.74	0.19	1.02	23.64	0.02	0.01	0.00	0.03	0.00	99.42
373	7.55	0.00	5.69	0.02	60.36	0.21	0.94	24.15	0.00	0.00	0.00	0.01	0.00	98.92
393	7.49	0.05	5.92	0.01	62.00	0.18	0.96	24.81	0.12	0.02	0.00	0.00	0.00	101.51
412	7.13	0.03	5.79	0.03	60.91	0.22	0.92	24.28	0.11	0.00	0.00	0.00	0.00	99.37
432	7.07	0.05	6.18	0.01	60.55	0.18	0.85	24.56	0.00	0.00	0.00	0.00	0.00	99.45
451	7.28	0.02	6.20	0.01	60.37	0.19	0.78	24.70	0.13	0.00	0.00	0.00	0.00	99.62
471	7.44	0.00	6.07	0.00	60.38	0.20	0.81	24.53	0.00	0.01	0.00	0.00	0.00	99.43
491	7.38	0.03	6.07	0.02	60.45	0.21	0.83	24.41	0.18	0.00	0.00	0.00	0.00	99.48
510	7.19	0.00	6.14	0.01	61.79	0.18	0.86	24.82	0.03	0.00	0.02	0.00	0.00	101.03
550	7.27	0.00	6.12	0.01	60.57	0.23	0.83	24.54	0.00	0.00	0.00	0.03	0.00	99.59
569	7.30	0.00	5.96	0.02	60.94	0.16	0.85	24.34	0.00	0.02	0.00	0.00	0.00	99.59
589	7.34	0.05	6.07	0.03	60.44	0.16	0.78	24.45	0.10	0.00	0.00	0.01	0.00	99.39
608	7.35	0.03	5.98	0.01	60.78	0.19	0.86	24.50	0.13	0.00	0.01	0.00	0.00	99.77
628	7.35	0.00	5.58	0.01	60.53	0.18	0.92	24.07	0.00	0.00	0.00	0.02	0.00	98.65
648	7.24	0.03	5.87	0.01	60.54	0.20	0.93	24.33	0.00	0.00	0.00	0.00	0.02	99.16
667	7.55	0.04	6.05	0.00	60.77	0.22	0.86	24.56	0.05	0.01	0.00	0.00	0.00	100.09
687	7.31	0.01	5.89	0.00	61.13	0.18	0.87	24.17	0.24	0.01	0.00	0.00	0.00	99.70
707	7.37	0.04	6.02	0.01	60.53	0.22	0.87	24.61	0.00	0.00	0.00	0.00	0.00	99.66
726	7.16	0.00	6.14	0.01	60.75	0.24	0.85	24.43	0.00	0.00	0.00	0.00	0.00	99.57
746	7.41	0.03	5.87	0.01	60.80	0.20	0.91	24.55	0.05	0.02	0.01	0.01	0.00	99.84
765	7.37	0.01	5.59	0.00	61.02	0.21	0.92	24.26	0.00	0.03	0.00	0.01	0.00	99.42
785	7.40	0.01	5.76	0.00	61.03	0.20	0.91	24.30	0.00	0.01	0.00	0.00	0.00	99.62

LV-RD-009-2A2 Plagioclase Rim to Rim

Distance (μm)	Na_2O	TiO_2	CaO	MgO	SiO_2	FeO	K_2O	Al_2O_3	F	MnO	Cl	Cr_2O_3	P_2O_5	Total
31	7.45	0.02	5.80	0.01	60.74	0.19	0.90	24.25	0.16	0.01	0.00	0.01	0.00	99.46
61	7.27	0.00	5.77	0.00	60.93	0.20	0.90	24.09	0.00	0.00	0.00	0.00	0.00	99.16
92	7.43	0.04	5.53	0.02	60.88	0.23	0.92	23.94	0.02	0.00	0.00	0.02	0.00	99.02
123	7.38	0.02	5.53	0.00	60.80	0.16	0.93	24.03	0.00	0.01	0.00	0.03	0.00	98.88
215	7.44	0.00	5.60	0.01	60.72	0.18	0.97	24.13	0.08	0.00	0.00	0.00	0.02	99.12
245	7.51	0.00	5.83	0.01	60.72	0.17	0.92	24.13	0.11	0.01	0.00	0.00	0.00	99.36
307	7.30	0.03	5.96	0.00	60.85	0.19	0.87	24.29	0.00	0.00	0.01	0.00	0.01	99.51
337	7.45	0.00	5.98	0.02	60.61	0.18	0.82	24.19	0.05	0.00	0.00	0.00	0.00	99.28
399	7.06	0.00	6.01	0.02	60.02	0.18	0.82	24.70	0.02	0.00	0.00	0.00	0.00	98.83
429	7.30	0.05	5.78	0.02	60.45	0.24	0.92	24.08	0.02	0.00	0.01	0.00	0.00	98.85
460	7.29	0.00	5.62	0.00	60.80	0.24	0.99	24.06	0.02	0.00	0.00	0.02	0.00	99.02
491	7.37	0.00	5.59	0.02	60.83	0.22	0.96	24.17	0.00	0.02	0.00	0.00	0.00	99.18
521	7.41	0.01	5.68	0.00	60.94	0.23	0.92	24.07	0.00	0.00	0.00	0.00	0.00	99.25
613	7.01	0.03	6.25	0.01	60.53	0.24	0.82	24.59	0.00	0.01	0.01	0.00	0.00	99.50
644	7.29	0.00	6.18	0.01	60.50	0.21	0.83	24.66	0.03	0.01	0.00	0.00	0.00	99.71
675	7.13	0.02	6.16	0.01	60.12	0.21	0.86	24.53	0.06	0.02	0.00	0.01	0.00	99.10
705	7.20	0.01	5.81	0.00	60.91	0.22	0.88	24.45	0.00	0.00	0.00	0.00	0.00	99.48
736	7.28	0.02	5.85	0.01	60.52	0.17	0.89	24.23	0.00	0.00	0.00	0.00	0.00	98.96
797	7.52	0.01	5.65	0.02	61.21	0.17	0.89	24.08	0.00	0.00	0.00	0.05	0.00	99.60
828	7.57	0.02	5.73	0.01	60.93	0.20	0.88	24.26	0.08	0.02	0.01	0.00	0.00	99.69
859	7.29	0.05	5.65	0.01	60.68	0.20	0.89	24.28	0.00	0.00	0.00	0.00	0.00	99.03

LV-MR-008-1-1 Plagioclase Core to Rim

Distance (μm)	Na_2O	TiO_2	CaO	MgO	SiO_2	FeO	K_2O	Al_2O_3	F	MnO	Cl	Cr_2O_3	P_2O_5	BaO	Total
21	8.50	0.00	4.83	0.00	61.69	24.26	0.13	0.90	0.00	0.00	0.00	0.01	0.01	0.11	100.43
47	9.09	0.06	4.85	0.00	59.90	23.61	0.19	0.96	0.01	0.00	0.00	0.00	0.03	0.07	98.77
73	9.03	0.03	5.08	0.01	60.03	24.05	0.20	0.88	0.00	0.00	0.00	0.00	0.02	0.08	99.41
99	9.13	0.11	5.39	0.00	59.61	24.22	0.17	0.88	0.00	0.00	0.00	0.00	0.02	0.08	99.61
125	9.16	0.08	5.05	0.00	59.90	23.97	0.09	0.96	0.07	0.00	0.00	0.00	0.00	0.07	99.31
151	9.18	0.00	4.78	0.01	60.24	23.63	0.18	0.96	0.00	0.00	0.00	0.00	0.01	0.03	99.02
177	9.24	0.02	4.86	0.00	60.20	23.83	0.18	1.00	0.00	0.00	0.00	0.00	0.00	0.07	99.41
203	9.18	0.03	4.74	0.01	60.20	23.64	0.15	1.04	0.00	0.00	0.00	0.00	0.01	0.03	99.03
229	9.00	0.03	5.12	0.00	59.65	24.03	0.18	0.90	0.00	0.00	0.00	0.00	0.00	0.06	98.96
255	9.06	0.07	5.18	0.00	59.41	23.93	0.18	0.89	0.00	0.00	0.00	0.00	0.00	0.08	98.78
281	8.46	0.00	4.87	0.00	61.54	23.98	0.09	0.90	0.00	0.00	0.00	0.00	0.00	0.08	99.90
307	9.11	0.06	4.96	0.00	59.92	23.71	0.14	0.93	0.00	0.00	0.00	0.00	0.01	0.12	98.96
333	9.05	0.00	4.86	0.00	60.26	23.58	0.11	0.92	0.06	0.00	0.00	0.00	0.01	0.10	98.92
359	8.69	0.00	5.66	0.00	58.98	24.36	0.13	0.76	0.00	0.00	0.00	0.00	0.02	0.06	98.65
385	9.21	0.00	4.87	0.00	60.04	23.67	0.17	0.94	0.00	0.00	0.00	0.00	0.01	0.08	98.99
411	8.73	0.00	5.88	0.00	58.42	24.48	0.09	0.74	0.13	0.00	0.00	0.00	0.00	0.05	98.47
437	7.98	0.00	7.56	0.00	56.53	26.10	0.16	0.51	0.04	0.00	0.00	0.00	0.03	0.08	98.96
463	8.90	0.00	5.25	0.00	59.44	23.97	0.14	0.90	0.02	0.00	0.00	0.00	0.01	0.14	98.76
489	9.29	0.00	4.58	0.00	60.42	23.41	0.20	1.02	0.00	0.00	0.00	0.00	0.01	0.11	99.04
515	9.28	0.00	4.46	0.00	60.51	23.43	0.16	1.05	0.02	0.00	0.00	0.00	0.01	0.06	98.98
541	8.32	0.06	4.15	0.00	62.02	23.67	0.17	1.07	0.00	0.00	0.00	0.00	0.00	0.16	99.62
567	9.07	0.00	4.11	0.00	60.76	23.11	0.23	1.11	0.00	0.00	0.01	0.00	0.01	0.16	98.56
593	9.04	0.00	4.18	0.01	60.96	23.18	0.16	1.14	0.04	0.00	0.00	0.00	0.01	0.11	98.81
619	8.76	0.02	4.49	0.01	60.03	23.73	0.15	1.02	0.00	0.00	0.00	0.00	0.00	0.15	98.36
645	8.88	0.00	4.60	0.02	60.40	23.73	0.19	0.95	0.00	0.00	0.01	0.00	0.00	0.15	98.92
697	8.87	0.07	4.19	0.01	60.56	23.29	0.23	1.08	0.09	0.00	0.00	0.00	0.00	0.22	98.57
749	8.85	0.08	4.38	0.00	60.50	23.44	0.14	1.00	0.00	0.00	0.00	0.00	0.00	0.16	98.55
801	8.56	0.01	4.11	0.00	62.51	23.33	0.14	1.13	0.00	0.01	0.01	0.00	0.03	0.18	100.00
827	9.26	0.00	4.15	0.00	60.79	23.16	0.18	1.16	0.01	0.00	0.00	0.00	0.01	0.15	98.87
853	9.26	0.08	4.03	0.00	61.16	22.97	0.13	1.27	0.00	0.00	000	0.00	0.01	0.14	99.04
879	9.30	0.04	4.01	0.01	61.45	22.83	0.13	1.22	0.00	0.00	0.00	0.00	0.00	0.05	99.04
905	9.17	0.05	4.17	0.00	60.90	22.95	0.18	1.20	0.00	0.00	0.00	0.00	0.00	0.15	98.76
931	9.32	0.02	4.04	0.00	61.05	22.90	0.16	1.22	0.00	0.00	0.01	0.00	0.00	0.15	98.87
957	9.48	0.00	3.64	0.00	61.93	22.62	0.15	1.33	0.00	0.00	0.01	0.00	0.01	0.14	99.29
983	9.43	0.02	3.74	0.00	61.84	22.88	0.13	1.29	0.00	0.00	0.00	0.00	0.00	0.15	99.49
1009	9.46	0.04	3.96	0.01	61.16	22.69	0.11	1.24	0.00	0.00	0.00	0.00	0.00	0.11	98.78
1035	9.57	0.01	3.64	0.01	61.88	22.64	0.08	1.33	0.00	0.00	0.00	0.00	0.00	0.14	99.29
1061	8.65	0.01	3.77	0.01	62.85	23.37	0.15	1.22	0.00	0.01	0.00	0.00	0.00	0.08	100.11

LV-MR-008-1-1 Plagioclase Core to Rim (continued)

Distance (μm)	Na_2O	TiO_2	CaO	MgO	SiO_2	FeO	K_2O	Al_2O_3	F	MnO	Cl	Cr_2O_3	P_2O_5	BaO	Total
1087	9.30	0.00	4.02	0.00	61.25	22.80	0.16	1.22	0.00	0.00	0.00	0.00	0.00	0.04	98.78
1113	9.42	0.00	3.80	0.00	61.39	23.05	0.19	1.28	0.00	0.00	0.00	0.00	0.00	0.10	99.24
1139	9.53	0.02	3.74	0.00	61.52	22.83	0.15	1.26	0.00	0.00	0.00	0.00	0.00	0.14	99.20
1191	9.25	0.00	4.55	0.00	60.55	23.23	0.16	1.05	0.00	0.00	0.00	0.00	0.00	0.03	98.81
1217	9.48	0.00	3.77	0.00	61.66	22.80	0.17	1.26	0.02	0.00	0.00	0.00	0.01	0.06	99.21
1243	9.47	0.00	3.67	0.00	61.88	22.68	0.14	1.32	0.00	0.00	0.00	0.00	0.00	0.05	99.22

LV-MR-008-1-2 Sanidine Core to Rim

Distance (μm)	Na_2O	TiO_2	CaO	MgO	SiO_2	FeO	K_2O	Al_2O_3	F	MnO	Cl	Cr_2O_3	P_2O_5	BaO	Total
13	4.38	0.00	0.21	0.00	64.41	0.07	11.30	19.10	0.05	0.00	0.00	0.00	0.00	0.70	100.20
41	4.42	0.00	0.20	0.01	63.23	0.08	11.46	19.20	0.00	0.00	0.00	0.00	0.00	0.84	99.44
69	4.46	0.03	0.24	0.02	62.88	0.11	11.32	19.07	0.00	0.00	0.00	0.00	0.01	0.93	99.05
97	4.38	0.05	0.20	0.02	62.90	0.09	11.37	19.23	0.00	0.00	0.00	0.00	0.00	1.12	99.36
125	4.39	0.00	0.25	0.01	62.48	0.13	11.32	19.16	0.00	0.00	0.00	0.00	0.01	1.35	99.09
153	4.35	0.00	0.23	0.00	62.78	0.12	11.18	19.30	0.00	0.00	0.00	0.00	0.00	1.43	99.40
181	4.35	0.01	0.24	0.01	63.16	0.13	11.44	19.21	0.01	0.00	0.00	0.00	0.00	1.04	99.60
209	4.61	0.00	0.20	0.01	63.72	0.06	11.63	18.97	0.00	0.00	0.00	0.00	0.00	0.48	99.67
237	4.38	0.02	0.21	0.01	63.48	0.08	11.59	18.98	0.05	0.00	0.00	0.00	0.00	0.48	99.25
265	4.46	0.00	0.20	0.02	63.67	0.10	11.46	19.23	0.04	0.00	0.00	0.00	0.00	0.62	99.77
293	4.11	0.00	0.20	0.00	64.48	0.06	10.82	19.24	0.00	0.00	0.00	0.00	0.00	0.65	99.57
321	4.40	0.02	0.20	0.00	62.88	0.12	11.49	19.02	0.00	0.00	0.00	0.00	0.00	0.90	99.01
349	4.44	0.00	0.21	0.00	63.24	0.13	11.70	18.98	0.00	0.00	0.00	0.00	0.00	0.50	99.20
377	4.41	0.00	0.22	0.00	63.60	0.11	11.43	18.97	0.00	0.00	0.00	0.00	0.00	0.68	99.43
405	4.46	0.02	0.21	0.00	63.01	0.12	11.41	19.12	0.00	0.00	0.00	0.00	0.00	0.89	99.25
433	4.37	0.03	0.21	0.00	62.88	0.10	11.36	19.05	0.00	0.00	0.00	0.00	0.00	1.07	99.07
461	4.45	0.00	0.20	0.00	62.85	0.10	11.22	19.19	0.00	0.00	0.00	0.00	0.00	1.13	99.14
489	4.42	0.00	0.22	0.00	63.27	0.09	11.38	19.17	0.00	0.00	0.00	0.00	0.00	0.85	99.41
517	4.49	0.00	0.21	0.00	63.01	0.11	11.34	19.24	0.00	0.00	0.00	0.00	0.00	1.06	99.46
545	4.32	0.00	0.22	0.00	63.11	0.04	11.59	18.94	0.00	0.00	0.00	0.00	0.00	0.80	99.00
573	4.40	0.05	0.20	0.00	64.17	0.06	11.20	19.07	0.00	0.00	0.00	0.00	0.00	0.54	99.69
601	4.43	0.00	0.21	0.00	63.93	0.05	11.61	19.18	0.00	0.00	0.00	0.00	0.00	0.29	99.70
629	4.59	0.01	0.21	0.00	63.83	0.06	11.58	19.14	0.01	0.00	0.00	0.00	0.00	0.30	99.73
657	4.50	0.00	0.18	0.00	63.72	0.01	11.64	19.06	0.00	0.00	0.00	0.00	0.00	0.17	99.27
685	4.55	0.00	0.19	0.00	63.66	0.02	11.73	19.04	0.00	0.00	0.00	0.00	0.00	0.23	99.43
713	4.50	0.02	0.19	0.00	63.57	0.07	11.75	18.96	0.00	0.00	0.00	0.00	0.00	0.28	99.33
741	4.46	0.03	0.18	0.00	63.77	0.09	11.64	19.01	0.00	0.00	0.00	0.00	0.00	0.29	99.47
769	4.47	0.02	0.20	0.00	63.34	0.03	11.54	18.90	0.00	0.00	0.00	0.00	0.00	0.53	99.02
797	4.45	0.05	0.19	0.00	63.50	0.03	11.68	19.07	0.00	0.00	0.00	0.00	0.00	0.46	99.42
825	4.46	0.09	0.17	0.00	63.78	0.09	11.74	18.99	0.00	0.00	0.00	0.00	0.00	0.35	99.67
853	4.19	0.07	0.18	0.01	64.69	0.05	11.18	19.00	0.00	0.00	0.01	0.00	0.00	0.52	99.89
881	4.41	0.00	0.20	0.00	63.54	0.08	11.66	18.83	0.14	0.01	0.01	0.00	0.00	0.36	99.17
909	4.40	0.02	0.20	0.00	63.34	0.05	11.60	18.94	0.00	0.00	0.01	0.00	0.00	0.47	99.02
937	4.43	0.02	0.18	0.00	63.12	0.08	11.69	18.83	0.00	0.00	0.00	0.00	0.01	0.48	98.84
965	4.39	0.01	0.20	0.00	63.44	0.10	11.54	18.92	0.00	0.00	0.00	0.00	0.00	0.56	99.14
993	4.43	0.01	0.21	0.00	63.49	0.05	11.55	18.99	0.01	0.00	0.00	0.00	0.00	0.57	99.30
1021	4.51	0.02	0.18	0.00	63.52	0.07	11.76	19.00	0.08	0.00	0.01	0.00	0.00	0.50	99.61
1049	4.40	0.13	0.20	0.00	63.25	0.06	11.61	18.83	0.07	0.00	0.00	0.00	0.00	0.49	99.01

LV-MR-008-1-2 Sanidine Core to Rim (continued)

Distance (μm)	Na_2O	TiO_2	CaO	MgO	SiO_2	FeO	K_2O	Al_2O_3	F	MnO	Cl	Cr_2O_3	P_2O_5	BaO	Total
1021	4.51	0.02	0.18	0.00	63.52	0.07	11.76	19.00	0.08	0.00	0.01	0.00	0.00	0.50	99.61
1049	4.40	0.13	0.20	0.00	63.25	0.06	11.61	18.83	0.07	0.00	0.00	0.00	0.00	0.49	99.01
1077	4.35	0.04	0.19	0.00	63.35	0.11	11.61	18.95	0.01	0.01	0.00	0.00	0.00	0.55	99.15
1105	4.45	0.00	0.18	0.00	63.59	0.03	11.55	18.87	0.08	0.00	0.00	0.00	0.00	0.52	99.25
1133	4.02	0.07	0.21	0.00	64.54	0.04	11.06	19.06	0.00	0.00	0.00	0.00	0.01	0.59	99.59
1161	4.22	0.03	0.22	0.00	63.08	0.05	11.43	18.81	0.00	0.00	0.00	0.00	0.00	0.50	98.34
1189	4.31	0.03	0.21	0.00	63.41	0.06	11.42	19.01	0.00	0.00	0.00	0.00	0.00	0.57	99.02
1217	4.27	0.00	0.19	0.00	63.51	0.04	11.43	18.97	0.00	0.00	0.00	0.00	0.00	0.50	98.91
1245	4.34	0.07	0.20	0.00	63.24	0.01	11.36	18.96	0.00	0.00	0.00	0.00	0.00	0.46	98.62

LV-MR-008-1-4-1 Plagioclase Core to Rim

Distance (μm)	Na_2O	TiO_2	CaO	MgO	SiO_2	FeO	K_2O	Al_2O_3	F	MnO	Cl	Cr_2O_3	P_2O_5	BaO	Total
60	9.65	0.00	4.14	0.01	60.62	0.22	1.22	22.95	0.06	0.00	0.00	0.00	0.05	0.00	98.89
96	7.57	0.00	8.35	0.00	55.50	0.11	0.43	26.67	0.08	0.00	0.00	0.00	0.01	0.01	98.70
132	9.46	0.00	4.78	0.00	60.11	0.20	0.98	23.57	0.00	0.00	0.00	0.00	0.00	0.00	99.10
168	9.38	0.00	4.61	0.00	60.45	0.18	1.10	23.32	0.00	0.00	0.00	0.00	0.02	0.01	99.07
276	9.59	0.00	4.30	0.00	60.82	0.10	1.15	23.11	0.09	0.00	0.00	0.00	0.01	0.00	99.14
312	9.54	0.00	4.18	0.00	61.16	0.15	1.19	23.04	0.00	0.00	0.00	0.00	0.03	0.00	99.28
348	9.46	0.00	4.51	0.00	60.58	0.13	1.10	23.32	0.00	0.00	0.00	0.00	0.07	0.01	99.16
384	7.20	0.00	8.01	0.00	56.23	0.24	0.48	26.67	0.00	0.00	0.00	0.00	0.07	0.01	98.90
420	9.06	0.00	5.15	0.00	59.68	0.17	0.77	23.77	0.00	0.00	0.00	0.00	0.06	0.00	98.66
456	8.97	0.00	5.46	0.00	59.54	0.22	0.84	24.14	0.00	0.00	0.00	0.00	0.06	0.01	99.24
492	8.97	0.00	4.42	0.00	61.00	0.18	1.03	23.28	0.00	0.00	0.00	0.00	0.11	0.00	98.99
528	9.06	0.00	4.55	0.00	60.68	0.20	1.03	23.61	0.01	0.00	0.00	0.00	0.01	0.01	99.16
564	9.32	0.06	4.49	0.00	60.57	0.16	1.05	23.58	0.00	0.00	0.00	0.00	0.02	0.00	99.26
600	9.33	0.00	4.04	0.00	61.56	0.14	1.19	23.04	0.00	0.00	0.00	0.00	0.06	0.00	99.35
636	9.31	0.00	4.02	0.00	61.66	0.16	1.22	22.91	0.00	0.00	0.00	0.00	0.06	0.00	99.33
672	8.57	0.00	6.03	0.01	58.74	0.21	0.79	24.48	0.00	0.00	0.00	0.00	0.06	0.00	98.89
708	9.52	0.00	4.09	0.01	61.22	0.19	1.20	22.88	0.00	0.00	0.00	0.00	0.03	0.00	99.14
744	9.29	0.00	4.29	0.02	61.63	0.15	1.10	23.35	0.00	0.00	0.00	0.00	0.07	0.01	99.91
780	9.55	0.00	4.18	0.02	61.17	0.15	1.14	23.13	0.00	0.00	0.01	0.00	0.02	0.00	99.36
816	8.95	0.04	5.52	0.01	59.33	0.14	0.84	24.34	0.00	0.00	0.00	0.00	0.04	0.02	99.23
888	9.65	0.02	4.16	0.01	61.21	0.17	1.25	23.21	0.00	0.00	0.00	0.00	0.05	0.03	99.76

LV-MR-008-1-5-1 Plagioclase Rim to Core

Distance (μm)	Na_2O	TiO_2	CaO	MgO	SiO_2	FeO	K_2O	Al_2O_3	F	MnO	Cl	Cr_2O_3	P_2O_5	BaO	Total
32	8.83	0.00	3.57	0.00	62.79	0.08	1.27	22.98	0.08	0.00	0.00	0.00	0.02	0.04	99.62
60	9.50	0.02	3.73	0.00	61.39	0.12	1.35	22.63	0.06	0.00	0.00	0.00	0.00	0.05	98.83
88	9.61	0.00	3.67	0.00	61.53	0.12	1.32	22.61	0.00	0.00	0.00	0.00	0.00	0.08	98.94
116	9.53	0.01	3.53	0.00	61.70	0.08	1.36	22.48	0.01	0.00	0.00	0.00	0.00	0.03	98.72
144	9.57	0.00	3.86	0.00	61.33	0.12	1.24	22.65	0.07	0.00	0.00	0.00	0.00	0.08	98.89
172	9.67	0.00	3.68	0.00	61.57	0.12	1.29	22.60	0.00	0.00	0.00	0.00	0.00	0.09	99.02
200	9.64	0.00	3.77	0.00	61.42	0.10	1.32	22.78	0.00	0.00	0.00	0.00	0.01	0.03	99.09
228	9.60	0.00	3.68	0.00	61.42	0.12	1.29	22.70	0.00	0.00	0.00	0.00	0.00	0.02	98.83
256	9.37	0.00	3.97	0.00	61.24	0.11	1.24	22.84	0.00	0.00	0.00	0.00	0.00	0.07	98.85
284	9.39	0.00	3.85	0.00	61.18	0.12	1.26	22.94	0.00	0.00	0.00	0.00	0.00	0.03	98.77
312	8.86	0.00	3.82	0.02	62.32	0.16	1.26	23.30	0.00	0.00	0.01	0.00	0.00	0.09	99.83
340	9.59	0.02	3.95	0.01	61.41	0.14	1.25	22.90	0.00	0.00	0.00	0.00	0.00	0.06	99.34
368	9.60	0.00	3.93	0.01	61.27	0.16	1.22	22.67	0.00	0.00	0.00	0.00	0.00	0.12	98.99
396	9.38	0.04	4.05	0.02	61.26	0.14	1.15	22.92	0.00	0.00	0.00	0.00	0.00	0.16	99.13
424	9.53	0.00	4.28	0.01	60.98	0.15	1.12	23.02	0.00	0.00	0.01	0.00	0.02	0.07	99.19
452	9.49	0.03	3.95	0.00	61.14	0.19	1.25	22.74	0.00	0.00	0.00	0.00	0.01	0.08	98.89
480	9.60	0.03	4.29	0.02	60.69	0.19	1.15	22.91	0.00	0.00	0.00	0.00	0.00	0.05	98.93
508	9.43	0.03	4.30	0.01	60.92	0.13	1.16	23.16	0.00	0.00	0.00	0.00	0.01	0.13	99.27
536	9.21	0.04	4.38	0.02	60.62	0.18	1.09	23.36	0.00	0.00	0.01	0.00	0.00	0.11	99.00
564	9.29	0.00	4.35	0.02	60.73	0.16	1.16	23.09	0.00	0.00	0.01	0.00	0.00	0.12	98.92

LV-MR-008-1-5-2 Plagioclase Core to Rim

Distance (μm)	Na_2O	TiO_2	CaO	MgO	SiO_2	FeO	K_2O	Al_2O_3	F	MnO	Cl	Cr_2O_3	P_2O_5	BaO	Total
34	8.03	0.00	5.83	0.00	59.91	0.15	0.72	25.05	0.00	0.00	0.00	0.00	0.02	0.06	99.77
60	8.40	0.02	6.34	0.01	58.19	0.17	0.70	25.07	0.00	0.00	0.00	0.00	0.04	0.09	99.02
86	8.85	0.01	5.53	0.00	59.24	0.18	0.81	24.34	0.00	0.00	0.00	0.00	0.02	0.11	99.08
112	8.68	0.00	5.73	0.00	59.15	0.17	0.81	24.52	0.00	0.00	0.00	0.00	0.01	0.11	99.18
138	8.76	0.04	5.74	0.00	58.56	0.11	0.79	24.70	0.00	0.00	0.00	0.00	0.02	0.08	98.82
164	8.78	0.00	5.63	0.00	59.57	0.15	0.82	24.24	0.00	0.00	0.00	0.00	0.01	0.06	99.26
190	9.25	0.00	4.88	0.01	60.02	0.13	0.96	23.73	0.00	0.00	0.00	0.00	0.03	0.06	99.08
216	9.28	0.07	4.34	0.00	60.78	0.14	1.11	23.22	0.00	0.00	0.00	0.00	0.01	0.09	99.04
242	9.30	0.06	3.77	0.00	61.59	0.16	1.25	22.90	0.00	0.00	0.01	0.00	0.01	0.06	99.11
268	9.48	0.00	3.97	0.00	61.26	0.17	1.25	22.99	0.12	0.00	0.00	0.00	0.01	0.00	99.21
294	8.52	0.00	3.45	0.01	62.93	0.15	1.40	22.90	0.00	0.00	0.01	0.00	0.00	0.06	99.43
320	9.48	0.03	3.69	0.01	61.90	0.13	1.34	22.63	0.00	0.00	0.00	0.00	0.00	0.10	99.31
346	9.34	0.01	3.79	0.01	61.64	0.11	1.28	22.88	0.00	0.00	0.01	0.00	0.00	0.07	99.14
372	9.16	0.00	3.97	0.00	61.24	0.15	1.21	22.93	0.01	0.00	0.00	0.00	0.00	0.04	98.72
398	9.29	0.00	3.83	0.01	61.80	0.14	1.27	22.79	0.00	0.00	0.01	0.00	0.00	0.03	99.16
424	9.43	0.02	3.65	0.01	61.58	0.14	1.28	22.72	0.00	0.00	0.00	0.00	0.00	0.07	98.91
450	9.25	0.00	3.98	0.00	61.26	0.12	1.26	22.89	0.00	0.00	0.00	0.00	0.00	0.12	98.89
476	9.15	0.00	3.81	0.01	61.43	0.16	1.22	22.73	0.00	0.00	0.00	0.00	0.00	0.07	98.58
502	9.28	0.02	4.42	0.01	60.51	0.17	1.04	23.12	0.00	0.00	0.00	0.00	0.00	0.07	98.64
528	9.40	0.00	3.90	0.00	61.20	0.12	1.24	22.88	0.00	0.00	0.00	0.00	0.00	0.07	98.80
554	8.77	0.08	3.48	0.00	63.11	0.19	1.21	23.17	0.02	0.00	0.00	0.00	0.01	0.05	100.08
580	9.16	0.05	4.48	0.01	60.82	0.20	1.12	23.38	0.06	0.00	0.00	0.00	0.00	0.03	99.28
606	9.27	0.03	3.98	0.00	61.33	0.17	1.19	23.11	0.05	0.00	0.00	0.00	0.01	0.05	99.17
632	9.15	0.13	4.08	0.01	61.14	0.21	1.19	23.01	0.00	0.00	0.00	0.00	0.00	0.06	98.99

LV-MR-008-1-6-1 Plagioclase Rim to Rim

Distance (μm)	Na_2O	TiO_2	CaO	MgO	SiO_2	FeO	K_2O	Al_2O_3	F	MnO	Cl	Cr_2O_3	P_2O_5	BaO	Total
30	8.71	0.00	3.93	0.00	62.71	0.12	1.19	23.45	0.00	0.00	0.01	0.00	0.01	0.06	100.18
58	9.41	0.00	4.67	0.00	60.25	0.18	1.05	23.58	0.07	0.00	0.01	0.00	0.02	0.11	99.31
86	9.46	0.00	4.16	0.01	60.95	0.18	1.16	23.21	0.08	0.00	0.00	0.00	0.02	0.09	99.29
114	9.57	0.02	4.34	0.01	60.91	0.14	1.16	23.23	0.00	0.00	0.01	0.00	0.02	0.14	99.55
142	9.44	0.04	4.12	0.00	61.26	0.22	1.19	23.08	0.00	0.00	0.00	0.00	0.00	0.04	99.40
170	9.52	0.00	4.29	0.01	61.04	0.18	1.17	23.25	0.14	0.00	0.00	0.00	0.00	0.08	99.62
198	9.44	0.02	4.05	0.00	61.43	0.15	1.18	23.20	0.08	0.00	0.00	0.00	0.01	0.09	99.62
226	9.50	0.07	3.76	0.01	61.64	0.15	1.29	22.88	0.00	0.00	0.01	0.00	0.00	0.12	99.41
254	9.58	0.03	3.77	0.00	61.66	0.16	1.33	22.85	0.04	0.00	0.01	0.00	0.00	0.05	99.46
282	9.53	0.04	3.91	0.00	61.29	0.19	1.28	22.91	0.15	0.00	0.01	0.00	0.01	0.06	99.29
310	9.21	0.07	3.60	0.00	62.71	0.17	1.35	23.24	0.14	0.00	0.01	0.00	0.00	0.00	100.43
338	9.40	0.00	4.21	0.00	60.86	0.17	1.20	23.15	0.19	0.00	0.01	0.00	0.00	0.02	99.11
366	9.56	0.00	4.00	0.00	61.14	0.13	1.24	22.80	0.06	0.00	0.01	0.00	0.00	0.03	98.94
394	9.54	0.00	3.96	0.00	61.18	0.17	1.22	23.03	0.07	0.00	0.00	0.00	0.01	0.04	99.19

LV-MR-008-1-6-2 Plagioclase Rim to Rim

Distance (μm)	Na_2O	TiO_2	CaO	MgO	SiO_2	FeO	K_2O	Al_2O_3	F	MnO	Cl	Cr_2O_3	P_2O_5	BaO	Total
39	8.57	0.02	3.98	0.02	62.40	0.19	1.18	23.48	0.01	0.00	0.00	0.00	0.00	0.03	99.87
75	9.33	0.11	4.18	0.01	60.74	0.18	1.23	22.81	0.00	0.00	0.00	0.00	0.03	0.02	98.64
111	9.52	0.06	4.05	0.01	61.23	0.18	1.21	22.98	0.13	0.00	0.01	0.00	0.00	0.03	99.36
147	9.40	0.00	4.27	0.01	61.14	0.15	1.19	23.00	0.00	0.00	0.01	0.00	0.02	0.06	99.24
183	9.43	0.00	4.12	0.02	61.25	0.15	1.22	23.00	0.09	0.00	0.01	0.00	0.02	0.03	99.28
219	9.41	0.02	3.96	0.01	61.01	0.13	1.27	22.72	0.00	0.00	0.00	0.00	0.01	0.06	98.60
255	9.66	0.03	3.94	0.02	61.42	0.20	1.28	22.79	0.00	0.00	0.00	0.00	0.01	0.06	99.41
291	9.58	0.03	4.05	0.01	61.14	0.19	1.26	22.83	0.00	0.00	0.00	0.00	0.04	0.01	99.12
327	9.43	0.13	4.22	0.01	61.01	0.20	1.20	23.09	0.01	0.00	0.00	0.00	0.01	0.05	99.35
363	9.70	0.02	3.75	0.01	61.66	0.20	1.37	22.39	0.08	0.00	0.01	0.00	0.01	0.04	99.18

LV-MR-008-1-7-2 Plagioclase Rim to Rim

Distance (μm)	Na_2O	TiO_2	CaO	MgO	SiO_2	FeO	K_2O	Al_2O_3	F	MnO	Cl	Cr_2O_3	P_2O_5	BaO	Total
22	8.62	0.00	4.91	0.00	60.41	0.16	0.81	23.90	0.00	0.00	0.01	0.00	0.00	0.00	98.81
52	9.16	0.00	4.93	0.00	59.95	0.21	0.96	23.57	0.06	0.00	0.00	0.00	0.00	0.02	98.83
82	8.89	0.05	5.61	0.00	59.40	0.16	0.82	24.02	0.05	0.00	0.00	0.00	0.01	0.00	98.99
112	9.09	0.00	5.35	0.00	59.16	0.23	0.84	23.82	0.00	0.00	0.00	0.00	0.01	0.02	98.53
142	8.84	0.00	5.67	0.00	58.98	0.22	0.79	24.21	0.00	0.00	0.00	0.00	0.00	0.02	98.72
172	9.57	0.00	4.43	0.00	60.92	0.15	1.13	22.97	0.00	0.00	0.00	0.00	0.01	0.02	99.19
202	9.28	0.00	4.67	0.00	60.33	0.14	1.03	23.45	0.01	0.00	0.00	0.00	0.00	0.02	98.92
262	9.05	0.00	4.06	0.00	63.57	0.20	1.02	22.25	0.00	0.00	0.01	0.00	0.00	0.01	100.17
292	9.71	0.00	4.34	0.00	60.69	0.17	1.11	22.97	0.00	0.00	0.00	0.00	0.01	0.00	99.00
322	8.50	0.04	5.98	0.02	59.04	0.11	0.76	24.84	0.00	0.00	0.00	0.00	0.00	0.07	99.35
352	9.65	0.10	4.46	0.01	60.67	0.12	1.07	23.34	0.00	0.00	0.00	0.00	0.00	0.02	99.44
382	9.85	0.07	4.49	0.01	60.57	0.13	1.08	23.49	0.00	0.00	0.00	0.00	0.00	0.02	99.70
412	10.02	0.06	3.57	0.00	61.50	0.07	1.36	22.42	0.04	0.00	0.00	0.00	0.01	0.10	99.11
442	10.04	0.04	3.62	0.00	61.58	0.12	1.34	22.52	0.00	0.00	0.00	0.00	0.00	0.04	99.29
472	9.76	0.07	4.05	0.01	61.14	0.11	1.17	23.01	0.02	0.00	0.00	0.00	0.01	0.03	99.38
502	9.87	0.10	3.95	0.00	61.46	0.11	1.34	22.80	0.00	0.00	0.00	0.00	0.01	0.06	99.69
532	9.81	0.05	4.04	0.00	61.21	0.14	1.25	23.12	0.02	0.00	0.00	0.00	0.02	0.05	99.69
562	9.84	0.08	3.89	0.00	61.26	0.18	1.36	22.81	0.00	0.00	0.00	0.00	0.01	0.05	99.48
592	9.86	0.00	3.63	0.00	61.62	0.12	1.39	22.63	0.00	0.00	0.00	0.00	0.00	0.05	99.29
622	9.03	0.09	3.74	0.00	62.82	0.17	1.19	23.20	0.06	0.00	0.00	0.00	0.00	0.02	100.29
652	9.80	0.05	3.99	0.01	61.15	0.17	1.22	23.03	0.00	0.00	0.00	0.00	0.01	0.03	99.46
682	9.60	0.02	4.03	0.00	61.22	0.14	1.20	23.01	0.06	0.00	0.00	0.00	0.01	0.07	99.32
712	9.93	0.00	3.78	0.00	61.47	0.16	1.21	22.79	0.00	0.00	0.00	0.00	0.02	0.09	99.43
742	9.74	0.03	4.38	0.00	60.70	0.16	1.10	23.23	0.06	0.00	0.00	0.00	0.00	0.11	99.49

LV-MR-008-1-10 Plagioclase Core to Rim

Distance (μm)	Na_2O	TiO_2	CaO	MgO	SiO_2	FeO	K_2O	Al_2O_3	F	MnO	Cl	Cr_2O_3	P_2O_5	BaO	Total
27	8.62	0.00	3.81	0.00	62.74	0.14	1.11	23.66	0.00	0.00	0.01	0.00	0.00	0.16	100.23
89	9.45	0.00	4.09	0.00	60.89	0.17	1.10	23.30	0.00	0.00	0.01	0.00	0.00	0.14	99.13
151	9.22	0.00	4.51	0.00	60.09	0.13	0.88	23.29	0.01	0.00	0.00	0.00	0.01	0.12	98.25
182	9.24	0.00	4.06	0.00	60.42	0.12	1.12	23.18	0.00	0.00	0.01	0.00	0.00	0.15	98.28
213	9.24	0.00	4.10	0.00	60.68	0.15	1.10	23.37	0.00	0.00	0.00	0.00	0.00	0.15	98.78
244	8.94	0.00	4.66	0.00	59.66	0.10	0.96	23.83	0.00	0.00	0.00	0.00	0.00	0.19	98.34
337	8.88	0.00	3.58	0.00	63.97	0.20	0.84	22.28	0.00	0.00	0.01	0.00	0.00	0.04	99.80
368	9.32	0.00	4.27	0.02	60.91	0.18	1.11	22.78	0.00	0.00	0.00	0.00	0.01	0.07	98.66
399	9.39	0.02	4.02	0.00	61.32	0.16	1.18	22.80	0.00	0.00	0.00	0.00	0.00	0.06	98.95
430	9.47	0.00	4.20	0.00	60.95	0.17	1.20	23.09	0.00	0.00	0.00	0.00	0.00	0.10	99.17
461	8.59	0.00	6.14	0.00	58.36	0.12	0.80	24.55	0.00	0.00	0.01	0.00	0.01	0.04	98.62
492	9.16	0.04	4.33	0.01	60.81	0.11	1.10	23.03	0.02	0.00	0.01	0.00	0.01	0.05	98.65
523	9.35	0.00	4.13	0.00	60.90	0.14	1.17	22.96	0.00	0.00	0.01	0.00	0.00	0.04	98.70
585	9.36	0.02	4.24	0.01	60.87	0.15	1.17	22.87	0.00	0.00	0.00	0.00	0.00	0.05	98.74
616	9.30	0.00	4.48	0.00	60.92	0.15	1.07	23.06	0.00	0.00	0.01	0.00	0.01	0.07	99.07
647	8.71	0.01	4.00	0.00	62.62	0.19	1.01	23.39	0.02	0.00	0.00	0.00	0.01	0.08	100.02
678	9.41	0.00	4.14	0.00	61.21	0.13	0.94	23.05	0.00	0.00	0.00	0.00	0.02	0.04	98.94
740	7.11	0.01	8.83	0.00	54.91	0.14	0.42	27.18	0.04	0.00	0.00	0.00	0.01	0.11	98.75
771	7.80	0.00	7.63	0.00	56.65	0.17	0.56	26.25	0.00	0.00	0.00	0.00	0.03	0.10	99.18

LV-MR-005-1-2 Plagioclase Rim to Rim

Distance (μm)	Na_2O	TiO_2	CaO	MgO	SiO_2	FeO	K_2O	Al_2O_3	F	MnO	Cl	Cr_2O_3	P_2O_5	BaO	Total
59	9.47	0.00	4.41	0.00	61.07	0.13	1.11	23.25	0.00	0.00	0.00	0.00	0.00	0.04	99.47
87	9.53	0.00	3.78	0.01	61.36	0.15	1.20	22.90	0.06	0.00	0.00	0.00	0.00	0.04	99.00
115	9.26	0.00	4.36	0.00	61.19	0.09	1.11	23.07	0.08	0.00	0.00	0.00	0.00	0.09	99.23
143	9.35	0.04	4.37	0.00	60.93	0.12	1.08	23.23	0.04	0.00	0.00	0.00	0.00	0.02	99.15
171	9.25	0.01	4.31	0.00	60.95	0.15	1.10	23.25	0.14	0.00	0.01	0.00	0.00	0.02	99.13
199	9.39	0.00	4.35	0.00	60.86	0.17	1.11	23.22	0.02	0.00	0.00	0.00	0.00	0.02	99.14
227	9.51	0.00	4.29	0.00	61.13	0.11	1.17	23.27	0.09	0.00	0.01	0.00	0.00	0.06	99.60
255	9.49	0.00	4.30	0.00	60.86	0.16	1.10	23.13	0.01	0.00	0.00	0.00	0.00	0.02	99.06
283	9.52	0.00	4.24	0.00	61.12	0.11	1.14	23.25	0.11	0.00	0.00	0.00	0.00	0.05	99.49
311	9.00	0.00	4.27	0.00	61.63	0.18	1.14	23.27	0.17	0.00	0.00	0.00	0.00	0.03	99.61
339	9.59	0.00	4.23	0.00	61.03	0.16	1.13	23.19	0.01	0.00	0.00	0.00	0.00	0.05	99.39
367	9.38	0.00	4.39	0.02	61.02	0.15	1.09	23.29	0.07	0.00	0.00	0.00	0.00	0.06	99.42
395	9.39	0.00	4.33	0.01	60.99	0.16	1.14	23.27	0.11	0.00	0.01	0.00	0.00	0.06	99.42
423	9.70	0.00	4.38	0.01	61.01	0.19	1.14	23.07	0.09	0.00	0.00	0.00	0.00	0.09	99.62
451	9.49	0.01	4.01	0.02	61.25	0.17	1.22	22.95	0.12	0.00	0.01	0.00	0.00	0.08	99.27
479	9.60	0.00	4.15	0.01	61.18	0.15	1.17	22.94	0.00	0.00	0.00	0.00	0.00	0.03	99.22
507	9.60	0.01	4.32	0.02	61.07	0.15	1.14	23.21	0.04	0.00	0.00	0.00	0.00	0.06	99.59
535	9.44	0.00	4.23	0.01	61.05	0.11	1.17	22.96	0.14	0.00	0.00	0.00	0.00	0.08	99.12
563	9.39	0.00	4.42	0.02	60.86	0.16	1.11	23.05	0.00	0.00	0.00	0.00	0.00	0.07	99.08
591	9.01	0.06	4.09	0.00	61.91	0.14	1.17	23.42	0.00	0.00	0.00	0.00	0.02	0.00	99.82
619	9.33	0.02	4.00	0.01	61.17	0.11	1.14	22.88	0.00	0.00	0.00	0.00	0.01	0.04	98.71
647	9.57	0.02	3.77	0.00	61.38	0.17	1.22	22.88	0.00	0.00	0.00	0.00	0.01	0.06	99.08
675	9.76	0.09	3.81	0.02	61.49	0.18	1.12	23.04	0.00	0.00	0.00	0.00	0.01	0.03	99.55
703	9.24	0.06	4.49	0.01	60.47	0.14	1.05	23.40	0.00	0.00	0.00	0.00	0.00	0.02	98.89
731	9.65	0.02	4.19	0.01	61.03	0.18	1.10	23.12	0.00	0.00	0.00	0.00	0.00	0.00	99.31
759	9.29	0.00	4.26	0.03	60.90	0.15	1.05	23.42	0.01	0.00	0.00	0.00	0.00	0.05	99.16
787	9.77	0.02	4.30	0.00	60.90	0.15	1.06	23.26	0.00	0.01	0.00	0.00	0.01	0.03	99.51
815	9.54	0.02	4.18	0.01	61.09	0.17	1.10	23.30	0.00	0.00	0.00	0.00	0.00	0.03	99.43
843	9.35	0.01	4.61	0.00	60.28	0.16	1.04	23.56	0.00	0.00	0.00	0.00	0.02	0.07	99.10
871	9.37	0.03	4.57	0.00	61.55	0.14	1.10	23.62	0.00	0.00	0.00	0.00	0.00	0.01	100.39
899	9.82	0.08	4.28	0.00	61.50	0.16	1.17	23.19	0.00	0.00	0.00	0.00	0.00	0.06	100.27
927	9.64	0.06	4.18	0.00	61.23	0.18	1.18	22.99	0.00	0.00	0.00	0.00	0.00	0.06	99.52

LV-MR-005-1-3 Plagioclase Core to Rim

Distance (μm)	Na_2O	TiO_2	CaO	MgO	SiO_2	FeO	K_2O	Al_2O_3	F	MnO	Cl	Cr_2O_3	P_2O_5	BaO	Total
32	4.18	0.02	9.57	0.01	57.61	0.14	0.26	26.86	0.20	0.00	0.00	0.00	0.03	0.07	98.85
60	5.92	0.02	9.48	0.00	56.77	0.09	0.27	26.55	0.01	0.00	0.00	0.00	0.03	0.07	99.19
88	5.72	0.02	8.29	0.02	58.92	0.11	0.34	25.65	0.04	0.00	0.00	0.00	0.02	0.13	99.22
116	6.47	0.00	8.93	0.01	57.25	0.13	0.29	26.08	0.07	0.00	0.00	0.00	0.02	0.12	99.34
144	6.91	0.00	9.42	0.00	56.00	0.12	0.26	26.54	0.01	0.00	0.00	0.00	0.05	0.13	99.42
172	6.63	0.10	10.16	0.00	55.43	0.11	0.21	27.03	0.07	0.00	0.00	0.00	0.01	0.08	99.79
200	7.05	0.13	9.43	0.00	56.23	0.09	0.25	26.32	0.05	0.00	0.00	0.00	0.04	0.05	99.61
228	7.34	0.02	8.92	0.01	56.57	0.09	0.28	25.87	0.00	0.00	0.00	0.00	0.02	0.09	99.21
256	7.46	0.00	8.95	0.00	57.10	0.13	0.28	25.78	0.04	0.00	0.00	0.00	0.02	0.08	99.82
284	7.09	0.11	9.37	0.01	56.09	0.11	0.27	26.22	0.00	0.01	0.00	0.00	0.01	0.11	99.38
312	7.05	0.00	9.21	0.01	56.35	0.17	0.28	26.48	0.00	0.00	0.00	0.00	0.02	0.01	99.57
340	8.63	0.00	6.86	0.01	59.44	0.12	0.43	24.18	0.07	0.00	0.00	0.00	0.02	0.02	99.76
368	9.23	0.00	5.88	0.01	60.81	0.19	0.52	23.54	0.00	0.00	0.00	0.00	0.01	0.17	100.35
396	9.63	0.07	5.33	0.00	62.10	0.17	0.68	22.78	0.00	0.00	0.00	0.00	0.01	0.07	100.83
424	10.25	0.02	4.30	0.00	63.43	0.17	0.85	22.26	0.00	0.00	0.00	0.00	0.00	0.11	101.40
452	10.11	0.00	4.03	0.00	63.77	0.14	0.81	21.95	0.00	0.00	0.00	0.00	0.01	0.00	100.82
480	10.34	0.00	3.84	0.00	64.13	0.11	0.84	21.76	0.00	0.00	0.00	0.00	0.02	0.01	101.04
508	9.97	0.00	4.01	0.00	63.64	0.11	0.86	21.91	0.00	0.00	0.00	0.00	0.00	0.05	100.53
536	9.89	0.00	4.22	0.01	63.39	0.10	0.82	22.19	0.01	0.00	0.00	0.00	0.01	0.03	100.65
564	9.29	0.02	3.38	0.00	64.25	0.10	2.28	21.31	0.00	0.00	0.00	0.00	0.01	0.08	100.71
592	3.98	0.08	0.11	0.01	65.54	0.10	11.80	18.20	0.18	0.00	0.00	0.00	0.01	0.89	100.83
620	3.89	0.00	0.12	0.01	65.29	0.07	12.03	17.90	0.12	0.00	0.00	0.00	0.03	0.89	100.30
648	3.85	0.00	0.10	0.00	65.39	0.06	11.95	17.98	0.09	0.00	0.00	0.00	0.01	0.83	100.21
676	3.96	0.00	0.08	0.00	65.62	0.07	12.24	17.95	0.00	0.00	0.00	0.00	0.03	0.66	100.62
732	3.88	0.00	0.08	0.00	65.89	0.09	12.12	17.83	0.00	0.00	0.00	0.00	0.02	0.40	100.33
760	3.95	0.00	0.07	0.00	65.69	0.06	12.25	17.84	0.00	0.00	0.00	0.00	0.02	0.47	100.34
788	3.94	0.00	0.13	0.00	65.50	0.05	11.70	17.92	0.02	0.00	0.00	0.00	0.02	0.66	99.93
816	3.96	0.00	0.11	0.00	64.87	0.09	11.89	17.93	0.00	0.00	0.00	0.00	0.02	0.79	99.66
844	3.88	0.03	0.11	0.00	65.42	0.09	12.07	17.87	0.02	0.00	0.00	0.00	0.02	0.74	100.24
872	4.06	0.00	0.12	0.00	65.62	0.04	11.85	18.29	0.04	0.00	0.00	0.00	0.00	0.77	100.78
900	4.30	0.01	0.14	0.00	65.36	0.04	11.71	18.10	0.05	0.00	0.00	0.00	0.01	0.96	100.66
928	4.16	0.03	0.12	0.00	65.26	0.06	11.89	18.03	0.06	0.02	0.00	0.00	0.00	1.00	100.59
956	4.14	0.05	0.12	0.00	65.10	0.06	11.96	17.96	0.16	0.02	0.00	0.00	0.01	0.84	100.35
984	4.13	0.09	0.10	0.00	65.00	0.06	11.92	18.07	0.05	0.01	0.00	0.00	0.00	0.88	100.27
1012	4.16	0.09	0.14	0.00	65.31	0.07	11.85	18.07	0.13	0.01	0.00	0.00	0.01	0.78	100.55
1040	4.17	0.08	0.14	0.00	65.31	0.04	11.98	17.81	0.06	0.02	0.00	0.00	0.00	0.75	100.34
1068	4.13	0.08	0.12	0.00	65.85	0.05	12.02	17.63	0.01	0.00	0.00	0.00	0.01	0.31	100.20
1096	4.09	0.02	0.11	0.00	65.84	0.10	12.19	17.94	0.09	0.00	0.00	0.00	0.00	0.37	100.71
1124	4.26	0.05	0.09	0.00	65.68	0.06	12.13	17.84	0.12	0.01	0.00	0.00	0.01	0.40	100.62

LV-MR-005-1-5 Plagioclase Core to Rim

Distance (μm)	Na_2O	TiO_2	CaO	MgO	SiO_2	FeO	K_2O	Al_2O_3	F	MnO	Cl	Cr_2O_3	P_2O_5	BaO	Total
18	8.73	0.00	4.14	0.01	61.86	0.16	1.13	23.24	0.00	0.00	0.00	0.00	0.01	0.00	99.29
49	9.31	0.00	4.15	0.01	60.84	0.17	1.11	22.89	0.00	0.00	0.01	0.00	0.01	0.09	98.58
80	9.24	0.00	4.32	0.02	61.13	0.15	1.11	22.97	0.00	0.00	0.01	0.00	0.02	0.04	99.01
111	9.22	0.00	3.91	0.01	61.40	0.14	1.22	22.48	0.00	0.00	0.01	0.00	0.01	0.07	98.45
173	9.37	0.00	4.37	0.00	60.66	0.11	1.13	22.88	0.00	0.00	0.01	0.00	0.02	0.05	98.59
204	9.14	0.00	4.45	0.00	60.60	0.16	1.11	23.10	0.00	0.00	0.01	0.00	0.00	0.06	98.61
235	8.97	0.00	4.99	0.01	60.24	0.20	0.94	23.58	0.00	0.00	0.00	0.00	0.00	0.03	98.97
266	9.21	0.00	4.48	0.00	60.68	0.14	1.08	23.32	0.01	0.00	0.00	0.00	0.01	0.15	99.08
297	9.14	0.05	4.25	0.00	60.98	0.16	1.09	23.15	0.00	0.00	0.00	0.00	0.00	0.05	98.87
328	9.05	0.16	3.71	0.00	62.42	0.19	1.21	23.19	0.01	0.00	0.00	0.00	0.01	0.06	100.00
359	9.37	0.07	3.88	0.00	61.05	0.19	1.20	22.95	0.11	0.00	0.00	0.00	0.02	0.11	98.90
390	9.38	0.08	3.75	0.00	61.06	0.17	1.20	22.73	0.04	0.02	0.00	0.00	0.01	0.06	98.48
421	9.46	0.11	3.78	0.00	61.41	0.15	1.30	22.70	0.02	0.00	0.00	0.00	0.02	0.12	99.06
452	9.55	0.15	3.55	0.00	61.46	0.16	1.26	22.75	0.15	0.00	0.00	0.00	0.01	0.04	99.02
483	9.10	0.11	5.04	0.00	59.58	0.17	0.88	23.93	0.01	0.02	0.00	0.00	0.00	0.11	98.96
514	9.32	0.09	4.38	0.00	60.01	0.17	1.03	23.38	0.00	0.00	0.00	0.00	0.02	0.14	98.53
545	9.52	0.15	3.96	0.00	60.92	0.16	1.19	22.97	0.00	0.00	0.00	0.00	0.00	0.02	98.89
576	9.63	0.18	3.84	0.00	61.15	0.20	1.19	22.97	0.08	0.00	0.00	0.00	0.01	0.10	99.31
607	9.70	0.07	3.84	0.00	61.41	0.20	1.21	23.07	0.06	0.00	0.00	0.00	0.01	0.06	99.61
638	9.12	0.05	3.54	0.01	62.73	0.18	1.31	22.88	0.00	0.00	0.00	0.00	0.00	0.09	99.91
669	9.50	0.13	3.85	0.00	61.41	0.13	1.22	22.68	0.00	0.00	0.00	0.00	0.00	0.10	99.01
700	9.40	0.15	4.18	0.00	61.14	0.21	1.14	23.07	0.00	0.00	0.00	0.00	0.00	0.10	99.39
731	9.50	0.10	4.08	0.00	61.27	0.13	1.16	22.91	0.00	0.00	0.00	0.00	0.00	0.10	99.25
762	9.33	0.12	4.27	0.00	60.82	0.13	1.05	23.09	0.00	0.00	0.00	0.00	0.00	0.05	98.85
793	9.40	0.08	4.24	0.00	60.95	0.16	1.13	23.02	0.00	0.00	0.00	0.00	0.00	0.09	99.06
824	9.75	0.09	4.09	0.00	61.21	0.17	1.20	22.85	0.01	0.00	0.00	0.00	0.00	0.06	99.42
855	9.47	0.08	4.14	0.00	60.85	0.20	1.13	22.93	0.01	0.00	0.00	0.00	0.00	0.06	98.86
886	9.40	0.15	4.21	0.00	60.71	0.15	1.10	23.00	0.00	0.00	0.00	0.00	0.00	0.07	98.79
917	9.46	0.02	4.33	0.00	60.92	0.15	1.14	23.03	0.00	0.00	0.00	0.00	0.00	0.08	99.13
948	8.83	0.00	4.22	0.00	61.55	0.17	1.13	23.25	0.04	0.00	0.00	0.03	0.00	0.02	99.23
979	9.57	0.00	4.22	0.01	60.88	0.18	1.11	23.02	0.04	0.00	0.00	0.00	0.00	0.02	99.02
1010	9.49	0.00	4.12	0.01	61.03	0.19	1.18	22.99	0.05	0.00	0.00	0.03	0.00	0.02	99.08
1041	9.62	0.00	3.46	0.00	62.04	0.15	1.42	22.40	0.07	0.00	0.00	0.00	0.00	0.02	99.15
1072	9.51	0.00	4.17	0.01	61.12	0.13	1.09	22.95	0.01	0.00	0.00	0.00	0.00	0.08	99.06
1103	9.75	0.00	3.81	0.01	61.30	0.16	1.20	22.98	0.12	0.00	0.00	0.00	0.00	0.01	99.29
1134	9.53	0.00	4.43	0.00	60.74	0.13	1.12	23.30	0.05	0.00	0.00	0.00	0.00	0.06	99.34
1165	9.39	0.00	3.99	0.01	61.02	0.12	1.25	22.81	0.01	0.00	0.00	0.00	0.00	0.06	98.65
1196	9.17	0.00	4.76	0.01	59.94	0.14	1.02	23.60	0.02	0.00	0.00	0.00	0.00	0.07	98.72

LV-MR-005-1-5 Plagioclase Core to Rim (continued)

Distance (μm)	Na_2O	TiO_2	CaO	MgO	SiO_2	FeO	K_2O	Al_2O_3	F	MnO	Cl	Cr_2O_3	P_2O_5	BaO	Total
1227	9.49	0.00	4.45	0.02	60.48	0.17	1.06	23.34	0.00	0.01	0.00	0.01	0.00	0.06	99.08
1258	9.01	0.01	4.35	0.01	61.69	0.16	1.07	23.61	0.00	0.00	0.00	0.00	0.00	0.07	99.98
1289	9.61	0.01	4.34	0.00	60.52	0.12	1.06	23.20	0.04	0.00	0.01	0.00	0.01	0.07	98.97
1320	9.57	0.00	4.28	0.02	60.63	0.12	1.07	23.16	0.11	0.00	0.00	0.00	0.00	0.08	98.99
1351	9.73	0.02	3.94	0.00	61.10	0.09	1.15	22.98	0.00	0.00	0.00	0.00	0.00	0.17	99.18
1382	9.73	0.03	4.00	0.01	61.03	0.11	1.18	22.92	0.08	0.00	0.00	0.00	0.01	0.06	99.13

LV-MR-005-1-6 Sanidine Rim to Rim

Distance (μm)	Na_2O	TiO_2	CaO	MgO	SiO_2	FeO	K_2O	Al_2O_3	F	MnO	Cl	Cr_2O_3	P_2O_5	BaO	Total
40	3.84	0.00	0.14	0.00	64.34	0.08	11.81	18.81	0.07	0.00	0.00	0.00	0.02	0.75	99.82
83	3.89	0.00	0.16	0.00	62.94	0.08	12.03	18.99	0.16	0.00	0.00	0.00	0.00	0.65	98.83
126	4.07	0.00	0.17	0.00	63.25	0.11	11.86	18.96	0.04	0.00	0.00	0.00	0.00	0.70	99.15
169	3.94	0.00	0.15	0.00	63.60	0.09	12.26	18.93	0.09	0.00	0.00	0.00	0.00	0.35	99.36
212	3.92	0.00	0.15	0.00	63.07	0.09	12.17	19.20	0.00	0.00	0.00	0.00	0.00	0.69	99.29
255	4.11	0.02	0.18	0.00	63.32	0.07	11.86	19.02	0.00	0.00	0.00	0.00	0.01	0.58	99.17
298	3.93	0.02	0.13	0.00	63.50	0.06	12.21	18.65	0.05	0.00	0.00	0.00	0.00	0.24	98.77
341	4.03	0.00	0.14	0.00	63.71	0.09	12.20	18.87	0.00	0.00	0.00	0.00	0.01	0.17	99.23
384	4.02	0.00	0.15	0.00	63.59	0.10	12.09	19.00	0.10	0.00	0.00	0.00	0.00	0.23	99.22
427	4.06	0.00	0.15	0.00	63.47	0.10	12.08	18.93	0.00	0.00	0.00	0.00	0.00	0.27	99.08
470	3.81	0.04	0.16	0.00	64.62	0.11	11.79	18.85	0.11	0.00	0.00	0.00	0.00	0.33	99.76
513	4.09	0.04	0.17	0.00	63.46	0.09	12.07	18.80	0.00	0.00	0.00	0.00	0.00	0.19	98.91
556	4.16	0.03	0.18	0.00	63.70	0.05	11.96	18.96	0.00	0.00	0.00	0.00	0.00	0.33	99.37
599	3.99	0.03	0.19	0.00	63.32	0.10	12.08	18.84	0.01	0.00	0.00	0.00	0.01	0.25	98.83
642	4.13	0.02	0.19	0.00	62.97	0.06	12.17	18.83	0.00	0.00	0.01	0.00	0.00	0.20	98.58
685	4.26	0.07	0.22	0.00	63.26	0.09	11.95	19.03	0.00	0.00	0.00	0.00	0.00	0.14	99.00
728	4.16	0.05	0.19	0.00	63.58	0.08	12.08	18.96	0.00	0.00	0.00	0.00	0.00	0.25	99.34
771	4.06	0.06	0.17	0.00	63.32	0.06	12.15	18.88	0.00	0.00	0.00	0.00	0.00	0.26	98.96
814	3.97	0.05	0.17	0.00	63.46	0.07	12.02	18.95	0.06	0.00	0.00	0.00	0.00	0.26	98.98
857	4.19	0.04	0.16	0.00	63.54	0.11	12.22	18.85	0.00	0.00	0.00	0.00	0.01	0.20	99.31
900	3.88	0.07	0.15	0.00	65.06	0.11	11.72	19.08	0.01	0.00	0.00	0.03	0.00	0.41	100.51
943	3.96	0.00	0.18	0.00	63.26	0.09	12.10	18.95	0.07	0.01	0.00	0.00	0.00	0.84	99.43
986	4.00	0.05	0.18	0.00	62.66	0.13	12.02	18.88	0.00	0.00	0.00	0.00	0.00	0.89	98.82
1029	3.96	0.03	0.21	0.00	62.96	0.09	12.07	19.12	0.01	0.03	0.00	0.01	0.00	0.85	99.34
1072	3.97	0.02	0.13	0.00	63.39	0.09	12.12	19.01	0.00	0.00	0.00	0.02	0.00	0.53	99.27
1115	4.00	0.02	0.17	0.00	63.38	0.07	12.05	18.91	0.00	0.00	0.00	0.04	0.00	0.72	99.35
1158	3.98	0.05	0.19	0.00	63.13	0.11	12.00	18.97	0.00	0.00	0.00	0.00	0.00	0.62	99.05
1201	4.02	0.00	0.15	0.00	63.17	0.11	11.89	19.16	0.00	0.03	0.00	0.03	0.00	0.79	99.35
1244	4.12	0.00	0.17	0.00	62.77	0.11	11.96	18.88	0.00	0.00	0.00	0.01	0.00	0.95	98.97
1287	4.06	0.00	0.16	0.00	63.59	0.09	12.23	18.97	0.00	0.00	0.00	0.03	0.01	0.30	99.43

LV-MR-005-1-8 Plagioclase Rim to Rim

Distance (μm)	Na_2O	TiO_2	CaO	MgO	SiO_2	FeO	K_2O	Al_2O_3	F	MnO	Cl	Cr_2O_3	P_2O_5	BaO	Total
19	8.90	0.00	3.84	0.00	62.90	0.14	1.18	23.04	0.00	0.00	0.00	0.00	0.00	0.04	100.04
39	9.16	0.02	4.43	0.01	60.68	0.18	1.08	23.22	0.00	0.00	0.00	0.00	0.01	0.04	98.84
58	9.18	0.00	4.49	0.00	60.45	0.16	1.01	23.20	0.00	0.00	0.01	0.00	0.01	0.06	98.57
77	9.21	0.17	4.60	0.00	60.30	0.18	1.03	23.10	0.00	0.00	0.00	0.00	0.00	0.07	98.68
96	9.39	0.00	4.38	0.00	61.08	0.16	1.07	23.23	0.00	0.00	0.00	0.00	0.01	0.09	99.40
116	9.44	0.00	4.40	0.01	60.57	0.19	1.08	23.18	0.00	0.00	0.00	0.00	0.01	0.13	99.00
212	8.21	0.11	6.25	0.00	59.56	0.15	0.67	24.84	0.00	0.00	0.00	0.00	0.02	0.03	99.84
232	9.25	0.05	4.56	0.00	60.28	0.21	1.03	23.64	0.05	0.00	0.01	0.00	0.01	0.06	99.12
251	7.78	0.05	8.01	0.01	55.58	0.18	0.47	26.41	0.10	0.00	0.01	0.00	0.02	0.05	98.63
270	8.97	0.02	5.37	0.00	59.21	0.18	0.82	24.07	0.11	0.00	0.01	0.00	0.01	0.06	98.76
309	8.93	0.00	5.60	0.00	59.07	0.17	0.79	24.24	0.04	0.00	0.00	0.00	0.00	0.05	98.88
328	6.99	0.01	9.15	0.00	54.68	0.17	0.40	27.39	0.00	0.00	0.01	0.00	0.01	0.03	98.83
347	6.87	0.10	9.58	0.01	54.26	0.19	0.36	27.30	0.09	0.00	0.00	0.00	0.00	0.04	98.76
367	8.80	0.06	5.98	0.00	58.79	0.16	0.72	24.39	0.00	0.00	0.01	0.00	0.01	0.05	98.97
386	7.20	0.05	8.96	0.00	54.66	0.15	0.44	27.03	0.01	0.00	0.01	0.00	0.01	0.07	98.58
405	8.52	0.02	4.13	0.00	61.97	0.14	1.13	23.22	0.00	0.00	0.00	0.00	0.00	0.12	99.23
425	9.41	0.07	4.36	0.01	60.62	0.18	1.04	23.39	0.09	0.00	0.00	0.00	0.01	0.07	99.20
444	9.53	0.00	3.77	0.01	61.83	0.24	1.28	22.76	0.00	0.00	0.00	0.00	0.02	0.04	99.48
463	9.29	0.02	4.61	0.00	60.50	0.17	1.08	23.29	0.11	0.00	0.00	0.00	0.03	0.04	99.08
483	9.31	0.00	4.50	0.00	60.70	0.18	1.08	23.17	0.07	0.00	0.00	0.00	0.00	0.08	99.05
502	9.34	0.01	4.56	0.01	60.75	0.22	1.00	23.13	0.00	0.00	0.00	0.00	0.01	0.09	99.11
521	9.60	0.00	3.72	0.01	61.51	0.16	1.26	22.54	0.05	0.00	0.00	0.00	0.02	0.03	98.87
540	9.44	0.02	4.32	0.00	60.62	0.18	1.13	23.08	0.00	0.00	0.00	0.00	0.04	0.07	98.91
560	9.29	0.00	4.40	0.00	60.65	0.18	1.04	23.32	0.00	0.00	0.00	0.00	0.00	0.07	98.96
579	9.53	0.02	4.17	0.01	60.75	0.22	1.11	22.88	0.00	0.00	0.00	0.00	0.01	0.03	98.72

LV-HCF-002-1-1 Plagioclase Rim to Rim

Distance (μm)	Na_2O	TiO_2	CaO	MgO	SiO_2	FeO	K_2O	Al_2O_3	F	MnO	Cl	Cr_2O_3	P_2O_5	BaO	Total
52	4.10	0.00	0.28	0.00	64.76	0.09	9.83	19.34	0.00	0.02	0.00	0.00	0.02	1.52	99.96
103	4.03	0.00	0.27	0.00	64.87	0.06	9.76	19.67	0.00	0.00	0.01	0.00	0.01	1.50	100.18
155	3.98	0.03	0.26	0.01	64.48	0.11	9.79	19.72	0.00	0.01	0.00	0.02	0.08	1.70	100.19
206	3.94	0.07	0.19	0.00	64.90	0.11	10.08	19.06	0.17	0.00	0.01	0.01	0.00	1.18	99.62
258	4.05	0.02	0.30	0.00	64.03	0.14	9.72	19.58	0.08	0.00	0.02	0.00	0.02	1.65	99.56
309	4.17	0.04	0.21	0.00	64.40	0.12	9.80	19.47	0.02	0.01	0.00	0.01	0.00	1.50	99.74
361	4.05	0.00	0.32	0.00	64.59	0.08	9.52	19.38	0.00	0.00	0.00	0.00	0.00	1.45	99.39
413	3.38	0.11	0.44	0.00	76.61	0.22	5.14	12.64	0.00	0.02	0.01	0.02	0.04	0.05	98.67
464	8.00	0.00	3.88	0.00	63.64	0.20	1.33	22.81	0.02	0.00	0.00	0.00	0.02	0.05	99.95
516	8.36	0.01	3.71	0.01	63.81	0.13	1.24	22.57	0.14	0.00	0.00	0.00	0.00	0.05	99.96
619	8.07	0.00	3.10	0.01	64.50	0.15	1.52	22.22	0.00	0.00	0.00	0.01	0.03	0.13	99.73
670	8.32	0.02	3.57	0.00	63.62	0.16	1.37	22.66	0.00	0.00	0.00	0.01	0.01	0.07	99.81
722	8.43	0.00	3.78	0.00	63.39	0.15	1.35	22.64	0.00	0.01	0.01	0.00	0.00	0.20	99.95
774	8.39	0.00	3.63	0.01	63.67	0.14	1.33	22.22	0.00	0.00	0.00	0.00	0.00	0.07	99.46
825	8.04	0.00	3.80	0.01	63.51	0.19	1.28	22.57	0.00	0.01	0.00	0.00	0.00	0.09	99.49
928	8.37	0.01	4.32	0.00	63.01	0.17	1.08	23.17	0.04	0.00	0.00	0.02	0.03	0.07	100.26
980	8.04	0.00	4.66	0.01	62.41	0.18	0.99	23.36	0.00	0.01	0.00	0.00	0.04	0.14	99.86
1031	8.36	0.01	4.81	0.01	62.72	0.20	0.96	23.52	0.18	0.04	0.00	0.00	0.01	0.05	100.79
1083	7.74	0.03	4.82	0.02	62.52	0.17	0.95	23.71	0.00	0.00	0.00	0.00	0.03	0.01	99.98
1134	8.12	0.03	4.62	0.01	62.31	0.20	1.01	23.50	0.00	0.01	0.00	0.01	0.02	0.11	99.95
1186	7.81	0.01	4.85	0.00	62.14	0.14	0.93	23.58	0.00	0.00	0.01	0.00	0.03	0.02	99.51
1238	7.97	0.00	5.05	0.01	61.97	0.19	0.93	23.67	0.00	0.01	0.00	0.01	0.00	0.05	99.85
1289	8.03	0.06	4.88	0.00	62.41	0.20	0.97	23.54	0.00	0.00	0.01	0.03	0.00	0.13	100.26
1341	8.32	0.01	4.90	0.00	61.79	0.19	0.94	23.71	0.12	0.00	0.00	0.00	0.00	0.09	100.01
1392	7.85	0.02	5.21	0.01	61.68	0.19	0.82	23.76	0.08	0.03	0.00	0.01	0.00	0.07	99.69
1444	8.09	0.00	4.99	0.02	62.33	0.17	0.88	23.80	0.00	0.00	0.00	0.00	0.00	0.18	100.46
1495	8.01	0.01	5.04	0.00	62.31	0.16	0.93	23.62	0.00	0.00	0.01	0.00	0.01	0.15	100.24
1547	7.59	0.01	5.26	0.01	61.85	0.21	0.86	23.91	0.14	0.01	0.00	0.03	0.01	0.04	99.89
1599	7.82	0.04	5.03	0.01	62.60	0.19	0.89	23.77	0.00	0.00	0.01	0.00	0.03	0.12	100.50
1650	7.83	0.02	5.03	0.00	62.39	0.20	0.89	23.68	0.14	0.01	0.00	0.00	0.00	0.04	100.17
1702	7.80	0.01	5.23	0.02	61.68	0.13	0.87	23.90	0.10	0.01	0.00	0.05	0.02	0.07	99.85
1753	7.86	0.01	5.11	0.00	62.22	0.16	0.90	23.66	0.00	0.00	0.00	0.00	0.00	0.18	100.09
1805	7.94	0.00	4.72	0.00	62.52	0.21	0.98	23.11	0.08	0.00	0.00	0.00	0.00	0.08	99.60
1856	8.00	0.00	4.46	0.00	62.97	0.16	1.03	23.23	0.00	0.00	0.01	0.03	0.04	0.16	100.08
1908	8.18	0.01	4.09	0.00	62.86	0.18	1.11	22.88	0.02	0.04	0.00	0.01	0.00	0.13	99.49
1960	8.13	0.00	4.22	0.00	63.29	0.16	1.15	22.84	0.00	0.01	0.00	0.00	0.01	0.11	99.90
2011	8.20	0.00	4.14	0.00	63.15	0.16	1.14	22.36	0.19	0.00	0.00	0.00	0.01	0.10	99.37
2063	8.05	0.02	4.70	0.00	62.45	0.19	1.02	22.91	0.06	0.01	0.00	0.03	0.00	0.08	99.50

LV-HCF-002-1-1 Plagioclase Rim to Rim (continued)

Distance (μm)	Na_2O	TiO_2	CaO	MgO	SiO_2	FeO	K_2O	Al_2O_3	F	MnO	Cl	Cr_2O_3	P_2O_5	BaO	Total
2114	7.87	0.00	4.67	0.03	62.45	0.16	0.95	23.02	0.00	0.02	0.00	0.01	0.03	0.08	99.30
2166	8.27	0.01	4.27	0.01	63.15	0.14	1.04	22.86	0.00	0.00	0.00	0.00	0.05	0.09	99.89
2217	7.70	0.00	5.54	0.00	61.11	0.21	0.78	24.04	0.00	0.02	0.01	0.02	0.00	0.04	99.46
2269	7.38	0.02	5.64	0.02	61.24	0.23	0.77	23.98	0.12	0.06	0.00	0.00	0.03	0.08	99.51
2321	7.82	0.01	5.59	0.00	61.41	0.19	0.79	24.16	0.02	0.00	0.00	0.02	0.00	0.10	100.09
2372	7.80	0.00	5.62	0.01	61.57	0.16	0.76	24.18	0.14	0.02	0.00	0.03	0.02	0.07	100.33
2424	7.95	0.05	5.84	0.01	61.14	0.21	0.77	24.11	0.10	0.01	0.00	0.00	0.00	0.00	100.15
2475	7.41	0.00	5.66	0.01	61.27	0.21	0.79	23.92	0.00	0.00	0.00	0.02	0.04	0.10	99.43
2527	7.70	0.00	5.88	0.00	61.47	0.20	0.74	24.25	0.00	0.00	0.00	0.03	0.00	0.06	100.33
2578	7.51	0.00	5.77	0.01	61.41	0.24	0.76	24.17	0.10	0.03	0.01	0.00	0.01	0.07	100.04
2630	7.76	0.00	5.40	0.02	61.69	0.22	0.81	23.92	0.04	0.01	0.00	0.00	0.06	0.07	99.99
2681	8.20	0.03	3.65	0.01	64.00	0.15	1.38	22.30	0.00	0.01	0.00	0.00	0.03	0.09	99.85
2733	8.28	0.01	3.55	0.00	63.40	0.17	1.31	21.94	0.00	0.00	0.00	0.03	0.03	0.10	98.81
2785	8.63	0.03	3.29	0.01	64.47	0.16	1.50	22.12	0.00	0.00	0.00	0.00	0.00	0.17	100.37
2836	7.62	0.01	3.65	0.01	63.00	0.19	2.00	22.16	0.00	0.01	0.00	0.00	0.03	0.17	98.83
2939	4.04	0.03	0.29	0.01	64.50	0.12	10.00	19.11	0.00	0.00	0.00	0.01	0.00	1.54	99.65
2991	3.93	0.02	0.26	0.00	64.21	0.10	9.81	18.95	0.00	0.04	0.02	0.00	0.04	1.46	98.84
3042	4.15	0.00	0.28	0.00	64.63	0.10	9.79	19.23	0.02	0.00	0.00	0.02	0.04	1.42	99.67
3094	4.21	0.00	0.29	0.00	64.54	0.11	9.71	19.28	0.00	0.00	0.00	0.00	0.01	1.48	99.63

LV-HCF-002-1-5 Plagioclase Rim to Rim

Distance (μm)	Na_2O	TiO_2	CaO	MgO	SiO_2	FeO	K_2O	Al_2O_3	F	MnO	Cl	Cr_2O_3	P_2O_5	BaO	Total
45	4.19	0.03	0.26	0.00	65.11	0.13	9.79	18.84	0.00	0.01	0.00	0.02	0.06	1.29	99.72
91	4.13	0.07	0.30	0.00	64.94	0.11	9.64	18.85	0.09	0.03	0.01	0.00	0.02	1.28	99.41
136	4.37	0.00	0.31	0.00	65.01	0.12	9.46	18.81	0.00	0.00	0.00	0.00	0.00	1.17	99.24
182	8.67	0.00	3.65	0.02	63.37	0.19	1.33	22.16	0.11	0.00	0.00	0.01	0.00	0.01	99.49
227	8.12	0.07	4.28	0.00	63.06	0.19	1.13	22.58	0.15	0.01	0.00	0.01	0.00	0.17	99.70
272	7.85	0.00	4.43	0.00	62.19	0.18	1.00	23.02	0.00	0.00	0.00	0.01	0.00	0.04	98.72
318	7.81	0.00	4.54	0.00	62.75	0.17	1.05	23.28	0.11	0.00	0.00	0.00	0.09	0.12	99.87
363	8.02	0.03	4.70	0.00	62.17	0.21	1.05	23.58	0.04	0.00	0.00	0.00	0.00	0.36	100.15
409	7.62	0.05	5.47	0.03	61.46	0.24	0.81	23.77	0.00	0.02	0.00	0.00	0.00	0.16	99.63
454	7.55	0.02	5.41	0.01	61.74	0.17	0.82	23.85	0.00	0.01	0.01	0.02	0.00	0.23	99.83
499	7.48	0.01	5.45	0.00	61.43	0.21	0.78	24.01	0.20	0.00	0.00	0.02	0.00	0.19	99.68
545	8.26	0.00	4.12	0.02	63.21	0.18	1.10	22.79	0.00	0.01	0.01	0.00	0.00	0.19	99.88
590	7.44	0.02	4.18	0.00	63.53	0.17	1.15	22.95	0.00	0.00	0.00	0.00	0.00	0.25	99.70
636	7.83	0.01	4.15	0.00	62.95	0.20	1.20	22.91	0.00	0.03	0.01	0.01	0.01	0.34	99.67
681	7.83	0.00	4.87	0.02	62.45	0.18	0.98	23.28	0.00	0.00	0.02	0.01	0.00	0.19	99.83
726	8.18	0.03	4.48	0.00	62.63	0.22	1.17	23.05	0.22	0.00	0.00	0.01	0.00	0.24	100.13
772	8.23	0.00	4.03	0.00	63.59	0.18	1.23	22.79	0.11	0.02	0.01	0.00	0.00	0.10	100.24
817	8.27	0.00	4.00	0.00	63.53	0.20	1.22	22.58	0.07	0.00	0.00	0.00	0.02	0.10	99.96
908	7.83	0.01	4.76	0.01	62.03	0.23	1.05	23.28	0.13	0.00	0.00	0.00	0.04	0.20	99.51
953	7.77	0.07	2.94	0.00	63.63	0.12	2.55	21.72	0.00	0.00	0.00	0.00	0.00	0.64	99.45
999	7.68	0.05	5.31	0.00	61.75	0.19	0.88	23.95	0.02	0.04	0.00	0.01	0.01	0.20	100.08
1044	7.50	0.04	5.89	0.00	60.90	0.20	0.72	24.27	0.00	0.00	0.00	0.01	0.02	0.23	99.77
1090	7.77	0.07	4.74	0.00	62.40	0.21	1.07	23.38	0.07	0.00	0.00	0.00	0.03	0.33	100.03
1135	8.21	0.07	4.15	0.00	62.91	0.21	1.18	22.73	0.00	0.00	0.01	0.00	0.02	0.14	99.62
1180	8.30	0.00	4.06	0.00	63.51	0.16	1.14	22.57	0.11	0.00	0.00	0.00	0.00	0.08	99.89
1226	7.92	0.03	4.55	0.01	62.26	0.21	1.10	23.13	0.04	0.00	0.00	0.01	0.09	0.25	99.58
1271	7.64	0.02	3.91	0.01	63.69	0.21	1.42	22.47	0.00	0.00	0.02	0.00	0.00	0.19	99.58
1317	7.62	0.00	4.80	0.01	61.66	0.14	0.97	23.52	0.20	0.00	0.00	0.00	0.05	0.19	99.08

LV-HCF-005-1A1-2 Sanidine Rim to Rim

Distance (μm)	Na_2O	TiO_2	CaO	MgO	SiO_2	FeO	K_2O	Al_2O_3	F	MnO	Cl	Cr_2O_3	P_2O_5	BaO	Total
35	4.00	0.00	0.26	0.01	64.12	0.11	10.02	19.44	0.10	0.00	0.01	0.00	0.01	1.26	99.29
71	3.92	0.00	0.24	0.00	64.22	0.10	9.90	19.44	0.14	0.01	0.00	0.01	0.01	1.34	99.27
106	4.08	0.00	0.23	0.00	64.96	0.09	9.86	19.44	0.00	0.02	0.00	0.00	0.00	1.31	99.99
141	4.11	0.04	0.27	0.00	64.65	0.08	9.80	19.45	0.00	0.00	0.02	0.01	0.01	1.45	99.85
177	4.14	0.02	0.22	0.00	64.48	0.04	9.74	19.25	0.04	0.03	0.00	0.00	0.01	1.48	99.43
212	3.86	0.00	0.26	0.00	64.65	0.10	10.05	19.53	0.02	0.00	0.00	0.00	0.01	1.55	100.02
247	4.04	0.02	0.26	0.01	64.61	0.07	10.07	19.40	0.08	0.00	0.02	0.00	0.02	1.52	100.08
283	4.03	0.00	0.27	0.00	64.32	0.09	9.77	19.48	0.00	0.05	0.01	0.00	0.03	1.65	99.68
318	4.17	0.01	0.28	0.01	64.75	0.10	9.85	19.43	0.00	0.00	0.01	0.02	0.00	1.53	100.16
353	3.99	0.00	0.30	0.01	64.21	0.10	9.84	19.37	0.04	0.00	0.00	0.01	0.00	1.41	99.25
389	3.79	0.03	0.28	0.00	64.16	0.09	9.86	19.58	0.16	0.04	0.00	0.00	0.00	1.38	99.30
424	4.04	0.06	0.24	0.00	64.44	0.10	9.85	19.50	0.00	0.01	0.00	0.00	0.00	1.42	99.67
459	3.74	0.05	0.25	0.00	64.80	0.12	9.86	19.47	0.12	0.03	0.01	0.00	0.01	1.38	99.80
495	4.12	0.08	0.26	0.00	65.07	0.11	9.97	19.49	0.00	0.00	0.01	0.00	0.04	1.35	100.48
530	4.14	0.03	0.22	0.00	64.75	0.10	9.92	19.34	0.00	0.02	0.00	0.02	0.02	1.26	99.81
565	4.09	0.00	0.24	0.00	64.87	0.13	9.84	19.15	0.00	0.00	0.00	0.00	0.00	1.46	99.78
601	4.20	0.00	0.24	0.01	65.06	0.10	9.91	19.55	0.00	0.02	0.01	0.02	0.04	1.46	100.61
636	4.28	0.00	0.26	0.00	64.60	0.12	9.97	19.18	0.14	0.00	0.01	0.00	0.01	1.39	99.88
671	3.96	0.03	0.25	0.00	64.19	0.08	9.70	19.33	0.00	0.04	0.01	0.00	0.05	1.29	98.92
707	4.02	0.00	0.25	0.00	64.06	0.09	9.82	19.48	0.08	0.00	0.00	0.00	0.04	1.37	99.16
742	3.97	0.03	0.23	0.00	64.72	0.08	9.93	19.19	0.00	0.00	0.00	0.00	0.04	1.33	99.51
777	4.11	0.00	0.28	0.00	64.85	0.12	10.00	19.23	0.00	0.01	0.00	0.00	0.07	1.29	99.95
813	4.22	0.01	0.25	0.00	64.62	0.14	9.96	19.57	0.02	0.00	0.01	0.02	0.00	1.52	100.30
848	3.95	0.00	0.24	0.01	64.65	0.09	9.96	19.20	0.00	0.02	0.01	0.00	0.02	1.35	99.48
883	4.18	0.03	0.25	0.00	65.22	0.11	9.99	19.55	0.02	0.00	0.00	0.00	0.00	1.51	100.85
919	4.15	0.03	0.28	0.00	64.95	0.14	10.11	19.27	0.00	0.00	0.00	0.00	0.00	1.48	100.41
954	4.07	0.03	0.26	0.00	64.88	0.06	9.94	19.28	0.00	0.02	0.00	0.00	0.00	1.46	100.00
989	4.04	0.01	0.26	0.00	64.86	0.14	9.85	19.33	0.16	0.00	0.00	0.01	0.03	1.29	99.92
1025	3.80	0.03	0.20	0.00	64.86	0.10	9.96	19.06	0.25	0.02	0.01	0.00	0.02	1.18	99.37
1060	3.99	0.02	0.26	0.00	64.91	0.12	9.99	19.48	0.02	0.00	0.00	0.01	0.00	1.37	100.15

LV-HCF-005-1A2-2 Plagioclase Rim to Rim

Distance (μm)	Na_2O	TiO_2	CaO	MgO	SiO_2	FeO	K_2O	Al_2O_3	F	MnO	Cl	Cr_2O_3	P_2O_5	BaO	Total
37	8.42	0.00	4.13	0.01	62.76	0.16	1.16	23.11	0.05	0.05	0.01	0.01	0.03	0.00	99.86
73	8.15	0.05	3.96	0.00	63.46	0.17	1.27	23.05	0.00	0.00	0.01	0.00	0.03	0.00	100.13
110	7.86	0.03	3.98	0.00	63.48	0.17	1.34	22.84	0.02	0.00	0.00	0.02	0.00	0.00	99.73
147	8.28	0.00	3.78	0.01	63.85	0.15	1.30	22.84	0.05	0.02	0.00	0.00	0.00	0.00	100.27
183	8.29	0.01	3.96	0.00	63.45	0.20	1.22	22.98	0.00	0.00	0.01	0.01	0.10	0.00	100.23
257	7.72	0.01	4.72	0.00	62.04	0.16	1.04	23.58	0.00	0.00	0.00	0.00	0.01	0.00	99.27
293	8.09	0.03	4.43	0.00	62.76	0.18	1.09	23.32	0.16	0.00	0.00	0.00	0.01	0.00	99.99
330	7.96	0.01	4.92	0.00	61.88	0.18	0.99	23.88	0.11	0.00	0.01	0.00	0.00	0.00	99.89
367	7.53	0.03	5.06	0.00	61.62	0.23	0.91	23.85	0.00	0.00	0.01	0.02	0.04	0.00	99.29
403	7.84	0.00	5.04	0.00	61.91	0.22	0.96	23.95	0.00	0.03	0.00	0.03	0.04	0.00	100.01
440	7.93	0.00	5.05	0.03	61.77	0.20	0.95	24.12	0.00	0.00	0.01	0.00	0.00	0.00	100.05
477	7.53	0.04	5.64	0.00	60.91	0.18	0.84	24.53	0.00	0.00	0.00	0.00	0.00	0.00	99.67
513	7.77	0.02	5.70	0.02	61.39	0.19	0.80	24.25	0.09	0.00	0.00	0.01	0.00	0.00	100.19
550	7.60	0.02	5.56	0.00	61.35	0.18	0.82	24.33	0.02	0.00	0.00	0.00	0.06	0.00	99.94
587	7.63	0.00	5.30	0.01	61.54	0.21	0.81	24.37	0.11	0.00	0.00	0.00	0.00	0.00	99.93
623	7.59	0.00	5.52	0.01	61.22	0.24	0.80	24.48	0.00	0.00	0.01	0.00	0.03	0.00	99.90
660	7.65	0.01	5.38	0.02	61.12	0.24	0.82	24.34	0.00	0.00	0.00	0.00	0.00	0.00	99.57
733	7.65	0.01	5.37	0.02	61.04	0.18	0.85	24.46	0.00	0.00	0.00	0.00	0.02	0.00	99.59
770	7.93	0.00	4.96	0.00	61.94	0.14	0.91	23.70	0.16	0.00	0.00	0.01	0.00	0.00	99.69
807	7.78	0.05	5.15	0.00	62.42	0.16	0.86	23.94	0.00	0.00	0.00	0.02	0.07	0.00	100.45
843	7.77	0.00	4.82	0.00	62.12	0.12	0.96	23.54	0.00	0.00	0.02	0.00	0.01	0.00	99.34
880	8.07	0.00	4.62	0.00	63.28	0.12	0.99	23.75	0.21	0.02	0.00	0.00	0.01	0.00	100.97
917	8.33	0.04	4.65	0.00	62.82	0.18	1.03	23.59	0.05	0.00	0.00	0.00	0.02	0.00	100.68
990	8.11	0.00	4.51	0.00	62.05	0.16	1.03	23.36	0.00	0.01	0.00	0.00	0.00	0.00	99.24
1027	8.08	0.02	4.35	0.00	61.95	0.22	1.04	23.27	0.16	0.00	0.00	0.00	0.01	0.00	99.02
1063	7.73	0.00	4.44	0.00	62.05	0.18	1.09	23.28	0.12	0.00	0.01	0.01	0.00	0.00	98.85

LV-HCF-005-1A3-1 Plagioclase Rim to Rim

Distance (μm)	Na_2O	TiO_2	CaO	MgO	SiO_2	FeO	K_2O	Al_2O_3	F	MnO	Cl	Cr_2O_3	P_2O_5	BaO	Total
33	8.35	0.00	3.91	0.02	63.36	0.13	1.18	22.99	0.05	0.00	0.00	0.02	0.04	0.00	100.02
65	8.05	0.00	4.17	0.00	63.37	0.16	1.20	23.20	0.25	0.00	0.00	0.00	0.00	0.00	100.30
98	8.15	0.00	4.03	0.00	63.39	0.13	1.24	23.05	0.14	0.00	0.00	0.00	0.00	0.00	100.06
131	8.39	0.00	4.05	0.00	63.71	0.12	1.22	23.23	0.11	0.00	0.02	0.00	0.00	0.00	100.80
196	8.31	0.00	4.39	0.01	62.92	0.17	1.09	23.67	0.18	0.00	0.00	0.00	0.02	0.00	100.69
229	8.40	0.02	3.97	0.00	63.19	0.13	1.21	23.10	0.14	0.00	0.00	0.00	0.01	0.00	100.11
262	8.30	0.00	4.25	0.00	63.36	0.17	1.19	23.31	0.32	0.00	0.00	0.00	0.00	0.00	100.77
294	8.22	0.00	4.49	0.00	63.07	0.19	1.04	23.29	0.14	0.00	0.01	0.00	0.00	0.00	100.39
327	8.41	0.00	4.35	0.01	63.45	0.16	0.80	23.09	0.27	0.00	0.01	0.00	0.07	0.00	100.50
360	8.07	0.01	4.35	0.00	63.06	0.16	1.04	23.04	0.00	0.00	0.01	0.00	0.06	0.00	99.80
392	7.43	0.00	5.44	0.00	60.14	0.15	0.85	25.54	0.00	0.00	0.01	0.00	0.02	0.00	99.59
425	7.63	0.06	5.55	0.00	61.71	0.17	0.84	24.34	0.00	0.00	0.01	0.00	0.00	0.00	100.31
458	7.52	0.06	4.93	0.03	62.23	0.17	0.93	23.91	0.18	0.00	0.00	0.00	0.05	0.00	99.95
490	7.37	0.03	5.59	0.01	61.32	0.17	0.85	24.40	0.00	0.00	0.01	0.00	0.00	0.00	99.76
523	7.82	0.04	4.90	0.00	62.08	0.14	1.00	23.83	0.16	0.00	0.00	0.00	0.02	0.00	99.91
556	7.84	0.02	4.84	0.00	61.46	0.17	0.90	23.60	0.21	0.00	0.03	0.03	0.05	0.00	99.04
589	7.98	0.00	5.24	0.01	62.28	0.16	0.89	24.08	0.02	0.00	0.00	0.02	0.00	0.00	100.67
654	7.76	0.00	5.35	0.01	62.22	0.17	0.84	24.15	0.00	0.02	0.01	0.01	0.00	0.00	100.53
687	7.96	0.04	5.22	0.00	62.21	0.17	0.84	24.29	0.02	0.00	0.00	0.00	0.03	0.00	100.76
719	7.91	0.01	5.05	0.00	62.21	0.15	0.92	23.99	0.00	0.01	0.00	0.00	0.04	0.00	100.30
752	7.82	0.00	4.57	0.00	62.75	0.19	1.06	24.21	0.00	0.00	0.00	0.00	0.02	0.00	100.62
785	8.19	0.02	4.12	0.01	63.06	0.22	1.23	23.18	0.00	0.01	0.01	0.00	0.00	0.00	100.06
818	8.11	0.00	4.34	0.00	63.26	0.17	1.15	23.34	0.00	0.00	0.00	0.00	0.00	0.00	100.36
883	8.46	0.06	3.76	0.01	63.60	0.16	1.29	22.09	0.23	0.00	0.00	0.02	0.00	0.00	99.57
916	8.26	0.00	4.16	0.00	63.37	0.18	1.23	23.14	0.12	0.01	0.00	0.00	0.05	0.00	100.46
948	8.42	0.00	3.93	0.00	63.82	0.18	1.20	22.89	0.00	0.01	0.00	0.00	0.06	0.00	100.50
981	8.00	0.00	4.18	0.00	63.00	0.16	1.15	23.25	0.00	0.00	0.00	0.01	0.00	0.00	99.75

LV-HCF-005-1A3-2 Plagioclase Rim to Rim

Distance (μm)	Na_2O	TiO_2	CaO	MgO	SiO_2	FeO	K_2O	Al_2O_3	F	MnO	Cl	Cr_2O_3	P_2O_5	BaO	Total
33	8.31	0.00	4.17	0.00	63.47	0.19	1.20	23.05	0.16	0.00	0.00	0.01	0.01	0.00	100.49
67	8.14	0.00	4.16	0.02	62.83	0.15	1.12	23.19	0.07	0.00	0.00	0.04	0.00	0.00	99.68
100	8.08	0.02	3.97	0.01	63.08	0.22	1.25	23.08	0.00	0.00	0.00	0.00	0.02	0.00	99.73
133	8.25	0.00	4.15	0.01	62.62	0.18	1.24	22.94	0.05	0.00	0.00	0.00	0.04	0.00	99.45
167	8.25	0.00	4.26	0.01	62.48	0.17	1.19	23.29	0.00	0.00	0.00	0.01	0.00	0.00	99.67
200	8.54	0.01	4.07	0.01	62.73	0.19	1.13	23.25	0.14	0.01	0.00	0.00	0.00	0.00	100.02
233	8.15	0.02	4.43	0.01	62.63	0.17	1.20	23.12	0.00	0.00	0.00	0.00	0.00	0.00	99.72
267	8.08	0.02	3.95	0.01	63.00	0.14	1.20	22.88	0.00	0.00	0.01	0.02	0.00	0.00	99.30
300	8.33	0.02	4.68	0.01	61.75	0.18	1.01	23.43	0.00	0.00	0.00	0.02	0.00	0.00	99.42
333	7.64	0.00	4.80	0.02	62.16	0.20	1.09	23.74	0.00	0.00	0.00	0.00	0.00	0.00	99.64
367	7.58	0.05	4.87	0.03	62.30	0.19	0.95	23.88	0.00	0.04	0.00	0.00	0.00	0.00	99.89
400	7.92	0.00	5.38	0.01	61.26	0.21	0.85	24.17	0.00	0.04	0.00	0.01	0.00	0.00	99.85
433	7.70	0.00	5.31	0.00	61.25	0.21	0.87	24.22	0.00	0.00	0.00	0.00	0.00	0.00	99.56
467	7.98	0.02	5.23	0.01	61.41	0.16	0.92	24.17	0.21	0.00	0.01	0.00	0.00	0.00	100.02
500	7.75	0.05	5.22	0.01	60.68	0.19	0.86	24.13	0.02	0.04	0.00	0.00	0.02	0.00	98.95
533	7.85	0.06	5.14	0.01	61.13	0.19	0.92	24.08	0.00	0.00	0.01	0.00	0.00	0.00	99.39
567	7.54	0.01	5.34	0.00	61.55	0.21	0.84	24.43	0.09	0.01	0.00	0.00	0.00	0.00	99.98
600	7.73	0.00	5.18	0.01	61.73	0.19	0.90	24.06	0.00	0.03	0.00	0.00	0.01	0.10	99.92
633	7.45	0.00	5.35	0.00	61.45	0.19	0.86	24.29	0.04	0.01	0.01	0.00	0.00	0.08	99.72
667	7.59	0.02	5.06	0.00	61.99	0.20	0.86	24.18	0.00	0.00	0.00	0.00	0.00	0.15	100.05
700	7.69	0.02	4.98	0.00	62.07	0.17	0.93	24.11	0.00	0.00	0.01	0.00	0.00	0.11	100.09
733	7.68	0.00	4.99	0.00	62.23	0.16	0.86	24.24	0.00	0.00	0.00	0.01	0.00	0.12	100.29
767	7.60	0.00	4.69	0.00	62.28	0.12	1.00	23.68	0.10	0.02	0.00	0.04	0.00	0.09	99.58
800	7.21	0.01	4.85	0.01	62.22	0.18	0.93	24.21	0.00	0.03	0.00	0.00	0.00	0.09	99.75
833	7.28	0.04	4.51	0.01	62.12	0.19	1.01	23.50	0.08	0.00	0.01	0.00	0.00	0.10	98.83
867	7.93	0.00	4.56	0.00	62.50	0.16	0.98	23.97	0.00	0.00	0.01	0.05	0.02	0.08	100.27
900	7.91	0.03	4.77	0.01	61.96	0.16	0.98	23.83	0.14	0.00	0.00	0.01	0.00	0.14	99.89
933	7.64	0.01	4.78	0.00	62.03	0.16	0.96	24.16	0.00	0.02	0.00	0.02	0.02	0.09	99.89
967	8.45	0.00	4.08	0.00	62.14	0.17	1.19	23.32	0.00	0.00	0.00	0.02	0.02	0.19	99.58
1000	7.78	0.08	3.85	0.00	62.78	0.18	1.22	23.23	0.04	0.00	0.00	0.00	0.02	0.12	99.30

LV-HCF-005-2A1 Plagioclase Rim to Rim

Distance (μm)	Na_2O	TiO_2	CaO	MgO	SiO_2	FeO	K_2O	Al_2O_3	F	MnO	Cl	Cr_2O_3	P_2O_5	BaO	Total
38	8.35	0.01	3.65	0.00	63.80	0.15	1.29	22.47	0.03	0.00	0.00	0.00	0.04	0.07	99.85
75	8.01	0.00	3.67	0.00	63.66	0.18	1.31	22.70	0.01	0.00	0.00	0.00	0.00	0.12	99.64
113	8.16	0.00	3.77	0.00	62.41	0.18	1.25	22.78	0.00	0.00	0.00	0.03	0.02	0.10	98.69
150	8.55	0.01	3.78	0.00	64.41	0.20	1.25	22.78	0.12	0.00	0.00	0.00	0.00	0.08	101.13
188	8.13	0.04	3.82	0.00	63.35	0.16	1.24	22.97	0.00	0.04	0.00	0.01	0.03	0.09	99.88
225	8.09	0.04	3.75	0.00	64.07	0.14	1.25	22.73	0.00	0.01	0.00	0.00	0.03	0.11	100.21
263	8.23	0.00	3.80	0.00	63.71	0.16	1.22	22.55	0.05	0.00	0.00	0.02	0.00	0.10	99.80
338	7.61	0.02	4.59	0.00	62.84	0.18	1.02	23.36	0.00	0.01	0.00	0.03	0.01	0.00	99.67
413	7.63	0.00	4.92	0.02	62.27	0.18	0.91	23.53	0.00	0.00	0.00	0.01	0.00	0.01	99.47
488	7.62	0.04	5.07	0.01	61.87	0.20	0.81	24.08	0.20	0.00	0.00	0.00	0.00	0.04	99.85
525	7.44	0.00	5.42	0.00	61.78	0.18	0.80	24.03	0.00	0.02	0.00	0.00	0.01	0.01	99.69
563	7.57	0.04	5.56	0.01	61.77	0.19	0.78	24.12	0.00	0.00	0.00	0.02	0.00	0.04	100.08
600	7.46	0.02	5.07	0.01	61.79	0.20	0.86	23.91	0.00	0.00	0.01	0.00	0.01	0.06	99.40
638	7.16	0.01	5.12	0.02	60.43	0.21	0.87	24.93	0.10	0.01	0.01	0.01	0.05	0.07	98.95
675	7.36	0.01	5.38	0.00	61.38	0.19	0.78	23.82	0.00	0.00	0.00	0.02	0.00	0.07	99.01
713	7.66	0.00	5.15	0.00	61.84	0.21	0.79	23.78	0.07	0.00	0.00	0.00	0.00	0.09	99.56
750	7.80	0.02	4.93	0.02	61.67	0.21	0.86	23.89	0.15	0.00	0.00	0.00	0.02	0.06	99.55
788	7.95	0.01	4.10	0.00	62.93	0.13	1.13	22.42	0.02	0.03	0.00	0.00	0.06	0.06	98.81
825	7.72	0.03	4.75	0.01	62.61	0.16	0.95	23.32	0.00	0.00	0.00	0.00	0.00	0.06	99.60
863	7.49	0.00	4.64	0.01	62.79	0.22	0.97	23.13	0.00	0.00	0.00	0.00	0.04	0.12	99.40
900	7.59	0.02	4.67	0.01	62.92	0.19	0.96	23.22	0.00	0.00	0.00	0.00	0.00	0.08	99.66
975	7.79	0.00	4.78	0.01	63.85	0.18	0.95	23.82	0.00	0.00	0.00	0.02	0.00	0.13	101.52
1013	7.62	0.01	4.82	0.00	61.81	0.17	0.90	23.41	0.10	0.01	0.00	0.01	0.06	0.08	98.96
1050	7.77	0.01	4.77	0.01	62.95	0.19	0.97	23.38	0.00	0.00	0.00	0.00	0.00	0.03	100.08
1088	7.61	0.02	5.09	0.02	62.11	0.18	0.90	23.59	0.00	0.00	0.00	0.00	0.00	0.09	99.62
1125	7.50	0.03	4.91	0.00	62.42	0.18	0.89	23.43	0.05	0.00	0.00	0.00	0.00	0.08	99.47
1163	7.88	0.04	4.45	0.02	62.87	0.18	1.00	23.13	0.06	0.01	0.00	0.00	0.00	0.11	99.69
1200	7.71	0.01	4.55	0.01	62.78	0.18	0.93	23.36	0.11	0.01	0.00	0.00	0.00	0.02	99.64
1238	7.83	0.00	4.56	0.01	62.73	0.20	1.01	23.20	0.08	0.00	0.01	0.02	0.00	0.11	99.71
1313	8.34	0.00	3.49	0.00	64.54	0.18	1.33	22.20	0.02	0.01	0.00	0.00	0.00	0.12	100.22
1350	7.94	0.01	3.45	0.00	64.13	0.13	1.31	22.07	0.03	0.02	0.00	0.01	0.00	0.09	99.17
1388	8.02	0.04	3.42	0.00	64.18	0.18	1.37	22.18	0.03	0.02	0.00	0.02	0.00	0.05	99.49

LV-HCF-006-1A3 Sanidine Rim to Rim

Distance (μm)	Na_2O	TiO_2	CaO	MgO	SiO_2	FeO	K_2O	Al_2O_3	F	MnO	Cl	Cr_2O_3	P_2O_5	BaO	Total
97	4.02	0.00	0.25	0.00	65.30	0.08	9.88	19.32	0.00	0.01	0.00	0.00	0.02	1.39	100.27
122	3.83	0.00	0.28	0.01	64.99	0.09	9.79	19.49	0.00	0.02	0.02	0.00	0.04	1.36	99.90
146	3.79	0.02	0.24	0.00	64.57	0.10	9.76	19.22	0.06	0.00	0.00	0.00	0.00	1.42	99.14
170	3.79	0.00	0.26	0.00	64.85	0.12	10.10	19.22	0.00	0.02	0.01	0.00	0.02	1.35	99.75
195	3.95	0.00	0.26	0.00	65.62	0.11	9.93	19.42	0.08	0.01	0.00	0.01	0.03	1.30	100.67
219	3.72	0.01	0.24	0.00	65.15	0.09	9.98	19.56	0.05	0.00	0.00	0.00	0.06	1.41	100.25
243	3.84	0.00	0.23	0.00	64.64	0.06	10.04	19.29	0.00	0.00	0.01	0.00	0.02	1.36	99.49
268	3.71	0.04	0.26	0.00	65.17	0.10	10.03	19.21	0.08	0.00	0.00	0.00	0.02	1.36	99.93
292	3.91	0.00	0.26	0.00	65.07	0.10	10.00	19.32	0.07	0.00	0.00	0.01	0.00	1.33	100.04
341	3.85	0.04	0.25	0.00	65.33	0.13	9.80	19.28	0.09	0.00	0.00	0.00	0.00	1.30	100.04
365	3.92	0.02	0.26	0.00	65.06	0.10	9.90	19.43	0.00	0.00	0.00	0.01	0.00	1.16	99.84
390	4.09	0.00	0.29	0.00	65.84	0.11	9.98	19.44	0.08	0.00	0.00	0.02	0.00	0.82	100.62
463	4.25	0.00	0.36	0.00	66.19	0.08	9.53	19.42	0.00	0.02	0.00	0.00	0.01	0.67	100.55
487	4.31	0.02	0.33	0.00	65.81	0.10	9.47	19.26	0.02	0.00	0.00	0.02	0.00	0.60	99.93
511	4.20	0.00	0.30	0.00	65.61	0.08	9.59	19.36	0.05	0.00	0.01	0.02	0.02	0.71	99.91
536	3.43	0.03	0.25	0.00	69.17	0.40	8.72	16.53	0.00	0.02	0.02	0.00	0.00	0.59	99.15
560	8.18	0.07	3.39	0.00	64.25	0.14	1.35	22.38	0.12	0.00	0.00	0.00	0.01	0.05	99.89
584	7.49	0.00	2.99	0.00	64.39	0.19	1.82	21.50	0.00	0.02	0.00	0.00	0.00	0.18	98.58
609	8.09	0.01	3.23	0.01	65.42	0.17	1.48	21.84	0.00	0.00	0.00	0.00	0.06	0.02	100.32
633	7.54	0.03	2.33	0.00	65.09	0.16	3.47	21.13	0.08	0.00	0.00	0.00	0.00	0.29	100.07
657	8.26	0.03	3.08	0.00	65.14	0.19	1.53	22.17	0.00	0.00	0.00	0.00	0.02	0.06	100.48
682	4.31	0.01	0.26	0.00	65.44	0.10	9.69	19.47	0.00	0.00	0.00	0.00	0.02	0.84	100.15
706	4.15	0.01	0.25	0.00	66.03	0.08	9.83	19.28	0.10	0.00	0.00	0.03	0.01	0.84	100.59
755	4.00	0.03	0.27	0.00	65.70	0.09	9.73	19.32	0.00	0.03	0.00	0.00	0.05	0.84	100.06
779	4.02	0.03	0.38	0.00	65.32	0.12	9.66	19.55	0.00	0.00	0.00	0.03	0.00	1.12	100.23
804	4.03	0.03	0.30	0.00	65.45	0.09	9.64	19.60	0.01	0.00	0.01	0.00	0.03	1.19	100.37
828	3.89	0.02	0.28	0.00	65.10	0.07	9.87	19.65	0.01	0.01	0.00	0.00	0.00	1.31	100.21
877	3.97	0.01	0.26	0.00	65.33	0.08	9.91	19.66	0.08	0.00	0.00	0.00	0.00	1.28	100.55
925	3.80	0.06	0.46	0.06	76.55	0.77	4.64	12.88	0.00	0.03	0.03	0.00	0.03	0.00	99.30
950	3.55	0.14	0.45	0.05	76.08	0.80	4.75	12.97	0.05	0.00	0.04	0.00	0.04	0.10	98.99
974	3.64	0.09	0.46	0.04	77.36	0.86	4.95	13.19	0.00	0.04	0.03	0.03	0.02	0.05	100.77

LV-HCF-006-2-3 Sanidine Rim to Rim

Distance (μm)	Na_2O	TiO_2	CaO	MgO	SiO_2	FeO	K_2O	Al_2O_3	F	MnO	Cl	Cr_2O_3	P_2O_5	BaO	Total
39	3.74	0.00	0.27	0.01	65.26	0.10	10.03	19.16	0.00	0.03	0.00	0.00	0.00	1.56	100.15
78	3.92	0.01	0.29	0.01	65.02	0.11	10.18	19.39	0.22	0.00	0.00	0.00	0.00	1.58	100.65
118	3.87	0.02	0.27	0.00	65.13	0.07	10.04	19.52	0.00	0.02	0.00	0.00	0.00	1.58	100.51
157	3.94	0.03	0.29	0.00	65.29	0.09	10.04	19.61	0.03	0.00	0.01	0.00	0.00	1.60	100.92
196	3.90	0.00	0.26	0.00	65.55	0.13	9.99	19.13	0.04	0.02	0.00	0.02	0.01	1.54	100.56
235	3.79	0.00	0.27	0.00	64.17	0.12	10.08	18.87	0.06	0.00	0.00	0.00	0.00	1.61	98.96
274	4.00	0.02	0.28	0.00	65.04	0.09	10.04	19.55	0.11	0.02	0.00	0.00	0.00	1.52	100.63
314	3.97	0.01	0.25	0.00	65.49	0.08	9.90	19.56	0.00	0.01	0.00	0.02	0.02	1.59	100.90
353	3.91	0.00	0.25	0.01	65.22	0.08	9.86	19.57	0.00	0.00	0.00	0.00	0.02	1.51	100.45
392	3.83	0.00	0.26	0.00	63.81	0.15	10.06	19.42	0.00	0.01	0.00	0.01	0.00	1.58	99.12
431	3.93	0.03	0.30	0.00	65.36	0.09	10.16	19.42	0.10	0.00	0.01	0.01	0.00	1.55	100.90
470	3.71	0.02	0.25	0.00	64.82	0.08	10.03	19.54	0.05	0.00	0.00	0.00	0.00	1.61	100.09
510	3.86	0.00	0.28	0.01	65.14	0.11	10.04	19.76	0.00	0.01	0.00	0.01	0.00	1.55	100.75
549	4.03	0.00	0.28	0.00	64.93	0.11	10.12	19.52	0.05	0.00	0.01	0.00	0.05	1.58	100.66
588	3.82	0.00	0.29	0.00	65.51	0.08	10.03	19.54	0.04	0.01	0.00	0.00	0.00	1.47	100.77

LV-HCF-006-2-4 Sanidine Rim to Rim

Distance (μm)	Na_2O	TiO_2	CaO	MgO	SiO_2	FeO	K_2O	Al_2O_3	F	MnO	Cl	Cr_2O_3	P_2O_5	BaO	Total
84	3.89	0.00	0.21	0.00	65.68	0.06	10.13	19.52	0.11	0.00	0.00	0.00	0.05	1.51	101.11
167	3.72	0.04	0.26	0.00	65.46	0.10	10.13	19.56	0.00	0.02	0.01	0.00	0.00	1.58	100.89
251	3.68	0.04	0.28	0.00	65.21	0.12	10.01	19.48	0.01	0.02	0.01	0.02	0.04	1.57	100.46
335	4.07	0.01	0.28	0.00	64.70	0.11	10.15	19.44	0.00	0.02	0.01	0.03	0.00	1.58	100.40
418	3.72	0.08	0.26	0.02	64.95	0.11	9.99	19.36	0.00	0.03	0.00	0.00	0.00	1.43	99.93
502	3.84	0.03	0.26	0.00	65.64	0.12	10.14	19.48	0.00	0.04	0.02	0.00	0.00	1.43	100.99
586	3.79	0.01	0.26	0.00	64.66	0.10	10.17	19.30	0.00	0.03	0.00	0.00	0.02	1.58	99.91
670	3.89	0.00	0.27	0.00	64.66	0.10	10.08	19.52	0.24	0.00	0.00	0.00	0.04	1.44	100.13
753	3.92	0.01	0.27	0.00	65.08	0.14	9.50	19.70	0.00	0.01	0.00	0.00	0.00	1.58	100.19
837	3.69	0.04	0.29	0.00	65.26	0.15	9.95	19.57	0.00	0.00	0.01	0.01	0.00	1.42	100.39
921	3.81	0.04	0.26	0.00	65.71	0.10	10.09	19.30	0.03	0.00	0.00	0.02	0.01	1.46	100.83
1004	4.07	0.04	0.29	0.00	64.39	0.11	10.18	19.47	0.00	0.05	0.00	0.01	0.00	1.54	100.15
1088	3.74	0.05	0.24	0.00	65.43	0.09	10.08	19.37	0.02	0.00	0.01	0.02	0.04	1.48	100.55
1172	3.68	0.00	0.25	0.00	65.23	0.07	10.04	19.36	0.03	0.00	0.00	0.00	0.00	1.57	100.24
1256	3.53	0.09	0.28	0.00	64.39	0.10	9.88	18.86	0.14	0.00	0.01	0.00	0.00	1.57	98.77
1339	3.72	0.04	0.26	0.00	64.99	0.07	10.17	19.43	0.05	0.03	0.00	0.00	0.01	1.61	100.37
1423	3.90	0.06	0.27	0.00	65.46	0.11	10.22	19.15	0.03	0.01	0.00	0.01	0.00	1.42	100.61
1507	3.92	0.00	0.28	0.01	65.32	0.11	10.08	19.30	0.00	0.00	0.00	0.00	0.03	1.52	100.56
1590	3.80	0.00	0.30	0.00	65.41	0.11	10.17	19.51	0.06	0.00	0.00	0.00	0.00	1.42	100.76
1674	4.12	0.02	0.24	0.00	65.69	0.11	10.24	19.32	0.00	0.00	0.01	0.02	0.00	1.35	101.11

LV-MR-004-1-1-2 Sanidine Core to Rim

Distance (μm)	Na_2O	TiO_2	CaO	MgO	SiO_2	FeO	K_2O	Al_2O_3	F	MnO	Cl	Cr_2O_3	P_2O_5	BaO	Total
26	4.20	65.26	11.59	0.16	0.00	0.09	0.00	19.14	0.02	0.00	0.05	0.02	0.00	0.11	100.60
48	4.47	63.91	11.87	0.19	0.00	0.02	0.01	18.84	0.06	0.00	0.06	0.00	0.00	0.07	99.49
70	4.49	63.71	12.25	0.17	0.00	0.00	0.01	18.74	0.09	0.00	0.05	0.02	0.00	0.13	99.67
92	4.39	63.61	12.02	0.16	0.00	0.00	0.00	18.76	0.08	0.00	0.04	0.02	0.00	0.01	99.08
114	4.53	63.63	11.98	0.17	0.00	0.00	0.02	18.91	0.04	0.00	0.04	0.02	0.01	0.03	99.37
136	4.34	63.51	11.94	0.14	0.00	0.00	0.00	18.69	0.00	0.00	0.07	0.01	0.00	0.01	98.70
158	4.34	63.56	11.98	0.13	0.00	0.00	0.00	18.76	0.05	0.00	0.06	0.01	0.00	0.05	98.94
180	4.41	63.41	11.97	0.16	0.00	0.00	0.00	18.79	0.06	0.00	0.06	0.01	0.00	0.14	99.01
202	4.47	63.67	11.94	0.16	0.00	0.00	0.00	18.91	0.05	0.00	0.05	0.01	0.00	0.12	99.36
224	4.60	63.50	12.04	0.15	0.00	0.00	0.00	18.82	0.08	0.00	0.07	0.02	0.00	0.13	99.40
246	4.46	63.77	11.66	0.17	0.00	0.00	0.00	18.97	0.00	0.00	0.06	0.01	0.01	0.09	99.18
268	4.49	63.59	11.65	0.17	0.00	0.00	0.00	18.75	0.00	0.00	0.05	0.00	0.01	0.15	98.86
290	4.65	63.82	11.67	0.17	0.00	0.00	0.00	18.82	0.00	0.00	0.05	0.01	0.00	0.09	99.26
312	4.50	63.49	11.71	0.18	0.00	0.00	0.00	18.84	0.09	0.00	0.06	0.01	0.00	0.15	99.03
334	4.50	63.67	11.69	0.14	0.00	0.01	0.00	18.85	0.00	0.00	0.02	0.00	0.01	0.11	98.98
356	4.53	63.54	11.77	0.16	0.00	0.00	0.00	18.78	0.00	0.00	0.02	0.01	0.07	0.14	98.99
378	4.39	63.65	11.83	0.14	0.00	0.00	0.00	18.77	0.00	0.00	0.04	0.00	0.01	0.16	98.99
400	4.54	63.58	11.61	0.15	0.00	0.00	0.00	18.66	0.00	0.00	0.04	0.00	0.01	0.20	98.80
422	4.43	62.90	11.73	0.18	0.00	0.12	0.00	18.71	0.00	0.00	0.06	0.01	0.11	0.40	98.57
444	4.46	63.61	11.63	0.19	0.00	0.00	0.00	18.94	0.00	0.00	0.03	0.02	0.01	0.40	99.27
466	4.45	63.55	11.89	0.17	0.00	0.07	0.00	19.08	0.00	0.00	0.07	0.02	0.00	0.55	99.80
488	4.42	63.31	11.93	0.17	0.00	0.02	0.00	19.05	0.06	0.00	0.07	0.00	0.00	0.55	99.58
510	4.50	63.64	11.96	0.16	0.00	0.00	0.00	18.98	0.03	0.00	0.11	0.01	0.00	0.37	99.76
532	4.39	63.67	11.88	0.15	0.00	0.00	0.00	18.94	0.08	0.00	0.10	0.02	0.00	0.32	99.54
554	4.57	63.65	12.06	0.14	0.00	0.00	0.00	18.96	0.02	0.00	0.11	0.01	0.00	0.36	99.86
576	4.35	63.45	12.00	0.14	0.00	0.09	0.00	18.86	0.02	0.00	0.13	0.00	0.01	0.25	99.25
598	4.27	63.65	12.01	0.13	0.00	0.00	0.00	19.09	0.08	0.00	0.11	0.01	0.00	0.38	99.73
620	4.50	63.55	12.04	0.15	0.00	0.00	0.00	18.96	0.09	0.00	0.08	0.02	0.01	0.31	99.70
664	4.44	63.78	12.06	0.11	0.00	0.00	0.00	18.93	0.05	0.00	0.09	0.00	0.00	0.22	99.68
686	4.48	64.06	12.08	0.10	0.00	0.09	0.00	19.09	0.00	0.00	0.12	0.00	0.00	0.22	100.19
708	4.44	63.61	12.07	0.13	0.00	0.00	0.00	18.86	0.00	0.00	0.10	0.00	0.00	0.28	99.50
730	4.44	63.78	11.93	0.13	0.00	0.07	0.00	18.75	0.00	0.00	0.09	0.00	0.00	0.32	99.49
752	4.49	63.58	11.87	0.17	0.00	0.00	0.00	18.78	0.00	0.00	0.06	0.00	0.01	0.30	99.25
774	4.44	63.30	11.93	0.15	0.00	0.05	0.00	18.76	0.00	0.00	0.06	0.00	0.00	0.36	99.03
796	4.44	63.75	12.04	0.17	0.00	0.00	0.00	18.81	0.00	0.00	0.10	0.00	0.00	0.32	99.63
818	4.42	63.52	12.16	0.16	0.00	0.00	0.00	18.65	0.00	0.00	0.10	0.00	0.00	0.27	99.27
840	4.49	63.30	11.91	0.16	0.00	0.10	0.00	18.84	0.00	0.00	0.08	0.00	0.00	0.53	99.37
862	4.32	62.69	11.79	0.16	0.00	0.01	0.00	18.89	0.00	0.00	0.08	0.00	0.00	0.81	98.74

LV-MR-004-1-1-2 Sanidine Core to Rim (continued)

Distance (μm)	Na_2O	TiO_2	CaO	MgO	SiO_2	FeO	K_2O	Al_2O_3	F	MnO	Cl	Cr_2O_3	P_2O_5	BaO	Total
884	4.53	62.83	11.57	0.19	0.00	0.09	0.00	19.04	0.00	0.00	0.12	0.00	0.00	0.81	99.14
906	4.56	62.61	11.22	0.20	0.00	0.00	0.01	19.52	0.08	0.00	0.11	0.01	0.00	1.40	99.72
928	4.38	61.25	11.37	0.18	0.00	0.02	0.00	19.17	0.09	0.00	0.09	0.01	0.03	0.92	97.49
950	4.54	63.26	11.67	0.18	0.00	0.00	0.00	19.02	0.05	0.00	0.08	0.02	0.00	0.79	99.60
972	4.43	63.08	11.60	0.17	0.00	0.00	0.00	19.13	0.09	0.00	0.10	0.01	0.00	0.85	99.44
994	4.35	63.16	11.52	0.17	0.00	0.00	0.00	19.06	0.10	0.00	0.11	0.00	0.00	0.68	99.15
1016	4.35	63.11	11.86	0.19	0.00	0.00	0.00	19.08	0.02	0.00	0.10	0.00	0.00	0.59	99.30
1038	4.49	63.30	11.90	0.16	0.00	0.00	0.00	18.79	0.05	0.00	0.11	0.00	0.00	0.44	99.24
1060	4.33	62.96	11.86	0.16	0.00	0.00	0.00	18.65	0.10	0.00	0.11	0.01	0.00	0.47	98.63
1082	4.32	62.66	11.87	0.17	0.00	0.04	0.00	19.02	0.11	0.00	0.12	0.02	0.01	0.39	98.70
1104	5.78	62.91	10.15	0.16	0.00	0.00	0.00	18.96	0.08	0.00	0.11	0.02	0.00	0.42	98.58

LV-MR-004-1-3 Sanidine Rim to Rim

Distance (μm)	Na_2O	TiO_2	CaO	MgO	SiO_2	FeO	K_2O	Al_2O_3	F	MnO	Cl	Cr_2O_3	P_2O_5	BaO	Total
24	4.34	0.05	0.15	0.00	65.52	0.08	11.15	18.98	0.00	0.01	0.00	0.00	0.00	0.13	100.41
47	4.58	0.00	0.19	0.00	63.89	0.06	11.70	18.95	0.00	0.00	0.00	0.00	0.00	0.14	99.52
70	4.53	0.05	0.20	0.00	64.19	0.10	11.60	18.71	0.01	0.00	0.00	0.00	0.02	0.07	99.48
93	4.52	0.00	0.21	0.00	64.30	0.07	11.61	18.88	0.00	0.00	0.00	0.00	0.00	0.11	99.69
116	4.64	0.12	0.17	0.00	64.13	0.07	11.55	18.73	0.00	0.00	0.00	0.00	0.00	0.11	99.51
139	4.37	0.10	0.13	0.00	63.41	0.11	11.58	18.75	0.00	0.00	0.00	0.00	0.01	0.61	99.07
162	4.32	0.07	0.20	0.00	62.56	0.09	11.29	18.97	0.00	0.01	0.00	0.00	0.00	1.13	98.64
185	4.27	0.00	0.21	0.00	62.67	0.12	11.20	18.99	0.07	0.02	0.00	0.00	0.01	1.27	98.78
208	4.33	0.00	0.18	0.00	62.67	0.09	11.50	18.98	0.00	0.01	0.00	0.00	0.00	1.24	99.00
231	4.32	0.07	0.17	0.00	62.86	0.06	11.37	19.08	0.08	0.01	0.00	0.00	0.01	1.10	99.11
254	4.23	0.00	0.20	0.00	64.38	0.08	11.18	19.24	0.21	0.00	0.01	0.00	0.00	1.11	100.54
277	4.35	0.00	0.18	0.00	62.78	0.10	11.43	19.24	0.12	0.00	0.01	0.00	0.00	1.43	99.59
300	4.30	0.02	0.20	0.00	62.98	0.05	11.48	19.10	0.21	0.00	0.00	0.00	0.00	1.32	99.57
323	4.29	0.05	0.18	0.00	62.90	0.11	11.56	18.80	0.10	0.00	0.01	0.00	0.00	1.22	99.18
346	4.27	0.05	0.18	0.00	62.64	0.08	11.57	18.97	0.17	0.00	0.00	0.00	0.00	1.10	98.96
369	4.38	0.02	0.18	0.00	62.95	0.04	11.60	18.62	0.13	0.00	0.00	0.00	0.00	1.14	99.02
392	4.29	0.00	0.20	0.00	62.77	0.14	11.63	18.91	0.21	0.00	0.00	0.00	0.00	1.00	99.06
415	4.27	0.00	0.18	0.00	62.60	0.08	11.65	18.88	0.10	0.00	0.01	0.00	0.00	0.98	98.71
438	4.35	0.06	0.19	0.00	63.02	0.08	11.44	18.95	0.00	0.00	0.01	0.00	0.00	0.81	98.91
461	4.34	0.02	0.20	0.00	62.67	0.06	11.57	18.94	0.00	0.00	0.00	0.00	0.00	1.00	98.78
484	4.04	0.01	0.17	0.00	64.39	0.09	11.15	18.83	0.00	0.00	0.00	0.00	0.02	0.66	99.35
507	4.30	0.02	0.19	0.00	63.20	0.08	11.75	18.98	0.04	0.00	0.01	0.00	0.02	0.79	99.35
530	4.25	0.00	0.18	0.00	63.14	0.14	11.68	19.03	0.11	0.00	0.01	0.00	0.03	0.99	99.50
553	4.28	0.09	0.17	0.00	62.82	0.11	11.71	19.00	0.06	0.00	0.00	0.00	0.01	1.09	99.30
576	4.11	0.02	0.19	0.00	63.44	0.07	11.70	18.94	0.06	0.00	0.00	0.00	0.01	0.59	99.10
599	4.32	0.00	0.15	0.00	63.37	0.06	11.97	18.92	0.00	0.00	0.00	0.00	0.02	0.60	99.42
622	4.44	0.00	0.17	0.00	63.50	0.10	11.83	18.84	0.06	0.00	0.00	0.00	0.02	0.57	99.49
645	4.34	0.00	0.18	0.00	63.76	0.11	11.94	18.68	0.10	0.00	0.00	0.00	0.00	0.32	99.39
668	4.53	0.13	0.17	0.01	64.22	0.12	11.75	18.79	0.00	0.00	0.00	0.00	0.01	0.27	100.00

LV-MR-004-1-4 Plagioclase Core to Rim

Distance (μm)	Na_2O	TiO_2	CaO	MgO	SiO_2	FeO	K_2O	Al_2O_3	F	MnO	Cl	Cr_2O_3	P_2O_5	BaO	Total
20	7.73	0.00	8.11	0.01	56.15	0.07	0.32	26.60	0.08	0.00	0.00	0.00	0.02	0.12	99.18
39	7.83	0.00	8.02	0.02	55.67	0.08	0.31	26.53	0.02	0.00	0.01	0.00	0.04	0.12	98.62
59	7.48	0.00	8.32	0.01	55.39	0.13	0.30	26.79	0.06	0.00	0.00	0.00	0.02	0.05	98.51
78	7.54	0.00	8.22	0.02	55.52	0.13	0.31	26.99	0.00	0.00	0.01	0.00	0.03	0.07	98.82
98	7.19	0.00	9.17	0.02	54.64	0.15	0.24	27.46	0.02	0.00	0.00	0.00	0.01	0.06	98.96
117	7.40	0.00	8.88	0.02	54.77	0.10	0.26	27.24	0.08	0.00	0.01	0.00	0.03	0.08	98.82
137	7.38	0.00	8.59	0.02	54.97	0.14	0.28	27.22	0.12	0.00	0.00	0.00	0.02	0.09	98.77
176	7.37	0.00	8.75	0.02	55.10	0.14	0.24	27.23	0.06	0.00	0.00	0.00	0.01	0.07	98.95
195	7.45	0.00	8.71	0.01	55.11	0.13	0.23	27.16	0.00	0.00	0.00	0.00	0.01	0.14	98.94
234	8.12	0.00	7.53	0.01	56.35	0.14	0.28	26.31	0.07	0.00	0.00	0.00	0.00	0.10	98.86
254	8.80	0.00	6.35	0.01	57.88	0.05	0.36	25.22	0.07	0.00	0.00	0.00	0.00	0.02	98.72
273	9.46	0.00	5.40	0.01	59.12	0.03	0.41	24.48	0.04	0.00	0.00	0.00	0.00	0.07	98.99
293	9.86	0.00	4.49	0.00	60.19	0.06	0.52	23.54	0.00	0.00	0.00	0.00	0.00	0.05	98.72
312	9.98	0.00	4.10	0.00	60.72	0.03	0.58	23.24	0.07	0.00	0.00	0.00	0.00	0.04	98.73
332	9.92	0.00	4.46	0.00	60.35	0.05	0.55	23.57	0.06	0.00	0.00	0.00	0.00	0.05	98.99
351	9.86	0.00	4.38	0.00	60.26	0.07	0.56	23.60	0.04	0.00	0.00	0.00	0.00	0.03	98.79
371	10.11	0.00	4.20	0.00	60.63	0.03	0.59	23.25	0.02	0.00	0.00	0.00	0.00	0.07	98.89
390	10.41	0.00	3.63	0.00	61.27	0.04	0.64	22.73	0.04	0.00	0.00	0.00	0.00	0.04	98.79

LV-MR-004-1-5 Sanidine Rim to Rim

Distance (μm)	Na_2O	TiO_2	CaO	MgO	SiO_2	FeO	K_2O	Al_2O_3	F	MnO	Cl	Cr_2O_3	P_2O_5	BaO	Total
24	4.55	0.03	0.14	0.00	64.29	0.09	11.04	19.04	0.00	0.04	0.00	0.02	0.00	0.29	99.51
47	4.44	0.02	0.16	0.00	63.69	0.08	11.91	18.76	0.00	0.00	0.00	0.01	0.00	0.19	99.26
70	4.42	0.00	0.17	0.00	63.37	0.08	11.96	18.65	0.00	0.11	0.00	0.00	0.00	0.22	98.94
93	4.23	0.00	0.14	0.00	63.59	0.07	12.13	18.78	0.00	0.00	0.00	0.01	0.00	0.29	99.23
116	4.28	0.11	0.16	0.01	63.42	0.07	11.93	18.84	0.00	0.00	0.00	0.01	0.00	0.49	99.31
139	4.24	0.00	0.19	0.00	63.04	0.09	11.67	18.91	0.00	0.00	0.00	0.01	0.00	0.76	98.91
162	4.41	0.00	0.12	0.00	63.57	0.07	11.87	19.04	0.00	0.04	0.00	0.01	0.00	0.33	99.43
185	4.31	0.00	0.17	0.00	63.58	0.04	11.90	18.69	0.00	0.00	0.00	0.02	0.01	0.32	99.03
208	4.16	0.05	0.20	0.00	62.56	0.07	11.79	19.21	0.00	0.00	0.00	0.01	0.00	0.63	98.70
231	4.36	0.05	0.13	0.01	63.13	0.10	11.86	19.34	0.00	0.12	0.00	0.01	0.00	0.65	99.71
254	4.15	0.00	0.15	0.00	64.47	0.03	11.59	19.00	0.00	0.00	0.01	0.00	0.00	0.65	100.04
277	4.30	0.00	0.19	0.01	63.10	0.06	11.87	18.94	0.00	0.00	0.02	0.00	0.00	0.88	99.36
300	4.37	0.00	0.16	0.00	63.07	0.04	11.82	18.96	0.00	0.00	0.00	0.00	0.00	0.91	99.33
323	4.29	0.02	0.20	0.00	62.47	0.06	11.68	18.95	0.00	0.09	0.00	0.00	0.01	1.21	98.93
346	4.19	0.00	0.18	0.00	62.52	0.05	11.63	18.95	0.00	0.00	0.01	0.01	0.01	1.43	98.98
369	4.26	0.01	0.19	0.01	62.23	0.05	11.48	19.09	0.00	0.00	0.00	0.00	0.00	1.46	98.77
392	4.23	0.00	0.21	0.00	62.03	0.08	11.55	19.02	0.00	0.06	0.00	0.01	0.00	1.48	98.64
415	4.20	0.00	0.19	0.00	62.48	0.07	11.57	19.16	0.00	0.00	0.01	0.00	0.00	1.46	99.14
438	4.28	0.00	0.19	0.00	62.30	0.08	11.64	19.17	0.00	0.00	0.01	0.01	0.01	1.55	99.23
461	4.28	0.01	0.17	0.00	62.28	0.06	11.72	18.98	0.00	0.04	0.02	0.00	0.01	1.37	98.92
484	4.03	0.00	0.14	0.00	63.42	0.13	11.40	19.13	0.00	0.00	0.00	0.00	0.01	1.15	99.41
507	4.14	0.10	0.18	0.01	62.65	0.10	11.54	19.17	0.00	0.00	0.00	0.00	0.00	1.22	99.08
530	4.29	0.04	0.14	0.01	62.70	0.10	11.43	19.01	0.00	0.00	0.00	0.00	0.00	1.24	98.95
553	4.83	0.02	0.15	0.00	62.86	0.12	10.99	19.14	0.00	0.06	0.00	0.00	0.00	1.10	99.24
576	4.39	0.10	0.20	0.00	62.69	0.11	11.30	19.01	0.00	0.00	0.02	0.00	0.00	1.23	99.04
599	4.26	0.02	0.18	0.01	62.30	0.09	11.83	19.14	0.00	0.00	0.00	0.00	0.00	1.27	99.09
622	4.20	0.10	0.19	0.00	62.46	0.12	11.70	19.07	0.00	0.00	0.00	0.00	0.00	1.18	99.03
645	4.16	0.08	0.18	0.00	62.46	0.11	11.61	19.09	0.00	0.00	0.00	0.00	0.00	1.17	98.87
668	4.23	0.07	0.17	0.01	62.87	0.08	11.75	19.23	0.00	0.00	0.00	0.00	0.00	1.20	99.62
691	4.17	0.00	0.19	0.01	62.27	0.12	11.70	19.10	0.00	0.00	0.00	0.00	0.00	1.20	98.76
714	4.30	0.02	0.16	0.00	63.01	0.12	11.51	19.23	0.00	0.00	0.00	0.02	0.00	1.12	99.47
737	4.27	0.01	0.19	0.00	62.52	0.10	11.57	19.13	0.00	0.00	0.00	0.02	0.00	1.18	98.97
760	4.49	0.04	0.19	0.00	62.15	0.09	11.57	19.08	0.00	0.00	0.00	0.04	0.01	1.17	98.83
783	4.35	0.03	0.17	0.00	62.56	0.09	11.57	19.14	0.00	0.00	0.00	0.02	0.00	1.19	99.10
806	4.29	0.01	0.17	0.00	62.56	0.11	11.53	19.13	0.00	0.00	0.00	0.03	0.01	1.22	99.03
829	4.37	0.04	0.17	0.00	62.50	0.11	11.46	19.07	0.00	0.00	0.00	0.02	0.00	1.24	98.98
852	4.28	0.02	0.17	0.00	62.35	0.06	11.71	19.08	0.00	0.00	0.00	0.03	0.00	1.29	98.99
875	4.33	0.01	0.20	0.00	62.41	0.11	11.51	19.21	0.00	0.01	0.00	0.01	0.00	1.12	98.91

LV-MR-004-1-5 Sanidine Rim to Rim (continued)

Distance (μm)	Na_2O	TiO_2	CaO	MgO	SiO_2	FeO	K_2O	Al_2O_3	F	MnO	Cl	Cr_2O_3	P_2O_5	BaO	Total
898	4.51	0.00	0.19	0.00	62.69	0.06	11.55	19.12	0.00	0.00	0.00	0.02	0.00	1.16	99.30
921	4.45	0.03	0.18	0.00	62.41	0.10	11.70	19.05	0.00	0.00	0.00	0.02	0.00	1.03	98.96
944	4.32	0.04	0.17	0.01	63.52	0.08	11.64	19.30	0.00	0.00	0.00	0.02	0.00	0.92	100.01
967	4.31	0.02	0.16	0.01	62.49	0.06	11.74	18.97	0.00	0.00	0.00	0.02	0.00	0.96	98.73
990	4.38	0.00	0.17	0.01	62.61	0.05	11.70	18.91	0.00	0.00	0.00	0.02	0.00	0.81	98.66
1013	4.46	0.09	0.19	0.01	62.83	0.08	11.75	18.82	0.00	0.00	0.00	0.01	0.00	0.88	99.10
1036	4.60	0.02	0.16	0.01	63.10	0.04	11.58	18.87	0.00	0.00	0.00	0.02	0.00	0.64	99.03

LV-MR-004-1-6 Plagioclase-Sanidine rim to rim

Distance (μm)	Na_2O	TiO_2	CaO	MgO	SiO_2	FeO	K_2O	Al_2O_3	F	MnO	Cl	Cr_2O_3	P_2O_5	BaO	Total
30	5.85	0.00	0.19	0.00	63.87	0.06	10.06	19.01	0.00	0.00	0.00	0.00	0.02	0.63	99.70
61	4.52	0.00	0.21	0.00	62.61	0.12	11.60	19.19	0.00	0.00	0.00	0.00	0.00	1.06	99.31
91	4.29	0.00	0.20	0.00	62.32	0.10	11.44	19.22	0.01	0.00	0.00	0.00	0.00	1.42	99.00
122	4.35	0.00	0.19	0.00	62.37	0.06	11.54	19.23	0.00	0.00	0.01	0.00	0.03	1.34	99.12
152	4.37	0.00	0.20	0.00	62.25	0.08	11.70	19.13	0.00	0.00	0.00	0.00	0.00	1.45	99.18
183	4.22	0.07	0.16	0.00	62.29	0.11	11.63	19.17	0.00	0.00	0.00	0.00	0.00	1.20	98.86
213	4.20	0.01	0.21	0.00	62.16	0.07	11.69	19.18	0.00	0.00	0.00	0.00	0.03	1.38	98.92
244	4.39	0.09	0.21	0.01	62.15	0.11	11.46	19.09	0.00	0.00	0.01	0.00	0.03	1.40	98.93
274	4.41	0.00	0.20	0.00	62.01	0.14	11.52	19.00	0.00	0.00	0.00	0.00	0.00	1.25	98.52
305	4.77	0.01	0.34	0.00	62.35	0.13	10.99	18.77	0.00	0.00	0.01	0.00	0.05	0.81	98.21
335	4.11	0.00	0.20	0.00	64.12	0.13	11.30	19.26	0.00	0.00	0.00	0.00	0.00	1.08	100.20
366	4.28	0.01	0.26	0.00	62.38	0.10	11.32	19.15	0.01	0.00	0.01	0.00	0.01	1.21	98.72
396	4.14	0.00	0.24	0.00	61.96	0.07	11.34	19.22	0.00	0.00	0.01	0.00	0.00	1.47	98.45
427	4.03	0.03	0.23	0.00	62.13	0.09	11.61	19.16	0.00	0.00	0.00	0.00	0.00	1.41	98.69
457	9.70	0.00	4.00	0.00	61.30	0.15	1.09	22.80	0.00	0.00	0.00	0.00	0.00	0.09	99.12
488	9.55	0.01	3.98	0.00	61.03	0.11	1.00	22.99	0.00	0.00	0.00	0.00	0.00	0.15	98.82
518	8.96	0.00	5.41	0.00	58.98	0.17	0.82	24.09	0.00	0.00	0.00	0.00	0.00	0.18	98.61
549	8.14	0.00	6.76	0.00	57.24	0.24	0.61	25.50	0.00	0.00	0.01	0.00	0.03	0.18	98.70
640	7.93	0.09	6.76	0.02	57.89	0.30	0.65	25.21	0.00	0.00	0.00	0.00	0.00	0.12	98.97
671	8.37	0.15	6.94	0.02	57.07	0.29	0.62	25.38	0.00	0.00	0.01	0.00	0.02	0.16	99.03
701	8.08	0.07	7.25	0.01	57.04	0.28	0.63	25.49	0.00	0.01	0.00	0.00	0.02	0.19	99.07
732	8.41	0.04	6.21	0.24	57.34	0.62	0.89	24.58	0.06	0.00	0.01	0.00	0.01	0.20	98.57
762	8.85	0.04	5.77	0.02	58.71	0.29	0.84	24.44	0.00	0.00	0.00	0.00	0.00	0.16	99.13
793	9.00	0.08	5.43	0.02	59.10	0.23	0.92	24.06	0.00	0.00	0.00	0.00	0.01	0.25	99.12
823	9.25	0.10	5.54	0.01	58.65	0.31	0.83	24.31	0.00	0.00	0.00	0.00	0.00	0.21	99.20
854	9.08	0.13	5.47	0.01	58.91	0.26	0.85	24.09	0.00	0.00	0.01	0.00	0.01	0.23	99.05
884	8.94	0.01	5.53	0.00	58.88	0.23	0.80	24.25	0.00	0.02	0.00	0.00	0.00	0.17	98.84
915	8.94	0.06	5.58	0.01	58.79	0.26	0.73	24.29	0.00	0.00	0.01	0.00	0.02	0.16	98.84
945	8.40	0.07	6.47	0.01	57.92	0.19	0.59	24.94	0.11	0.00	0.00	0.00	0.01	0.09	98.75
976	8.79	0.00	5.85	0.02	58.77	0.17	0.74	24.48	0.17	0.00	0.01	0.00	0.00	0.13	99.05
1006	8.20	0.10	7.33	0.00	56.98	0.22	0.55	25.77	0.07	0.00	0.01	0.00	0.02	0.02	99.24
1037	9.00	0.09	5.94	0.01	58.55	0.21	0.71	24.54	0.02	0.00	0.00	0.00	0.00	0.12	99.19
1067	8.96	0.04	5.89	0.00	58.67	0.28	0.75	24.50	0.07	0.00	0.00	0.00	0.00	0.16	99.29
1098	9.01	0.13	5.83	0.01	58.85	0.28	0.77	24.36	0.07	0.00	0.01	0.00	0.01	0.12	99.41
1128	8.95	0.12	5.87	0.00	58.81	0.22	0.75	24.35	0.12	0.00	0.00	0.00	0.01	0.13	99.26
1159	8.86	0.04	6.15	0.01	58.20	0.28	0.71	24.53	0.12	0.00	0.00	0.00	0.00	0.17	99.02
1189	8.54	0.06	6.88	0.02	57.07	0.26	0.62	25.52	0.12	0.00	0.00	0.00	0.02	0.11	99.18
1220	8.42	0.00	6.94	0.01	57.09	0.24	0.63	25.13	0.05	0.00	0.00	0.00	0.00	0.12	98.62

LV-MR-004-1-6 Plagioclase-Sanidine rim to rim (continued)

Distance (μm)	Na_2O	TiO_2	CaO	MgO	SiO_2	FeO	K_2O	Al_2O_3	F	MnO	Cl	Cr_2O_3	P_2O_5	BaO	Total
1281	8.48	0.03	6.80	0.00	57.39	0.27	0.63	25.18	0.00	0.00	0.00	0.00	0.01	0.18	98.98
1311	9.78	0.04	4.65	0.01	60.12	0.22	0.90	23.66	0.00	0.00	0.00	0.00	0.00	0.16	99.54

LV-MR-004-1-7 Plagioclase Core to Rim

Distance (μm)	Na_2O	TiO_2	CaO	MgO	SiO_2	FeO	K_2O	Al_2O_3	F	MnO	Cl	Cr_2O_3	P_2O_5	BaO	Total
21	8.12	0.10	6.03	0.01	58.75	0.18	0.69	24.73	0.05	0.00	0.01	0.00	0.00	0.13	98.78
41	8.69	0.02	5.99	0.00	58.54	0.10	0.66	24.37	0.06	0.00	0.00	0.00	0.00	0.06	98.47
62	8.82	0.04	5.99	0.00	58.57	0.15	0.68	24.70	0.05	0.00	0.00	0.00	0.01	0.02	99.00
83	8.85	0.06	5.86	0.00	58.76	0.20	0.67	24.71	0.19	0.00	0.01	0.00	0.03	0.09	99.33
103	8.63	0.13	5.81	0.02	58.69	0.14	0.70	24.54	0.16	0.00	0.00	0.00	0.00	0.06	98.79
124	8.69	0.00	5.89	0.00	58.67	0.17	0.70	24.53	0.10	0.00	0.00	0.00	0.00	0.14	98.85
145	8.89	0.13	5.98	0.01	58.42	0.22	0.68	24.53	0.18	0.00	0.01	0.00	0.01	0.15	99.13
165	8.83	0.00	5.94	0.02	58.27	0.25	0.73	24.60	0.14	0.00	0.01	0.00	0.02	0.12	98.86
186	8.75	0.10	6.00	0.00	58.48	0.16	0.70	24.64	0.14	0.00	0.01	0.00	0.02	0.07	99.01
207	8.82	0.00	5.94	0.02	58.16	0.15	0.65	24.77	0.07	0.00	0.01	0.00	0.03	0.04	98.63
227	8.29	0.00	5.75	0.00	59.34	0.18	0.64	24.57	0.00	0.00	0.01	0.00	0.02	0.08	98.88
248	8.60	0.04	5.94	0.00	58.74	0.20	0.71	24.57	0.06	0.00	0.00	0.00	0.00	0.18	99.01
269	8.71	0.00	5.97	0.00	58.37	0.26	0.71	24.61	0.10	0.00	0.00	0.00	0.00	0.19	98.88
290	8.69	0.00	5.91	0.01	58.58	0.20	0.68	24.46	0.00	0.00	0.00	0.00	0.01	0.17	98.70
310	8.55	0.00	6.03	0.00	58.48	0.21	0.68	24.71	0.00	0.00	0.00	0.00	0.00	0.12	98.76
331	8.68	0.00	5.84	0.00	58.74	0.26	0.68	24.48	0.00	0.00	0.00	0.00	0.01	0.15	98.84
352	9.01	0.00	5.19	0.00	59.67	0.19	0.76	23.95	0.00	0.00	0.00	0.00	0.00	0.11	98.89
372	9.13	0.00	5.09	0.00	59.69	0.16	0.83	23.96	0.00	0.00	0.00	0.00	0.00	0.10	98.96
393	8.98	0.00	4.69	0.00	60.05	0.19	1.18	23.48	0.00	0.00	0.00	0.00	0.01	0.07	98.64
414	9.58	0.00	4.13	0.00	61.26	0.15	1.05	23.01	0.00	0.00	0.00	0.00	0.00	0.08	99.26
434	8.75	0.02	5.11	0.01	60.35	0.22	0.79	24.18	0.06	0.00	0.00	0.00	0.00	0.04	99.49
455	9.65	0.00	4.69	0.02	60.32	0.19	0.79	23.69	0.00	0.00	0.00	0.00	0.01	0.06	99.42
476	9.55	0.02	4.31	0.01	60.53	0.15	1.02	23.22	0.00	0.00	0.01	0.00	0.02	0.06	98.91
496	9.65	0.07	4.13	0.01	60.74	0.15	1.04	22.97	0.15	0.00	0.00	0.00	0.00	0.06	98.90
517	9.58	0.02	4.33	0.01	60.58	0.16	0.93	23.29	0.13	0.00	0.00	0.00	0.00	0.06	99.02

LV-DM-001-1-2 Plagioclase Rim to Rim

Distance (μm)	Na_2O	TiO_2	CaO	MgO	SiO_2	FeO	K_2O	Al_2O_3	F	MnO	Cl	Cr_2O_3	P_2O_5	BaO	Total
17	9.18	0.00	3.85	0.01	62.44	0.12	1.08	23.51	0.02	0.00	0.00	0.00	0.00	0.07	100.27
52	9.73	0.02	4.00	0.01	61.05	0.14	1.08	23.11	0.00	0.00	0.00	0.00	0.02	0.11	99.26
87	9.40	0.00	4.16	0.00	61.07	0.12	1.06	23.30	0.00	0.00	0.00	0.00	0.01	0.12	99.24
122	9.59	0.07	4.10	0.00	60.86	0.19	1.10	23.13	0.01	0.00	0.00	0.00	0.02	0.07	99.13
157	9.39	0.00	4.22	0.00	60.54	0.16	1.08	23.20	0.00	0.00	0.00	0.00	0.01	0.13	98.72
192	9.50	0.00	4.21	0.01	60.62	0.09	1.08	23.14	0.00	0.00	0.00	0.00	0.02	0.13	98.80
227	9.30	0.02	4.21	0.00	60.31	0.15	1.03	23.26	0.06	0.00	0.00	0.00	0.02	0.12	98.46
262	9.28	0.00	4.45	0.00	60.30	0.20	0.95	23.50	0.00	0.00	0.00	0.00	0.02	0.12	98.82
332	9.60	0.00	4.44	0.00	60.28	0.17	1.02	23.51	0.00	0.00	0.00	0.00	0.02	0.15	99.19
367	8.86	0.00	4.43	0.00	61.97	0.19	1.01	23.65	0.07	0.00	0.00	0.00	0.00	0.10	100.25
402	9.38	0.00	4.31	0.00	60.55	0.19	1.08	23.22	0.09	0.00	0.00	0.00	0.00	0.07	98.83
437	9.60	0.00	4.22	0.01	60.76	0.20	1.04	23.32	0.07	0.00	0.01	0.00	0.00	0.07	99.25
472	9.38	0.00	4.37	0.01	60.57	0.11	1.06	23.32	0.02	0.00	0.00	0.00	0.00	0.05	98.89
507	9.59	0.00	4.24	0.00	60.76	0.21	1.08	23.30	0.08	0.00	0.00	0.00	0.00	0.01	99.23
542	9.44	0.00	4.30	0.01	60.72	0.18	1.06	23.35	0.11	0.00	0.00	0.00	0.00	0.07	99.19
577	9.55	0.00	4.24	0.00	60.59	0.12	1.07	23.21	0.18	0.00	0.00	0.00	0.00	0.08	98.97
612	9.37	0.02	4.26	0.00	60.65	0.21	1.07	23.39	0.02	0.00	0.00	0.00	0.00	0.10	99.07
647	9.48	0.00	4.28	0.00	60.76	0.23	1.07	23.11	0.05	0.00	0.00	0.00	0.00	0.00	98.95
682	9.44	0.00	4.42	0.01	60.71	0.18	1.03	23.53	0.00	0.00	0.00	0.00	0.00	0.08	99.39
717	8.59	0.00	3.81	0.00	62.22	0.28	1.05	23.30	0.00	0.00	0.00	0.00	0.01	0.07	99.32
787	9.56	0.00	4.14	0.00	60.68	0.20	1.03	23.19	0.00	0.00	0.00	0.00	0.00	0.08	98.89
822	9.55	0.00	4.19	0.01	60.37	0.17	1.06	23.09	0.06	0.00	0.00	0.00	0.01	0.06	98.54
857	9.64	0.00	4.03	0.00	60.74	0.17	1.07	23.20	0.00	0.00	0.00	0.00	0.00	0.04	98.89
892	9.59	0.01	4.09	0.00	60.70	0.16	1.07	23.14	0.00	0.00	0.00	0.00	0.00	0.05	98.80
927	9.61	0.05	3.90	0.00	60.68	0.23	1.08	23.14	0.00	0.00	0.01	0.00	0.00	0.12	98.82
997	9.44	0.00	3.95	0.01	60.94	0.22	1.16	22.96	0.00	0.00	0.00	0.00	0.00	0.07	98.74
1032	9.48	0.02	3.83	0.01	61.04	0.22	1.08	22.80	0.00	0.00	0.00	0.00	0.00	0.07	98.54
1067	9.05	0.02	4.00	0.00	62.06	0.08	1.16	23.06	0.09	0.00	0.00	0.00	0.00	0.03	99.51
1102	9.50	0.00	4.11	0.00	60.98	0.11	1.13	22.94	0.13	0.00	0.00	0.00	0.02	0.00	98.86
1137	9.55	0.03	4.09	0.00	60.91	0.09	1.14	22.89	0.07	0.00	0.00	0.00	0.01	0.03	98.77
1172	9.42	0.00	3.96	0.01	61.11	0.10	1.14	23.06	0.00	0.00	0.00	0.00	0.00	0.03	98.83
1207	9.37	0.00	4.03	0.00	60.97	0.17	1.15	22.88	0.09	0.00	0.00	0.00	0.00	0.02	98.64
1242	9.55	0.01	4.11	0.00	60.87	0.12	1.16	23.02	0.02	0.00	0.00	0.00	0.01	0.02	98.87
1277	9.47	0.00	4.12	0.00	60.82	0.14	1.16	22.96	0.13	0.00	0.00	0.00	0.00	0.08	98.81
1312	9.58	0.00	4.30	0.00	60.79	0.13	1.15	23.08	0.00	0.00	0.00	0.00	0.01	0.02	99.06
1347	9.51	0.00	4.34	0.00	60.34	0.12	1.10	23.28	0.00	0.00	0.00	0.00	0.00	0.00	98.68
1382	9.29	0.06	4.21	0.00	60.62	0.09	1.09	23.25	0.06	0.00	0.00	0.00	0.02	0.02	98.68
1417	8.71	0.00	4.29	0.00	61.41	0.17	1.09	23.45	0.00	0.00	0.00	0.00	0.01	0.08	99.22

LV-DM-001-1-2 Plagioclase Rim to Rim (continued)

Distance (μm)	Na_2O	TiO_2	CaO	MgO	SiO_2	FeO	K_2O	Al_2O_3	F	MnO	Cl	Cr_2O_3	P_2O_5	BaO	Total
1452	9.44	0.00	4.19	0.00	60.61	0.19	1.05	23.11	0.00	0.00	0.00	0.00	0.03	0.08	98.69
1487	9.50	0.00	4.30	0.00	60.66	0.18	1.05	23.39	0.00	0.00	0.01	0.00	0.01	0.06	99.16
1522	9.34	0.00	4.10	0.00	60.94	0.17	1.10	23.29	0.00	0.00	0.00	0.00	0.02	0.15	99.12
1557	9.56	0.00	4.26	0.00	60.46	0.18	1.04	23.25	0.00	0.00	0.00	0.00	0.01	0.07	98.83
1592	9.30	0.00	4.55	0.00	60.18	0.15	1.01	23.56	0.05	0.00	0.00	0.00	0.03	0.08	98.86
1627	9.16	0.00	4.69	0.00	60.20	0.17	0.97	23.43	0.00	0.00	0.01	0.00	0.02	0.11	98.75
1662	9.29	0.00	4.20	0.00	60.68	0.18	1.02	23.24	0.00	0.00	0.01	0.00	0.02	0.10	98.73
1697	9.53	0.01	4.34	0.00	60.57	0.15	1.04	23.18	0.00	0.00	0.00	0.00	0.03	0.10	98.95
1732	9.18	0.02	4.27	0.00	60.70	0.18	1.03	23.31	0.00	0.00	0.00	0.00	0.01	0.06	98.77

LV-DM-001-1-3 Sanidine

Distance (μm)	Na_2O	TiO_2	CaO	MgO	SiO_2	FeO	K_2O	Al_2O_3	F	MnO	Cl	Cr_2O_3	P_2O_5	BaO	Total
67	7.21	0.00	0.23	0.01	65.09	0.05	6.93	19.40	0.00	0.00	0.00	0.00	0.00	0.72	99.65
120	3.98	0.00	0.14	0.01	62.85	0.06	12.12	18.76	0.05	0.00	0.00	0.00	0.00	0.64	98.57
173	3.91	0.00	0.16	0.01	63.18	0.08	11.98	18.89	0.09	0.00	0.00	0.00	0.01	0.64	98.90
226	4.00	0.00	0.14	0.01	62.90	0.11	12.20	18.70	0.01	0.01	0.00	0.00	0.01	0.70	98.79
385	9.48	0.00	3.89	0.01	60.81	0.11	1.04	23.03	0.09	0.00	0.00	0.00	0.02	0.04	98.48
438	9.63	0.00	3.92	0.01	61.14	0.14	0.98	22.75	0.00	0.00	0.00	0.00	0.02	0.04	98.62
544	9.64	0.00	3.82	0.01	61.27	0.10	1.10	22.60	0.08	0.00	0.00	0.00	0.01	0.07	98.67
597	8.85	0.05	4.52	0.00	60.74	0.19	0.96	23.82	0.00	0.00	0.00	0.00	0.02	0.04	99.19
650	4.07	0.10	0.18	0.00	62.84	0.10	11.90	19.29	0.00	0.00	0.01	0.00	0.02	1.21	99.72
703	3.98	0.02	0.17	0.00	63.12	0.10	12.25	19.05	0.00	0.00	0.01	0.00	0.01	0.58	99.28
756	3.89	0.09	0.20	0.00	62.43	0.11	12.09	19.18	0.00	0.00	0.01	0.00	0.01	1.07	99.08
809	3.96	0.00	0.19	0.00	62.94	0.13	12.06	19.17	0.00	0.00	0.00	0.00	0.02	1.12	99.58
862	4.02	0.07	0.20	0.01	62.56	0.07	11.89	19.21	0.00	0.00	0.00	0.00	0.02	0.97	99.01
915	4.04	0.03	0.24	0.01	62.96	0.14	11.75	19.01	0.00	0.00	0.00	0.00	0.02	0.95	99.17
968	4.01	0.10	0.23	0.00	62.56	0.09	12.01	19.14	0.00	0.00	0.01	0.00	0.01	1.13	99.29
1021	4.08	0.07	0.26	0.01	62.68	0.08	11.91	19.18	0.00	0.00	0.00	0.00	0.02	1.11	99.39
1074	4.04	0.03	0.24	0.00	62.95	0.08	11.93	19.31	0.00	0.00	0.01	0.01	0.02	1.03	99.64
1127	3.90	0.01	0.26	0.00	64.01	0.07	11.48	19.19	0.00	0.00	0.00	0.00	0.01	0.93	99.85
1180	4.00	0.00	0.28	0.00	62.46	0.09	11.97	19.14	0.13	0.00	0.00	0.00	0.01	1.08	99.10
1233	4.12	0.02	0.30	0.00	62.37	0.13	11.72	19.24	0.00	0.00	0.00	0.00	0.01	1.07	98.97
1286	4.00	0.00	0.13	0.00	63.13	0.07	12.18	18.65	0.02	0.00	0.00	0.00	0.00	0.50	98.67
1339	4.02	0.04	0.12	0.00	63.30	0.11	12.23	18.85	0.00	0.00	0.00	0.00	0.01	0.40	99.08
1392	4.02	0.05	0.26	0.00	62.41	0.12	12.02	19.29	0.00	0.00	0.00	0.00	0.01	1.00	99.17
1445	4.04	0.05	0.27	0.00	62.21	0.08	11.96	19.19	0.00	0.01	0.00	0.00	0.01	1.15	98.97
1498	3.90	0.06	0.23	0.00	62.29	0.09	12.05	19.07	0.00	0.00	0.01	0.00	0.01	1.17	98.86
1551	3.94	0.06	0.23	0.00	62.17	0.12	11.93	18.88	0.00	0.00	0.00	0.00	0.02	1.12	98.46
1604	4.22	0.01	0.16	0.00	62.85	0.09	11.90	18.98	0.00	0.00	0.00	0.00	0.00	0.88	99.10
1657	4.09	0.02	0.16	0.00	64.20	0.11	11.38	19.13	0.00	0.00	0.00	0.00	0.01	0.79	99.88
1710	4.01	0.00	0.16	0.00	63.25	0.15	11.99	19.11	0.00	0.00	0.00	0.00	0.01	0.88	99.55
1763	3.92	0.00	0.17	0.00	62.86	0.13	12.14	19.14	0.00	0.00	0.00	0.00	0.01	0.83	99.21
1816	3.99	0.00	0.15	0.00	62.92	0.09	12.12	19.26	0.00	0.00	0.00	0.00	0.01	0.88	99.44
1869	4.02	0.02	0.19	0.00	63.03	0.11	12.04	19.09	0.00	0.00	0.00	0.00	0.01	0.72	99.22
1975	4.00	0.00	0.21	0.00	62.70	0.12	12.01	19.18	0.00	0.00	0.00	0.00	0.01	0.79	99.03
2028	4.03	0.00	0.25	0.00	62.56	0.08	11.92	19.27	0.00	0.00	0.00	0.00	0.00	1.18	99.28
2081	3.80	0.00	0.12	0.00	63.87	0.12	12.11	19.08	0.00	0.00	0.00	0.00	0.02	0.43	99.55
2134	3.96	0.07	0.16	0.00	63.42	0.12	12.38	18.99	0.00	0.00	0.00	0.00	0.01	0.22	99.32
2187	3.92	0.01	0.15	0.01	64.78	0.04	11.73	19.03	0.00	0.00	0.00	0.00	0.00	0.17	99.84
2240	4.01	0.00	0.16	0.01	63.75	0.02	12.30	19.00	0.00	0.00	0.00	0.00	0.00	0.18	99.43

LV-DM-001-1-3 Sanidine (continued)

Distance (μm)	Na_2O	TiO_2	CaO	MgO	SiO_2	FeO	K_2O	Al_2O_3	F	MnO	Cl	Cr_2O_3	P_2O_5	BaO	Total
2293	3.97	0.01	0.15	0.01	63.69	0.05	12.26	18.75	0.00	0.00	0.00	0.00	0.00	0.22	99.10
2346	4.09	0.00	0.15	0.01	63.88	0.02	12.36	18.93	0.00	0.00	0.00	0.00	0.00	0.20	99.62
2399	4.08	0.00	0.14	0.02	63.81	0.05	12.31	18.85	0.00	0.00	0.00	0.00	0.01	0.15	99.43
2452	4.07	0.00	0.17	0.00	63.70	0.07	12.23	18.95	0.00	0.00	0.00	0.00	0.01	0.24	99.44
2505	3.95	0.02	0.15	0.00	63.58	0.06	12.43	18.73	0.05	0.00	0.00	0.00	0.01	0.21	99.17
2558	4.09	0.00	0.16	0.00	63.90	0.02	12.08	18.85	0.00	0.00	0.00	0.00	0.00	0.17	99.28
2611	4.27	0.02	0.14	0.01	63.91	0.05	12.04	19.02	0.00	0.00	0.00	0.00	0.01	0.24	99.71
2664	4.14	0.00	0.16	0.01	63.33	0.04	12.07	18.84	0.00	0.00	0.00	0.00	0.00	0.27	98.87
2717	3.77	0.07	0.13	0.00	64.88	0.10	11.25	19.13	0.00	0.00	0.00	0.00	0.02	0.28	99.62
2770	3.85	0.00	0.16	0.00	63.74	0.05	11.76	18.92	0.15	0.00	0.00	0.00	0.01	0.33	98.90
2823	3.92	0.01	0.13	0.00	63.42	0.07	11.93	18.84	0.02	0.00	0.00	0.00	0.02	0.32	98.67
2876	4.11	0.04	0.16	0.00	63.54	0.09	11.72	18.93	0.06	0.00	0.00	0.00	0.03	0.48	99.12
2929	4.07	0.04	0.15	0.00	63.41	0.08	11.75	18.94	0.00	0.00	0.00	0.00	0.01	0.45	98.90
3035	3.98	0.07	0.18	0.00	63.42	0.07	11.75	18.91	0.00	0.00	0.00	0.00	0.02	0.54	98.94
3088	4.10	0.03	0.16	0.00	63.27	0.09	11.69	18.86	0.00	0.00	0.00	0.00	0.01	0.56	98.76
3141	5.32	0.06	0.12	0.00	63.48	0.07	9.93	18.98	0.07	0.00	0.00	0.00	0.02	0.59	98.60
3194	6.38	0.04	0.21	0.00	64.06	0.10	7.97	19.18	0.00	0.00	0.00	0.00	0.02	0.63	98.59

LV-DM-001-1-4-1 Plagioclase

Distance (μm)	Na_2O	TiO_2	CaO	MgO	SiO_2	FeO	K_2O	Al_2O_3	F	MnO	Cl	Cr_2O_3	P_2O_5	BaO	Total
34	9.25	0.00	3.99	0.00	61.76	0.15	0.97	23.31	0.12	0.00	0.00	0.00	0.02	0.12	99.64
64	9.44	0.07	4.69	0.00	59.99	0.16	0.80	23.66	0.11	0.00	0.00	0.00	0.02	0.04	98.93
94	9.17	0.05	4.36	0.00	60.66	0.12	0.97	23.36	0.00	0.00	0.00	0.00	0.01	0.02	98.71
124	9.55	0.07	4.29	0.00	60.79	0.20	0.96	23.45	0.00	0.00	0.00	0.00	0.02	0.08	99.42
154	9.15	0.00	4.57	0.00	60.30	0.16	0.92	23.88	0.05	0.00	0.00	0.00	0.02	0.11	99.14
184	9.26	0.00	4.33	0.00	60.40	0.18	1.00	23.51	0.00	0.00	0.00	0.00	0.04	0.08	98.80
214	9.58	0.00	4.23	0.00	60.66	0.13	1.01	23.45	0.00	0.00	0.00	0.00	0.01	0.10	99.16
244	9.31	0.02	4.31	0.00	60.51	0.15	1.02	23.20	0.00	0.00	0.00	0.00	0.01	0.09	98.62
274	9.41	0.03	4.21	0.01	60.51	0.15	1.03	23.25	0.00	0.00	0.00	0.00	0.03	0.10	98.71
334	8.93	0.02	4.17	0.00	61.90	0.10	0.96	23.50	0.00	0.00	0.00	0.00	0.00	0.02	99.59
364	9.36	0.02	4.37	0.00	60.35	0.10	0.95	23.37	0.00	0.00	0.00	0.00	0.01	0.07	98.60
394	9.10	0.00	4.92	0.00	59.93	0.18	0.88	23.64	0.00	0.00	0.00	0.00	0.00	0.02	98.67
424	9.18	0.00	4.38	0.00	60.44	0.13	0.98	23.40	0.00	0.00	0.00	0.00	0.00	0.00	98.51
484	9.28	0.03	4.22	0.00	61.19	0.16	1.02	23.30	0.00	0.00	0.00	0.00	0.00	0.02	99.20
514	9.42	0.00	4.43	0.00	60.44	0.15	0.97	23.52	0.00	0.00	0.00	0.00	0.00	0.00	98.93
544	9.14	0.03	4.30	0.00	60.58	0.15	1.00	23.25	0.00	0.00	0.00	0.00	0.00	0.00	98.45
574	9.33	0.00	4.30	0.00	60.93	0.17	1.01	23.31	0.00	0.00	0.00	0.00	0.00	0.03	99.07
604	9.35	0.00	4.22	0.00	60.78	0.17	1.07	23.27	0.00	0.00	0.00	0.00	0.02	0.06	98.94
634	8.13	0.04	5.78	0.01	59.64	0.15	0.66	24.95	0.10	0.00	0.00	0.00	0.01	0.01	99.43
694	9.19	0.00	4.57	0.02	60.20	0.21	0.94	23.59	0.14	0.00	0.00	0.00	0.00	0.05	98.85
724	9.49	0.01	3.92	0.01	61.23	0.15	1.08	22.92	0.09	0.00	0.00	0.00	0.00	0.01	98.86
754	9.58	0.02	3.78	0.01	61.39	0.14	1.14	22.83	0.18	0.00	0.00	0.00	0.00	0.07	99.05

LV-DM-001-1-4-2 Plagioclase

Distance (μm)	Na_2O	TiO_2	CaO	MgO	SiO_2	FeO	K_2O	Al_2O_3	F	MnO	Cl	Cr_2O_3	P_2O_5	BaO	Total
35	8.57	0.00	3.87	0.01	63.21	0.15	0.49	23.29	0.04	0.00	0.00	0.00	0.01	0.05	99.67
89	9.42	0.00	4.60	0.01	60.20	0.17	0.86	23.51	0.07	0.00	0.00	0.00	0.01	0.08	98.89
116	8.87	0.00	5.71	0.01	58.66	0.18	0.80	24.50	0.00	0.00	0.00	0.00	0.00	0.03	98.76
170	9.86	0.00	3.53	0.02	61.78	0.18	1.26	22.83	0.07	0.00	0.00	0.00	0.01	0.10	99.62
197	9.79	0.00	3.48	0.00	61.80	0.20	1.31	22.83	0.18	0.00	0.00	0.00	0.00	0.14	99.65
224	9.44	0.00	4.05	0.00	61.17	0.14	1.13	23.28	0.14	0.00	0.00	0.00	0.01	0.10	99.40
251	9.87	0.00	3.46	0.00	61.79	0.16	1.34	22.66	0.02	0.00	0.00	0.00	0.01	0.07	99.38
278	9.85	0.00	4.04	0.01	60.86	0.17	1.21	23.22	0.07	0.00	0.00	0.00	0.00	0.08	99.49
305	9.45	0.00	3.56	0.00	63.06	0.10	1.34	23.41	0.02	0.00	0.00	0.00	0.00	0.00	100.92
332	10.00	0.00	3.56	0.00	62.13	0.18	1.28	23.03	0.00	0.00	0.00	0.00	0.01	0.00	100.18
359	10.01	0.01	3.80	0.01	61.75	0.21	1.24	22.99	0.02	0.00	0.00	0.00	0.03	0.00	100.04
386	9.75	0.02	4.10	0.00	61.09	0.12	1.12	23.15	0.09	0.00	0.00	0.00	0.04	0.02	99.46
413	9.05	0.07	5.82	0.00	58.74	0.12	0.72	24.89	0.00	0.00	0.00	0.00	0.02	0.00	99.43
440	9.74	0.00	4.24	0.00	60.91	0.14	1.09	23.35	0.00	0.00	0.00	0.00	0.02	0.02	99.50
467	9.99	0.00	3.98	0.00	61.11	0.16	1.15	22.94	0.04	0.00	0.00	0.00	0.01	0.02	99.37
494	9.67	0.04	4.44	0.00	60.39	0.14	1.02	23.39	0.00	0.00	0.01	0.00	0.02	0.00	99.10
521	9.66	0.00	4.20	0.00	60.75	0.10	1.05	23.10	0.06	0.00	0.00	0.00	0.01	0.00	98.91
548	9.18	0.00	3.59	0.00	65.52	0.20	0.90	20.99	0.00	0.00	0.01	0.00	0.02	0.00	100.39

LV-DM-001-1-1-5 Plagioclase Rim to Rim

Distance (μm)	Na_2O	TiO_2	CaO	MgO	SiO_2	FeO	K_2O	Al_2O_3	F	MnO	Cl	Cr_2O_3	P_2O_5	BaO	Total
38	8.95	0.00	3.79	0.01	62.17	0.15	1.17	22.94	0.00	0.00	0.00	0.00	0.01	0.01	99.18
66	9.65	0.00	3.96	0.01	60.92	0.19	1.10	22.96	0.00	0.00	0.00	0.00	0.01	0.00	98.80
94	9.58	0.00	3.99	0.00	60.92	0.16	1.17	22.98	0.00	0.00	0.01	0.00	0.02	0.01	98.84
122	9.76	0.02	3.84	0.00	61.35	0.20	1.19	22.79	0.00	0.00	0.00	0.00	0.02	0.04	99.21
150	9.85	0.00	3.61	0.00	61.35	0.10	1.19	22.68	0.00	0.00	0.00	0.00	0.00	0.01	98.81
178	9.86	0.02	3.65	0.00	61.50	0.19	1.17	22.71	0.00	0.00	0.00	0.00	0.01	0.00	99.12
206	9.89	0.00	3.59	0.00	61.38	0.14	1.23	22.31	0.00	0.00	0.00	0.00	0.02	0.00	98.55
234	9.80	0.00	3.86	0.00	61.39	0.17	1.19	22.61	0.00	0.00	0.00	0.00	0.02	0.00	99.03
262	9.79	0.00	3.63	0.00	61.65	0.16	1.17	22.65	0.00	0.00	0.00	0.00	0.01	0.00	99.05
290	9.62	0.00	3.62	0.00	61.42	0.15	1.15	22.62	0.00	0.00	0.00	0.00	0.02	0.00	98.60
318	9.00	0.04	3.48	0.00	62.93	0.20	1.19	22.88	0.00	0.00	0.00	0.00	0.00	0.04	99.75
346	9.83	0.06	3.69	0.00	61.58	0.16	1.19	22.57	0.00	0.00	0.00	0.00	0.00	0.08	99.16
374	9.71	0.14	3.76	0.00	61.36	0.18	1.19	22.79	0.00	0.00	0.00	0.00	0.00	0.04	99.17
402	9.62	0.02	3.99	0.00	61.19	0.12	1.04	22.83	0.04	0.00	0.00	0.00	0.00	0.08	98.91
430	9.62	0.10	4.09	0.00	61.33	0.23	1.08	23.09	0.00	0.00	0.00	0.00	0.00	0.05	99.57
458	9.86	0.05	3.93	0.01	61.35	0.17	1.11	22.87	0.02	0.00	0.00	0.00	0.00	0.05	99.41
486	9.63	0.03	3.87	0.01	61.43	0.15	1.17	22.89	0.11	0.00	0.00	0.00	0.00	0.04	99.27
514	9.79	0.08	3.89	0.00	61.18	0.17	1.11	22.87	0.00	0.00	0.00	0.00	0.00	0.06	99.15
542	9.76	0.06	3.98	0.01	61.14	0.16	1.08	23.05	0.00	0.00	0.00	0.00	0.00	0.08	99.32
570	9.73	0.03	4.02	0.01	61.32	0.15	1.10	23.08	0.02	0.00	0.00	0.00	0.00	0.05	99.50
598	9.29	0.00	3.94	0.02	61.73	0.21	1.12	23.29	0.14	0.00	0.00	0.00	0.00	0.00	99.69
626	9.58	0.07	4.31	0.01	60.71	0.17	1.05	23.04	0.07	0.00	0.00	0.00	0.01	0.00	98.99
654	9.58	0.00	4.20	0.02	61.15	0.16	1.09	23.25	0.04	0.00	0.00	0.00	0.01	0.00	99.48
682	9.60	0.00	4.11	0.00	60.97	0.15	1.07	23.07	0.01	0.00	0.00	0.00	0.00	0.00	98.99
710	9.78	0.00	4.13	0.03	60.93	0.21	0.85	23.17	0.14	0.00	0.00	0.00	0.00	0.00	99.17

APPENDIX B. EPMA ANALYSES OF ORTHOPYROXENE, AMPHIBOLE AND BIOTITE. ERRONEOUS DATA HAVE BEEN REMOVED.

LV-RD-008-1A2 Orthopyroxene Rim to Rim

Distance (μm)	Na_2O	TiO_2	CaO	MgO	SiO_2	FeO	K_2O	Al_2O_3	F	MnO	Cl	Cr_2O_3	P_2O_5	Total
69	0.00	0.08	1.02	15.76	51.63	29.73	0.01	0.40	0.00	1.34	0.00	0.00	0.01	99.97
139	0.03	0.11	1.09	16.74	51.94	28.77	0.01	0.40	0.00	1.34	0.00	0.00	0.00	100.42
208	0.00	0.12	1.04	17.78	51.88	27.66	0.01	0.47	0.00	1.25	0.00	0.00	0.00	100.20
278	0.03	0.13	1.04	17.60	52.51	27.65	0.00	0.45	0.00	1.30	0.00	0.00	0.02	100.73
347	0.04	0.12	1.08	17.55	51.44	27.43	0.01	0.45	0.00	1.27	0.01	0.00	0.02	99.43
416	0.21	0.14	1.07	17.77	51.60	27.60	0.03	0.47	0.00	1.18	0.06	0.01	0.06	100.17
486	0.04	0.07	1.06	17.70	52.10	27.85	0.00	0.44	0.00	1.26	0.00	0.00	0.00	100.53
555	0.02	0.12	1.01	16.37	51.35	29.15	0.01	0.42	0.00	1.32	0.02	0.00	0.04	99.82
625	0.00	0.14	0.99	15.71	51.29	30.39	0.03	0.32	0.09	1.40	0.00	0.00	0.00	100.31
694	1.21	0.15	1.33	11.21	56.79	22.71	1.26	4.21	0.11	0.99	0.04	0.02	0.17	100.13

LV-RD-008-2A1-1 Orthopyroxene Rim to Rim

Distance (μm)	Na_2O	TiO_2	CaO	MgO	SiO_2	FeO	K_2O	Al_2O_3	F	MnO	Cl	Cr_2O_3	P_2O_5	Total
24	0.04	0.13	1.04	16.34	51.41	28.91	0.00	0.40	0.00	1.31	0.01	0.00	0.00	99.58
48	0.01	0.12	1.03	16.72	51.83	28.43	0.00	0.37	0.00	1.24	0.00	0.00	0.03	99.79
72	0.06	0.09	1.06	17.13	51.60	28.16	0.00	0.36	0.00	1.22	0.01	0.01	0.02	99.70
96	0.03	0.08	1.02	17.44	52.12	27.89	0.00	0.32	0.00	1.23	0.00	0.00	0.01	100.14
120	0.07	0.10	1.00	17.29	52.01	27.94	0.00	0.30	0.00	1.21	0.01	0.00	0.01	99.95
144	0.04	0.09	1.03	17.44	51.94	27.84	0.01	0.33	0.00	1.26	0.00	0.00	0.05	100.02
168	0.00	0.11	1.02	17.42	52.13	27.80	0.00	0.40	0.09	1.23	0.00	0.01	0.05	100.23
192	0.01	0.10	1.05	17.06	52.17	28.31	0.00	0.35	0.00	1.22	0.00	0.00	0.01	100.26
216	0.04	0.11	1.04	16.27	51.55	29.25	0.00	0.39	0.01	1.36	0.01	0.05	0.00	100.08
240	0.00	0.12	1.08	17.30	52.16	28.29	0.00	0.47	0.04	1.29	0.00	0.02	0.00	100.75
264	0.00	0.08	1.05	17.54	52.12	27.74	0.00	0.44	0.00	1.20	0.00	0.04	0.00	100.22
288	0.03	0.11	1.06	17.28	52.18	27.94	0.00	0.42	0.00	1.22	0.00	0.00	0.04	100.27
312	0.03	0.14	1.08	17.27	51.54	27.23	0.00	0.49	0.00	1.21	0.00	0.00	0.00	99.01
336	0.06	0.15	1.06	17.64	52.12	27.61	0.00	0.39	0.00	1.21	0.00	0.00	0.06	100.31
360	0.00	0.11	1.05	17.70	53.22	28.58	0.01	0.42	0.00	1.21	0.00	0.00	0.04	102.34
384	0.01	0.11	1.10	17.00	52.19	27.70	0.00	0.44	0.00	1.27	0.00	0.03	0.01	99.85
408	0.02	0.07	2.53	16.82	50.31	27.11	0.00	0.41	0.00	1.27	0.01	0.00	1.33	99.88
432	0.02	0.13	1.08	17.18	51.97	28.06	0.01	0.46	0.00	1.28	0.00	0.01	0.02	100.24
456	0.00	0.11	1.10	16.82	51.21	28.18	0.00	0.49	0.00	1.22	0.00	0.02	0.00	99.15
480	0.00	0.18	1.07	16.97	51.55	28.49	0.00	0.43	0.00	1.26	0.01	0.00	0.03	99.99

LV-RD-009-1A4 Orthopyroxene Rim to Rim

Analysis Point	Na_2O	TiO_2	CaO	MgO	SiO_2	FeO	K_2O	Al_2O_3	F	MnO	Cl	Cr_2O_3	P_2O_5	Total
2	0.01	0.11	1.11	15.70	51.15	30.86	0.01	0.24	0.00	1.39	0.00	0.00	0.00	100.58
3	0.04	0.10	1.12	16.12	51.68	30.05	0.00	0.30	0.00	1.39	0.02	0.01	0.00	100.81
4	0.01	0.08	1.15	16.47	52.02	29.77	0.00	0.25	0.00	1.33	0.00	0.01	0.00	101.10
5	0.00	0.11	1.11	16.53	51.60	29.53	0.00	0.40	0.00	1.37	0.00	0.01	0.00	100.64
6	0.01	0.15	1.19	16.17	51.68	29.66	0.00	0.37	0.00	1.39	0.00	0.01	0.00	100.63
7	0.00	0.11	1.07	16.13	51.50	30.02	0.00	0.40	0.00	1.35	0.00	0.01	0.00	100.59
8	0.06	0.09	1.12	15.47	51.21	30.91	0.00	0.35	0.00	1.31	0.00	0.00	0.00	100.53

LV-RD-009-2A5 Orthopyroxene Rim to Rim

Analysis Point	Na_2O	TiO_2	CaO	MgO	SiO_2	FeO	K_2O	Al_2O_3	F	MnO	Cl	Cr_2O_3	P_2O_5	Total
1	0.07	0.14	1.06	15.36	50.69	31.00	0.01	0.36	0.00	1.44	0.01	0.00	0.00	100.14
2	0.02	0.11	1.15	16.24	51.62	29.72	0.00	0.40	0.00	1.40	0.01	0.01	0.00	100.66
3	0.02	0.11	1.18	16.65	51.33	29.22	0.00	0.29	0.01	1.38	0.01	0.00	0.00	100.21
4	0.06	0.10	1.11	15.88	50.97	29.88	0.00	0.30	0.00	1.38	0.00	0.02	0.00	99.68
5	0.06	0.09	1.16	15.25	51.12	30.50	0.02	0.29	0.00	1.35	0.00	0.02	0.00	99.86
6	0.02	0.14	1.12	16.29	51.33	29.68	0.01	0.37	0.01	1.37	0.00	0.01	0.00	100.35
7	0.00	0.11	1.10	16.09	51.63	29.83	0.00	0.29	0.00	1.37	0.00	0.00	0.00	100.43
8	0.01	0.11	1.11	16.03	50.89	29.55	0.00	0.36	0.00	1.35	0.00	0.05	0.00	99.47

LV-MR-008-1-7-1 Biotite Rim to Rim

Distance (μm)	Na_2O	CaO	MgO	SiO_2	FeO	Al_2O_3	K_2O	Total
39	1.35	46.42	0.63	10.01	10.24	5.68	19.28	93.59
76	1.38	46.45	0.65	10.33	10.07	5.52	19.18	93.57
113	1.44	46.62	0.66	10.25	9.70	5.63	19.68	93.98
150	1.26	45.57	0.67	10.15	9.41	5.64	19.63	92.32
187	1.41	46.49	0.69	10.16	9.62	5.72	20.74	94.83
224	1.20	46.25	0.66	10.07	9.45	5.72	20.77	94.13
261	1.43	46.46	0.68	10.17	9.61	5.77	20.27	94.40
298	1.06	45.27	0.64	9.67	9.44	5.78	21.87	93.72
335	1.42	45.91	0.73	10.16	9.41	6.09	20.14	93.86
372	1.58	45.32	0.74	10.27	9.16	6.68	21.05	94.79
409	1.59	44.85	0.85	10.28	8.64	7.08	20.67	93.96
446	1.47	45.77	0.74	10.38	9.13	6.47	20.16	94.10
483	1.45	46.29	0.66	10.22	9.47	6.05	20.58	94.72
520	1.36	46.53	0.67	10.24	9.51	5.73	20.58	94.60
557	1.42	46.41	0.71	10.33	9.62	5.89	20.31	94.69
594	1.41	46.45	0.67	10.51	9.92	5.75	19.76	94.46
631	1.39	46.68	0.67	10.28	10.00	5.84	19.50	94.35
668	1.41	47.40	0.71	10.52	10.08	5.96	19.85	95.94
705	1.40	46.85	0.65	10.31	10.16	5.72	18.99	94.09
742	1.39	46.85	0.69	10.41	10.07	5.83	18.96	94.19

LV-MR-005-1-1 Amphibole Rim to Rim

Distance (μm)	Na_2O	CaO	MgO	SiO_2	FeO	Al_2O_3	K_2O	Total
32	1.39	10.86	10.94	47.03	17.18	5.81	0.65	93.87
64	1.32	10.95	11.08	47.14	16.87	5.92	0.64	93.92
96	1.31	11.01	11.42	47.38	16.42	5.51	0.61	93.65
128	1.34	10.99	11.21	47.20	16.94	5.72	0.63	94.04
160	1.35	10.89	11.42	47.19	16.63	5.81	0.65	93.94
192	1.50	11.03	11.56	46.48	16.25	6.61	0.69	94.11
224	2.02	11.13	11.04	43.44	14.88	9.79	0.69	92.98
256	1.94	11.12	12.28	44.35	13.07	9.52	0.68	92.96
288	2.03	11.13	12.01	43.99	13.40	9.47	0.70	92.73
320	2.00	11.01	11.92	44.29	13.79	9.66	0.67	93.33
352	2.07	11.15	11.51	44.03	14.02	9.65	0.72	93.15
384	2.02	11.19	11.83	44.18	13.92	9.50	0.70	93.34
416	1.92	11.09	11.38	43.92	14.40	9.32	0.65	92.68
448	1.87	11.27	11.34	43.94	14.25	9.12	0.66	92.44
480	1.64	11.26	12.41	46.07	13.44	7.52	0.70	93.04
512	1.91	11.44	12.24	45.02	13.71	8.82	0.66	93.80
544	1.56	11.22	12.71	47.25	13.66	6.73	0.64	93.77
576	1.53	11.15	11.73	46.57	15.26	6.84	0.64	93.73
608	1.38	11.03	11.10	46.67	16.64	5.84	0.66	93.32
640	1.29	10.98	10.81	46.92	17.17	5.95	0.67	93.79
672	1.36	10.88	11.01	46.74	17.12	6.03	0.69	93.82
704	1.34	10.79	11.13	47.27	17.06	5.74	0.64	93.97
736	1.29	10.89	11.17	47.04	17.39	5.80	0.66	94.23
768	1.34	10.90	11.36	47.13	16.72	5.98	0.63	94.06

LV-MR-005-1-2 Amphibole Rim to Rim

Distance (μm)	Na_2O	CaO	MgO	SiO_2	FeO	Al_2O_3	K_2O	Total
31	1.37	10.76	11.11	46.89	16.93	6.06	0.70	93.83
63	1.36	10.85	11.12	46.43	16.38	6.00	0.66	92.79
95	1.34	10.77	11.07	46.64	16.95	6.09	0.66	93.52
159	1.39	10.79	11.29	47.08	16.61	6.08	0.65	93.87
191	1.93	10.97	9.98	43.20	16.43	9.41	0.69	92.60
223	2.09	10.93	12.47	43.92	12.35	10.20	0.68	92.63
255	2.09	10.87	13.32	44.77	11.84	9.70	0.66	93.24
287	2.17	10.90	13.53	44.67	11.04	9.83	0.67	92.81
319	2.02	11.08	12.17	43.92	13.66	9.97	0.78	93.59
351	1.50	11.03	12.28	46.76	14.14	6.78	0.65	93.14
383	1.35	10.98	11.62	47.10	16.18	5.87	0.65	93.75
415	1.34	10.89	11.34	46.98	16.69	5.75	0.64	93.63
447	1.25	10.91	11.44	47.20	16.86	5.67	0.66	93.99
479	1.35	10.92	11.22	46.74	16.81	5.98	0.69	93.72

LV-MR-005-1-1-2 Amphibole Rim to Rim

Distance (μm)	Na_2O	CaO	MgO	SiO_2	FeO	Al_2O_3	K_2O	Total
52	1.28	10.93	11.22	47.65	16.88	5.75	0.67	94.37
105	1.45	10.91	10.86	46.66	17.38	6.32	0.75	94.32
158	1.35	10.89	10.97	46.42	16.87	6.14	0.71	93.35
211	1.41	10.97	11.24	46.63	16.92	6.10	0.73	94.01
264	1.33	11.02	11.42	46.87	16.99	5.99	0.73	94.35
317	1.34	10.84	10.94	46.85	17.35	5.84	0.69	93.85
370	1.38	10.95	10.95	46.90	17.36	5.95	0.71	94.20
423	1.38	10.97	11.21	46.86	16.94	6.07	0.72	94.14
476	1.26	11.00	11.37	46.98	16.84	6.01	0.66	94.11
529	1.49	11.05	10.94	46.18	17.14	6.61	0.70	94.10
582	2.01	10.89	9.87	42.74	17.59	10.03	0.64	93.76
635	2.12	10.96	11.75	43.67	14.24	10.00	0.54	93.29
688	2.37	10.81	14.13	44.38	11.30	10.45	0.51	93.95
741	1.59	11.02	13.15	46.89	13.60	7.10	0.68	94.03
794	1.98	10.84	11.80	43.60	14.61	9.86	0.81	93.50
847	2.21	11.08	12.49	44.01	13.43	10.20	0.57	93.97
900	2.00	10.94	12.71	44.29	13.11	9.62	0.74	93.42
953	2.00	10.92	10.40	43.36	16.33	9.91	0.58	93.50
1006	1.43	10.77	11.58	46.83	16.36	6.31	0.67	93.95
1059	1.34	10.93	11.24	47.00	17.42	6.00	0.67	94.59
1112	1.37	10.82	10.97	47.18	17.01	6.03	0.71	94.08
1165	1.25	10.75	11.08	46.86	16.71	5.98	0.71	93.35
1218	1.32	10.70	11.27	46.95	16.81	6.00	0.68	93.74
1271	1.33	10.90	11.30	47.36	16.92	5.72	0.68	94.21
1324	1.39	10.61	11.04	46.93	17.03	5.91	0.70	93.61

LV-MR-001-1-11 Amphibole Rim to Rim

Distance (μm)	Na_2O	CaO	MgO	SiO_2	FeO	Al_2O_3	K_2O	Total
16	1.56	10.09	8.20	44.86	21.65	6.39	0.78	93.54
36	1.58	10.01	8.31	44.77	20.71	6.66	0.81	92.84
56	1.55	10.13	8.34	44.60	21.22	6.61	0.79	93.23
76	1.51	10.25	8.26	45.14	22.09	6.29	0.75	94.28
96	1.52	10.24	7.92	45.17	22.29	6.22	0.79	94.14
116	1.54	10.39	9.13	45.64	19.70	6.15	0.75	93.29
136	1.55	10.48	9.72	45.79	19.20	6.26	0.75	93.76
156	1.53	10.68	10.76	46.49	17.57	6.34	0.76	94.12
176	1.75	10.63	9.82	44.40	18.57	7.67	0.89	93.73
196	1.67	10.68	10.34	45.47	17.87	6.96	0.84	93.82
216	1.56	10.74	10.76	46.09	17.23	6.51	0.78	93.68
236	1.53	10.61	10.62	46.13	17.49	6.50	0.76	93.63
256	1.53	10.61	10.62	46.12	17.38	6.12	0.75	93.12
276	1.52	10.61	10.71	46.30	17.68	6.22	0.72	93.75
296	1.45	10.63	10.46	46.19	17.56	6.15	0.77	93.21
316	1.50	10.51	10.14	45.95	18.07	6.27	0.78	93.21
336	1.52	10.08	7.70	44.56	21.45	6.42	0.76	92.50
356	1.49	10.10	8.36	44.23	20.40	6.82	0.80	92.21
376	1.75	9.92	8.66	46.40	20.51	6.59	0.76	94.58

LV-MR-001-1-12 Amphibole Rim to Rim

Distance (μm)	Na_2O	CaO	MgO	SiO_2	FeO	Al_2O_3	K_2O	Total
16	1.99	10.16	8.92	42.27	18.52	9.46	1.05	92.38
36	2.03	10.48	9.61	42.34	17.72	9.70	1.05	92.93
56	2.13	10.25	9.39	42.23	17.95	9.62	1.05	92.61
76	2.13	10.31	9.33	42.14	18.55	9.59	1.06	93.10
96	2.02	10.27	9.37	42.19	17.97	9.51	1.06	92.40
116	2.10	10.23	9.33	42.27	18.44	9.61	1.04	93.01
136	2.13	10.26	7.94	41.92	19.83	9.31	1.05	92.44
156	2.12	10.11	9.30	42.04	18.35	9.70	1.04	92.66
176	2.20	10.37	9.42	41.81	17.93	10.20	1.05	92.98
196	2.12	10.37	9.50	42.13	17.55	10.11	1.02	92.78
216	2.10	10.20	9.10	41.85	18.37	9.96	0.99	92.56
236	2.04	10.14	9.44	42.37	17.87	9.52	0.99	92.39
256	2.12	10.38	9.29	41.89	18.08	9.93	1.09	92.77
276	1.50	10.12	8.33	44.84	21.22	6.61	0.79	93.41
296	2.06	10.18	9.24	42.35	18.00	9.58	0.99	92.40
316	1.20	10.29	7.75	41.72	20.09	9.46	1.05	92.33
336	2.03	10.30	8.04	41.92	20.00	9.33	1.05	92.66
356	1.62	9.65	9.73	41.54	19.74	9.67	0.88	92.81
376	1.49	9.91	7.90	44.75	21.17	6.58	0.85	92.64

LV-MR-004-1-9 Amphibole Rim to Rim

Distance (μm)	Na_2O	CaO	MgO	SiO_2	FeO	Al_2O_3	K_2O	Total
30	1.58	44.42	0.82	10.09	8.04	7.01	21.18	93.13
60	1.71	44.82	0.87	10.11	8.37	6.88	21.13	93.88
90	1.68	44.81	0.82	10.19	8.38	6.82	21.22	93.92
120	1.56	44.79	0.82	10.34	8.39	6.97	21.41	94.25
150	1.73	44.73	0.89	10.22	8.58	6.91	21.49	94.54
180	1.80	43.69	0.98	10.50	8.65	7.93	20.50	94.06
210	0.92	38.51	7.84	1.75	11.19	12.45	18.58	91.23
240	2.11	42.08	0.84	10.86	9.14	10.40	18.40	93.83
270	2.27	43.50	0.84	10.61	9.00	10.51	18.27	95.00
300	2.19	42.66	0.75	10.68	8.89	9.83	18.83	93.82
330	1.69	45.28	0.82	10.40	9.48	6.86	18.95	93.47
360	2.03	44.15	0.79	10.74	10.20	8.87	16.32	93.11
390	1.69	45.47	0.77	10.58	10.13	6.98	18.02	93.63
420	1.56	46.23	0.73	10.48	9.88	6.09	18.23	93.20
450	1.67	44.93	0.81	10.35	9.09	6.98	18.70	92.52
480	1.72	44.04	0.90	10.29	8.10	7.52	20.09	92.66
510	1.62	45.03	0.81	10.28	8.50	6.70	20.60	93.54
540	1.63	45.93	0.75	10.29	8.54	6.41	19.98	93.53
570	1.62	45.80	0.72	10.20	8.70	6.21	20.45	93.72
600	1.64	45.50	0.80	10.36	8.36	6.55	20.17	93.39
630	1.60	45.31	0.77	10.13	8.47	6.51	21.80	94.59
660	1.60	45.42	0.77	10.37	8.27	6.43	21.35	94.21
690	1.62	44.89	0.79	9.99	8.10	6.56	21.79	93.74
720	1.61	45.33	0.76	10.17	8.17	6.37	22.31	94.73

LV-DM-001-1-1 Biotite Rim to Rim

Distance (μm)	Na_2O	CaO	MgO	SiO_2	FeO	Al_2O_3	K_2O	Total
30	1.46	10.01	10.76	45.87	18.58	6.48	0.78	93.93
75	1.43	10.05	10.87	45.78	18.69	6.54	0.79	94.14
120	1.39	10.05	10.70	46.27	18.70	6.21	0.76	94.07
165	1.49	10.03	10.55	46.21	18.61	6.29	0.73	93.91
210	1.43	9.97	10.62	45.95	18.30	6.36	0.78	93.42
255	1.45	10.01	10.58	46.32	18.63	6.31	0.73	94.03
300	1.45	10.06	10.40	45.96	18.58	6.41	0.79	93.64
345	1.49	9.95	10.53	45.73	18.74	6.46	0.79	93.68
390	1.45	10.03	10.55	46.21	18.52	6.17	0.80	93.73
435	1.43	10.17	10.52	46.30	18.79	6.15	0.72	94.08
480	1.34	10.30	10.50	46.47	18.35	5.87	0.68	93.51
525	1.33	10.19	10.40	46.86	18.41	5.79	0.67	93.64
570	1.40	10.13	10.62	46.80	18.73	5.73	0.67	94.09
615	1.43	10.00	10.20	46.39	18.69	5.87	0.72	93.31
660	1.48	9.97	10.46	46.43	18.96	6.04	0.62	93.94
705	1.42	9.89	10.35	46.25	18.75	5.82	0.64	93.11
750	1.46	10.26	10.52	46.11	18.31	6.10	0.70	93.44
795	1.46	10.56	10.67	47.44	18.70	5.94	0.65	95.42
840	1.42	10.20	10.56	46.47	18.48	5.78	0.69	93.60
885	1.61	9.98	10.61	45.66	18.40	6.73	0.84	93.83
930	1.34	10.35	10.52	45.89	18.10	6.17	0.77	93.14
1020	1.52	10.20	10.51	45.50	18.61	6.65	0.82	93.82
1065	1.55	10.11	10.64	45.85	18.30	6.63	0.82	93.91
1110	1.56	10.13	10.73	45.58	18.40	6.69	0.84	93.92
1155	1.54	10.11	10.43	45.69	18.29	6.63	0.79	93.48
1200	1.56	9.76	10.47	45.37	19.30	6.63	0.82	93.91
1245	1.56	9.68	10.32	45.46	19.30	6.86	0.83	94.00
1290	1.64	9.78	10.40	45.40	18.80	6.76	0.79	93.57
1335	1.48	10.36	10.25	46.51	18.26	6.19	0.79	93.84
1380	1.43	10.42	10.63	46.36	17.91	6.06	0.70	93.51
1425	1.46	10.31	10.55	46.26	18.16	6.31	0.72	93.78
1470	1.55	10.29	10.54	46.04	17.97	6.31	0.76	93.45
1515	1.38	10.33	10.47	46.08	18.66	6.17	0.69	93.78
1560	1.42	10.24	10.66	46.14	18.28	6.23	0.74	93.72
1605	1.49	10.29	10.64	46.85	17.80	6.32	0.78	94.16
1650	1.46	10.40	10.63	45.95	18.01	6.45	0.79	93.69
1695	1.43	10.12	10.69	46.09	18.56	6.38	0.73	94.00
1740	1.49	9.50	10.51	45.37	19.18	6.57	0.78	93.39
1785	1.54	10.22	10.63	45.88	18.00	6.67	0.85	93.78

LV-DM-001-1-6 Biotite Rim to Rim

Distance (μm)	Na_2O	CaO	MgO	SiO_2	FeO	Al_2O_3	K_2O	Total
56	1.49	10.78	10.37	45.61	17.84	6.76	0.85	93.69
106	1.49	10.95	11.07	46.05	16.90	6.79	0.86	94.10
156	1.51	10.90	11.16	46.06	17.03	6.88	0.85	94.39
206	1.61	10.44	10.87	46.51	16.39	7.13	1.00	93.95
256	1.52	10.89	11.12	46.10	16.82	6.63	0.84	93.92
306	1.56	10.90	10.80	45.42	16.85	7.32	0.83	93.68
356	1.60	10.83	10.85	45.79	17.25	6.98	0.86	94.16
406	1.43	10.95	11.50	47.09	16.43	6.24	0.71	94.34
456	1.48	10.80	11.65	47.04	16.16	5.92	0.68	93.73
506	1.48	10.86	11.52	46.42	16.34	6.27	0.77	93.65
556	1.60	10.81	10.59	45.19	16.56	7.14	0.91	92.81
606	1.44	10.84	11.35	46.62	15.90	6.26	0.81	93.23
656	1.45	10.71	11.38	46.58	15.79	6.19	0.73	92.82
706	1.57	10.70	11.07	46.46	15.97	6.46	0.80	93.04
756	1.50	10.48	11.39	45.56	15.75	6.14	0.68	91.51
806	1.52	10.84	11.25	46.60	16.27	6.25	0.72	93.46
856	1.46	10.91	11.23	46.72	16.18	6.18	0.72	93.40
906	1.56	10.60	11.11	45.89	16.37	6.70	0.90	93.14
956	1.37	10.82	11.92	47.75	15.99	5.63	0.67	94.16
1006	1.50	11.00	11.37	46.66	16.23	6.45	0.76	93.97
1056	1.47	10.84	11.28	46.22	16.56	6.34	0.75	93.44
1106	1.54	11.03	11.37	46.29	16.56	6.44	0.79	94.02
1156	1.57	10.76	10.99	45.91	15.96	6.51	0.81	92.51
1206	1.69	9.76	10.14	47.93	15.11	7.50	1.37	93.49
1256	1.59	10.83	11.32	46.36	16.64	6.62	0.71	94.07
1306	1.62	10.73	11.13	46.06	16.65	6.92	0.78	93.88
1356	1.64	10.90	11.37	46.06	16.36	6.73	0.81	93.87
1406	1.67	10.82	11.31	45.73	16.30	7.06	0.88	93.77
1456	1.63	10.72	11.25	45.89	16.28	6.85	0.87	93.49
1506	1.43	1.11	0.82	69.43	1.39	11.59	4.47	90.25

LV-DM-001-1-7 Amphibole Rim to Rim

Distance (μm)	Na_2O	CaO	MgO	SiO_2	FeO	Al_2O_3	K_2O	Total
47	1.38	10.86	9.75	45.39	19.14	6.73	0.83	94.08
100	1.58	10.66	9.89	46.25	19.12	6.78	0.89	95.18
153	1.43	10.68	10.06	46.25	19.02	6.08	0.77	94.28
206	1.90	10.77	9.62	51.39	18.62	5.64	0.76	98.71
259	1.38	10.71	10.22	46.31	18.75	6.00	0.74	94.10
365	1.40	10.78	10.13	46.46	18.70	6.08	0.72	94.26
418	1.37	10.71	10.14	46.49	19.05	6.15	0.76	94.66
471	1.44	10.50	10.38	46.86	18.86	5.67	0.74	94.44
524	1.37	10.50	10.09	46.17	19.40	6.29	0.81	94.62
577	1.51	10.62	9.49	45.84	18.45	6.37	0.81	93.09
683	1.44	10.76	10.07	45.46	18.50	6.48	0.80	93.51
736	1.38	10.89	9.97	45.41	17.83	6.44	0.76	92.69
789	1.44	10.90	10.11	45.84	18.29	6.63	0.85	94.07
842	1.52	10.55	10.05	46.14	18.05	6.27	0.78	93.36
948	1.46	10.81	10.32	45.85	18.16	6.47	0.81	93.87
1001	1.49	10.97	10.00	45.78	18.24	6.79	0.84	94.11
1054	1.53	10.74	10.12	45.67	17.93	6.83	0.85	93.67

LV-DM-001-1-8 Biotite Rim to Rim

Distance (μm)	Na_2O	CaO	MgO	SiO_2	FeO	Al_2O_3	K_2O	Total
47	1.38	10.86	9.75	45.39	19.14	6.73	0.83	94.08
100	1.58	10.66	9.89	46.25	19.12	6.78	0.89	95.18
153	1.43	10.68	10.06	46.25	19.02	6.08	0.77	94.28
206	1.90	10.77	9.62	51.39	18.62	5.64	0.76	98.71
259	1.38	10.71	10.22	46.31	18.75	6.00	0.74	94.10
365	1.40	10.78	10.13	46.46	18.70	6.08	0.72	94.26
418	1.37	10.71	10.14	46.49	19.05	6.15	0.76	94.66
471	1.44	10.50	10.38	46.86	18.86	5.67	0.74	94.44
524	1.37	10.50	10.09	46.17	19.40	6.29	0.81	94.62
577	1.51	10.62	9.49	45.84	18.45	6.37	0.81	93.09
683	1.44	10.76	10.07	45.46	18.50	6.48	0.80	93.51
736	1.38	10.89	9.97	45.41	17.83	6.44	0.76	92.69
789	1.44	10.90	10.11	45.84	18.29	6.63	0.85	94.07
842	1.52	10.55	10.05	46.14	18.05	6.27	0.78	93.36
948	1.46	10.81	10.32	45.85	18.16	6.47	0.81	93.87
1001	1.49	10.97	10.00	45.78	18.24	6.79	0.84	94.11
1054	1.53	10.74	10.12	45.67	17.93	6.83	0.85	93.67

LV-DM-001-1-9 Amphibole Rim to Rim

Distance (μm)	Na_2O	CaO	MgO	SiO_2	FeO	Al_2O_3	K_2O	Total
87	1.42	10.68	11.27	46.43	16.40	6.44	0.76	93.40
165	1.08	10.45	13.12	49.51	15.20	4.13	0.48	93.96
399	0.82	9.74	13.80	52.46	14.17	2.82	0.31	94.13
477	1.07	10.48	12.48	48.65	16.14	4.51	0.52	93.85
555	1.39	10.37	11.37	46.64	17.43	6.11	0.73	94.03
633	1.57	10.63	10.80	46.38	17.46	6.35	0.81	93.99
711	1.35	10.60	11.39	46.65	17.08	5.97	0.71	93.76
789	1.38	10.54	11.23	46.23	17.09	5.92	0.74	93.14
867	1.45	10.57	10.84	46.18	17.49	6.48	0.74	93.75
945	1.54	10.68	10.88	46.47	17.54	6.57	0.75	94.43
1023	1.49	10.50	10.96	46.18	17.17	6.57	0.74	93.61
1101	1.43	10.58	10.91	46.26	17.31	6.71	0.80	93.99
1179	1.53	10.56	10.80	45.53	17.61	6.92	0.81	93.77
1257	1.50	10.66	11.02	46.09	16.92	6.68	0.85	93.71
1335	1.49	10.75	11.09	45.93	16.98	6.69	0.79	93.73
1413	1.56	10.67	10.98	45.64	17.09	6.80	0.81	93.56
1491	1.56	10.77	10.72	45.43	17.50	6.97	0.79	93.73
1569	1.45	10.69	9.98	44.95	18.52	6.99	0.83	93.41

APPENDIX C. $^{40}AR/^{39}AR$ AGE DATA. ERRONEOUS DATA HAVE BEEN REMOVED.

LV-RD-005, Single Crystal Plagioclase, J = 0.0002396 ± 0.16%

4 amu discrimination = 1.0737 ± 0.10%, $^{40}/^{39}K$ = 0.0979 ± 21.04%, $^{36}/^{37}Ca$ = 0.000206 ± 4.60%, $^{39}/^{37}Ca$ = 0.000785 ± 3.61%

Crystal	T (C)	t (min.)	^{36}Ar	^{37}Ar	^{38}Ar	^{39}Ar	^{40}Ar	$\%^{40}Ar^*$	Ca/K	$^{40}Ar^*/^{39}ArK$	Age (Ma)	1s.d.
1	1600	1	0.015	0.684	0.011	0.322	3.074	49.4	10.249527	1.8882	0.82	0.22
2	1600	1	0.022	1.508	0.014	0.608	4.963	17.9	11.973423	0.9532	0.41	0.02
3	1600	1	0.012	1.425	0.018	0.692	4.153	117.0	9.9351122	3.8977	1.68	0.10
4	1600	1	0.017	0.938	0.010	0.435	3.739	37.6	10.404872	1.6776	0.73	0.21
5	1600	1	0.019	0.684	0.040	0.293	3.697	1.5	11.267308	0.1064	0.05	0.36
6	1600	1	0.018	1.782	0.019	0.950	5.690	64.6	9.0476617	2.6613	1.15	0.08
7	1600	1	0.026	1.097	0.019	0.688	5.871	7.3	7.6877482	0.4442	0.19	0.14
8	1600	1	0.018	0.960	0.090	0.487	4.999	54.9	9.5093903	3.8259	1.65	0.20
9	1600	1	0.019	1.080	0.015	0.552	4.385	31.3	9.4381333	1.4855	0.64	0.15
10	1600	1	0.037	2.265	0.024	1.426	12.997	40.7	7.6581862	3.2956	1.42	0.10
11	1600	1	0.029	3.787	0.037	2.171	11.339	54.7	8.4121634	2.4437	1.06	0.05
12	1600	1	0.026	3.137	0.029	1.575	9.589	55.0	9.6076062	2.7747	1.20	0.09
13	1600	1	0.024	2.015	0.021	1.055	5.714	25.6	9.2128851	0.9347	0.40	0.08
14	1600	1	0.035	1.338	0.021	0.904	8.609	11.1	7.1350827	0.8699	0.38	0.10

note: isotope beams in mV rlsd = released, error in age includes J error, all errors 1 sigma
(36Ar through 40Ar are measured beam intensities, corrected for decay in age calculations)

LV-RD-008, Multiple Crystal Fusions, Plagioclase, J = 0.000235 ± 0.19%

4 amu discrimination = 1.0835 ± 0.30%, $^{40}/^{39}K$ = 0.0979 ± 21.04%, $^{36}/^{37}Ca$ = 0.000206 ± 4.60%, $^{39}/^{37}Ca$ = 0.000785 ± 3.61%

Crystal	T (C)	t (min.)	^{36}Ar	^{37}Ar	^{38}Ar	^{39}Ar	^{40}Ar	$\%^{40}Ar^*$	Ca/K	$^{40}Ar^*/^{39}ArK$	Age (Ma)	1s.d.
1	1600	1	0.067	2.495	0.038	1.989	18.304	22.7	7.6094771	1.8378	0.78	0.04
2	1600	1	0.087	2.599	0.043	2.095	25.411	22.9	7.5254194	2.5553	1.08	0.09
3	1600	1	0.076	1.519	0.025	1.009	20.976	20.4	9.1364608	3.8299	1.62	0.20
4	1600	1	0.042	0.944	0.025	0.874	12.113	43.8	6.5500726	4.8334	2.05	0.10
note: isotope beams in mV rlsd = released, error in age includes J error, all errors 1 sigma										Mean ± s.d. =	1.38	0.56
(36Ar through 40Ar are measured beam intensities, corrected for decay in age calculations)												

LV-RD-009, Multiple Crystal Fusions, Plagioclase, J = 0.000241 ± 0.16%

4 amu discrimination = 1.0737 ± 0.10%, $^{40}/^{39}$K = 0.0979 ± 21.04%, $^{36}/^{37}$Ca = 0.000206 ± 4.60%, $^{39}/^{37}$Ca = 0.000785 ± 3.61%

Crystal	T (C)	t (min.)	^{36}Ar	^{37}Ar	^{38}Ar	^{39}Ar	^{40}Ar	%^{40}Ar*	Ca/K	^{40}Ar*/^{39}ArK	Age (Ma)	1s.d.
1	1600	1	0.019	1.139	0.012	0.648	5.996	62.7	8.5664373	3.5826	1.56	0.22
2	1600	1	0.012	0.584	0.060	0.415	4.243	132.0	6.8548924	6.0465	2.63	0.31
3	1600	1	0.021	0.457	0.019	0.690	6.219	48.3	3.2228869	2.7609	1.20	0.20
4	1600	1	0.015	0.772	0.016	0.496	3.580	78.5	7.5833886	1.8864	0.82	0.23
5	1600	1	0.022	0.642	0.010	0.478	6.847	50.3	6.5418952	4.9180	2.14	0.31
6	1600	1	0.022	0.260	0.013	0.318	4.514	3.3	3.9794185	0.2806	0.12	0.51
7	1600	1	0.022	0.544	0.022	0.585	5.473	32.1	4.5267389	1.9716	0.86	0.24
8	1600	1	0.026	0.126	0.012	0.357	6.535	19.3	1.7166835	2.6251	1.14	0.48
										Mean ± s.d. =	1.31	0.79
										Wtd mean age = (6 fusions)	1.09	0.20

note: isotope beams in mV rlsd = released, error in age includes J error, all errors 1 sigma
(36Ar through 40Ar are measured beam intensities, corrected for decay in age calculations)

LV-RD Combined, Single and Multiple Laser Fusions, Plagioclase

4 amu discrimination (1-14, 1-8) = 1.0737 ± 0.10%, 4 amu discrimination (1-4) = 1.0835 ±0.30% $^{40}/^{39}K$ = 0.0979 ± 21.04%, $^{36}/^{37}Ca$ = 0.000206 ± 4.60%, $^{39}/^{37}Ca$ = 0.000785 ± 3.61%

Crystal	T (C)	t (min.)	^{36}Ar	^{37}Ar	^{38}Ar	^{39}Ar	^{40}Ar	%^{40}Ar*	Ca/K	$^{40}Ar^*/^{39}ArK$	Age (Ma)	1s.d.
1	1600	1	0.015	0.684	0.011	0.322	3.074	49.4	10.249527	1.8882	0.82	0.22
2	1600	1	0.022	1.508	0.014	0.608	4.963	17.9	11.973423	0.9532	0.41	0.02
3	1600	1	0.012	1.425	0.018	0.692	4.153	117.0	9.9351122	3.8977	1.68	0.10
4	1600	1	0.017	0.938	0.010	0.435	3.739	37.6	10.404872	1.6776	0.73	0.21
5	1600	1	0.019	0.684	0.040	0.293	3.697	1.5	11.267308	0.1064	0.05	0.36
6	1600	1	0.018	1.782	0.019	0.950	5.690	64.6	9.0476617	2.6613	1.15	0.08
7	1600	1	0.026	1.097	0.019	0.688	5.871	7.3	7.6877482	0.4442	0.19	0.14
8	1600	1	0.018	0.960	0.090	0.487	4.999	54.9	9.5093903	3.8259	1.65	0.20
9	1600	1	0.019	1.080	0.015	0.552	4.385	31.3	9.4381333	1.4855	0.64	0.15
10	1600	1	0.037	2.265	0.024	1.426	12.997	40.7	7.6581862	3.2956	1.42	0.10
11	1600	1	0.029	3.787	0.037	2.171	11.339	54.7	8.4121634	2.4437	1.06	0.05
12	1600	1	0.026	3.137	0.029	1.575	9.589	55.0	9.6076062	2.7747	1.20	0.09
13	1600	1	0.024	2.015	0.021	1.055	5.714	25.6	9.2128851	0.9347	0.40	0.08
14	1600	1	0.035	1.338	0.021	0.904	8.609	11.1	7.1350827	0.8699	0.38	0.10
1	1600	1	0.019	1.139	0.012	0.648	5.996	62.7	8.5664373	3.5826	1.56	0.22
2	1600	1	0.012	0.584	0.060	0.415	4.243	132.0	6.8548924	6.0465	2.63	0.31
3	1600	1	0.021	0.457	0.019	0.690	6.219	48.3	3.2228869	2.7609	1.20	0.20
4	1600	1	0.015	0.772	0.016	0.496	3.580	78.5	7.5833886	1.8864	0.82	0.23
5	1600	1	0.022	0.642	0.010	0.478	6.847	50.3	6.5418952	4.9180	2.14	0.31
6	1600	1	0.022	0.260	0.013	0.318	4.514	3.3	3.9794185	0.2806	0.12	0.51
7	1600	1	0.022	0.544	0.022	0.585	5.473	32.1	4.5267389	1.9716	0.86	0.24
8	1600	1	0.026	0.126	0.012	0.357	6.535	19.3	1.7166835	2.6251	1.14	0.48
1	1600	1	0.067	2.495	0.038	1.989	18.304	22.7	7.6094771	1.8378	0.78	0.04
2	1600	1	0.087	2.599	0.043	2.095	25.411	22.9	7.5254194	2.5553	1.08	0.09
3	1600	1	0.076	1.519	0.025	1.009	20.976	20.4	9.1364608	3.8299	1.62	0.20
4	1600	1	0.042	0.944	0.025	0.874	12.113	43.8	6.5500726	4.8334	2.05	0.10
note: isotope beams in mV rlsd = released, error in age includes J error, all errors 1 sigma										Mean ± s.d. =	1.07	0.65
(36Ar through 40Ar are measured beam intensities, corrected for decay in age calculations)										Wtd mean age = (3 fusions)	411.00	0.02

LV-MR-008, Single Crystal Fusion, Sanidine, J = 0.000238 ± 0.16%

4 amu discrimination = 1.0835 ± 0.30%, $^{40}/^{39}$K = 0.0979 ± 21.04%, $^{36}/^{37}$Ca = 0.000206 ± 4.60%, $^{39}/^{37}$Ca = 0.000785 ± 3.61%

Crystal	T (C)	t (min.)	^{36}Ar	^{37}Ar	^{38}Ar	^{39}Ar	^{40}Ar	%^{40}Ar*	Ca/K	^{40}Ar*/^{39}ArK	Age (ka)	1s.d.
1	1600	1	0.142	0.332	0.978	72.584	129.051	67.7	0.0277986	1385.0530	514.00	9.00
2	1600	1	0.783	0.224	0.701	44.338	273.154	21.2	0.0307042	1542.0550	564.00	12.00
3	1600	1	0.588	0.324	0.817	51.762	229.462	29.1	0.0380418	1522.9842	558.00	11.00
4	1600	1	0.104	0.376	1.041	78.126	127.848	75.2	0.0292495	1422.3376	526.00	9.00
5	1600	1	0.125	0.453	0.984	72.146	132.210	72.1	0.0381604	1545.2396	565.00	9.00
6	1600	1	1.668	0.367	1.305	75.706	551.643	16.6	0.029462	1425.4559	527.00	14.00
7	1600	1	0.159	0.324	0.778	51.462	105.890	57.8	0.0382636	1360.3341	506.00	10.00
8	1600	1	0.069	0.278	0.861	63.232	101.358	79.7	0.0267198	1472.4377	542.00	9.00
9	1600	1	0.465	0.426	1.082	74.892	225.446	42.0	0.0345701	1481.8811	545.00	10.00
10	1600	1	0.164	0.185	0.566	38.904	94.345	52.3	0.0289004	1456.7337	537.00	10.00
11	1600	1	0.093	0.298	0.864	64.239	107.093	74.4	0.0281931	1428.5759	528.00	10.00
12	1600	1	0.253	0.226	0.717	49.652	132.456	46.8	0.0276629	1447.3321	534.00	10.00
13	1600	1	0.091	0.282	0.817	60.588	99.034	73.2	0.0282871	1366.5035	508.00	9.00
14	1600	1	0.056	0.111	0.317	22.479	41.898	67.8	0.0300104	1381.9572	513.00	10.00
15	1600	1	0.326	0.291	0.872	64.153	172.715	46.9	0.0275678	1472.4377	542.00	11.00
16	1600	1	0.459	0.259	0.795	54.224	198.853	35.9	0.0290291	1551.6142	567.00	10.00
17	1600	1	0.060	0.181	0.548	39.529	63.364	74.5	0.0278284	1338.7947	499.00	9.00
18	1600	1	0.043	0.197	0.486	37.258	58.401	81.3	0.0321346	1431.6976	529.00	9.00
19	1600	1	1.106	0.277	0.451	50.754	346.618	19.3	0.0331693	1570.7803	573.00	9.00
20	1600	1	0.282	0.227	0.673	46.526	140.097	44.2	0.0296521	1561.1893	570.00	10.00
21	1600	1	0.075	0.218	0.595	47.085	82.739	74.4	0.0281384	1510.3055	554.00	9.00
22	1600	1	0.188	0.178	0.537	38.355	100.567	48.7	0.0282049	1472.4377	542.00	10.00
23	1600	1	0.153	0.115	0.609	43.765	97.088	56.4	0.0159696	1434.8210	530.00	10.00
24	1600	1	0.030	0.113	0.306	22.728	36.049	83.5	0.0302164	1437.9462	531.00	12.00
25	1600	1	0.041	0.158	0.462	34.617	53.826	81.1	0.0277392	1406.7722	521.00	10.00
26	1600	1	0.080	0.147	0.431	29.893	59.072	64.7	0.0298864	1437.9462	531.00	12.00
27	1600	1	0.199	0.138	0.377	26.205	87.499	48.3	0.0320052	1469.2934	541.00	11.00
28	1600	1	0.035	0.136	0.324	24.659	40.000	81.1	0.0335189	1441.0731	532.00	10.00
29	1600	1	0.096	0.180	0.554	41.013	77.993	66.4	0.0266733	1437.9462	531.00	10.00
30	1600	1	0.765	0.187	0.633	38.253	256.332	18.1	0.02971	1416.1063	524.00	14.00
										Mean ± s.d. =	536.13	19.47
										Wtd mean age = (23 fusions)	534.30	2.75
										Isochron age = (17 fusions)	525.10	1.55

LV-HCF-002, Single Crystal Sanidine, J = 0.000238 ± 0.16%

4 amu discrimination = 1.0737 ± 0.10%, $^{40}/^{39}K$ = 0.0979 ± 21.04%, $^{36}/^{37}Ca$ = 0.000206 ± 4.60%, $^{39}/^{37}Ca$ = 0.000785 ± 3.61%

Crystal	T (C)	t (min.)	^{36}Ar	^{37}Ar	^{38}Ar	^{39}Ar	^{40}Ar	$\%^{40}Ar^*$	Ca/K	$^{40}Ar^*/^{39}ArK$	Age (ka)	1s.d.
1	1600	1	0.024	0.085	0.133	9.990	13.420	64.7	0.0405117	815.4621	320.00	11.00
2	1600	1	0.019	0.062	0.091	6.510	8.550	64.5	0.0453459	702.7269	279.00	21.00
3	1600	1	0.025	0.147	0.233	16.898	18.887	70.7	0.0414199	776.6788	306.00	15.00
4	1600	1	0.017	0.080	0.128	9.418	10.669	76.6	0.0404444	771.1628	304.00	13.00
5	1600	1	0.023	0.045	0.058	3.726	8.458	50.8	0.0575041	985.1280	380.00	47.00
6	1600	1	0.015	0.045	0.054	3.926	6.276	77.7	0.0545747	930.7887	361.00	19.00
7	1600	1	0.035	0.093	0.138	9.318	14.384	43.3	0.0475213	757.3997	299.00	16.00
8	1600	1	0.146	0.045	0.090	5.040	43.231	9.9	0.0425118	922.2610	358.00	31.00
9	1600	1	0.023	0.074	0.113	8.514	12.000	63.8	0.0413833	826.5985	324.00	13.00
10	1600	1	0.028	0.055	0.078	5.805	11.205	48.3	0.0451116	848.9454	332.00	15.00
11	1600	1	0.043	0.750	0.111	7.646	15.768	34.6	0.4670978	760.1492	300.00	19.00
12	1600	1	0.013	0.037	0.032	1.897	2.955	75.2	0.0928684	664.8150	265.00	64.00
13	1600	1	0.022	0.045	0.071	4.870	8.046	50.0	0.0439958	798.8038	314.00	26.00
14	1600	1	0.044	0.467	0.084	5.963	14.763	34.7	0.3729246	832.1759	326.00	29.00
15	1600	1	0.032	0.431	0.124	8.781	12.184	48.1	0.233714	605.8304	243.00	22.00
16	1600	1	0.220	0.101	0.171	13.679	17.166	50.3	0.0351555	1011.0681	389.00	26.00
17	1600	1	0.028	0.059	0.071	5.632	10.099	51.9	0.049879	877.0187	342.00	32.00
note: isotope beams in mV rlsd = released, error in age includes J error, all errors 1 sigma										Mean ± s.d. =	320.12	38.83
(36Ar through 40Ar are measured beam intensities, corrected for decay in age calculations)										Wtd mean age = (16 fusions)	320.00	6.50
										Isochron age = (9 fusions)	312.00	7.00

LV-HCF-006, Multiple Crystal Fusions, Sanidine, J = 0.000240 ± 0.29%

4 amu discrimination = 1.0669 ± 0.27%, $^{40}/^{39}$K = 0.0979 ± 21.04%, $^{36}/^{37}$Ca = 0.000206 ±4.60%, $^{39}/^{37}$Ca = 0.000785 ± 3.61%

Crystal	T (C)	t (min.)	^{36}Ar	^{37}Ar	^{38}Ar	^{39}Ar	^{40}Ar	%^{40}Ar*	Ca/K	^{40}Ar*/^{39}ArK	Age (ka)	1s.d.
1	1600	1	0.030	0.228	0.421	31.490	30.505	75.5	0.0378218	742.9171	296.00	10.00
2	1600	1	0.216	0.427	0.893	64.098	108.000	42.0	0.0347987	767.4707	305.00	10.00
3	1600	1	2.682	0.377	1.197	52.856	795.184	6.8	0.0372586	1183.3820	451.00	10.00
4	1600	1	0.331	0.244	0.499	33.410	116.649	21.3	0.0381499	808.6666	320.00	10.00
5	1600	1	0.510	0.392	0.900	60.988	207.315	30.8	0.0335754	1198.2302	456.00	11.00
6	1600	1	0.108	0.274	0.487	36.618	56.826	47.0	0.0390873	772.9437	307.00	10.00
7	1600	1	0.315	0.307	0.616	44.411	128.258	31.2	0.03611	1002.6425	389.00	16.00
8	1600	1	0.640	0.251	0.546	31.843	203.599	13.1	0.0411756	934.3295	365.00	24.00
9	1600	1	0.103	0.157	0.277	20.544	42.367	35.0	0.0399204	753.8147	300.00	11.00
10	1600	1	0.050	0.213	0.396	29.496	34.527	62.0	0.0377221	745.6392	297.00	10.00
11	1600	1	0.101	0.177	0.334	23.571	44.187	38.5	0.0392261	753.8147	300.00	12.00
12	1600	1	0.034	0.170	0.265	20.588	23.795	67.5	0.0431335	775.6825	308.00	12.00
13	1600	1	0.329	0.713	0.383	23.150	112.635	19.8	0.1608917	1077.6810	415.00	11.00
14	1600	1	0.478	0.340	0.637	42.933	161.410	17.4	0.0413683	710.3688	284.00	11.00
15	1600	1	0.300	0.149	0.314	19.478	101.031	18.8	0.0399596	1071.8703	413.00	21.00
16	1600	1	0.047	2.040	0.048	2.876	13.043	18.6	3.7092327	762.0037	303.00	34.00
17	1600	1	0.540	0.183	0.362	21.083	162.583	8.7	0.0453418	726.6159	290.00	20.00
18	1600	1	0.083	0.131	0.024	17.148	35.081	38.4	0.0399059	811.4252	321.00	15.00
19	1600	1	0.135	0.127	0.246	16.200	51.678	30.3	0.0409514	1048.6920	405.00	13.00
20	1600	1	0.025	0.100	0.172	11.724	14.392	69.7	0.0445558	786.6528	312.00	13.00
note: isotope beams in mV rlsd = released, error in age includes J error, all errors 1 sigma										Mean ± s.d. =	341.85	57.49
(36Ar through 40Ar are measured beam intensities, corrected for decay in age calculations)										Wtd mean age = (14 fusions)	304.50	3.90
										Isochron age = (14 fusions)	295.00	3.05

LV-HCF-005, Single Crystal Fusion, Sanidine, J = 0.0002388 ± 0.15%

4 amu discrimination = 1.0737 ± 0.10%, $^{40}/^{39}K$ = 0.0979 ± 21.04%, $^{36}/^{37}Ca$ = 0.000206 ± 4.60%, $^{39}/^{37}Ca$ = 0.000785 ± 3.61%

Crystal	T (C)	t (min.)	^{36}Ar	^{37}Ar	^{38}Ar	^{39}Ar	^{40}Ar	%^{40}Ar*	Ca/K	$^{40}Ar^*/^{39}ArK$	Age (ka)	1s.d.
1	1600	1	0.035	0.106	0.161	11.591	15.806	53.1	0.0462929	678.7454	271.00	14.00
2	1600	1	0.084	0.232	0.383	27.099	43.398	48.2	0.0433374	812.7302	320.00	58.00
3	1600	1	0.027	0.129	0.229	16.951	18.456	71.4	0.0385232	757.6027	300.00	11.00
4	1600	1	0.045	0.137	0.237	17.140	23.028	53.6	0.0404611	713.9385	284.00	12.00
5	1600	1	0.031	4.293	0.061	3.887	8.303	27.3	5.5998449	452.2099	185.00	45.00
6	1600	1	0.300	0.309	0.580	38.226	105.787	21.0	0.0409193	619.7626	249.00	21.00
7	1600	1	0.036	0.081	0.129	9.545	14.847	48.9	0.0429574	708.5077	282.00	17.00
8	1600	1	0.037	0.244	0.446	34.452	34.085	71.5	0.0358511	727.5420	289.00	11.00
9	1600	1	0.034	0.347	0.635	47.881	44.850	80.3	0.0366855	798.8910	315.00	10.00
10	1600	1	0.046	1.798	0.419	30.300	32.310	71.9	0.3004057	798.8910	315.00	11.00
11	1600	1	0.089	0.264	0.490	35.886	50.191	56.3	0.0372397	843.3119	331.00	10.00
12	1600	1	0.439	0.214	0.447	28.032	138.244	14.4	0.0386445	776.8278	307.00	12.00
13	1600	1	0.195	0.222	0.477	32.467	78.257	34.5	0.0346129	913.5131	356.00	10.00
14	1600	1	0.029	0.203	0.397	28.998	28.992	85.6	0.0354369	893.7586	349.00	12.00
15	1600	1	0.053	0.063	0.095	6.150	18.609	49.9	0.0518555	1629.6520	593.00	24.00
16	1600	1	0.084	0.240	0.368	26.152	41.600	52.6	0.0464553	893.7586	349.00	11.00
17	1600	1	0.058	0.150	0.298	21.179	29.646	59.7	0.035852	874.0806	342.00	11.00
18	1600	1	0.025	0.076	0.018	8.830	11.472	91.3	0.0435694	1159.6067	441.00	14.00
19	1600	1	0.035	0.062	0.092	7.197	12.084	65.7	0.0436083	1048.1542	403.00	22.00
20	1600	1	0.028	0.286	0.065	4.586	9.508	83.4	0.3157148	1649.0313	599.00	29.00
21	1600	1	0.026	0.062	0.094	6.680	9.631	88.0	0.0469834	1153.6821	439.00	21.00
22	1600	1	0.026	0.043	0.041	3.264	6.968	88.0	0.0666883	1613.5518	588.00	56.00
23	1600	1	0.028	0.187	0.053	3.552	7.554	79.1	0.2665173	1470.6404	543.00	36.00
24	1600	1	0.026	0.044	0.064	4.277	8.144	88.8	0.0520767	1613.5518	588.00	35.00
										Mean ± s.d. =	376.58	121.26
										Wtd mean age = (10 fusions)	297.00	6.50
										Isochron age = (5 fusions)	329.30	25.50

note: isotope beams in mV rlsd = released, error in age includes J error, all errors 1 sigma
(36Ar through 40Ar are measured beam intensities, corrected for decay in age calculations)

LV-MR-004, Single & Multiple Crystal Fusions, Sanidine, J = 0.000236 ± 0.17%

4 amu discrimination = 1.0835 ± 0.30%, $^{40}/^{39}$K = 0.0979 ± 21.04%, $^{36}/^{37}$Ca = 0.000206 ± 4.60%, $^{39}/^{37}$Ca = 0.000785 ± 3.61%

Crystal	T (C)	t (min.)	^{36}Ar	^{37}Ar	^{38}Ar	^{39}Ar	^{40}Ar	%^{40}Ar*	Ca/K	^{40}Ar*/^{39}ArK	Age (ka)	1s.d.
1	1600	1	0.063	0.299	0.906	68.979	40.373	49.4	0.0248273	283.9079	117.00	9.00
2	1600	1	0.133	0.384	0.859	62.293	57.783	31.9	0.0353076	298.9696	123.00	10.00
3	1600	1	0.057	0.182	0.548	39.982	29.086	44.4	0.0260725	311.5592	128.00	10.00
4	1600	1	0.226	0.331	0.609	42.852	76.098	16.9	0.0442419	306.5192	126.00	10.00
5	1600	1	0.212	0.324	0.961	69.120	84.418	26.9	0.0268483	336.8435	138.00	10.00
6	1600	1	0.059	0.346	0.759	57.428	37.840	52.0	0.0345087	339.3796	139.00	10.00
7	1600	1	0.030	0.279	0.971	72.153	33.089	65.8	0.0221475	293.9434	121.00	9.00
8	1600	1	0.036	0.228	0.759	55.995	27.997	58.6	0.0233217	278.8985	115.00	9.00
9	1600	1	0.038	0.207	0.592	46.110	25.794	56.4	0.0257128	298.9696	123.00	9.00
10	1600	1	0.131	0.310	0.969	71.804	62.179	36.3	0.0247279	319.1298	131.00	9.00
11	1600	1	0.106	0.277	0.985	74.225	59.237	44.6	0.0213749	362.2683	148.00	10.00
12	1600	1	0.083	0.298	0.942	69.900	45.256	40.6	0.0248076	261.4092	108.00	9.00
13	1600	1	0.016	0.212	0.601	44.824	19.437	71.8	0.0275307	288.9229	119.00	9.00
14	1600	1	0.024	0.159	0.370	27.136	13.736	53.5	0.0341071	236.5419	98.00	9.00
15	1600	1	0.020	0.187	0.516	39.798	18.827	67.1	0.027351	293.9434	121.00	9.00
16	1600	1	0.019	0.150	0.416	31.369	15.324	66.5	0.0278345	291.4325	120.00	9.00
17	1600	1	0.107	0.260	0.601	43.289	43.791	28.9	0.0349614	291.4325	120.00	9.00
18	1600	1	0.032	0.216	0.693	52.240	26.330	58.8	0.0240682	283.9079	117.00	9.00
19	1600	1	0.024	0.134	0.416	30.431	14.859	55.1	0.0256319	239.0224	99.00	9.00
20	1600	1	0.055	0.252	0.506	38.189	29.195	44.9	0.0384111	334.3088	137.00	9.00
22	1600	1	0.022	0.196	0.545	40.036	19.035	64.1	0.0284969	281.4025	116.00	9.00
23	1600	1	0.056	0.160	0.364	26.823	24.167	35.9	0.0347221	309.0385	127.00	9.00
24	1600	1	0.019	0.135	0.385	28.707	14.847	67.3	0.027374	311.5592	128.00	9.00
25	1600	1	0.044	0.155	0.427	30.269	21.457	42.2	0.0298076	281.4025	116.00	10.00
26	1600	1	0.247	0.040	0.865	64.749	93.543	23.5	0.003596	352.0815	144.00	10.00
27	1600	1	0.194	1.477	0.625	45.994	69.821	21.0	0.1869356	326.7130	134.00	11.00
28	1600	1	0.054	0.484	0.616	45.432	30.677	46.4	0.0620127	306.5192	126.00	9.00
										Mean ± s.d. =	123.67	11.93
										Wtd mean age =	124.00	2.20
										(26 fusions)		
										Isochron age =	118.20	0.85
										(16 fusions)		

note: isotope beams in mV rlsd = released, error in age includes J error, all errors 1 sigma
(36Ar through 40Ar are measured beam intensities, corrected for decay in age calculations)

LV-MR-001, Single Crystal Fusion, Sanidine, J = 0.000243 ± 0.29%

4 amu discrimination = 1.0669 ± 0.27%, $^{40}/^{39}$K = 0.0979 ± 21.04%, $^{36}/^{37}$Ca = 0.000206 ± 4.60%, $^{39}/^{37}$Ca = 0.000785 ± 3.61%

Crystal	T (C)	t (min.)	^{36}Ar	^{37}Ar	^{38}Ar	^{39}Ar	^{40}Ar	%^{40}Ar*	Ca/K	^{40}Ar*/^{39}ArK	Age (ka)	1s.d.
1	1600	1	0.069	0.398	0.597	43.847	32.144	35.8	0.0494197	251.4578	107.00	10.00
2	1600	1	0.025	0.165	0.456	34.182	17.620	57.6	0.0277375	275.7295	117.00	9.00
3	1600	1	0.022	0.610	0.362	26.033	13.166	55.7	0.134648	249.0380	106.00	9.00
4	1600	1	0.185	0.337	0.603	44.293	64.931	17.5	0.0437197	261.1503	111.00	9.00
5	1600	1	0.036	0.113	0.361	27.508	17.643	42.2	0.0236048	251.4578	107.00	9.00
6	1600	1	0.030	0.184	0.570	42.395	20.286	51.9	0.0249393	232.1370	99.00	9.00
7	1600	1	0.026	0.179	0.416	31.405	16.942	55.6	0.0327518	275.7295	117.00	9.00
8	1600	1	0.023	0.163	0.531	42.365	18.828	59.3	0.0221086	246.6195	105.00	9.00
9	1600	1	0.020	0.208	0.525	39.553	18.179	64.5	0.0302179	275.7295	117.00	10.00
10	1600	1	0.110	0.180	0.568	40.452	42.705	24.4	0.025569	256.3014	109.00	11.00
11	1600	1	0.027	0.105	0.278	21.231	12.788	45.0	0.0284184	236.9592	101.00	10.00
note: isotope beams in mV rlsd = released, error in age includes J error, all errors 1 sigma										Mean ± s.d. =	108.73	6.26
(36Ar through 40Ar are measured beam intensities, corrected for decay in age calculations)										Wtd mean age = (11 fusions)	108.70	2.80
										Isochron age = (7 fusions)	94.30	1.65

LV-DM-001, Single Crystal Fusion, Sanidine, J = 0.000240 ± 0.17%

4 amu discrimination = 1.0835 ± 0.30%, $^{40}/^{39}$K = 0.0979 ± 21.04%, $^{36}/^{37}$Ca = 0.000206 ± 4.60%, $^{39}/^{37}$Ca = 0.000785 ± 3.61%

Crystal	T (C)	t (min.)	^{36}Ar	^{37}Ar	^{38}Ar	^{39}Ar	^{40}Ar	%^{40}Ar*	Ca/K	^{40}Ar*/^{39}ArK	Age (ka)	1s.d.
1	1600	1	0.140	0.341	1.131	83.856	58.736	26.8	0.0250145	184.0986	78.00	9.00
2	1600	1	0.477	0.581	1.318	96.108	150.128	9.0	0.0371869	143.2935	61.00	12.00
3	1600	1	0.052	0.273	0.867	65.719	27.774	39.3	0.0255531	152.8601	65.00	9.00
4	1600	1	0.083	0.374	1.216	89.935	43.421	33.6	0.0255808	157.6514	67.00	9.00
5	1600	1	0.144	0.727	1.422	108.225	63.543	25.4	0.0413219	148.0741	63.00	9.00
6	1600	1	0.187	0.519	1.758	132.745	82.690	25.6	0.0240503	160.0490	68.00	9.00
7	1600	1	0.127	0.292	1.102	80.934	51.741	22.1	0.0221934	138.5181	59.00	9.00
8	1600	1	0.503	0.947	1.351	93.997	158.680	9.0	0.0619744	155.2551	66.00	9.00
9	1600	1	0.246	0.720	1.687	128.245	100.525	23.2	0.0345354	184.0986	78.00	9.00
10	1600	1	0.063	0.334	0.941	73.482	34.012	36.1	0.02796	160.0490	68.00	9.00
11	1600	1	0.072	0.337	1.062	81.959	39.849	37.3	0.0252933	176.8697	75.00	9.00
12	1600	1	0.071	0.294	1.056	79.057	37.628	34.9	0.0228759	160.0490	68.00	9.00
13	1600	1	0.365	0.369	1.062	77.731	113.178	7.0	0.0292015	102.8710	44.00	9.00
14	1600	1	0.616	0.569	1.403	98.200	192.831	8.9	0.035643	179.2780	76.00	10.00
15	1600	1	0.880	0.267	1.128	74.969	253.856	3.2	0.0219079	112.3480	48.00	11.00
16	1600	1	0.174	0.691	1.137	83.523	65.145	18.0	0.0508917	140.9051	60.00	9.00
17	1600	1	0.131	0.310	1.324	97.617	59.735	34.5	0.0195347	232.5995	98.00	9.00
18	1600	1	0.065	0.217	0.900	67.926	31.473	30.4	0.0196515	133.7480	57.00	9.00
19	1600	1	0.178	0.310	1.153	86.155	67.717	16.1	0.0221336	150.4665	64.00	9.00
20	1600	1	0.680	0.405	1.106	76.658	205.487	7.0	0.032499	193.7558	82.00	10.00
21	1600	1	0.194	0.194	0.803	58.471	39.932	24.5	0.0204095	162.4480	69.00	9.00
22	1600	1	0.626	0.313	0.991	65.502	187.606	6.5	0.0293942	191.3395	81.00	10.00
23	1600	1	0.160	0.550	0.800	57.372	56.916	17.2	0.058971	169.6529	72.00	9.00
24	1600	1	0.049	0.251	0.918	69.685	27.906	37.1	0.0221567	140.9051	60.00	9.00
25	1600	1	0.089	0.297	0.680	51.619	36.565	26.2	0.0353932	179.2780	76.00	9.00
26	1600	1	0.175	0.295	0.906	66.512	62.191	16.1	0.0272831	150.4665	64.00	9.00
27	1600	1	0.057	0.198	0.665	48.960	25.532	29.8	0.0248769	145.6831	62.00	9.00
28	1600	1	0.070	0.246	0.700	52.808	30.253	27.6	0.0286555	150.4665	64.00	9.00
										Mean ± s.d. =	67.61	10.77
										Wtd mean age =	68.60	1.75
										(27 fusions)		
										Isochron age =	64.90	0.90
										(10 fusions)		

note: isotope beams in mV rlsd = released, error in age includes J error, all errors 1 sigma

(36Ar through 40Ar are measured beam intensities, corrected for decay in age calculations)

REFERENCES

Aslan, Z., 2005, Petrography and Petrology of the Calc-Alkaline Sarihan Granitoid (NE Turkey): An Example of Magma Mingling and Mixing: Turkish Journal of Earth Sciences, v. 14, p. 185-207.

Bachman, O and Bergantz, G.W., 2003, Rejuvenation of the Fish Canyon magma body: A window into the evolution of large-volume silicic magma systems: Geology, v. 31, no. 9, p. 789-792.

Bachman, O and Bergantz, G.W., 2004, On the Origin of Crystal-poor Rhyolites: Extracted from Batholithic Crystal Mushes: Journal of Petrology, vol. 45, no. 8, p. 1565-1582.

Bailey, R. A., Dalrymple, G.B., and Lanphere, M.A., 1976, Volcanism, Structure, and Geochronology of the Long Valley Caldera, Mono County, California: Journal of Geophysical Research, v. 81, no. 5, p. 725-744.

Bailey, R. A., 1989, Geologic map of Long Valley caldera, Mono Inyo Craters volcanic chain, and vicinity, eastern California: US Geological Survey Miscellaneous Investigations Series I-1933, scale 62,500.

Bailey, R.A., 2004, Eruptive History and Chemical Evolution of the Precaldera and Postcaldera Basalt-Dacite Sequences, Long Valley, California: Implications for Magma Sources, Current Seismic Unrest, and Future Volcanism: U.S. Geological Survey Professional Paper 1692, p. 1-75

Davies, G.R., Halliday, A.N., Mahood, G.A., and Hall, C.M., 1994 Isotopic constraints on the production rates, crystallization histories and residence times of pre-caldera silicic magmas, Long Valley, California: Earth and Planetary Science Letters, v. 125, iss. 1-4, p 17-37.

Ginibre, C., Worner, ,G., Kronz, A., 2004, Structure and Dynamics of the Laacher See Magma Chamber (Eifler, Germany) from Major and Trace Element Zoning in Sanidine: a Cathodoluminescence and Electron Microprobe Study: Journal of Petrology, v. 45, no. 11, p. 2197-2223.

Gualda, G.A.R. and Ghiorso, M.S., 2014, The Bishop Tuff giant magma body: an alternative to the Standard Model: Contributions to Mineralogy and Petrology, v. 166, p. 755-775.

Heumann, A., and Davies, G.R., 1997, Isotopic and Chemical Evolution of the Post-Caldera Rhyolitic System at Long Valley, California: v. 38, no. 12, p. 1661-1678.

Heumann, A., Davies, G.R., and Elliott, T., 2002, Crystallization history of rhyolites at Long Valley, California, inferred from combined U-series and Rb- Sr Isotope systematics: Geochemica et Cosmochimica Acta, v. 66, no. 10, p. 1821-1837.

Hibbard, M.J., 1981, The Magma Mixing Origin of Mantled Feldspars: Contributions to Mineral Petrology, v. 76, p. 158-170.

Hildreth, W., 1977, The magma chamber of the Bishop Tuff: gradients in temperature, pressure, and composition: University of California – Berkeley p. 1-328.

Hildreth, W., 1981, Gradients in Silicic Magma Chambers: Implications for Lithospheric Magmatism: Journal of Geophysical Research, v. 86, no. B11, p. 10153-10192.

Hildreth, W., 2004, Volcanological perspectives on Long Valley, Mammoth Mountain, and Mono Craters: several contiguous but discrete systems: Journal of Volcanology and Geothermal Research, v. 136, p. 169-198.

Hill, D.P., 2004, Unrest in the Long Valley Caldera, 1978-2004, *in* Troise, C., De Natale, G. and Kilburn, C.R.J. (eds) 2006: Mechanisms of Activity and Unrest at Large Calderas: Geological Society, London, v. 269, p. 1-24.

Huppert, H.E., and Sparks, S.J., 1988, The Generation of Granitic Magmas by Intrusion of Basalt into Continental Crust: Journal of Petrology, v. 29, iss. 3, p. 599-624.

Jerram, D.A., and Martin, V.M., 2008, Understanding crystal populations and their significance through the magma plumbing system, *in* Annen, C.A. and Zellmer G.F. (eds) 2008, Dynamics of crustal magma transfer, storage and differentiation: Geological Society Special Publications, London, v. 304, p. 13-148.

L'Heureux, I. and Folwer, A.D., 1994, A nonlinear dynamical model of oscillatory zoning in plagioclase: American Mineralogist, v. 79, p. 885-891.

Loomis, T., 1982, Numerical simulations of crystallization processes of plagioclase in complex melts: the origin of major and oscillatory zoning in plagioclase: Contributions to Mineralogy and Petrology, v. 81, .iss. 3, p. 219-229.

McDougall, I. and Harrison, M.T., 1999, Geochronology and Thermochronology By The $^{40}Ar/^{39}Ar$ Method: New York, Oxford University of Press, 241 p.

Mankiken, E.A., Gromme, S., Dalrymple, M.A., Lanphere, M.A., Bailey, R.A., 1986, Paleomagnetism and K-Ar Ages of Volcanic Rocks From Long Valley Caldera, California: Journal of Geophysical Research, v. 91, no. B1, p. 633-652.

Metz, J.M., and Mahood, G.A., 1985, Precursors to the Bishop Tuff Eruption: Glass Mountain, Long Valley, California: Journal of Geophysical Research, v. 90, iss. B13, 9.11121-11126

Perugini, D., Busa, T., Poli, G., and Nazzareni, S., 2003, The Role of Chaotic Dynamics and Flow Fields in the Development of Disequilibrium Textures in Volcanic Rocks: Journal of Petrology, v. 44, no. 4, p. 733-756.

Perkins, M.E. and Nash, B.P., 2002, Explosive silicic volcanism of the Yellowstone hotspot: The ash fall tuff record: Bulletin of the Geological Society of America, v. 114, no. 3 p. 367-381.

Rowe, M.C., Wolff, J.A., Gardner, J.N., Ramos, F.C., Teasdale, R., Heikoop, C.E., 2007, Development of a Continental Volcanic Field: Petrogenesis of Pre-caldera Intermediate And Silicic Rocks and Origin of the Bandelier Magmas, Jemez Mountains (New Mexico, USA): Journal of Petrology: v. 48, no. 11, p. 2063 – 2091.

Scherbakov, V.D., Plechov, P.Y., Izbekov, P.E., Shipman, J.S., 2010, Plagioclase zoning as a n indicator of magma processes at Bezymianny Volcano, Kamchhatka: Contributions to Mineralogy and Petrology, v. 162, iss. 1, p. 83-99.

Smith R.L., 1979, Ash-Flow Magmatism: GSA Special Papers, v. 180, p. 5-28.

Smith, R.L., and Bailey, R.A., 1966, The Bandelier Tuff: A study of ash-flow eruption cycles from zoned magma chambers: Bulletin of Volcanology, v. 29, no.1, p. 83-103.

Smith, R.B. and Braile, L.W., 1994, The Yellowstone hotspot, Journal of Volcanology and Geothermal Research: v. 61, p. 121-129,135-187.

Simon, J.I., Weis, D., DePaolo, D.J., Renne, P.R., Mundil, R., and Schmitt, A.K., 2014, Assimilation of preexisting Pleistocene intrusions at Long Valley by periodic magma recharges accelerates rhyolite generation: rethinking the melting model: Contributions to Mineralogy and Petrology, v. 167, p. 1-34.

Spell, T.L., and McDougall, I., 2003, Characterization and calibration of $^{40}Ar/^{39}Ar$ dating standards: Chemical Geology, v. 198, p. 189-211.

Wendt, I. and Carl, C., 1991, The statistical distribution of the mean squared weighted deviation: Chemical Geology: Isotope Geoscience section, v. 86, iss. 4. P. 275-285.

Wolff, J.A., Ramos, F.C., 2003, PB isotope variations among Bandelier Tuff feldspars: No evidence for a long-lived silicic magma chamber: Geology, v. 31, no. 6, p. 533-536.

CURRICULUM VITAE

William Joseph
josepw1@unlv.nevada.edu
1-(847)-863-8595

Education

Master's in Geology with a focus on Volcanology and Igneous Petrology, University of Nevada, Las Vegas – In Progress

Honors
Bernada E French Scholarship, 2015
Edwards and Olswang Scholarship, 2015
Most Outstanding TA Award, 2015

Bachelor of Arts in Geology, DePauw University – May 2014

Honors
Dr. Charles L. Beiber Scholarship, 2012
E.R. "Rock" Smith Award, 2013
Dean's List, 2012, Fall 2013, Fall 2014

Publications

Dobbs, S, Joseph, W.T., Kunkel, F., Cope, T., 2013. Mesozoic Structural and Stratigraphic Framework of the Yanshan Fold-Thrust Belt: A Record of Contractile and Extensional Tectonics in NE China: Geological Society of America: Abstracts with Programs, v. 45, No. 7.

Joseph, W.T., 2016 Characterizing Crystal Assemblages for the Petrogenesis of Post-Collapse Rhyolites in the Long Valley Caldera, CA: Geological Society of America: Abstracts with Programs, v. 48, no. 7.